UNIVERSITE DE LYON

CNRS & ECOLE NORMALE SUPERIEURE DE LYON

Unité de Mathématiques Pures et Appliquées

Habilitation à Diriger des Recherches

Analyse quantitative de modèles structurés issus de la biologie

Chimiotactisme, fronts d'invasion, polymérisation, polarisation

Vincent Calvez

Soutenue publiquement le 4 décembre 2015 devant le jury composé de

Laurent Desvillettes	Institut de Mathématiques de Jussieu
Odo Diekmann	Universiteit Utrecht
Sylvain Gandon	Centre d'Ecologie Fonctionnelle et Evolutive
Emmanuel Grenier	Ecole Normale Supérieure de Lyon
Benoît Perthame	Université Pierre et Marie Curie
Laure Saint-Raymond	Ecole Normale Supérieure de Paris
Emmanuel Trélat	Université Pierre et Marie Curie

après avis de

Laurent Desvillettes
Odo Diekmann
Emmanuel Trélat

Remerciements

Ce travail de recherche n'aurait certainement pas vu le jour sans l'engagement de Benoît Perthame à former des jeunes étudiants à l'interface entre les mathématiques et la biologie. Je fus l'un de ceux là. Depuis, j'ai toujours pu compter sur son soutien et lui en suis infiniment reconnaissant. J'ai pu également bénéficier de l'hospitalité et des lumières de José Antonio Carrillo tout au long de ces jeunes années, et surtout à l'occasion d'un semestre thématique au Centre de Recerca Matemàtica, Barcelona.

Je suis très honoré de voir réunies dans le jury des personnalités très importantes à mes yeux. Je tiens à remercier chaudement Laurent Desvillettes, Odo Diekmann, et Emmanuel Trélat d'avoir pris soin de rapporter mon mémoire d'habilitation. Je dois beaucoup à Emmanuel Grenier qui m'a soutenu à mon arrivée à Lyon, et m'a offert de participer à l'aventure Numed. Je suis très reconnaissant à Laure Saint-Raymond d'avoir accepté de faire le déplacement pour participer au jury, ainsi qu'à Sylvain Gandon d'avoir accepté de jouer le jeu de l'interdisciplinarité.

Mes recherches n'auraient pas connu cet élan sans la thèse de Jonathan Saragosti, dans l'équipe de Pascal Silberzan et Axel Buguin. Le travail expérimental de Jonathan et son ouverture d'esprit mathématique ont permis d'élaborer de nouveaux modèles et de les valider. Comme toujours, le travail d'analyse a un temps de maturation beaucoup plus long, mais je ne désespère pas d'arriver à clôre la partie mathématique du programme avant ma retraite.

Ce travail de recherche est le fruit de nombreuses collaborations. J'ai beaucoup appris au contact de nombreux mathématiciens et biologistes. Je souhaite les remercier dans ces lignes, en espérant n'oublier personne : Nikolaos Bournaveas pour les équations hyperboliques et son accueil à Edinburgh, Lucilla Corrias pour l'équation de Keller-Segel, Nicolas Meunier pour ses intuitions et son rôle précieux à l'interface, Natacha Lenuzza et Franck Mouthon pour tout ce que je sais (de terrifiant) sur les maladies à prion, Marie Doumic et Pierre Gabriel pour les équations de croissance-fragmentation, Hossein Khonsari pour sa volonté d'appliquer les mathématiques à la médecine, Raphaël Voituriez pour les modèles et la richesse de leurs comportements, Hugues Berry pour la diffusion intra-cellulaire, Didier Bresch pour les modèles de mécano-biologie, Sepideh Mirrahimi pour les équations de Hamilton-Jacobi, Grégoire Nadin qui m'a appris tout ce que je sais des équations de réaction-diffusion, Stéphane Gaubert pour sa redoutable perspicacité, Thomas Gallouët pour les systèmes de particules, Gaël Raoul pour sa grande exigence, et Christian Schmeiser pour les équations cinétiques et son accueil à Vienne...

J'ai pu bénéficier d'un environnement de recherche extrêmement stimulant à l'Ecole Normale Supérieure de Lyon, ainsi qu'à l'Université Claude Bernard. J'ai beaucoup appris sur le numérique grâce à Paul Vigneaux, avec qui je partage (entre multiples choses) un certain regard sur la BD. Recherche et amitié mêlées, tout ne saurait bien sûr se résumer à l'orgnisation d'un Cemracs (mais ce n'est pas rien déjà :). L'absence momentanée d'article cosigné ne rend guère compte de la fréquence et de l'intensité des séances de travail avec Thomas Lepoutre C'est aussi l'occasion de saluer Jimmy Garnier qui a accepté de se joindre à l'aventure. J'ai pu bénéficier de riches discussions avec des collègues d'autres disciplines, Sophie Pantalacci, Arezki Boudaoud, Pablo Jensen, Stéphane Vincent, Freddy Bouchet. Je les remercie vivement. Et aussi, bien sûr, les collègues et amis de l'Institut Camille Jordan, Violaine Louvet, Thierry Dumont, Francis Filbet, Julien Vovelle, Simon Masnou, Daniel Leroux, Sylvie Benzoni-Gavage, Miguel Rodrigues, Jean Bérard, Anne-Laure Fougères (certains sont partis vers d'autres cieux entre-temps).

L'organisation d'un trimestre thématique sous l'égide du Labex Milyon a été un évènement important de cette période. Cela n'aurait pu se faire sans la coordination des équipes maths-bio de Lyon, avec Fabien Crauste, Hugues Berry, Laurent Pujo-Menjouet, Thomas Lepoutre, Benjamin Ribba, Olivier Gandrillon, Samuel Bernard, Mostafa Adimy, Je remercie Bertrand Rémy pour sa confiance, ainsi que Carine Sevestre pour avoir rendu cela possible en toute sérénité.

Au quotidien, je m'en remets aveuglément à Magalie Le Borgne, Virginia Goncalves et Sandy Artero. Hommage leur est rendu à chaque occasion, en voici une nouvelle !

Je remercie plus généralement l'ensemble de l'UMPA, et ses directeurs successifs, Damien Gaboriau, Laurent Berger, Emmanuel Giroux et Albert Fathi, ainsi qu'à mon cher directeur d'équipe, Denis Serre. J'en profite pour saluer tous les membres de l'UMPA passés et présents. J'ai une pensée pour Gérard Lasseur, parti trop tôt.

Je remercie également l'équipe du DMA pour cette opportunité qui m'est offerte d'y séjourner régulièrement, et en particulier Bertrand Maury pour les stimulantes discussions là-bas.

Que serait Lyon sans MathàLyon (et dans toute la région...) ? En tout cas MathàLyon ne serait pas sans les pères fondateurs qui eurent cette fabuleuse idée de dupliquer l'exposition internationale des mathématiques, ni sans l'énergie (et les réseaux) de l'infatigable Régis Goiffon, sans le travail de coordination de Fabien Vignes-Tourneret et maintenant Thomas Lepoutre, et enfin les interventions des mathématiciens lyonnais dans les classes de collges et de lyces.

Je n'allais sûrement pas oublier les étudiants qui m'ont accordé leur confiance pour encadrer leurs travaux de thèse, et en particulier Emeric Bouin à qui une partie de ce mémoire doit beaucoup. Sans son travail acharné, le mystère des fronts qui accélèrent serait sans doute resté à couvert. Je remercie également Laetitia Giraldi, Thibault Bourgeron et Chris Henderson qui ont accepté de rejoindre l'UMPA comme post-doctorants.

Enfin, l'heure est venue de saluer les amis lyonnais, avec qui nous partageons beaucoup de temps (hors les murs) et c'est précieux : Paul, Mikael, Christophe, Grégory, Thomas, sans oublier Marielle, Laure, Anne, Delphine, et tous les enfants. Cyril et Ophélie étaient là aussi.

Il est toute une bande d'amis ici ou ailleurs que je n'aurai pas la place de saluer. Ils se reconnaitront s'ils tombent jamais sur ce texte. Je conclus en remerciant du fond du coeur toute ma famille et celle de Flore. Merci à Flore, dont le sourire ne cesse de s'agrandir. Ce mémoire est pour Timothée et Ophélie, sans oublier Elise.

Table of contents

Introduction

This memoir contains an overview of selected works I achieved between 2008 and 2015 in collaboration with several co-authors. Some results were obtained very recently, for the sake of completeness of this memoir, and are first reported in the following lines.

Biological motivations

My work is almost exclusively motivated by biological problems. I had the unique opportunity to interact with largely open-minded biologists and biophysicists. This led to very interesting and challenging mathematical problems. Some results had a clear biological interpretation. This memoir is structured from the point of view of biological applications:

(1) **Self-organization of aggregating particles.** (Chapter 1) – This part has a strong mathematical flavor. It was early motivated by the thorough analysis of the Keller-Segel model for chemotaxis, and in particular the critical two-dimensional case [**BDP06**]. The goal is to investigate the long-time asymptotics of a mean-field equation for diffusing and self-attracting particles. My contribution to this problem is a **gradient flow interpretation** for this type of equation in the Wasserstein space, and its consequences. Unfortunately, up to now, original features could be derived with full generality only for the one-dimensional case, although some extensions are possible for the higher-dimensional case when the interaction kernel is newtonian. The reason why techniques fail in higher dimension is not clear so far.

(2) **Dynamics of structured populations,** including bacterial chemotaxis (Chapter 2), evolution of dispersal evolution in age-structured populations (Chapter 3), and growth-fragmentation processes (Chapter 4) – Although these problems are apparently unrelated, they are intimately connected from the point of view of analysis and mathematical techniques.

On the contrary to several works in the literature that rely on multiscale models to derive macroscopic models in a suitable scaling limit, I attempt to keep the multiscale nature of model as far as possible during the analysis. There are strong biological motivations to do so. In collaboration with a group of biophysicists at Institut Curie (Paris), we showed that the mesoscopic scale is appropriate to accurately describe **migrating bands of chemotactic bacteria** [**23**], an old problem dating back to Keller and Segel [**KS71**], after the seminal work of Adler [**Adl66**].

Another motivation comes from the interplay between ecology and evolution. Numerous examples have been reported in the literature where ecological and evolutionary aspects are both acting at comparable time scales [**CBBB12, Le13**]. An important problem in evolutionary biology related to these issues is **dispersal evolution** [**Ron07**]. Recent field studies revealed that rapid evolution may occur at the margins of an invasive species range [**TBW+01, PBWS06**].

Another field of evolutionary biology in which it is of paramount importance to track the structure of the population is **the evolutionary theory of aging**, dating back to Hamilton [**Ham66**], see [**Ros94, Cha94**] for two important monographs on this subject. The purpose of this theory is to unravel the role of mutations with age-specific effects. In collaboration with a group of evolutionary biologists at ISEM (Montpellier), we have derived quantitative results for the maladaptation of an age-structured population to a changing environment.

Finally, the modelling of **biophysical polymerization processes** has raised a lot of interest in the past decades due to the increasing prevalence of amyloid diseases (*e.g.* CreutzfeldtJakob or Alzheimer's disease). My contribution to this modelling effort consists in a general analysis of optimal control of linear growth-fragmentation processes, where the combination of inhomogeneous growth and fragmentation exhibits unexpected dynamics.

(3) **Cell polarization,** including spontaneous yeast polarization, and biomechanical models for tip-growing cells (Chapter 5) – The possibility of yeast cell spontaneous polarization was described in [**WSAWL03**]. A feedback loop based on active transport along actin fibers was proposed to account for symmetry breaking. Analogy with the Keller-Segel system enables to analyse this instability beyond linear analysis. On the other hand, the coupling between biomechanical models for walled cell expansion, and heterogeneous distribution of growth pattern, is studied from the point of view of linear stability, and numerical simulations.

Mathematical contents

This memoir deals with the study of various linear and nonlinear Partial Differential Equations. Let me emphasize that, since biological models are not derived from first principles as in physics, generally they are not equipped with nice structures such as energy or entropy dissipation, that usually drive mathematical analysis. Hence, it is required to develop dedicated strategies to address each problem. However, some fruitful analogies between seemingly unrelated problems allow to transfer successful methodologies from one to each other. Various tools of PDE analysis have been used and developed in the course of my research:

(1) **Nonlinear Entropy methods** have been used for the systems of Keller-Segel type (aggregating particles and spontaneous polarization). As the Keller-Segel system coincides with the Smoluchowski-Poisson model for gravitation, it is equipped with a dissipated free energy, and entropy methods are available. The seminal work of Otto [**Ott01**] provided very powerful calculus in order to deal with such models. However, this has been extensively developed in the case of a convex interacting kernel, which is the exact opposite of the case at hand. We have spent much effort in disentangling the competition between (nonlinear) diffusion and aggregation in this context. This boils down to studying the geometry of the gradient flow of a convex + concave energy functional. The more interesting case arises when the convex and the concave contributions have the same homogeneity.

Surprisingly, similar entropy methods enable to investigate one-dimensional models for heterogeneous distribution of polarity markers. However, the methods fail in the higher-dimensional case, which makes full sense from the point of view of symmetry breaking. Nonetheless, we can get some heuristics about the higher-dimensional case.

(2) Existence of **travelling waves** for reaction-diffusion equations and related problems usually relies on comparison techniques using the construction of refined sub- and supersolutions. We have extended this analysis to multiscale problems such as kinetic transport equations – where the diffusive part is replaced by a transport-scattering operator – or mutation-selection-diffusion – where the reaction part is replaced by a mutation-selection

process. In the latter, the lack of comparison principle makes the analysis much more elaborate however. One noticeable exception in this program is the existence of **solitary waves** for the run-and-tumble equation describing migrating bands of chemotactic bacteria. Apparently, this problem does not belong to any large class of classical travelling waves problems. Accordingly, it is necessary to develop ad-hoc methods to establish this result.

(3) **Hamilton-Jacobi equations** arise naturally when seeking spreading properties of reaction-diffusion equations with monostable linearity in long time/large space [**Fre86**, **ES89**]. The propagation of level sets of the population density satisfy a Hamilton-Jacobi equation in the asymptotic limit, as in the approximation of geometric optics. This is intimately related to the *pulled* nature of the front, for which dynamics are driven by small density of individuals. Actually, the connection between reaction-diffusion equations and Hamilton-Jacobi equations originated from the theory of large deviations. Interestingly enough, this enables to derive quantitative results, *e.g.* asymptotic speed of propagation.

Recently, the same methodology was applied successfully to deriving the equations of adaptive dynamics [**GMMo98**] from mutation-selection deterministic PDE models [**DJMP05**, **Per07**]. Again, the dynamics are driven by the fate of rare mutants (*i.e.* low density of individuals).

An important aspect of this memoir consists in extending this approach to multiscale models. This requires tools from homogenization of Hamilton-Jacobi equations, and comparison principles when available. An important outcome is the quantitative description of velocity-jump processes in the large deviation regime, and also evolutionary dynamics in spatially structured populations, or age-structured populations.

(4) In the search for **optimal control** in discrete growth-fragmentation processes, we analysed a Ruelle-Perron-Frobenius operator in a max-plus setting. Under suitable irreducibility assumptions on the control matrices, we solved a max-plus eigenvalue problem, or equivalently, an ergodic Hamilton-Jacobi equation. The connection with the weak KAM theory of Fathi [**Fat97**, **FS04**, **Fat12**] is sketched in this memoir, and various dynamical properties of optimal trajectories are shown.

Major contributions

In my opinion, the major contributions contained in this memoir are the following:

(1) A sharp contraction estimate in Wasserstein distance for aggregating particles with linear diffusion and logarithmic interaction in one dimension of space (and also in two dimensions with radial symmetry), see Theorem 1.5.

(2) The existence of travelling waves for a kinetic model of chemotactic bacteria, which has been validated on biological experiments, see Section 2.2, and especially Theorem 2.15.

(3) Front acceleration in some models of structured populations. This emphasizes the importance of an accurate multiscale analysis of front propagation, as the dynamics can be very different at the various scales. For instance, propagation can accelerate at the mesoscopic scale (for a kinetic model), whereas it spreads linearly at the macroscopic scale (in the diffusive limit), compare Theorems 3.1 and 3.2.

(4) The existence of a Lyapunov exponent and a stable value function which encodes the infinite horizon pay-off of the optimal control problem $\dot{x} \in \mathcal{M}x$, where $\mathcal{M}$ is a compact set of irreducible Metzler matrices, Theorem 4.4.

A tale of two travellers

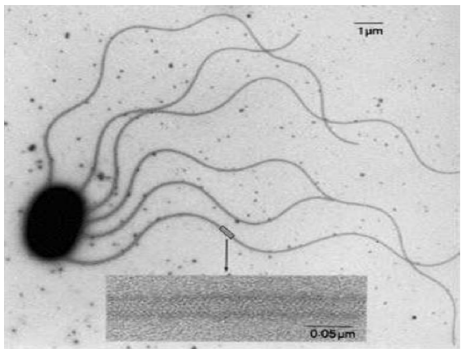

I finish this introduction by presenting two main characters that play a prominent role in this memoir, namely *Escherichia coli* and *Bufo marinus*. Further, they make the link between Chapter 2 and Chapter 3. They share the following features:

(i) they spread spatially, the former within migrating bands (Figure 0.1), and the latter in invasion fronts (Figure 0.2);

(ii) the population is structured with respect to a mesoscopic variable, velocity for *E. coli*, and dispersal for *B. marinus*. Both mesoscopic variables influence spatial displacements of individuals;

(iii) it is of paramount importance to keep the multiscale nature of the problem during mathematical analysis, in order to capture the spreading behaviour of the whole population.

Concentration waves of chemotactic bacteria *E. coli* were described in the seminal article by J. Adler[**Adl66**]. They inspired the second article of E.F. Keller and L.A. Segel about mathematical modelling of chemotaxis in 1971 [**KS71**]. Mesoscopic models describing this remarkable propagation phenomenon were proposed independantly in [**XHPE10**], and [**24, 23**]. Relevance of modelling at the mesoscopic scale relies on tracking experiments. They reveal the directional distribution of individuals, and in particular the spatially dependent biases of trajectories (see Figure 2.9). The velocity-jump process introduced by Stroock [**Str74**] and Alt [**Alt80**], can describe accurately those pulse waves, see Section 2.2.

One salient example of current species' invasion is the progression of cane toads in Australia. The invasion front accelerates since the introduction of *B. marinus* in the thirties [**PBWS06, UPSS08**]. Such acceleration is correlated with heterogeneity of the population with respect to morphology[**PBWS06**], and dispersal strategy [**LBS$^+$13, BPS14**]. It was postulated that a combination of mutation-selection processes and invasion dynamics may lead to spatial sorting individuals having the highest dispersal abilities at the edge of the front [**SBP11**]. This implies an apparent selection of the fastest individuals, which in turn speeds up the front. A minimal model for spatial sorting is analysed in Section 3.2.

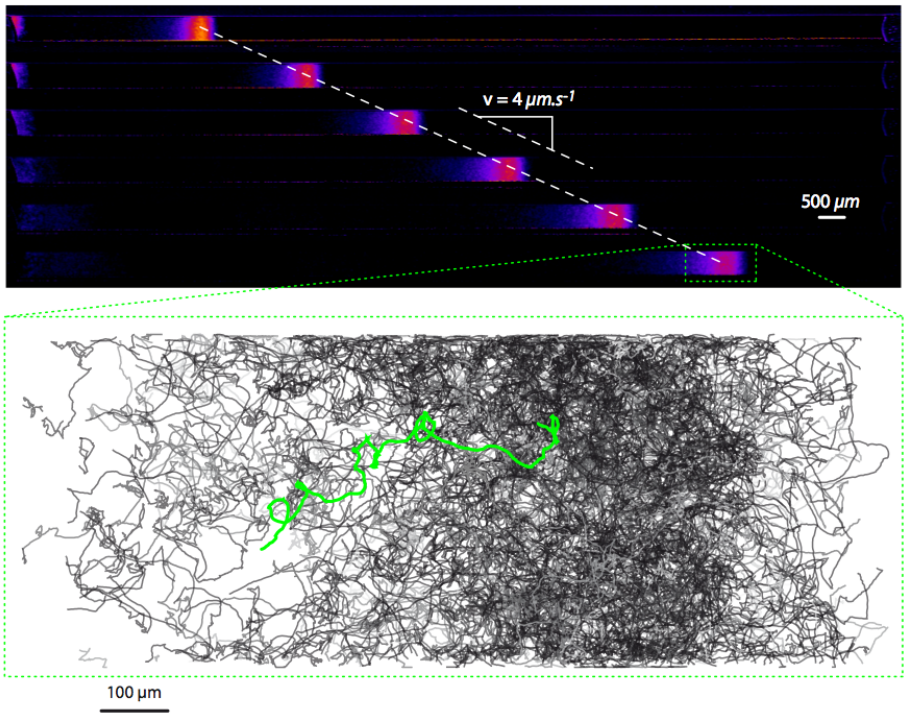

FIGURE 0.1. Concentration waves of bacteria in a microchannel [23]. (top) A solitary wave of high density of bacteria travels from left to right with constant speed and almost constant profile. (bottom) Massive tracking experiments reveal the mesoscopic structure of the wave. (Courtesy of J. Saragosti)

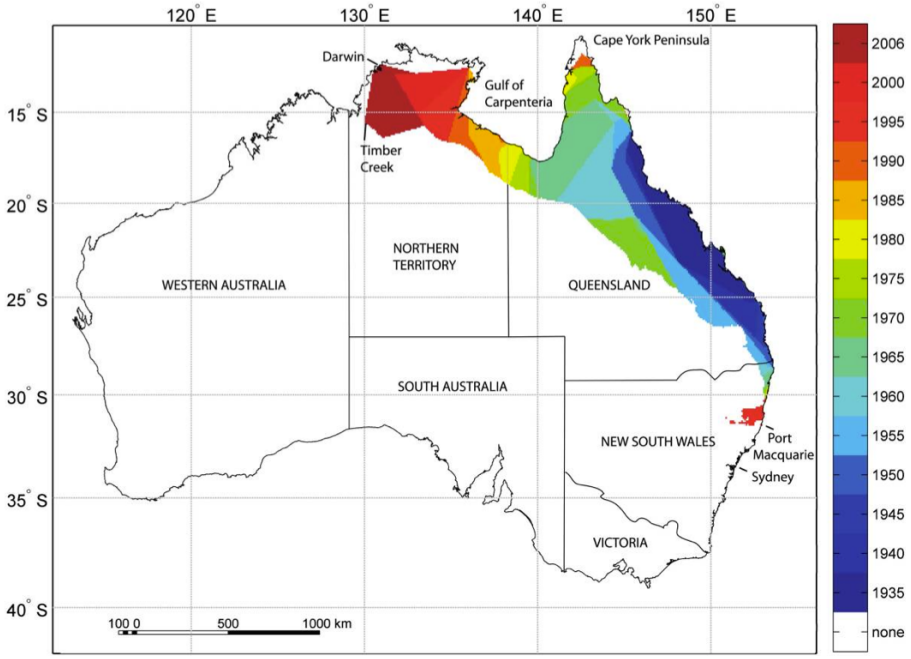

FIGURE 0.2. Propagation of cane toads *B. marinus* in Australia from 1935 to 2008 [**UPSS08**]. The speed of invasion ranges from 10 km/yr in the early stages of the invasion, to 50 km/yr at present time in the northern area.

Author's list of publications (2008–2015)

[1] O. Bénichou, V. Calvez, N. Meunier, and R. Voituriez. Front acceleration by dynamic selection in Fisher population waves. *Phys. Rev. E*, 2012.

[2] E. Bouin and V. Calvez. A kinetic eikonal equation. *C. R. Math. Acad. Sci. Paris*, 2012.

[3] E. Bouin and V. Calvez. Travelling waves for the cane toads equation with bounded traits. *Nonlinearity*, 2014.

[4] E. Bouin, V. Calvez, N. Meunier, S. Mirrahimi, B. Perthame, G. Raoul, and R. Voituriez. Invasion fronts with variable motility: phenotype selection, spatial sorting and wave acceleration. *C. R. Math. Acad. Sci. Paris*, 2012.

[5] E. Bouin, V. Calvez, and G. Nadin. Hyperbolic traveling waves driven by growth. *Math. Models Methods Appl. Sci.*, 2013.

[6] E. Bouin, V. Calvez, and G. Nadin. Propagation in a Kinetic Reaction-Transport Equation: Travelling Waves And Accelerating Fronts. *Archive for Rational Mechanics and Analysis*, 2015.

[7] N. Bournaveas and V. Calvez. Global existence for the kinetic chemotaxis model without pointwise memory effects, and including internal variables. *Kinetic and Related Models*, 2008.

[8] N. Bournaveas and V. Calvez. Critical mass phenomenon for a chemotaxis kinetic model with spherically symmetric initial data. *Annales de l'Institut Henri Poincare (C) Non Linear Analysis*, 2009.

[9] N. Bournaveas and V. Calvez. The one-dimensional Keller–Segel model with fractional diffusion of cells. *Nonlinearity*, 2010.

[10] V. Calvez, R. Hawkins, N. Meunier, and R. Voituriez. Analysis of a Nonlocal Model for Spontaneous Cell Polarization. *SIAM J. Appl. Math.*, 2012.

[11] V. Calvez and J. Carrillo. Refined asymptotics for the subcritical Keller-Segel system and related functional inequalities. *Proceedings of the American Mathematical Society*, 2012.

[12] V. Calvez and L. Corrias. Blow-up dynamics of self-attracting diffusive particles driven by competing convexities. *Discrete and Continuous Dynamical Systems - Series B*, 2013.

[13] V. Calvez, L. Corrias, and M. A. Ebde. Blow-up, Concentration Phenomenon and Global Existence for the Keller–Segel Model in High Dimension. *Communications in Partial Differential Equations*, 2012.

[14] V. Calvez, M. Doumic, and P. Gabriel. Self-similarity in a general aggregation–fragmentation problem. Application to fitness analysis. *Journal de mathématiques pures et appliquées*, 2012.

[15] V. Calvez and P. Gabriel. Optimal growth for linear processes with affine control. 2012. arXiv: 1203.5189.

[16] V. Calvez, P. Gabriel, and S. Gaubert. Non-linear eigenvalue problems arising from growth maximization of positive linear dynamical systems. 2014. arXiv: 1404.1868.

[17] V. Calvez and T. Gallouët. Particle approximation of the one dimensional Keller-Segel equation, stability and rigidity of the blow-up. 2014. arXiv: 1404.0139.

[18] V. Calvez and L. Giraldi. Pattern selection in a biomechanical model for the growth of walled cells. 2015. arXiv: 1502.05638.

[19] V. Calvez, N. Lenuzza, M. Doumic, J.-P. Deslys, F. Mouthon, and B. Perthame. Prion dynamics with size dependency–strain phenomena. *Journal of Biological Dynamics*, 2010.

[20] V. Calvez, N. Lenuzza, D. Oelz, J.-P. Deslys, P. Laurent, F. Mouthon, and B. Perthame. Size distribution dependence of prion aggregates infectivity. *Mathematical biosciences*, 2009.

[21] V. Calvez, G. Raoul, and C. Schmeiser. Confinement by biased velocity jumps: Aggregation of *escherichia coli*. *Kinetic and Related Models*, 2015.

[22] R. H. Khonsari, J. Olivier, P. Vigneaux, S. Sanchez, P. Tafforeau, P. E. Ahlberg, F. D. Rocco, D. Bresch, P. Corre, A. Ohazama, P. T. Sharpe, and V. Calvez. A mathematical model for mechanotransduction at the early steps of suture formation. *Proceedings of the Royal Society of London B: Biological Sciences*, 2013.

[23] J. Saragosti, V. Calvez, N. Bournaveas, B. Perthame, A. Buguin, and P. Silberzan. Directional persistence of chemotactic bacteria in a traveling concentration wave. *PNAS*, 2011.

[24] J. Saragosti, V. Calvez, N. Bournaveas, A. Buguin, P. Silberzan, and B. Perthame. Mathematical Description of Bacterial Traveling Pulses. *PLoS Comput. Biol.*, 2010.

CHAPTER 1

The Keller-Segel model viewed as a gradient flow

This chapter presents the contents of articles [11], [12], and [17], written in collaboration with J.A. Carrillo, T. Gallouët, and L. Corrias.

Summary

{1.1} The Keller-Segel system is briefly introduced. {1.1.1} It exhibits a remarkable dichotomy between global existence and blow-up of solutions in the two-dimensional case. The proof of global existence relies on a sharp functional inequality, namely the logarithmic HLS inequality. {1.1.2} The Keller-Segel system possesses a gradient flow structure in the space of probability measures, endowed with the Wasserstein metric.

{1.2} The one-dimensional case is analyzed thoroughly, up to a generalization of the problem, including power-like diffusion, and non Newtonian interaction. {1.2.1} In particular, the same dichotomy holds in the one-dimensional case with linear diffusion, and logarithmic interaction. {1.2.2} The one-dimensional Wasserstein distance coincides with the L^2 distance in Lagrangian formulation. {1.2.3} The competition between dispersion and aggregation can be interpreted as a balance between two contributions having opposite convexities. In particular, the logarithmic HLS inequality is a consequence of the Jensen inequality in both the one- and the two-dimensional case. However, this methodology seems to fail in dimension higher than three. {1.2.4} The same methodology enables to prove sharp exponential convergence towards steady state in the subcritical case. {1.2.5} This methodology can be extended to problems with power-like diffusion and interaction kernel. {1.2.6} Blow-up of solution is an immediate consequence of negativity of the free energy. However, unconditional blow-up in the supercritical case is much more difficult to obtain. Some insightful renormalization is presented, but the final result relies on a conjectured stability extimate.

{1.3} To gain analytical insights, it is fruitful to analyse a finite-dimensional version of the continuous problem. A deterministic particle scheme achieves this aim. {1.3.1} It is used to investigate the first aggregate at the blow-up time. {1.3.2} It is also used to study the attraction dominating regime, where the interaction term overwhelms the diffusion part regarding homogeneity.

1.1. Introduction and selected state of the art

I first recall some basic facts relative to the celebrated Keller-Segel model. It was introduced in the early 70's in a series of papers by E.F. Keller and L.A. Segel in order to describe self-organization of amoebae and bacteria colonies [**KS70a**, **KS70b**, **KS71**], see also [**TMPA08**, **HP09**] for two comprehensive reviews.

This model describes only motion of cells: it ignores cellular division, and death. Cells randomly diffuse, and are attracted by a chemical signal. The cell density is denoted by $\rho(t,x)$, and the

concentration of the chemical signal is denoted by $S(t,x)$. The Keller-Segel system consists of two partial differential equations. It writes in its simplest version as:

$$\begin{cases} \partial_t \rho = \Delta\rho - \chi\nabla\cdot(\rho\nabla S) \quad , \quad t>0,\ x\in\mathbb{R}^d\,, \\ -\Delta S = \rho \end{cases} \tag{1.1}$$

where $\chi>0$ is the chemo-sensitivity: it measures the influence of the gradient of chemical on the biased motion of cells. The first equation in (1.1) is conservative. So, there is another parameter in the model, namely the total number of cells $M=\int_{\mathbb{R}^d}\rho_0(x)\,dx=\int_{\mathbb{R}^d}\rho(t,x)\,dx$. We restrict to $M=1$ without loss of generality. Hence, $\rho(t,\cdot)$ will denote a probability density throughout this chapter.

The second equation of the system states that the signal is produced by the cells, and it diffuses so fast that it the equation is at quasi-stationary equilibrium. Thus, it acts as a self-attracting potential since χ is assumed to be positive. Note that in dimension $d=2$, we have the following representation of S, as the convolution with the Green's function of the Laplacian,

$$S(t,x) = -\frac{1}{2\pi}\int_{\mathbb{R}^2}\log|x-y|\rho(t,y)\,dy\,. \tag{1.2}$$

1.1.1. A simple dichotomy in 2D. Equation (1.1) expresses a competition between diffusion of cells and aggregation. One of the main feature is that solutions of (1.1) may become unbounded after a finite time. This is of course an idealization of possible aggregates, or clusters of cells.

1.1.1.1. *The free energy $\mathcal{F}[\rho]$.* One of the fruitful consequences of working with the simplified version of the Keller-Segel system (1.1) is that it comes with a rich mathematical structure[1]. The Keller-Segel system is endowed with a free energy $\mathcal{F}$,

$$\mathcal{F}[\rho] = \int_{\mathbb{R}^d}\rho\log\rho\,dx - \frac{\chi}{2}\int_{\mathbb{R}^d}\rho(x)S(x)\,dx\,. \tag{1.3}$$

We have (see [**BDP06**] for a rigorous justification)

$$\frac{d}{dt}\mathcal{F}[\rho(t)] = -\int_{\mathbb{R}^d}\rho\left|\nabla\left(\log\rho-\chi S\right)\right|^2\,dx \le 0\,. \tag{1.4}$$

There has been a large amount of studies devoted to the analysis of (1.1) using the free energy structure, see [**Bla11**] for a recent review. The two-dimensional case has attracted most of the attention due to biological relevance and mathematical elegance. In order to present the main result, let me discuss the action of dilations on the free energy. In the 2D case, the free energy reads as follows

$$\mathcal{F}[\rho] = \int_{\mathbb{R}^2}\rho(x)\log\rho(x)\,dx + \frac{\chi}{4\pi}\iint_{\mathbb{R}^2\times\mathbb{R}^2}\log|x-y|\rho(x)\rho(y)\,dxdy\,. \tag{1.5}$$

Since the total number of cells is conserved, we consider mass-preserving dilations such as $\rho_\lambda(y)=\lambda^{-2}\rho(\lambda^{-1}y)$. The free energy becomes,

$$\mathcal{F}[\rho_\lambda] = \mathcal{F}[\rho_\lambda] - 2\log\lambda + \frac{\chi}{4\pi}\log\lambda = \mathcal{F}[\rho_\lambda] + 2\left(\frac{\chi}{8\pi}-1\right)\log\lambda\,.$$

It is logarithmically homogeneous with respect to mass-preserving dilations. Furthermore, notice that the behaviour of the free energy depends on the value of χ. If $\chi<8\pi$, then $\mathcal{F}[\rho_\lambda]\to+\infty$ as $\lambda\to0$. This is ruled out by the *a priori* boundedness of the free energy $\mathcal{F}[\rho(t)]\le\mathcal{F}[\rho_0]$ (1.4). Therefore no concentration ($\lambda\ll1$) is expected in the subcritical case $\chi<8\pi$. In the supercritical case $\chi>8\pi$ however, we have $\mathcal{F}[\rho_\lambda]\to+\infty$ as $\lambda\to+\infty$. Therefore no dispersion ($\lambda\gg1$) of the cell density is expected in this case. Furthermore, we have $\mathcal{F}[\rho_\lambda]\to-\infty$ as $\lambda\to0$ in the latter case, and collapse of the cell density may occur, as it is compatible with the decay of the free energy.

[1] This remains true if the equation for S is the more realistic parabolic equation $\tau\partial_t S - D_S\Delta S=\rho$, see [**CC08**, **BCK+14**]. However, this structure breaks down if the advection speed is a nonlinear function of the gradient ∇S, as in Section 2.2.

1.1.1.2. *Global existence vs. blow-up.* It is remarkable that these expectations are indeed correct. This is a consequence of the homogeneity of the Keller-Segel system.

Theorem 1.1: Global existence vs. blow-up [BDP06]

Assume that the initial data satisfies $\rho_0\left(|\log\rho_0| + (1+|x|^2)\right) \in L^1$. Then, the following dichotomy holds true,

- If $\chi > 8\pi$, then the solution blows up in finite time (aggregation overcomes dispersion).
- If $\chi < 8\pi$, then the solution is global in time (dispersion overcomes aggregation). Moreover, the density converges to a self-similar vanishing profile.

In the subcritical regime, the nonlinear term (chemotaxis) becomes so small that the solution behaves like the solution of the heat equation. Indeed, the appropriate self-similar change of variables is the same as for the heat equation,

$$y = \frac{x}{\sqrt{1+2t}}\,, \qquad \tau = \frac{1}{2}\log(1+2t)\,. \tag{1.6}$$

The only difference is that the asymptotic self-similar profile is not a Gaussian function. It is a minimizer of the rescaled free energy. I will come back to this point later on.

1.1.1.3. *The logarithmic Hardy-Littlewood-Sobolev inequality.* Global existence in the two-dimensional case is intimately related to the following logarithmic Hardy-Littlewood-Sobolev functional inequality.

Theorem 1.2: The logarithmic HLS inequality [CL92]

There exists a constant $C(d)$ such that, for all probability density ρ with finite entropy, the following inequality holds true,

$$-\iint_{\mathbb{R}^d\times\mathbb{R}^d} \log\left(|z-z'|\right)\rho(z)\rho(z')\,dzdz' \le \frac{1}{d}\int_{\mathbb{R}^d}\log\left(\rho(z)\right)\rho(z)\,dz + C(d)\,. \tag{1.7}$$

Moreover, equality is satisfied for the extremal functions which are obtained by translations and dilations of

$$\mu(x) = \frac{1}{|\mathbb{S}^d|}\left(\frac{2}{1+|x|^2}\right)^d\,.$$

It is an endpoint inequality in the family of Hardy-Littlewood-Sobolev inequalities [**CL92**, **Bec93**]. The proof of Theorem 1.2 in any dimension, including the uniqueness of the extremal functions, is due to Carlen and Loss using the machinery of competing symmetries [**CL92**]. I also refer to [**DC12**, **CD14**] for recent developments in this direction.

Inequality (1.7) enables to measure in an optimal way the balance between diffusion and self-attraction at the level of the energy (1.5) [**DP04**].

1.1.1.4. *The critical case $\chi = 8\pi$.* Blanchet, Carrillo and Masmoudi [**BCM08**] proved that blow-up occurs in infinite time if the second moment of the initial density is finite, $\int_{\mathbb{R}^2}|x|^2\rho_0(x)\,dx < +\infty$. More recently, Blanchet, Carlen and Carrillo analysed thoroughly the case of initial data with infinite second moment [**BCC12**]. In fact, there exists a family of stationary states with infinite second moment. They prove stability of each of these equilibria using the free energy functional associated to a nonlinear diffusion equation of Fast-Diffusion type. The key observation is that this free energy is also a Lyapunov functional for the Keller-Segel system (1.1) with critical parameter

$\chi = 8\pi$. Moreover, this alternative Lyapunov functional possesses nice convexity properties, on the contrary to (1.3), see also [**CCL10**]. This result was refined in [**CF13**].

1.1.2. An enlightening gradient flow structure. The Keller-Segel system is part of a larger class of models of self-interacting particles, that have raised a considerable interest since the pioneering works of Jordan, Kinderlehrer and Otto [**JKO98**], McCann [**McC97**] and Otto [**Ott01**]. They deal with mean-field models of diffusing particles (with a possible nonlinear diffusion), in an external potential field V, interacting via the interaction kernel W,

$$\partial_t \rho = \Delta \rho^\alpha + \nabla \cdot (\rho \nabla V + \rho \nabla (W * \rho)) \,, \quad t > 0, \; x \in \mathbb{R}^d \,. \tag{1.8}$$

This system also possesses a free energy structure, generalizing (1.5),

$$\mathcal{F}[\rho] = \frac{1}{\alpha - 1} \int_{\mathbb{R}^d} \rho(x)^\alpha \, dx + \int_{\mathbb{R}^d} V(x) \rho(x) \, dx + \frac{1}{2} \iint_{\mathbb{R}^d \times \mathbb{R}^d} W(x-y) \rho(x) \rho(y) \, dx dy \,. \tag{1.9}$$

1.1.2.1. *Monge-Kantorovich Optimal transport and McCann's displacement convexity.* McCann proved that functional (1.9) enjoys remarkable convexity properties when the interpolation between probability measures follows the transport map of optimal euclidean transportation described by Brenier [**Bre91**]. Displacement interpolation consists in pushing forward a probability measure onto another one by using optimal paths in the euclidean space.

The problem of optimal transportation reads as follows [**Vil03, Vil09**]: Being given two probability measures on $\mathbb{R}^d$, μ and ν, find a transport map $T : \mathbb{R}^d \to \mathbb{R}^d$ that pushes forward μ onto ν with minimal global cost,

$$W_2(\mu, \nu) = \min_{T : T \# \mu = \nu} \left(\int_{\mathbb{R}^d} |x - T(x)|^2 \, d\mu(x) \right)^{1/2} . \tag{1.10}$$

Brenier proved that, if $\mu(x)$ and $\nu(z)$ are probability densities, and if ν has a finite second moment, then T is the unique gradient of a convex function $T = \nabla \phi$ that pushes forward $\mu(x)\,dx$ onto $\nu(z)\,dz$. The minimal cost of displacement (1.10) between the two probability measures is called the Wasserstein distance $\mathcal{W}_2(\mu, \nu)$.

McCann's displacement interpolation does the following thing: Being given two probability densities ρ_0 and ρ_1, define $T_t = (1-t)\mathrm{Id} + t \nabla \phi$, where $\nabla \phi$ pushes forward ρ_0 onto ρ_1 at minimal cost. The interpolation path in the space of probability measures is $\rho_t = (T_t \# \rho_0)$. McCann proved that the function $t \mapsto \mathcal{F}[\rho_t]$ is convex if the following conditions are fulfilled:

- $\alpha \geq 1 - 1/d$,
- V and W are convex.

The first condition is satisfied for the Keller-Segel system, but the interaction potential $W(x) = \log |x|$ is not convex.

1.1.2.2. *The gradient flow structure by Otto.* Beyond, there is an additional structure described by Otto [**Ott01**]: equation (1.8) coincides with the gradient flow of functional (1.9) in the space of probability measures endowed with the Wasserstein metric [**AGS08**]. This remarkable feature implies of course monotonicity of the functional along the trajectory, but it contains much more structure as we shall see later on.

In order to clarify this structure, I present below a basic example. Consider a smooth, convex potential $V : \mathbb{R}^d \to \mathbb{R}$, and the associated gradient flow in the euclidean space $\mathbb{R}^d$,

$$\dot{x}(t) = -\nabla V(x(t)) \,. \tag{1.11}$$

Also, denote by $X(t, x)$ the flow of the ODE (1.11). The corresponding advection PDE describes the motion of a cloud of particles, without interactions, following the gradient flow (1.11). It

reads

$$\partial_t \rho = \nabla \cdot (\rho \nabla V) \,. \tag{1.12}$$

Clearly, the solution is obtained by pushing-forward the initial density (or measure) ρ_0 by the flow of (1.11): $\rho(t,\cdot) = X(t,\cdot)\#\rho_0$, that is $\rho_0(x) = \rho(t, X(t,x)) \det D_x X(t,x)$. Equivalently, for any test function φ we have,

$$\int_{\mathbb{R}^d} \varphi(y)\rho(t,y)\,dy = \int_{\mathbb{R}^d} \varphi(X(t,x))\rho_0(x)\,dx\,.$$

On the other hand, the functional $\int_{\mathbb{R}^d} V(x)\rho(x)\,dx$ is nonincreasing along the trajectories of the advection equation (1.12), since it measures the potential energy of the cloud of particles following independent trajectories.

If one is seeking a convexity property for the functional $\int_{\mathbb{R}^d} V(x)\rho(x)\,dx$, associated with a gradient flow structure inherited from (1.11) in the space of probability measures, the interpolation between measures should follow lines in the euclidean space. This is the main feature of McCann's displacement interpolation $\rho_t = (T_t\#\rho_0)$. Accordingly, for the advection PDE (1.12) to inherit the gradient flow structure of (1.11), the metric on the space of probability measures should derive from the euclidean metric in $\mathbb{R}^d$. This is indeed encoded in the Wasserstein distance (1.10).

Interestingly enough, this approach can be generalized to interaction functionals $\iint_{\mathbb{R}^d\times\mathbb{R}^d} \rho(x)W(x-y)\rho(y)\,dxdy$, and even to internal energy functionals such as $\frac{1}{\alpha-1}\int_{\mathbb{R}^d}\rho(x)^\alpha\,dx$, coming from diffusion processes, for which no (deterministic) characteristics are available.

The theory of gradient flows is very well documented for displacement convex functionals, or more generally λ–convex functionals [**AGS08**]. However, the interaction kernel arising in the Keller-Segel equation is not λ–convex (1.5). Together with Blanchet and Carrillo, we proved in [**BCC08**] that the Keller-Segel system is indeed the gradient flow of the free energy functional in the subcritical case $\chi < 8\pi$.

1.2. The one-dimensional case

1.2.1. Two (good) reasons to restrict to the one-dimensional case. The one-dimensional case is much easier to figure out than the higher-dimensional case, since optimal transportation plans, and thus the Wasserstein distance, are explicit (see Section 1.2.2).

On the other hand, there is a one-dimensional analog of the two-dimensional Keller-Segel system that shares similar features. The idea is to replace the Green's function of the one-dimensional Laplacian, $S(t,x) = -\frac{1}{2}|x| * \rho(t,x)$, by a logarithmic interaction, $S(t,x) = -\log|x| * \rho(t,x)$. The one-dimensional Keller-Segel system with logarithmic interaction reads:

$$\partial_t \rho = \partial_x^2 \rho + \chi \partial_x \left(\rho \partial_x \left(\log|x| * \rho\right)\right), \quad t > 0\,, \quad x \in \mathbb{R}\,, \tag{1.13}$$

The same dichotomy as in Theorem 1.1 holds true [**CPSt07**]. The critical parameter value is $\chi = 2$.

Theorem 1.3: Global existence vs. blow-up, the one-dimensional case [CPSt07]

Assume that the initial data satisfies $\rho_0\left(|\log\rho_0| + (1+|x|^2)\right) \in L^1$. If $\chi > 2$, then the solution blows up in finite time. If $\chi < 2$, then the solution is global in time.

The main drawback of restricting to the one-dimensional case is that few results obtained in this context can be generalized to higher dimension using the following approach (see below for a discussion).

1.2.2. Optimal transportation and the gradient flow structure in 1D. The gradient flow structure can be reformulated in 1D using the inverse cumulative distribution function, that encodes the spatial distribution of the density in a Lagrangian formulation.

1.2.2.1. *Lagrangian reformulation.* The cumulative distribution function associated to the density $\rho(t,\cdot)$ is defined as follows,

$$F(t,x) = \int_{-\infty}^{x} \rho(t,y)\,dy\,, \quad x \in \mathbb{R}\,,$$

and its pseudo inverse $X(t,\cdot) : (0,1) \to \mathbb{R}$ is,

$$X(t,m) = \inf\{x \in \mathbb{R} \,|\, F(t,x) > m\}\,.$$

It encodes the position of particles, as a function of the partial mass $m \in (0,1)$. The link with optimal transportation is the following: the transport map between two measures $\mu(z)\,dz$ and $\rho(x)\,dx$ is given by $X \circ Z^{-1}$ [**Vil03**].

The nonlinear equation governing the evolution of $X(t,m)$ can be easily deduced from (1.13),

$$-\partial_t X(t,m) = \partial_m\left(\frac{1}{\partial_m X(t,m)}\right) + \chi \int_0^1 \frac{1}{X(t,m) - X(t,m')}\,dm'\,. \tag{1.14}$$

The second contribution is singular. It has to be understood through the following weak formulation: for any test function φ,

$$\begin{aligned}\frac{d}{dt}\int_0^1 \varphi(X(m,t))\,dm &= \int_0^1 \varphi''(X(m,t))\,dm \\ &\quad - \frac{\chi}{2}\iint_{(0,1)^2} \frac{\varphi'(X(t,m)) - \varphi'(X(t,m'))}{X(t,m) - X(t,m')}\,dmdm'\,,\end{aligned} \tag{1.15}$$

together with the (formal) boundary conditions:

$$\partial_m X(t,0) = \partial_m X(t,1) = +\infty\,, \quad X(t,0) = -\infty \quad \text{and} \quad X(t,1) = +\infty\,. \tag{1.16}$$

Finally, the free energy $\mathcal{F}$ reads as follows within this new formulation:

$$\mathcal{F}[\rho] = \mathcal{E}[X] = -\int_{(0,1)} \log\left(\frac{dX}{dm}\right) dm + \frac{\chi}{2}\iint_{(0,1)^2} \log|X(m) - X(m')|\,dmdm'\,. \tag{1.17}$$

1.2.2.2. *Gradient flow structure.* The Wasserstein distance between two probability densities $\rho(x)\,dx$ and $\mu(z)\,dz$ coincides with the L^2 distance between the inverse distribution functions,

$$\mathcal{W}_2(\rho,\mu) = \|X - Z\|_{L^2(0,1)}\,.$$

The formal link between the PDE (1.14) and the functional (1.17) is contained in the following claim.

Claim 1.4. *The integro-differential equation* (1.14) *is the gradient flow of the functional* $\mathcal{E}[X]$ *for the Hilbertian structure over* $L^2(0,1)$*:*

$$\dot{X} = -\nabla_{L^2}\,\mathcal{E}[X]\,. \tag{1.18}$$

This claim was proven rigorously in the subcritical case [**BCC08**].

1.2.2.3. *Blow-up of solutions.* Theorem 1.1, and its one-dimensional analog, Theorem 1.3, assert that the solution cannot be global in time when the parameter χ is above the critical value, and the variance is finite initially. In fact, this is a direct consequence of the logarithmic homogenetity of the free energy functional $\mathcal{E}$ (1.17), combined with the gradient flow structure. Indeed, Euler's formula for logarithmic homogeneous functions[2] yields the following identity,

$$\langle X, \nabla \mathcal{E}[X] \rangle = -1 + \frac{\chi}{2} .$$

On the other hand, by computing the time evolution of the variance of the density $\int |x|^2 \rho(t,x)\, dx = \|X(t)\|^2$, we get immediately,

$$\frac{d}{dt} \|X(t)\|^2 = 2 \left\langle X(t), \dot{X}(t) \right\rangle = -2 \left\langle X(t), \nabla \mathcal{E}[X(t)] \right\rangle = 2 - \chi . \tag{1.19}$$

Therefore, the variance cannot remain nonnegative for all time in the supercritical case $\chi > 2$.

1.2.3. Competition between concave and convex contributions in functional inequalities. The functional $\mathcal{F}$ is not displacement convex. However, it behaves globally as a convex functional in the following sense: it possesses a unique minimizer (up to dilations and translations) which is characterized as being the critical point of the functional. Alternatively speaking: if you are given a critical point of the energy, then you know it is a global minimizer.

1.2.3.1. *Competing convexities.* The formulation (1.17) suggests that convexity should play a crucial role here: the increment $X(m) - X(m')$ can be written as $\int_{m'}^{m} \frac{dX}{dm}(\sigma)\, d\sigma$, and Jensen's inequality enables to exchange the integral and the concave function log in order to bound the functional from below. Following this approach, Carrillo and I found a new proof of the logarithmic Hardy-Littlewood-Sobolev inequality, valid only in dimensions $d = 1, 2$.

▸ *Sketch of proof.* We restrict to the one-dimensional case. The first claim is that stationary states μ of the one-dimensional Keller-Segel equation with logarithmic interaction (1.13) are characterized by the following identity: for all test function φ, we have

$$\int_{\mathbb{R}} \varphi'(z) \mu(z)\, dz = \frac{1}{2} \iint_{\mathbb{R}\times\mathbb{R}} \left(\int_0^1 \varphi' \left([z,z']_t \right) dt \right) \mu(z)\mu(z')\, dz dz' , \tag{1.20}$$

where $[z,z']_t = (1-t)z + tz'$ is the linear interpolation between z and z'. This is a direct consequence of the weak formulation of the stationary state equation,

$$-\mu'(z) = \mu(z) \partial_z \left(\log|z| * \mu(z) \right) ,$$

after doubling the variables. Next, we evaluate the difference between the free energies of two densities, ρ and μ. We introduce the nonincreasing map $\phi' : \mathbb{R} \to \mathbb{R}$ pushing forward $\mu(z)\, dz$ onto $\rho(x)\, dx$.

$$\begin{aligned} \mathcal{F}[\rho] - \mathcal{F}[\mu] = & \int_{\mathbb{R}} \rho(x) \log \rho(x)\, dx - \int_{\mathbb{R}} \mu(z) \log \mu(z)\, dz \\ & + \iint_{\mathbb{R}\times\mathbb{R}} \rho(x) \log(|x-x'|) \rho(x')\, dx dx' - \iint_{\mathbb{R}\times\mathbb{R}} \mu(z) \log(|z-z'|) \mu(z')\, dz dz' \end{aligned}$$

Applying the change of variable $x = \phi'(z)$, we obtain

$$\begin{aligned} \mathcal{F}[\rho] - \mathcal{F}[\mu] &= -\int_{\mathbb{R}} \log\left(\phi''(z)\right) \mu(z)\, dz + \iint_{\mathbb{R}\times\mathbb{R}} \log\left(\frac{\phi'(z) - \phi'(z')}{z - z'} \right) \mu(z)\mu(z')\, dz dz' \\ &= -\int_{\mathbb{R}} \log\left(\phi''(z)\right) \mu(z)\, dz + \iint_{\mathbb{R}\times\mathbb{R}} \log\left(\int_0^1 \phi'' \left([z,z']_t \right) dt \right) \mu(z)\mu(z')\, dz dz' \end{aligned}$$

Finally, applying Jensen's inequality with the convex function $-\log$ we obtain the result,

$$\mathcal{F}[\rho] - \mathcal{F}[\mu] \geq -\int_{\mathbb{R}} \log\left(\phi''(z)\right) \mu(z)\, dz + \iint_{\mathbb{R}\times\mathbb{R}} \left(\int_0^1 \log\left(\phi'' \left([z,z']_t \right) \right) dt \right) \mu(z)\mu(z')\, dz dz' = 0 .$$

The last quantity vanishes when applying (1.20) with $\varphi' = \log \phi''$. ◂

[2] Here, $\mathcal{E}[\lambda X] = \mathcal{E}[X] + (-1 + \chi/2) \log \lambda$.

The same lines can be adapted (with some ad-hoc convexity inequality) for proving a similar result in the subcritical case $\chi < 2$ (see [11] for the details). In particular, we could prove that the rescaled energy functional

$$\mathcal{F}_{\mathbf{resc}}[\rho] = \mathcal{F}[\rho] + \frac{1}{2}\int_{\mathbb{R}} |x|^2 \rho(x)\,dx\,, \tag{1.21}$$

possesses a unique minimizer, which is characterized as being a stationary state of the rescaled Keller-Segel equation after the self-similar change of variables (1.6).

1.2.3.2. *Failure of the methodology in higher dimension.* Unfortunately, adapting this approach to the higher dimensional case yields unexpected technical obstructions that I was not able to overcome.

▸ *Obstruction in higher dimension.* When applying the same methodology in higher dimension, we end up with the following issue: let $\nabla\phi : \mathbb{R}^d \to \mathbb{R}^d$ be the optimal transport map pushing forward $\mu(z)\,dz$ onto $\rho(x)\,dx$. Then we have[3]

$$\begin{aligned}
\mathcal{F}[\rho] - \mathcal{F}[\mu] &= -\frac{1}{d}\int_{\mathbb{R}^d} \log\big(\det D^2\phi(z)\big)\,\mu(z)\,dz + \iint_{\mathbb{R}^d\times\mathbb{R}^d} \log\left(\frac{|\nabla\phi(z)-\nabla\phi(z')|}{|z-z'|}\right)\mu(z)\mu(z')\,dzdz'\\
&\geq -\frac{1}{d}\int_{\mathbb{R}^d} \log\big(\det D^2\phi(z)\big)\,\mu(z)\,dz + \iint_{\mathbb{R}^d\times\mathbb{R}^d} \log\left(\frac{\langle\nabla\phi(z)-\nabla\phi(z'),z-z'\rangle}{|z-z'|^2}\right)\mu(z)\mu(z')\,dzdz'\,,\\
&= -\frac{1}{d}\int_{\mathbb{R}^d} \log\big(\det D^2\phi(z)\big)\,\mu(z)\,dz + \iint_{\mathbb{R}^d\times\mathbb{R}^d} \log\left(\int_{t=0}^1 D^2\phi(\zeta)\left(\frac{\xi}{|\xi|},\frac{\xi}{|\xi|}\right)dt\right)\mu(z)\mu(z')\,dzdz'\,,
\end{aligned}$$

by Cauchy-Schwarz' inequality, where $\zeta = [z,z']_t$ and $\xi = z - z'$. By introducing the convex decomposition of the Hessian,

$$D^2\phi(\zeta) = \sum_{i=1}^d \lambda_i(\zeta) v_i(\zeta)\otimes v_i(\zeta)\,,\quad \sum_{i=1}^d v_i(\zeta)\otimes v_i(\zeta) = \mathrm{Id}\,, \tag{1.22}$$

we deduce

$$\begin{aligned}
\mathcal{F}[\rho] - \mathcal{F}[\mu] &\geq -\frac{1}{d}\int_{\mathbb{R}^d}\sum_{i=1}^d \log(\lambda_i(z))\mu(z)\,dz + \iint_{\mathbb{R}^d\times\mathbb{R}^d}\log\left(\int_{t=0}^1\sum_{i=1}^d \lambda_i(\zeta)\left(v_i(\zeta)\cdot\frac{\xi}{|\xi|}\right)^2 dt\right)\mu(z)\mu(z')\,dzdz'\,,\\
&\geq -\frac{1}{d}\int_{\mathbb{R}^d}\sum_{i=1}^d \log(\lambda_i(z))\mu(z)\,dz + \iint_{\mathbb{R}^d\times\mathbb{R}^d}\int_{t=0}^1\sum_{i=1}^d \log\left(\lambda_i(\zeta)\right)\left(v_i(\zeta)\cdot\frac{\xi}{|\xi|}\right)^2\mu(z)\mu(z')\;dtdzdz'\,,
\end{aligned}$$

by Jensen's inequality, since we have $\sum_{i=1}^d (v_i(\zeta)\cdot\xi)^2 = |\xi|^2$. After rearranging the last contribution, we obtain eventually,

$$\mathcal{F}[\rho] - \mathcal{F}[\mu] \geq \sum_{i=1}^d \int_{\zeta\in\mathbb{R}^d}\log(\lambda_i(\zeta))\left[-\frac{1}{d}\mu(\zeta) + \int_{t=0}^1\int_{\xi\in\mathbb{R}^d}\left(v_i(\zeta)\cdot\frac{\xi}{|\xi|}\right)^2\mu(\zeta-t\xi)\mu(\zeta+(1-t)\xi)\,d\xi dt\right]. \tag{1.23}$$

In dimension $d = 1$, the quantity between brackets $[\dots]$ is identically zero if, and only if, μ is a stationary state. However, this is not the case in higher dimension for each $i = 1\dots d$ (although this is true in average). In fact, the following relation holds: for each decomposition as in (1.22), we have

$$\sum_{i=1}^d \int_{\zeta\in\mathbb{R}^d}\lambda_i(\zeta)\left[-\frac{1}{d}\mu(\zeta) + \int_{t=0}^1\int_{\xi\in\mathbb{R}^d}\left(v_i(\zeta)\cdot\frac{\xi}{|\xi|}\right)^2\mu(\zeta-t\xi)\mu(\zeta+(1-t)\xi)\,d\xi dt\right] = 0\,.$$

However, this is not sufficient to conclude that the r.h.s. of (1.23) vanishes, as in the one-dimensional case. ◂

[3] Here, $\mathcal{F}$ is defined with the choice of constants that makes the logarithmic HLS inequality correct, *i.e.*

$$\mathcal{F}[\rho] = \frac{1}{d}\int_{\mathbb{R}^d}\log\left(\rho(z)\right)\rho(z)\,dz + \iint_{\mathbb{R}^d\times\mathbb{R}^d}\log\left(|z-z'|\right)\rho(z)\rho(z')\,dzdz'\,.$$

1.2.3.3. *Partial results in the radially symmetric case (see also Section 1.2.5).* Quite unexpectedly, our approach still works in the two-dimensional radially symmetric case, but not in the case $d \geq 3$. More generally, we are able to prove[4] analogous inequalities for functionals within the family (1.9) in the case of equal homogeneities, *i.e.* $W(x) = |x|^\gamma/\gamma$, with $\gamma = d(1-\alpha)$, and $V = 0$, under the restriction of radial symmetry[5], and the condition $\alpha \geq 1$, and $\gamma \in (-d, 2-d]$. The extremal case $\gamma = -d$ is ruled out for integrability reasons. On the other hand, the case $\gamma = 2-d$, which corresponds to a Newtonian interaction potential, appears to be an extremal case for some mysterious reason. In fact, hypergeometric functions pop up in the computation of convolutions like $W * \rho$ when ρ is radially symmetric. These hypergeometric functions enjoy some intricated convexity properties under the restriction $\gamma \leq 2-d$. This convexity structure is necessary for our approach. The logarithmic case corresponds to $\gamma = 0$, which yields the restriction $d \leq 2$.

This is work in progress, together with J.A. Carrillo and F. Hoffmann.

1.2.4. Exponential relaxation in self-similar variables. As mentioned above, it is natural to rescale the equation in the subcritical regime, since dispersion overcomes aggregation of particles. The system (1.13) writes as follows after the change of variables (1.6),

$$\partial_\tau \rho - \partial_y(y\rho) = \partial_{yy}\rho + \chi \partial_y\left(\rho \partial_y\left(\log|y| * \rho\right)\right), \quad \tau > 0, \quad y \in \mathbb{R}, \tag{1.24}$$

where we keep denoting the density by ρ in the new variables (τ, y), by a slight abuse of notations. We assume without loss of generality that the center of mass is zero, *i.e.* $\int_{\mathbb{R}} y\rho(t,y)\,dy = 0$.

Theorem 1.5: Exponentially fast convergence in the subcritical case [11]

Assume that $d = 1, 2$ and χ is below the critical value. In the case $d = 2$ assume in addition that the initial data ρ_0 is radially symmetric. Then, the solution of (1.24) converges exponentially fast towards the unique stationary state ν in Wasserstein distance (1.10). More precisely, the following explicit estimate holds true for solutions of (1.24):

$$\mathcal{W}_2(\rho_\tau, \mu) \leq \exp(-\tau)\mathcal{W}_2(\rho_0, \mu). \tag{1.25}$$

Of course, this result is closely related to the (almost) convexity structure of the (rescaled) functional energy (1.21), since (1.24) is the gradient flow of (1.21).

Remarkably, the rate of convergence does not depend on the parameter χ, even if it is arbitrarily close to the critical value.

Exponential relaxation in the subcritical two-dimensional case without the radial symmetry condition was proven recently by Campos and Dolbeault using a very powerful linearization technique and related functional inequalities [**CD14**] (see also the earlier work of [**BDEF10**] for the case of small χ). They obtained a rate of convergence which is twice faster for radially symmetric solutions, as compared to solutions without any symmetry. The set of admissible initial data was enlarged by Ergaña and Mischler [**EM13**]. I also refer to Montaru [**Mon15**] for yet another approach in the two-dimensional radially symmetric case.

▸ *Sketch of proof.* We restrict here to the one-dimensional case. We denote by $\partial_y\psi(\tau, y)$ the map that pushes forward $\rho(t,y)\,dy$ onto $\mu(z)\,dz$, and by $\partial_z\phi(\tau, z)$ the reverse map that pushes forward $\mu(z)\,dz$

[4] These are unpublished results.

[5] The condition of radial symmetry is usually not a restriction for proving such functional inequalities since the functionals are non-increasing under the action of decreasing rearrangement.

onto $\rho(t,y)\,dy$. The evolution of $w(\tau) = \frac{1}{2}W_2(\rho(\tau),\mu)^2 = \frac{1}{2}\int_{\mathbb{R}}|\partial_z\phi(\tau,z)-z|^2\mu(z)\,dz$ is computed as follows,

$$\begin{aligned}\frac{dw}{d\tau}(\tau) &= \int_{\mathbb{R}}(\partial_y\psi(\tau,y)-y)\left(\partial_y\left(\log\rho(\tau,y)+\chi\log|y|*\rho(\tau,y)+\frac{|y|^2}{2}\right)\right)\rho(\tau,y)\,dy\\ &= -\int_{\mathbb{R}}\partial_y^2\psi(\tau,y)\rho(\tau,y)\,dy+\frac{\chi}{2}\iint_{\mathbb{R}\times\mathbb{R}}\frac{\partial_y\psi(\tau,y)-\partial_y\psi(\tau,y')}{y-y'}\rho(\tau,y)\rho(\tau,y')\,dydy'\\ &\quad-\frac{1}{2}\iint_{\mathbb{R}\times\mathbb{R}}(\partial_y\psi(\tau,y)-\partial_y\psi(\tau,y'))(y-y')\rho(\tau,y)\rho(\tau,y')\,dydy'\\ &\quad+2\int_{\mathbb{R}}\partial_y\psi(\tau,y)y\rho(\tau,y)\,dy+1-\frac{\chi}{2}-\int_{\mathbb{R}}|y|^2\rho(\tau,y)\,dy\,,\end{aligned}$$

We follow the same lines as in the proof of Theorem 1.2. We make the change of variables $y=\partial_z\phi(\tau,z)$

$$\begin{aligned}\frac{dw}{d\tau}(\tau) &= -\int_{\mathbb{R}}\left(\partial_z^2\phi(\tau,z)\right)^{-1}\mu(z)\,dz\\ &\quad+\iint_{\mathbb{R}\times\mathbb{R}}\left[\frac{\chi}{2}\left(\frac{\partial_z\phi(\tau,z)-\partial_z\phi(t,z')}{z-z'}\right)^{-1}-\frac{|z-z'|^2}{2}\left(\frac{\partial_z\phi(\tau,z)-\partial_z\phi(t,z')}{z-z'}\right)\right]\mu(z)\mu(z')\,dzdz'\\ &\quad+2\int_{\mathbb{R}}z\partial_z\phi(\tau,z)\mu(z)\,dz+\int_{\mathbb{R}}|z|^2\mu(z)\,dz-\int_{\mathbb{R}}|\partial_z\phi(\tau,z)|^2\mu(z)\,dz\\ &\le -\int_{\mathbb{R}}\left(\partial_z^2\phi(\tau,z)\right)^{-1}\mu(z)\,dz\\ &\quad+\iint_{\mathbb{R}\times\mathbb{R}}\left[\left(\frac{\chi}{2}+\frac{|z-z'|^2}{2}\right)\int_0^1\left(\partial_z^2\phi(t,[z,z']_s)\right)^{-1}ds-|z-z'|^2\right]\mu(z)\mu(z')\,dzdz'\\ &\quad-\int_{\mathbb{R}}|\partial_z\phi(\tau,z)-z|^2\mu(z)\,dz+2\int_{\mathbb{R}}|z|^2\mu(z)\,dz\\ &= -\int_{\mathbb{R}}\left(\partial_z^2\phi(\tau,z)\right)^{-1}\mu(z)\,dz+\iint_{\mathbb{R}\times\mathbb{R}}\left[\left(\frac{\chi}{2}+\frac{|z-z'|^2}{2}\right)\int_0^1\left(\partial_z^2\phi(t,[z,z']_s)\right)^{-1}ds\right]\mu(z)\mu(z')\,dzdz'\\ &\quad-\int_{\mathbb{R}}|\partial_z\phi(\tau,z)-z|^2\mu(z)\,dz\,.\end{aligned}$$

There, we have applied the modified Jensen's inequality

$$\frac{\chi}{2}\left(\int_0^1u(s)\,ds\right)^{-1}-\frac{|z-z'|^2}{2}\left(\int_0^1u(s)\,ds\right)\le\left(\frac{\chi}{2}+\frac{|z-z'|^2}{2}\right)\int_0^1(u(s))^{-1}\,ds-|z-z'|^2\,,$$

for which equality holds true if and only if $u(s)=1$ a.e. on $(0,1)$. Finally, we conclude by using the following (weak) characterization of the stationary state, analogous to (1.20): for all test function φ, we have

$$\begin{aligned}\int_{\mathbb{R}}\varphi'(z)\mu(z)\,dz &= \frac{\chi}{2}\iint_{\mathbb{R}\times\mathbb{R}}\left(\int_0^1\varphi'\left([z,z']_t\right)\,dt\right)\mu(z)\mu(z')\,dzdz'\\ &\quad+\frac{1}{2}\iint_{\mathbb{R}\times\mathbb{R}}|z-z'|^2\left(\int_0^1\varphi'\left([z,z']_t\right)\,dt\right)\mu(z)\mu(z')\,dzdz'\,.\end{aligned}\tag{1.26}$$

We obtain eventually the inequality $\frac{dw}{d\tau}(\tau)\le -2w(\tau)$, which yields exponential convergence (1.25). ◂

1.2.5. A larger family of functionals and equations[6]. Together with Carrillo, we have investigated how the previous methodology can be extended to variants of (1.1), where the interaction is not obtained through the convolution with a logarithmic kernel, and the diffusion is possibly nonlinear. These results remain unpublished since the entire picture is not completely satisfactory so far.

We consider the following equation

$$\partial_t\rho=\Delta\rho^\alpha+\chi\nabla\cdot\left(\rho\nabla\left(\frac{|x|^\gamma}{\gamma}*\rho\right)\right),\quad t>0\,,\quad x\in\mathbb{R}^d\,,\tag{1.27}$$

[6]The content of this section is still under progress, in collaboration with J.A. Carrillo and F. Hoffmann.

It is a generalization of (1.1) with a nonlinear diffusion and a homogeneous interaction. The case $(\alpha, \gamma) = (1, 2-d)$ corresponds to the classical Keller-Segel system (up to constants).

The associated free energy writes as follows,

$$\mathcal{F}[\rho] = \frac{1}{\alpha-1}\int_{\mathbb{R}^d} \rho(x)^\alpha\, dx + \frac{\chi}{2\gamma}\iint_{\mathbb{R}^d\times\mathbb{R}^d} \frac{|x-y|^\gamma}{\gamma}\rho(x)\rho(y)\, dxdy\,. \tag{1.28}$$

1.2.5.1. *Classification.* We can define three regimes, depending on the relative values of the exponents α and γ,

$d(\alpha-1)+\gamma = 0$: This is the *fair-competition* regime, where homogeneities of the two competing contributions exactly balance. Among this regime, we separate the subcritical, the critical and the supercritical case, according to the value of the parameter χ.

$d(\alpha-1)+\gamma > 0$: This is the *diffusion-dominating* regime. Diffusion is strong, and is expected to overcome aggregation, whatever χ is.

$d(\alpha-1)+\gamma < 0$: This is the *attraction-dominating* regime. This regime is poorly understood. Self-attraction is strong, and can overcome the regularizing effect of diffusion whatever χ is, but there also exist global in time regular solutions under smallness assumptions in some critical L^p space.

I discuss briefly some partial results concerning functional inequalities, and their extremal functions. They can be obtained directly by using the same methodology as explained previously. I refer to [**Bed11b**, **KY12**, **CCV15**] for similar results using different approaches, namely comparison principles for the equation on the cumulative mass function in the radially symmetric case.

1.2.5.2. *The one-dimensional case.* In the one-dimensional case, we have the following statement that generalizes the logarithmic case $\gamma = 0$.

Claim 1.6 (The fair-competition regime). *Assume $\alpha - 1 + \gamma = 0$. For all $\gamma \in (-1, 0)$ there exists a critical parameter $\chi^*(\gamma) > 0$, such that*

(i) For $0 < \chi < \chi^*$ the functional (1.28) is positive everywhere.

(ii) For $\chi = \chi^*$ the functional (1.28) possesses a unique minimizer μ (up to dilations and translations) which satisfies $\mathcal{F}[\mu] = 0$. The minimizer is characterized as being a stationary state of (1.27)

(iii) For $\chi > \chi^*$ there exists a cone of densities for which the functional $\mathcal{F}$ takes negative values.

The proof of existence of a minimizer is equivalent to proving a sharp modified HLS inequality. This was performed using concentration-compactness techniques in higher dimension in [**BCL08**] for some special choice of the exponents, namely $\gamma = 2-d$, and $\alpha = (2d-2)/d$, see also [**Bed11a**, **KY12**] for more recent developments. Our methodology of competing convexities applies here, exactly in the same way as in the proof of Theorem 1.2.

The analog of Theorem 1.5 concerning exponential relaxation in the subcritical case $\chi < \chi^*$ is under current investigation. Additional difficulties arise because of the non zero homogeneity of the functional (see also Section 1.2.6).

1.2.5.3. *The higher dimensional case.* Our methodology can be extended in higher dimension under radial symmetry conditions. For instance, in the fair competition regime $d(\alpha-1)+\gamma = 0$, under the restriction $\gamma \in (-d, 2-d]$, we are able to prove the analog of Theorem 1.6. However, as mentioned above in Section 1.2.3.3, this requires a careful treatment of hypergeometric functions which appears to be highly technical, and does not help to gain a clear understanding of the whole picture.

1.2.6. Renormalization of the one-dimensional fair-competition regime. Let me comment on the behaviour of solutions to (1.27) in the one-dimensional fair-competition regime $\alpha-1+\gamma = 0$.

1.2.6.1. *Blow-up of solutions with negative energy.* The time evolution of the variance writes as follows,

$$\frac{d}{dt}\int_{\mathbb{R}} |x|^2 \rho(t,x)\,dx = 2(\alpha-1)\mathcal{F}[\rho(t)]\,. \tag{1.29}$$

This identity is a direct consequence of the homogeneity of the problem, as in Section 1.2.2.3. If the trajectory enters the negative cone of energy at some time $t = t_0$, $\mathcal{F}[\rho(t_0)] < 0$, it remains there since the free energy is nonincreasing along the trajectory $\mathcal{F}[\rho(t)] \searrow$. Then, the solution cannot exist globally because the variance would become negative otherwise, due to (1.29).

It is an open problem to prove or disprove that blow-up always occur, in the case where $\mathcal{F}[\rho_0] > 0$[7] There are some interesting renormalizations that may help to make some progress in this direction for the general case without symmetry. Since the problem is homogeneous, it is natural to define the renormalized density as follows

$$\hat\rho(t,y) = \sigma(t)\rho(t,\sigma(t)y)\,, \quad \sigma(t)^2 = \int_{\mathbb{R}} |x|^2\rho(t,x)\,dx\,. \tag{1.30}$$

It is defined such as $\int_{\mathbb{R}} |y|^2\hat\rho(t,y)\,dy = 1$.

1.2.6.2. *Reformulation in Lagrangian variables.* As previously, $X(t,m)$ denotes the inverse cumulative distribution function of the density $\rho(t,x)$. We deal with the gradient flow of the homogeneous functional

$$\mathcal{E}[X] = \frac{1}{\alpha-1}\int_0^1 (X'(m))^{1-\alpha}\,dm + \frac{\chi}{2}\iint_{(0,1)^2} \log|X(m)-X(m')|^\gamma\,dmdm'\,.$$

Euler's formula for homogeneous functions yields that

$$\frac{d}{dt}\|X(t)\|^2 = 2\left\langle X(t), \dot X(t)\right\rangle = -2\left\langle X(t), \nabla\mathcal{E}[X(t)]\right\rangle = -2\gamma\mathcal{E}[X(t)]\,, \tag{1.31}$$

which is precisely (1.29).

We have $\sigma(t) = \|X(t)\|_{L^2(0,1)}$. $Y(t) = X(t)/\|X(t)\|$. Using the two identities,

$$\dot X(t) = -\nabla\mathcal{E}[X(t)]\,, \tag{1.32}$$

$$\frac{d}{dt}\sigma(t)^2 = -2\gamma\mathcal{E}[X(t)]\,, \tag{1.33}$$

we can compute the evolution of the renormalized positions of the particles, $Y(t) = X(t)/\sigma(t)$. It writes eventually as

$$\dot Y(t) = \sigma(t)^{\gamma/2-1}\left(-\nabla\mathcal{E}[Y(t)] + \gamma\mathcal{E}[Y(t)]Y(t)\right)\,. \tag{1.34}$$

Interesting enough, the functional $\mathcal{E}$ is also a Lyapunov functional for the renormalized flow $Y(t)$,

$$\frac{d}{dt}\mathcal{E}[Y(t)] = \sigma(t)^{\gamma/2-1}\left(-\|\nabla\mathcal{E}[Y(t)]\|^2 + \gamma^2\mathcal{E}[Y(t)]^2\right) = -\sigma(t)^{\gamma/2-1}\mathcal{H}[Y(t)] \le 0\,. \tag{1.35}$$

where $\mathcal{H}[Y] = \|\nabla\mathcal{E}[Y]\|^2 - \gamma^2\mathcal{E}[Y]^2$ is the renormalized energy dissipation. It is nonnegative, as can be seen from the Euler's formula $\langle Y, \nabla\mathcal{E}[Y]\rangle = \gamma\mathcal{E}[Y]$, and the Cauchy-Schwarz inequality.

[7] This problem was answered positively by Bedrossian and Kim in the radially symmetric case in any dimension for the Newtonian case, *i.e.* $\gamma = 2-d$ [**BK13**, Theorem 5]. They used a comparison principle on the cumulative mass distribution.

1.2.6.3. *Blow-up under conditions on $\mathcal{H}$.* The key observation is that the functional $\mathcal{H}$ cannot vanish in the cone of nonnegative energy, as stated in the following claim.

LEMMA 1.7. *If $\mathcal{H}[Y]=0$, then $\mathcal{E}[Y]<0$.*

▸ *Sketch of proof.* It follows from the Cauchy-Schwarz inequality that $\mathcal{H}[Y]=0$ if and only if there exists π such that $\nabla\mathcal{E}[Y]+\pi Y=0$. Taking the scalar product with Y, we obtain that $\gamma\mathcal{E}[Y]+\pi=0$. Therefore $\pi=-\gamma\mathcal{E}[Y]\geq 0$ if Y is in the cone of nonnegative energy. To sum up, Y is a critical point of the rescaled energy $\mathcal{E}[X]+\frac{\pi}{2}\|X\|^2$, for some $\pi\geq 0$. Using the same methodology as in [**11**], we can prove that Y is in fact a *global minimizer* of $\mathcal{E}[X]+\frac{\pi}{2}\|X\|^2$. This is a contradiction, for homogeneity reasons: since we are in the supercritical case, there exists Z_0 such that $\mathcal{E}[Z_0]<0$. Hence, $\lim_{\lambda\to 0}\mathcal{E}[\lambda Z_0]+\frac{\pi}{2}\|\lambda Z_0\|^2=-\infty$. This is a contradiction with the fact that the rescaled energy $\mathcal{E}[X]+\frac{\pi}{2}\|X\|^2$ possesses a global minimizer. ◂

If we could prove the following uniform estimate

$$(\exists\delta>0)\ (\forall Y)\quad (\mathcal{E}[Y]\geq 0)\Rightarrow(\mathcal{H}[Y]\geq\delta)\,, \tag{1.36}$$

then we would be able to prove that any solution starting from the cone of nonnegative energy would eventually blow-up. The intermediate step would consist in proving that any solution eventually enters the cone of negative energy, as a consequence of (1.35).

LEMMA 1.8. *Assume that $\alpha-1+\gamma=0$, and $\chi>\chi^*$. If the estimate (1.36) holds true, then any trajectory eventually enters the cone of negative energy.*

▸ *Sketch of proof.* Assume that we have $\mathcal{E}[X(t)]\geq 0$ for all $t\geq 0$. The combination of (1.33) and (1.35) implies that the quantity $\omega(t)=\sigma(t)^{2-\gamma}$ satisfies

$$\frac{d^2\omega}{dt^2}(t)=\frac{\gamma(2-\gamma)}{\omega(t)}\mathcal{H}[Y(t)]\leq\delta\frac{\gamma(2-\gamma)}{\omega(t)}\,. \tag{1.37}$$

Then, multiplying both sides by $\dot\omega$ which is nonnegative as long as the solution lies in the cone of nonnegative energy by (1.33), we obtain

$$\frac12\frac{d}{dt}\left(\dot\omega(t)^2\right)+\delta(-\gamma)(2-\gamma)\frac{d}{dt}\left(\log\omega(t)\right)\leq 0\,.$$

We deduce after time integration that $\log\omega(t)$ is a priori bounded from above. This is enough to prove uniform boundedness of $\omega(t)$, and $\sigma(t)$ along the trajectory. Back to (1.35) and $\mathcal{H}[X(t)]\geq\delta$, we deduce that there exists a constant C depending on X_0, such that $\frac{d}{dt}\mathcal{E}[Y(t)]\leq -C\delta$. Therefore, the solution necessarily enters the cone of nonnegative energy. ◂

Open Problem(s) 1.9

Prove (or disprove) that all reasonable solutions of (1.27) blow-up in the one-dimensional fair-competition regime when χ is above the critical value. To prove this statement, it is enough to prove the uniform estimate (1.36).

1.3. Deterministic particle schemes, a Lagrangian point of view

We take advantage of the one-dimensional Lagrangian formulation to design a semi-discrete particle numerical scheme which possesses the same geometrical structure as the continuous problem. The strategy is as follows: we discretize the free energy $\mathcal{E}$ in Lagrangian coordinates, that is, the mass is equally distributed over N particles. Then, we consider the time continuous gradient flow with respect to the euclidean distance in $\mathbb{R}^N$. This is very much inspired by [**GT06**], and by the previous discussion about the analytical consequences of the geometry of the problem, *i.e.* the gradient flow of a homogeneous functional, on the behaviour of solutions.

The numerical scheme is designed in the following way: (i) we denote by $(X_i)_{1\le i\le N}$ the position of N particles carrying the same fraction of the unit mass. We assume that they are ordered as follows, $X_1 < X_2 < \cdots < X_N$. This assumption comes from the monotonicity of the inverse distribution function $X(t,m)$ with respect to m; (ii) we opt for a simple discretization of $\mathcal{E}$ (1.17):

$$\mathcal{E}_N[X] = -\sum_{i=1}^{N-1} \log(X_{i+1}-X_i) + \frac{\chi}{2N}\sum_{1\le i\ne j\le N} \log|X_i - X_j|; \tag{1.38}$$

(iii) we take the finite-dimensional euclidean gradient flow of $\mathcal{E}_N$ in $\mathbb{R}^N$, $\dot X(t) = -\nabla\mathcal{E}_N[X(t)]$,

$$\dot X_i = -\frac{1}{X_{i+1}-X_i} + \frac{1}{X_i - X_{i-1}} + \frac{\chi}{N}\sum_{j\ne i}\frac{1}{X_j - X_i}, \tag{1.39}$$

complemented with the dynamics of the extremal points

$$\begin{cases} \dot X_1 = -\dfrac{1}{X_2 - X_1} + \dfrac{\chi}{N}\displaystyle\sum_{j>1}\frac{1}{X_j - X_1} \\ \dot X_N = \dfrac{1}{X_N - X_{N-1}} + \dfrac{\chi}{N}\displaystyle\sum_{j<N}\frac{1}{X_j - X_N} \end{cases} \tag{1.40}$$

Note that these "boundary conditions" are equivalent to set two fictious particles $X_0 = -\infty$, and $X_{N+1} = +\infty$.

To sum up, we have discretized the one-dimensional Keller-Segel model with logarithmic interaction in such a way that it possesses a similar geometry. Therefore it captures the same features as the continuous system, in particular the dichotomy presented in Theorem 1.1.

First, the blow-up phenomenon in the supercritical case can be simply deduced from the logarithmic homogeneity of (1.38) with respect to dilations $X_\lambda = \lambda X$, as in Section 1.2.2.3. In fact, we have

$$\frac{1}{2}\frac{d}{dt}\|X(t)\|^2 = (N-1)\left(1 - \frac{\chi}{2}\right).$$

We see that blow-up occurs when $\chi > 2$, exactly as in the continuous model.

The proof of global existence follows from some discrete version of the logarithmic HLS inequality which is proven exactly as in the continuous case (Theorem 1.2), using the Jensen inequality. Finally, exponentially fast convergence of the rescaled solution $Y(\tau) = (\sqrt{1+2t})X(t)$ towards the unique stationary state in the subcritical regime $\chi < 2$ is adapted from the proof of Theorem 1.5. Details are contained in [**BCC08**].

I would not recommand the deterministic particle scheme (1.39) for practical purposes. I refer to [**Fil06**] for more efficient schemes from a computational viewpoint. However, I believe it provides us with a nice toy model in order to analyse subtle effects arising in the Keller-Segel equation, since it enables to reduce the dimension of the problem. In fact, even the case of three particles only exhibits quite informative behaviours, see [**17**].

1.3.1. A closer look at the first aggregate at the blow-up time. Together with Th. Gallouët we have tried to identify the number of particles involved in the first aggregate at the blow-up time. For instance, a phase-plane analysis of the three-particles system ($N = 3$) clearly shows that the first aggregate contains generically the minimal number of particles required for making an aggregate (2 or 3, depending on χ). There is one noticeable exception: the symmetrical case where the particle in the center is equally distant from the extremal ones.

The main challenge was to prove that, generically, the first aggregate contains exactly the critical number of particles (and not more). This question was raised in the two-dimensional continuous setting by [**CP81**]. A constructive partial answer was given in [**HV96**] in the radial case using

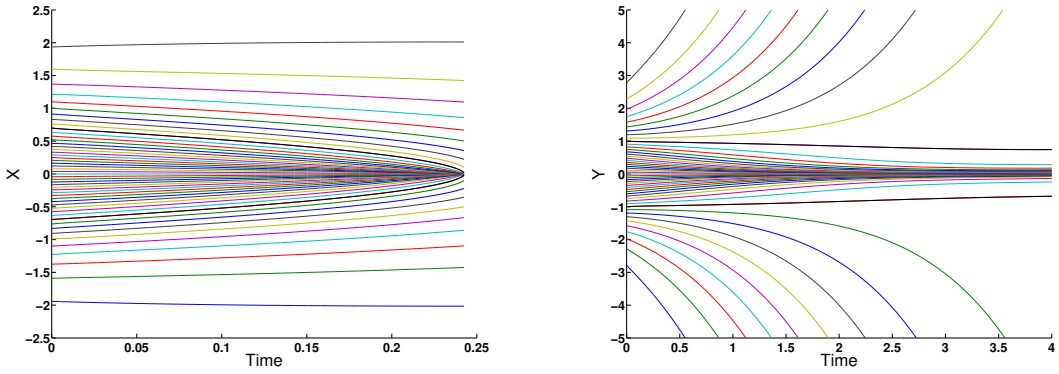

FIGURE 1.1. Numerical simulations of the discrete gradient flow (1.39)–(1.40) with $N = 49$ particles. The minimal number of particles to form an aggregate is $k = 31$. The initial data is a random perturbation of a symmetric configuration. (Left) Blow-up occurs by merging the minimal number of particles. The blow-up time is approximately $T = 0.24$. (Right) After a parabolic zoom, particles in the outer set are sent to infinity, and particles in the inner set converges towards a critical profile.

formal matching asymptotics. It was extensively studied in [**Suz05**]. More recently, Raphaël and Schweyer [**RS13**] proved stability of the blow-up mechanism described in [**HV96**] when χ is close to (and upper than) the critical value. More precisely, they showed that for initial data close to the critical mass stationary state $\mu(x) = \frac{8}{(1+|x|^2)^2}$ in some weighted space with second order regularity, the solution blows-up in a finite time T at the rate $\sqrt{T-t}\exp\left(-\sqrt{\frac{1}{2}|\log(T-t)|}+\mathcal{O}(1)\right)$, with the profile μ, up to a small correction.

The stability result obtained in [**17**] in the discrete setting can be summarized as follows: there exists an open set of initial data $\mathcal{D}$ such that for any $X(0) = (X_1(0),\dots,X_N(0)) \in D$, exactly the minimal number of particles gather when the solution blows-up. Let denote by k the minimal number of particles required for blow-up, defined so as $\frac{2N}{k+1} < \chi < \frac{2N}{k}$[8]. It means that $k-1$ particles forming an isolated subsystem of (1.39) cannot blow-up, because they do not carry enough mass. When starting from a configuration where k consecutive particles are close to each other, and the other $N-k$ are far apart, then this configuration is maintained until the blow-up time.

We also proved a rigidity result: up to extraction of a subsequence, the parabolic rescaling $Y(\tau) = (X(t)-\overline{X})/\sqrt{2\beta(T-t)}$ converges towards some profile Y_∞ which is a critical point of the partial rescaled energy,

$$\mathcal{E}_{\text{zoom}}[Y] = -\sum_{i\in\mathcal{I}\setminus\{\max\mathcal{I}\}}\log(Y_{i+1}-Y_i) + \frac{\chi}{2N}\sum_{\substack{(i,j)\in\mathcal{I}\times\mathcal{I}\\ i\neq j}}\log|Y_i-Y_j| - \frac{\beta}{2}\sum_{i\in\mathcal{I}}|Y_i|^2\,, \tag{1.41}$$

where $\beta = (k-1)\left(\frac{k\chi}{2N}-1\right) > 0$, and $\mathcal{I}$ is the set of particles taking part in the first aggregate, $|\mathcal{I}| = k$. Note the opposite sign of the last contribution as compared to (1.21), because this is a zoom in, as opposed to a zoom out.

Convergence holds for particles in the aggregate, whereas outer particles are sent to ∞ after a parabolic zoom. Alternatively speaking, k, and only k, particles blow-up at the same rate, see Figure 1.1.

[8] Equality cases are excluded for technical reasons.

We believe that convergence towards Y_∞ holds without extraction of subsequences. However, we were not able to prove it due to some technical obstruction.

Open Problem(s) 1.10

(i) For a given number of particles N, for all initial configurations, except the ones with a particular symmetry, exactly the minimal number of particles aggregate at the blow-up time.

(ii) After a proper parabolic rescaling, the k particles that aggregate converge towards a configuration which is critical for the free energy (1.41).

1.3.2. About the attraction-dominating regime. As emphasized above, the peculiar structure of the two-dimensional Keller-Segel model is a consequence of the logarithmic homogeneity, which is common for the entropy (diffusion) and the interaction energy (aggregation). What if this balance is broken? This holds for the Keller-Segel system (1.1) in dimension $d \geq 3$. There exists several studies about this problem in the literature [**BN94**, **CPZ04**, **KS10**, **Bed11b**].

Let me present briefly some results about the equation (1.27) in the one-dimensional case, for the attraction-dominating regime, namely $\alpha - 1 + \gamma < 0$. This is a caricature of the higher-dimensional Keller-Segel system (1.1) [**12**]. As opposed to the two dimensional case, several blow-up criteria are available. For instance, the solution blows-up in finite time when

$$C\left(\frac{1}{1-\alpha} - \frac{1}{\gamma}\right)\left(\int_{\mathbb{R}} |x|^2 \rho_0(x)\, dx\right)^{(1-\alpha)/2} + \mathcal{F}[\rho_0] < 0\,,$$

where C is some absolute constant. On the other hand, the solution is global in time if $\|\rho_0\|_{L^p}$ is small enough, where the critical exponent is given by $p = \dfrac{2-\alpha}{1+\gamma} > 1$.

As compared to the two-dimensional Keller-Segel system, the dichotomy between global existence and blow-up is not so clear. In fact, two different thresholds, concerning two different quantities (some critical L^p norm, on the one hand, the variance and the free energy on the other hand), are available.

Together with L. Corrias, we investigated the finite-dimensional problem, analogous to (1.39) in order to gain some insight on the toy model. We have adapted to the deterministic particle scheme the proofs guaranteeing either global existence, or blow-up of the cloud of particles. Noticeably, the phase-plane analysis in the case of three particles clearly shows that the situation is quite complex, despite the huge dimension reduction. For instance, it is difficult to determine the frontier between global existence and blow-up within a tractable analytical criterion.

1.4. Conclusion

The mathematical analysis of the Keller-Segel model has been remarkably active in the past decade. My contributions are far from answering general questions. They are rather focused on some specific aspects of the model. I tried to understand in an original way the competition between dispersion and self-attraction of cells. I was very enthusiastic with the one-dimensional case, for which the elegant geometric structure yields "optimal" proofs. However, this approach seems difficult to extrapolate to higher dimension, except in some specific cases. This failure is still not completely understood, leaving open some possible directions of research. Meanwhile, I decided to devote a larger fraction of my time to the study of swimming bacteria colonies, using more realistic models, based on an fruitful collaboration with a group of biophysicists. This is the purpose of the next Chapter.

CHAPTER 2

Mesoscopic modelling of chemotactic bacterial populations

This chapter presents the contents of articles [7], [8], [24], [23], [21], written in collaboration with N. Bournaveas, B. Perthame, J. Saragosti, A. Buguin, P. Silberzan, G. Raoul, and C. Schmeiser.

In addition, it contains original results on the existence of pulse waves for the kinetic model.

Summary

{2.1} Velocity-jump models are introduced to describe biased motion of cells at the mesoscopic scale. {2.1.1} The Alt model describes the evolution of cell density in phase space (position, velocity). The tumbling kernel indicates the frequency of turning. Chemical concentrations can influence tumbling rates, resulting in biased motion, *i.e.* chemotaxis. {2.1.2} In the case of spatial gradient sensing, dichotomy between global existence and blow-up is proven, similarly as for the two-dimensional Keller-Segel model, but in the spherically symmetric case only. {2.1.3} On the contrary, some bacteria experience temporal sensing. Existence of stationary clusters is proven at the mesoscopic scale. This amounts to prove monotonicity of the macroscopic cell density, by deciphering velocity profiles.

{2.2} Velocity-jump models are used to describe accurately lab experiments, {2.2.1} in which bands of bacteria are moving accross a microchannel at constant speed. {2.2.2} The problem is very different from classical reaction-diffusion travelling waves, as biased transport is the dominant effect here. {2.2.3} The diffusive limit of the velocity-jump process with temporal sensing yields a macroscopic advection-diffusion model which is different from the Keller-Segel model. Existence of travelling waves is established via analytical computations. Both the wave speed and the density profile agree with a first set of experimental data in which biases are small. {2.2.4} When biases are large, the mesoscopic model also fit experimental data very well. Moreover, existence of travelling waves is established.

2.1. Kinetic models for chemotaxis

I review below various aspects of kinetic models for chemotaxis, as opposed to parabolic models such as the Keller-Segel model (Chapter 1). Kinetic models for chemotaxis were developed by Alt [**Alt80**] (see also [**ODA88**]), following a stochastic process introduced in [**Str74**] after the seminal tracking experiments by Berg and Brown [**BB72**], Macnab and Koshland [**MK72**].

Kinetic models are well adapted to the mesoscopic description of velocity-jump processes, where each cell alternates between straight runs, and reorientation events (jumps in the velocity space). It is clear that a unique model cannot reproduce all strategies of cell locomotion, from the run-and-tumble process of the swimming bacteria *E. coli* to the polarized motion of amoeboid cells and leukocytes [**Bra01**]. However we point out, as in [**Alt80, ODA88**], that kinetic models can

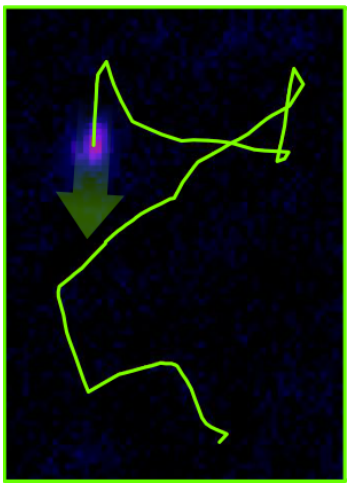

FIGURE 2.1. Typical trajectory of the swimming bacteria *E. coli*. Motion alternates between run phases (straight motion), and reorientation events (tumble). At the mesoscopic scale, it is reasonable to assume that both duration of run and duration of tumble follow Poisson distributions, but the timescale of run is one order of magnitude longer. (Courtesy of J. Saragosti)

distinguish between various strategies since the description takes place at the mesoscopic scale. For this, several choices for the reorientation kernel can be made.

We refer to [**Sch93**, **EO05**, **Loc07**, **Xue13**, **PTV15**] for further developments on velocity jump processes for bacterial and amoeboid motion that will not be discussed here. They include possible rotational diffusion during the run phase, or dynamics of a subcellular molecular network that transduces the external chemotactic signal inside the cell.

2.1.1. The Alt model and the tumbling kernel. The cell population is described by the density $f(t,x,v)$ at time ($t \in \mathbb{R}_+$), with respect to position ($x \in \mathbb{R}^d$) and velocity ($v \in V$). We assume throughout this chapter that the set of velocity V is bounded. For the sake of clarity, we normalize the velocity variable such as the measure of V has a unit value:

$$|V| = 1\,.$$

2.1.1.1. *The Alt model.* It reads as follows [**Alt80**, **ODA88**],

$$\underbrace{\partial_t f(t,x,v) + v\cdot\nabla_x f(t,x,v)}_{run} = \underbrace{\int_{v'\in V} \mathbf{T}(t,x,v,v')f(t,x,v')\,dv' - \boldsymbol{\lambda}(t,x,v)f(t,x,v)}_{tumble} \tag{2.1}$$

The free transport operator describes the phase of run, when the cell moves in a straight motion (but see [**Sch93**, **Loc07**] for more general models, including rotational diffusion during the run phase). The right-hand-side describes the reorientation process. The tumbling kernel $\mathbf{T}(t,x,v,v')$ denotes the frequency of reorientation from v' (pre-tumble velocity) to v (post-tumble velocity). The intensity of the Poisson process governing the reorientation events is

$$\boldsymbol{\lambda}(t,x,v) = \int_{v''\in V} \mathbf{T}(t,x,v'',v)\,dv''\,,$$

such that the equation (2.1) preserves the total number of cells. When a cell changes direction, a new velocity v is chosen according to the p.d.f.

$$K(t,x,v,v') = \frac{\mathbf{T}(t,x,v,v')}{\boldsymbol{\lambda}(t,x,v')}\,.$$

In other words, we can decompose the rate of reorientation as

$$\mathbf{T}(t,x,v,v') = K(t,x,v,v')\boldsymbol{\lambda}(t,x,v')\,,$$

where K is the conditional probability kernel, given that the cell has changed direction.

2.1.1.2. *The tumbling kernel: spatial vs. temporal sensing.* For the tumbling kernel $\mathbf{T}$, we will essentially consider two case studies:

(1) The case of *spatial sensing*, where the cell is able to measure spatial gradients of some chemical cues, for example by sending protrusions or pseudopodia. This usually coincides with the ability to polarize in the direction of the gradient. This is the case for amoeboid motion, *e.g.* amoebae or leukocytes [**Bra01**].

(2) The case of *temporal sensing*, where the cell is able to measure temporal variations of some chemical signal. This usually coincides with relative fast motion together with some memory effect. This is very well documented for *E. coli* (see [**Ber04**] and references therein).

2.1.1.3. *Dynamics of the chemoattractants.* Before we develop further these two cases, we discuss some basic facts about the modelling of the chemical signal. We shall distinguish between two opposite dynamics: production or consumption of the chemoattractant. It is not the goal of the present memoir to investigate very sophisticated chemical kinetics, hence we restrict to very simple reaction terms.

We shall denote by $S(t,x)$ the concentration of a chemoattractant produced by the cell population. This case has been extensively studied in the literature of chemotaxis modelling, as it is the basis of a very interesting positive feedback which leads to cell aggregation: when cells start to aggregate, the local concentration increases, enhancing the attraction of cells. We will mainly consider the following reaction-diffusion equation,

$$\nu\partial_t S = D_S\Delta S - \alpha S + \beta\rho\,, \quad \rho(t,x) = \int_{v\in V} f(t,x,v)\,dv\,, \tag{2.2}$$

where $\nu \in \{0,1\}$. The case $\nu = 0$ corresponds to the usual quasi-stationary approximation. This choice generally simplifies the analysis. However it is hardly relevant in the case of bacteria chemotaxis, for which effective diffusion of bacteria is comparable to the diffusion coefficient of chemoattractants [**24**].

We shall denote by $N(t,x)$ the concentration of a chemoattractant consumed by the cell population.

$$\partial_t N = D_N\Delta N - \gamma\rho N\,, \quad \rho(t,x) = \int_{v\in V} f(t,x,v)\,dv\,. \tag{2.3}$$

This will be used for the modelling of bacterial solitary waves, see Section 2.2.

2.1.2. Spatial sensing (blow-up vs. global existence). Here, we consider the case where an individual cell is able to measure the spatial gradient of a chemical signal at a given position x. Then, it is natural to consider that it chooses a post-tumble velocity v as a function of $v\cdot\nabla S$. If $v\cdot\nabla S \geq 0$, the direction is favorable, whereas if $v\cdot\nabla S \leq 0$ then the direction is unfavorable.

2.1.2.1. *Global existence in the case of sublinear dependency upon the gradient.* As compared to the Keller-Segel model, it is natural to address well-posedness of the kinetic equation (2.1) coupled to the reaction-diffusion equation (2.2). The articles [**7**, **8**], both written in collaboration with N. Bournaveas, contain the following result:

Theorem 2.1: Sublinear gradient dependency implies global existence [**8**]

Assume $d = 2$, V is bounded, and the tumbling kernel can be crudely bounded by the gradient $\|\nabla S\|_{L^\infty}$, with a sublinear estimate for some $\theta \in [0,1)$:

$$T(t,x,v,v') \lesssim \|\nabla S(t,\cdot)\|_{L^\infty}^{\theta} . \tag{2.4}$$

Then the solution of the coupled system (2.1)-(2.2), with $\nu = 0$, is global in time.

REMARK 2.2. *(1) Only the case $\nu = 0$ is treated in* [**7**, **8**]. *However it is expected that the same method leads to a similar result in the case $\nu = 1$.*

(2) The estimate (2.4) is crude as it is uniform with respect to x, and v. It is possible to refine this hypothesis, by assuming delocalization effects for instance, see [**CMPS04**, **HKS05**, **CDSM⁺06**, **BCGP08**]. *There, it is assumed that an individual cell measures the chemoattractant at some finite distance of its location:*

$$T(t,x,v,v') \lesssim |\nabla S(t,x+\varepsilon v)| ,$$
$$\text{or} \quad T(t,x,v,v') \lesssim |\nabla S(t,x-\varepsilon v')| ,$$

for some $\varepsilon > 0$, and dimension is $d = 2,3$. The former case presumes that cells can sense the gradient by sending protrusions in the direction v within the range ε. Note that here, v denotes the post-tumbling velocity, so the former estimate has to be interpreted as the cell browsing various possible directions. The latter case presumes that cells measure the gradient backward in time, with some delay $\varepsilon > 0$ (here, v' denotes the pre-tumbling velocity). Note that the same delay should be substracted to the time variable in order to be consistent.

▸ *Sketch of proof.* The proof of global existence relies on semi-group estimates based on the Duhamel formula, using the nonnegative nonlocal contribution $\int_{v'\in V} \mathbf{T}(t,x,v,v') f(t,x,v')\,dv'$ as a source term. The key argument consists in applying dispersion estimates for the free transport operator [**BD85**, **CP96**]: if f is the solution of the free transport equation

$$\partial_t f + v\cdot\nabla_x f = 0 ,$$

with initial datum f_0, then for all $p \geq q \geq 1$ the following decay estimate holds true,

$$\|f(t,\cdot,\cdot)\|_{L^p_x L^q_v} \leq \frac{1}{t^{d(1/q-1/p)}} \|f_0\|_{L^q_x L^p_v} . \tag{2.5}$$

Using the Duhamel formula for (2.1), and taking the $L^p_x L^q_v$ norm, we get

$$\|\rho(t,x)\|_{L^p_x} \lesssim \int_0^t \|\nabla S(t-s,x)\|_{L^\infty}^{\theta} \|\rho(t-s,x-sv)\|_{L^p_x L^q_v}\, ds .$$

The dispersion estimate (2.5) enables to control the last contribution,

$$\|\rho(t,x)\|_{L^p_x} \lesssim \int_0^t \frac{1}{s^{2(1/q-1/p)}} \|\nabla S(t-s,x)\|_{L^\infty}^{\theta} \|\rho(t-s,x)\|_{L^q_x L^p_v}\, ds ,$$

but $\rho(t-s,x)$ does not depend on v, so the $L^q_x L^p_v$ norm is in fact a L^q_x norm only, that can be interpolated between L^1_x and L^p_x. Recall that $\|\rho\|_{L^1_x}$ is constant by conservation of the total number of cells. On the other hand, the gradient ∇S is estimated using the following Sobolev estimate,

$$\|\nabla S\|_{L^\infty_x} \lesssim \|\rho\|_{L^1_x}^{1-p'/2} \|\rho\|_{L^p_x}^{p'/2} , \; 2 < p < \infty .$$

We obtain eventually

$$\|\rho(t,x)\|_{L^p_x} \lesssim \int_0^t \frac{1}{s^{2(1/p'-1/q')}} \|\rho(t-s,x)\|_{L^p_x}^{\theta p'/2+p'/q'}\, ds .$$

In order to apply the Gronwall lemma, it remains to show the existence of a couple of exponents (p, q) such that both the conditions $1/p' - 1/q' < 1/2$ (time integrability), and $\theta/2 \le 1/p' - 1/q'$ (sublinear growth) hold. This yields the constraint $\theta < 1$. ◂

2.1.2.2. *A remarkable dichotomy at the kinetic level.* The sublinear condition (2.4) makes a lot of sense in view of the following result [8]. Let $d = 2$, and consider a simple kinetic model for chemotaxis with the following rule: cells can browse post-tumbling directions, and orientate accordingly after the tumble. They choose only favorable directions ($v \cdot \nabla S \ge 0$), with a rate proportional to $\chi|\nabla S|$, for some positive χ[1]. Therefore the tumbling rate reads $\mathbf{T} = \chi(v \cdot \nabla S)_+$,

$$\begin{cases} \partial_t f + v \cdot \nabla_x f = \chi(v \cdot \nabla S)_+ \rho - \omega |\nabla S| f \,, \qquad t > 0 \,, \ x \in \mathbb{R}^2 \\ -\Delta S + \alpha S = \rho \end{cases} \tag{2.6}$$

where ω is a renormalization constant, so that the equation for the cell density is conservative. We assume in addition that the total number of cells is renormalized to unit value,

$$\iint f(t,x,v)\, dxdv = \iint f_0(x,v)\, dxdv = 1 \,. \tag{2.7}$$

The Keller-Segel system can be formally obtained as the diffusion limit of (2.6)[2] (up to some minor modifications, see [8]). Therefore, the following question arises naturally:

> *To which extent the system (2.6) can exhibit a nice dichotomy analogous to the two-dimensional Keller-Segel system? (see Theorem 1.1)*

The following result is somehow the kinetic version of Theorem 1.1.

Theorem 2.3: Global existence vs. blow-up in the spherically symmetric case [8]

Assume $d = 2$, V is a ball or a sphere, and the initial datum f_0 has spherical symmetry. There exist two explicit constants $0 < \chi_*(V) < \chi^*(V)$ such that the following dichotomy holds true,

- if $\chi > \chi^*(V)$ then the solution blows up in finite time.
- if $\chi < \chi_*(V)$ (and f_0 is not too singular) then the solution is global in time.

This result can be viewed as a kinetic analog of Theorem 1.1. However, the kinetic model is of hyperbolic type, and this significantly changes some details of the proof. Moreover, the two-dimensional Keller-Segel system is equipped with a time-decreasing free energy. This monotonicity argument, together with a suitable functional inequality, yields global existence with a sharp constant (Section 1.1.1.3). Here, we believe that the upper threshold χ^* is essentially optimal, since it coincides with the classical threshold for the Keller-Segel equation in the diffusion limit. On the other hand, we believe that the lower threshold χ_* is not optimal.

▸ *Sketch of proof.* The blow-up for large mass was proven by a similar argument as in the parabolic case. The spatial variance of the density was computed carefully. It was shown that it cannot remain nonnegative forever.

[1] This rule was suggested to us by B. Perthame

[2] For rigorous derivation of diffusion limits from kinetic equations towards the Keller-Segel model, we refer to [**OH02**, **CMPS04**, **HKS05**, **FLP05**, **CDSM⁺06**], and references therein. It is not our purpose to develop this theory here, as we aim to focus on the analysis at the mesoscopic scale.

By differentiating twice the second moment, we obtain:

$$
\begin{aligned}
I(t) &= \frac{1}{2}\iint_{\mathbb{R}^2\times V} |x|^2 f(t,x,v)\,dvdx\,,\\
\frac{dI}{dt}(t) &= \frac{1}{2}\iint_{\mathbb{R}^2\times V} (x\cdot v) f(t,x,v)\,dvdx\,,\\
\frac{d^2I}{dt^2}(t) &\le c_1 M - c_2\chi M^2 - \omega\int_{\mathbb{R}^2}(x\cdot j)|\nabla S|\,dx\,,
\end{aligned}
\tag{2.8}
$$

where $j(t,x) = \int v f(t,x,v)\,dv$ is the macroscopic flux. The first two contributions are similar to the parabolic case, except that the variance is derived twice in time (essentially because the problem is of hyperbolic type). However, the last contribution is not immediate to handle with. Fortunately, we can make the following observation under spherically symmetric conditions,

$$
\omega\int_{\mathbb{R}^2}(x\cdot j)|\nabla S|\,dx = \frac{dJ}{dt}\,,\quad \text{where } J \text{ is a nonnegative quantity, } J(t)\ge 0\,.
$$

The heuristics goes as follows:

$$
\left\{\begin{array}{l}\partial_t\rho = -\nabla\cdot j\\ \rho = -\nabla\cdot\nabla S\end{array}\right.\quad\Longrightarrow\quad \text{“ } j\nabla S \approx \frac{1}{2}\partial_t\left(\nabla^{-1}\rho\right)^2\text{ ”}\,.
$$

This can be made rigorous in the case of spherical symmetry. As a consequence, by integrating back in time (2.8), we deduce that the spatial variance I is bounded above by a negative parabola, if χ is large enough. This is an obstruction to global existence.

Concerning the global existence for small parameter χ, we were lacking a Lyapunov functional, as in the parabolic case. Also, the methodology used in the proof of Theorem 2.1 fails in the case $\theta = 1$. Eventually, it was proven via an ad-hoc comparison argument.

The following stationary function acts as a mildly singular supersolution, which is admissible when χ is small, and f is spherically symmetric,

$$
k(x,v) = \left\{\begin{array}{ll}|x|^{-\gamma} & \text{if}\quad (v\cdot x)<0\\ |\Pi_{v^\perp}x|^{-\gamma} & \text{if}\quad (v\cdot x)>0\,,\end{array}\right.
\tag{2.9}
$$

where $\Pi_{v^\perp}$ denotes the orthogonal projection on $v^\perp$, and $\gamma\in(0,1)$ is arbitrary, but the latter determines the constant $\chi_*(V)$[3]. More precisely, the following inequality holds true under the condition $\chi<\chi_*(V,\gamma)$,

$$
(\forall x,v)\quad v\cdot\nabla_x k(x,v) \ge \chi\,(v\cdot\nabla S(t,x))_+\int_{v'}k(x,v')\,dv'\,.
\tag{2.10}
$$

With this estimate at hand, we could prove: $(\forall t>0)\ f(t,x,v)\le k(x,v)$, provided the comparison holds true at $t=0$.

Heuristics for (2.9). The spherically symmetric assumption arises as a condition for getting the following crucial bound,

$$
(\forall t,x)\quad |\nabla S(t,x)| \le \frac{1}{2\pi}|x|^{-1}\,,
$$

that holds true in the radially symmetric case, using (2.7).

Searching for a stationary super-solution $k(x,v)$ of the kinetic equation (2.6), it is useful to drop the negative loss term in the r.h.s. Then, we end up with the sufficient condition

$$
v\cdot\nabla_x k(x,v) \gtrsim \chi|x|^{-1}\int_{v'}k(x,v')\,dv'\,.
\tag{2.11}
$$

By neglecting the dependency on the velocity $k(x,v)\approx K(x)$, we are dealing with

$$
-\nabla_x K(x) \gtrsim \chi M|x|^{-1}K(x)\,.
$$

This motivates the choice $K(x)\approx|x|^{-\gamma}$, with $\gamma=\mathcal{O}(\chi)$. The full velocity profile (2.9) is reconstructed *a posteriori* so as to fulfill (2.11). Finally, integrability with respect to velocity imposes $\gamma<1$, thus the smallness condition on χ. ◂

[3]In fact, this constant should be denoted as $\chi_*(V,\gamma)$.

REMARK 2.4. *Similarly as in Section 1.2, a similar dichotomy is expected to hold for a logarithmic spatial interaction kernel, in one dimension of space. This point was addressed in* [St11].

We conclude this Section by some open questions related to the previous results.

Open Problem(s) 2.5

(1) Relax the assumption on spherically symmetric data.

(2) Prove similar results in dimension $d = 3$ or higher: global existence under smallness assumption in a suitable Sobolev norm, and blow-up for small spatial variance.

(3) Search for a self-similar stationary state in the subcritical two-dimensional case.

2.1.3. Temporal sensing (cluster formation). Here, we consider the case where an individual cell is able to measure time variations of the chemical signal along its trajectory. This implicitly assumes some memory effect, which enables the cell to make temporal comparisons. Then, under the (questionable) assumption that the memory is (much) shorter than the typical run length, it is reasonable to formulate $\mathbf{T}$ as a function of the material derivative of the chemical concentration along the pre-tumble velocity v' [DS05],

$$\mathbf{T}(t,x,v,v') = \psi\left(\left.\frac{DS}{Dt}\right|_{v'}\right) = \psi\left(\partial_t S + v'\cdot\nabla_x S\right), \tag{2.12}$$

where ψ is a bounded, nonnegative, nonincreasing function. It expresses how a single cell responds to temporal variations of the signal along its trajectory, by modulating the rate of tumbling, or equivalently, by modulating the length of runs. If $\frac{DS}{Dt} > 0$ then the direction is favorable so the bacteria reduces the rate of tumbling, and vice-versa.

More sophisticated models consider that an individual cell performs a time convolution, with zero mean, to achieve this comparison. The convolution kernel was measured experimentally [SBB86]. This has raised a lot of interest recently from the point of view of optimal strategies [dG04, CG05, CV10]. Other models involve some internal state variables that describe the intracellular signalling pathway controlling the occurrence of tumbling [EO05, Loc07, Xue13, PTV15]. We will not discuss further these more realistic models in the present memoir.

2.1.3.1. *Formal diffusion limit.* As a preliminary step, it is instructive to consider the diffusion limit of the kinetic model. This helps to gain some insight about the dynamics of (2.1). The diffusion limit is valid when chemotaxis results in a small bias on the modulation of tumbling: we write

$$\psi = \psi_0(1+\varepsilon\phi), \tag{2.13}$$

where ϕ is a nonincreasing function of order one, and $\varepsilon > 0$ is the relative amplitude of the chemotactic biases. Formal computations yield the following drift-diffusion equation for the macroscopic density $\rho(t,x)$ in the limit $\varepsilon \to 0$,

$$\partial_t\rho = D_\rho\Delta\rho - \nabla\cdot(\rho\mathbf{u}), \quad \mathbf{u} = -\int_{v\in V} v\phi\,(v\cdot\nabla S)\,dv, \tag{2.14}$$

where the macroscopic advection speed $\mathbf{u}$ averages out the individual velocities modulated by the renormalized tumbling rate. As compared to (1.1), equation (2.14) is more nonlinear. In fact the Keller-Segel equation would derive from a linear response function ϕ[4].

[4]In fact, choosing a linear function ϕ is inconsistent with the nonnegativity constraint on ψ for large gradients ∇S at some given $\varepsilon > 0$. More generally, the Keller-Segel equation is usually derived from the kinetic equation (2.1) under the assumption of shallow gradients [EO04].

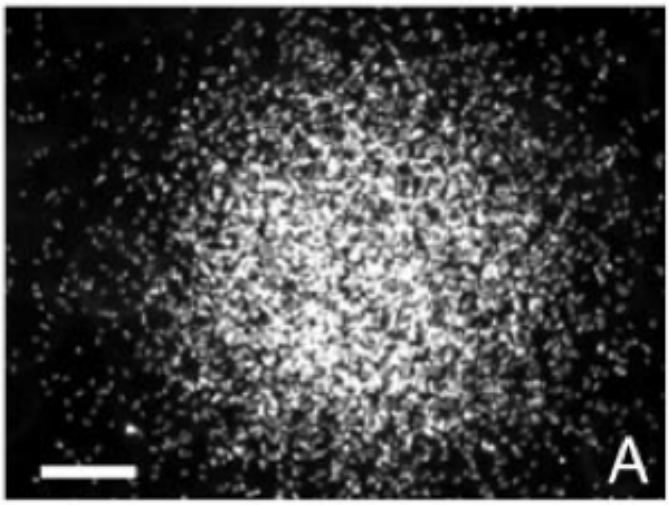

FIGURE 2.2. Stationary cluster of motile bacteria, as observed experimentally in [**MBBO03**].

2.1.3.2. *A specific choice for the response function ϕ.* There are some evidence that bacteria significantly amplifies small time variations of the signal concentration [**Ber04**, **EO05**, **Xue13**]. This can be put into the mathematical formalism by choosing the binary response function $\phi\left(\frac{DS}{Dt}\right) = -\chi \text{sign}\left(\frac{DS}{Dt}\right)$, for some $\chi > 0$. Then, the diffusion limit writes

$$\partial_t \rho = D_\rho \Delta \rho + \chi \nabla \cdot \left(\rho \frac{\nabla S}{|\nabla S|} \right). \tag{2.15}$$

2.1.3.3. *Stationary states of the macroscopic problem.* Radially symmetric stationary distributions of (2.15) exist in any dimension[5]. They are exponentially decaying,

$$\rho_\infty(x) = \frac{M\chi}{|\mathbb{S}^{d-1}| D_\rho} \exp\left(-\frac{\chi}{D_\rho} |x| \right), \tag{2.16}$$

where M denotes the total number of cells. Radially symmetric and exponentially decreasing stationary clusters were observed in colonies of bacteria [**MBBO03**] (see Figure 2.2). In particular, their typical radius essentially does not depend on the number of cells, which is the case for (2.16). This would not be the case for the Keller-Segel system.

2.1.3.4. *Stationary states of the mesoscopic problem.* It is natural to ask the same question at the kinetic level: does the tumbling kernel (2.12) leads to spatial confinement of the biased velocity-jump process? Alternatively speaking,

Do their exist stationary states for the coupled system (2.1)–(2.2)?

We will answer positively to this question. As a by-product, we will prove the existence of kinetic travelling waves of chemotactic bacteria in Section 2.2.4.2. The latter result is in my opinion one of the main outcome of this memoir, yet not published. As opposed to other parts of the memoir, I will provide detailed proofs of the following statement in order to prepare the demonstration of existence of travelling waves (Section 2.2.4.2).

[5] The one-dimensional case has a nice structure. When coupled to the Poisson equation $-\partial_x^2 S = \rho$, it is possible to reduce the problem to a single conservation law on $u = -\partial_x S$, *i.e.* the antiderivative of ρ. Then nonlinear stability boils down to stability of zero-speed shock waves for scalar diffusive conservation law, see [**Ser02**]. Note that the same reduction is at the basis of refined analysis of the two-dimensional, radially symmetric Keller-Segel system.

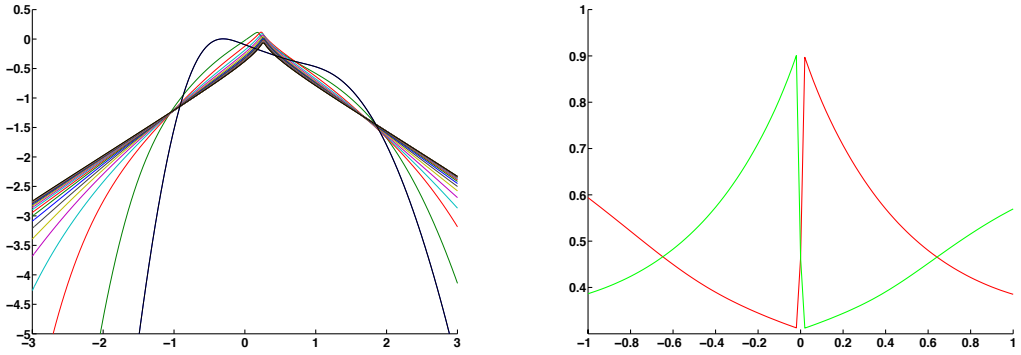

FIGURE 2.3. (Left) Macroscopic density $\rho(x)$ of the stationary state, (Right) Velocity profiles, resp. $F_-(v)$ and $F_+(v)$.

For the rest of this Section, we restrict to dimension $d = 1$.

We first answer the confinement issue when the chemical signal S is frozen. That is, we assume that S is a given, symmetrically monotonic, concentration. Hence, S is unimodal with a unique maximum point located at $x = 0$. Then, the system is decoupled, and (2.1) is a linear equation. The tumbling kernel simply reads

$$\mathbf{T}(t,x,v,v') = 1 + \chi(\operatorname{sign} x)(\operatorname{sign} v'). \tag{2.17}$$

The interpretation goes as follows: favorable directions are pointing towards $x = 0$ (maximum of the signal), *i.e.* $xv < 0$. When a cell moves in a favorable direction, it tumbles with rate $1-\chi$, whereas it tumbles with rate $1+\chi$ when it moves in a unfavorable direction. With such a tumbling kernel, the bacteria population is indeed confined in space, meaning that there exists a unique exponentially decreasing equilibrium.

Theorem 2.6: Exponential confinement by biased velocity-jump processes [21]

Assume $d = 1$, $\chi \in (0,1)$, and V is a bounded symmetric velocity set such that $|V| = 1$. There exists a symmetric density $f \in L^1 \cap L^\infty(\mathbb{R}\times V)$ solution of the following (linear) stationary problem,

$$v\partial_x f(x,v) = \int_{v'\in V} (1+\chi \operatorname{sign}(v'x)) f(x,v')\,dv' - (1+\chi\operatorname{sign}(vx)) f(x,v).$$

Moreover, there exists an exponent $\lambda > 0$, and two velocity profiles $F_\pm(v)$ with $F_+(-v) = F_-(v)$, such that the renormalized density $e^{\lambda|x|} f(x,v)$ converges exponentially fast to $F_\pm(v)$ as $x \to \pm\infty$ in $L^2(v^2 dv)$.

▸ *Sketch of proof.* We recall below the main lines of the proof, since they will be of great importance in the proofs of Theorems 2.6 and 2.15 below. We refer to [21] for the details.

We introduce the following notations for the sets of positive and negative velocities: $V^+ = V \cap \mathbb{R}_+$ and $V^- = V \cap \mathbb{R}_-$.

Step #1. Identification of the asymptotic profile. The stationary distribution is solution to the linear problem

$$v\partial_x f(x,v) + T(x,v) f(x,v) - \int_V T(x,v') f(x,v')\,dv' = 0, \quad T(x,v) = 1+\chi\operatorname{sign}(xv). \tag{2.18}$$

Exponential confinement of the stationary distribution is expected as $|x| \to \infty$, as for the diffusion limit (2.16). Hence, we make the following ansatz for $x > 0$,

$$f(x,v) \sim e^{-\lambda x} F_+(v) \quad \text{as} \quad x \to +\infty\,.$$

The key point is to identify λ and F_+. We plug the ansatz into (2.18),

$$-\lambda v F_+(v) + T_+(v) F_+(v) = \int_V T_+(v') F_+(v')\, dv'\,,$$

It yields,

$$F_+(v) = \frac{1}{T_+(v) - \lambda v}\,, \quad \text{and} \quad \int_V \frac{T_+(v)}{T_+(v) - \lambda v}\, dv = 1\,,$$

where we have opted for the normalization

$$\int_V T_+(v) F_+(v)\, dv = 1\,.$$

By convexity of $\lambda \mapsto (T_+(v) - \lambda v)^{-1}$, and the following condition on the derivative at $\lambda = 0$,

$$\frac{d}{d\lambda}\left(\int_V \frac{T_+(v)}{T_+(v) - \lambda v}\, dv\right)\bigg|_{\lambda=0} = \int_V \frac{v}{T_+(v)}\, dv < 0 \quad \textit{(mean algebraic run length is negative)}\,,$$

there exists a unique $\lambda > 0$ which satisfies $\int_V \frac{T_+(v)}{T_+(v)-\lambda v}\, dv = 1$ under the constraint that F_+ remains positive. Of course, $\lambda = 0$ is also a solution, but it does not correspond to a global integrable stationary distribution, since it does not decay spatially.

Step #2. Connection with the Milne problem. One key observation is that the function $u(x,v) = e^{\lambda x}(F_+(v))^{-1} f(x,v)$ verifies a kinetic equation on the half space $\mathbb{R}_+ \times V$, which satisfies the maximum principle,

$$v\partial_x u(x,v) = \int_V \frac{T_+(v')F_+(v')}{F_+(v)}(u(x,v') - u(x,v))\, dv'\,, \quad x > 0\,,\ v \in V\,. \tag{2.19}$$

However, we have no idea yet about the incoming data, *i.e.* the inward velocity profile $(u(0,v))_{v>0}$. For the "boundary value" at $x = +\infty$, we just impose boundedness of u. This prescribes uniquely u as a solution of the so-called Milne problem in radiative transfer theory [**BSS84**]: being given the inward velocity profile $\varphi^+(v) = F_+(v)u(0,v)$ for $v > 0$, there exists a unique $u \in L^\infty(\mathbb{R}_+ \times V)$, such that

$$\begin{cases} v\partial_x u(x,v) = \displaystyle\int_V \frac{T_+(v')F_+(v')}{F_+(v)}(u(x,v') - u(x,v))\, dv'\,, \quad x > 0\,,\ v \in V \\ u(0,v) = (F_+(v))^{-1}\varphi^+(v)\,, \quad v > 0\,. \end{cases} \tag{2.20}$$

Moreover, by the maximum principle, we have

$$\|u\|_{L^\infty(\mathbb{R}_+\times V)} \le \|u(0,\cdot)\|_{L^\infty(V^+)}\,.$$

Step #3. A fixed point argument. We define the linear map $\mathbf{B} : \mathcal{C}^0(V^+) \to \mathcal{C}^0(V^+)$ as follows,

$$(\forall v \in V^+) \quad \left(\mathbf{B}\varphi^+\right)(v) = F_+(-v)u(0,-v)\,,$$

so as being a fixed point is equivalent to verifying $f(0,v) = f(0,-v)$, which is the desired boundary condition at $x = 0$ coming from the symmetry of the problem. Compactness is required in order to apply the Krein-Rutman theorem. It can be deduced from classical averaging lemma, since the outward velocity profile is given by

$$u(0,v) = \int_0^{+\infty} e^{-t} A(-tF_+(v)v)\, dt\,, \quad v < 0\,, \tag{2.21}$$

where the macroscopic quantity A is defined as,

$$A(x) = \int_V T_+(v')F_+(v')u(x,v')\, dv'\,.$$

One-dimensional averaging lemma guarantees that $A(x)$ has Hölder regularity [**GLPS88**, Lemma 7]. As a consequence, $(u(0,v))_{v\in V^-}$ has Hölder regularity also. Alternatively speaking, negative velocities at $x = 0$ necessarily emerge after some tumbling event, for which regularization occurs via velocity averaging. On the other hand, positivity is an immediate consequence of (2.21).

Applying the Krein-Rutman theorem, there exists a profile φ^+, associated with a dominant eigenvalue Λ such that $\mathbf{B}\varphi^+ = \Lambda\varphi^+$. We deduce that $\Lambda = 1$ from the conservation law

$$\partial_x \left(\int v f(x,v)\, dv \right) = 0 \quad \Rightarrow \quad \int v f(x,v)\, dv = 0 .$$

The velocity profile φ^+ is such that the symmetric boundary condition $f(0,v) = f(0,-v)$ is satisfied.

Step #4. Refined asymptotic behaviour as $|x| \to \infty$. The exponent $\lambda > 0$ comes from an additional conservation law: by multiplying (2.19) against $vF_+(v)^2$, we obtain

$$\begin{aligned} &\partial_x \left(\int_V v^2 F_+(v)^2 u(x,v)\, dv \right) \\ &= \left(\int_V T_+(v') F_+(v') u(x,v')\, dv' \right) \left(\int_V v F_+(v)\, dv \right) - \left(\int_V T_+(v') F_+(v')\, dv' \right) \left(\int_V v F_+(v) u(x,v)\, dv \right) = 0 , \end{aligned}$$

since $\int_V v F_+(v)\, dv = 0$, and $\int_V v F_+(v) u(x,v)\, dv = e^{\lambda x} \int v f(x,v)\, dv = 0$. We define accordingly $\mu > 0$ such that

$$(\forall x > 0) \qquad \int_V v^2 F_+(v)^2 (u(x,v) - \mu)\, dv = 0 . \tag{2.22}$$

Then, it is possible to prove exponential decay towards the asymptotic profile as $x \to +\infty$ using second order entropy method with respect to the space variable. In fact, the two auxiliary quantities

$$E_0(x) = \int_V v^2 F_+(v)^2 \left(u(x,v) - \mu \right)^2 dv , \quad \text{and} \quad E_1(x) = \int_V v T_+(v) F_+(v)^2 \left(u(x,v) - \mu \right)^2 dv ,$$

satisfies the following system of (in)equalities,

$$\begin{cases} \dfrac{dE_0}{dx}(x) = 2\lambda E_0(x) - 2E_1(x) \\ \dfrac{dE_1}{dx}(x) \le -2\kappa E_0(x) , \end{cases} , \quad \text{where} \quad \kappa = \left(\inf_{v \in V} \frac{T_+(v)}{v^2 F_+(v)} \right)^2 \left(\int_V v^2 (F_+(v))^2\, dv \right) .$$

It yields the second-order damped differential inequality,

$$-\frac{1}{2} \frac{d^2 E_0}{dx^2}(x) + \lambda \frac{dE_0}{dx}(x) + 2\kappa E_0(x) \le 0 .$$

Using the "boundary condition" $E_0 \in L^\infty$, we can deduce that there exists a constant C depending on $E_0(0)$, $\frac{dE_0}{dx}(0)$, λ and β, such that,

$$E_0(x) \le C e^{-\beta x} , \quad \text{where } \beta \text{ is the positive root of } \frac{1}{2}\beta^2 + \lambda\beta - 2\kappa = 0 .$$

As a conclusion, we have obtained the following weighted L^2 estimate,

$$(\forall x > 0) \quad \left\| \frac{f(x,v)}{e^{-\lambda x} F_+(v)} - \mu \right\|_{L^2(v^2 F_+(v)^2 dv)} \le C e^{-\beta x} . \tag{2.23}$$

Appendix. About the regularity of $I(x)$ and $f(x,v)$. Finally, we investigate the regularity of the macroscopic quantity

$$I(x) = \int_V T(x,v') f(x,v')\, dv' .$$

LEMMA 2.7. *Suppose that f is normalized, say $\|f\|_{L^1(\mathbb{R}\times V)} = 1$. For any $\alpha \in (0,1)$, there exists a constant C_α depending on α, V and χ, such that*

$$\|I\|_{\mathcal{C}^{0,\alpha}} \le C_\alpha . \tag{2.24}$$

As a by-product, there exists a constant depending on V and χ such that,

$$\sup_{v \in V} f(x,v) \le C e^{-\lambda x} . \tag{2.25}$$

▹ *Proof of the lemma.* Recall that $u(x,v) = e^{\lambda x} (F_+(v))^{-1} f(x,v)$ is bounded,

$$\|u\|_{L^\infty(\mathbb{R}_+ \times V)} \le \|u^+(0,\cdot)\|_{L^\infty(V^+)} \le C \|f^+(0,\cdot)\|_{L^\infty(V^+)} . \tag{2.26}$$

Consequently, $v\partial_x u = \int F_+^{-1} T_+' F_+' (u' - u)\, dv' \in L^\infty$. We deduce from the one-dimensional averaging lemma [**GLPS88**] that $A(x) = \int T_+' F_+' u'\, dv' \in \mathcal{C}^{0,\alpha}$, for any $\alpha \in (0,1)$,

$$[A]_{\mathcal{C}^{0,\alpha}} \le C_\alpha \|v\partial_x u\|_{L^\infty}^{\alpha} \|u\|_{L^\infty}^{1-\alpha} \le C_\alpha \|u\|_{L^\infty} \le C_\alpha \|f^+(0,\cdot)\|_{L^\infty(V^+)} .$$

On the other hand, recall that

$$f^+(0,v) = \int_0^{+\infty} I(sv)\exp(-T^- s)\,ds\,,$$

in order to get $\|f^+(0,\cdot)\|_{L^\infty(V^+)} \le C\|I\|_{L^\infty}$. Consequently, $I(x) = e^{-\lambda x}A(x)$ is bounded and has global Hölder regularity on $\mathbb{R}_+$, with a constant depending on $\|I\|_{L^\infty}$. This enables to conclude, using interpolation, and the normalization $\|f\|_{L^1(\mathbb{R}\times V)} = 1$. Indeed, we have for any $\eta > 0$

$$I(x) \le I(y) + C_\alpha \|I\|_{L^\infty}|x-y|^\alpha\,,$$
$$\eta I(x) \le \|I\|_{L^1(\mathbb{R}_+)} + C_\alpha\|I\|_{L^\infty}\eta^{1+\alpha}\,.$$

Taking the supremum with respect to x, and choosing η such that $C_\alpha\eta^\alpha = 1/2$, we obtain

$$\|I\|_{L^\infty} \le \frac{2}{\eta}\|I\|_{L^1} \le C_\alpha\|f\|_{L^1(\mathbb{R}_+\times V)}\,.$$

As a by-product, the L^∞ bound (2.26) translates into (2.25). This concludes the proof of the lemma. ◁ ◀

The previous theorem resolves the linear problem only. In order to prove the existence of a stationary cluster for the coupled system (2.1)-(2.2), it is necessary to prove that the chemical signal S is symmetrically decreasing. This would be consistent with the starting hypothesis that $\partial_x S$ changes sign only at the origin $x = 0$. This would be immediate provided that ρ itself is symmetrically decreasing. However, this last statement requires more work to be proven with full generality. This is the purpose of the next statement.

Theorem 2.8: Monotonicity of the macroscopic density (Calvez, not yet published)

Assume $d = 1$, $\chi \in (0,1)$, and V is a symmetric combination of at most two intervals: $V = (-1/2, 1/2)$, or $V = (-v_0 - 1/2, -v_0) \cup (v_0, v_0 + 1/2)$ for some $v_0 > 0$. Let f be the stationary solution of the linear kinetic equation described in Theorem 2.6. Then, the macroscopic density $\rho(x) = \int_V f(x,v)\,dv$ is decreasing for $x > 0$ (and increasing for $x < 0$ by symmetry).

▸ *Sketch of proof.* Before giving the main lines of the proof, it is interesting to notice that the monotonicity of ρ is not clear at first sight. In fact, numerical simulations show that for a fixed velocity v, $f(x,v)$ can achieve its maximum value at positive x_*. Some overshoot phenomena may occur for the highest velocities, see Figure 2.4[6]. Therefore, the monotonicity of $\rho(x) = \int f(x,v)\,dv$ for $x > 0$ can only result from compensations between lower and higher velocities. The key of the proof of Theorem 2.8 relies on the refined description of velocity profiles in order to capture these compensations.

By symmetry, we restrict to $x > 0$. The superscript $^+$ (resp. $^-$) corresponds to positive velocities (resp. negative velocities). We also introduce the notations $\rho^+(x) = \int_{v>0} f^+(x,v)\,dv$, resp. $\rho^-(x) = \int_{v<0} f^-(x,v)\,dv$, for the number of particles moving to the right, resp. to the left. The number of reorientations per unit of time is denoted by

$$I(x) = \int T(v)f(x,v)\,dv = \int_{v>0} T^+ f^+(x,v)\,dv + \int_{v<0} T^- f^-(x,v)\,dv = T^+\rho^+(x) + T^-\rho^-(x)\,.$$

According to these notations, the stationary problem for the density f for $x > 0$ reads as follows,

$$\begin{cases} v\partial_x f^+(x,v) = I(x) - T^+ f^+(x,v)\,, & v > 0 \\ v\partial_x f^-(x,v) = I(x) - T^- f^-(x,v)\,, & v < 0 \end{cases} \tag{2.27}$$

where $T^+ = 1+\chi$, and $T^- = 1-\chi$. A first observation is that $I(x)$ is one of the natural macroscopic quantities associated with the system (2.27) (as well as the equilibrium flux $J(x) = \int vf\,dv$ which is identically zero). Thus, we aim to prove first that $I(x)$ is decreasing for $x > 0$. We will deduce as a corollary that $\rho(x)$ behaves in the same way.

[6] Laurent Gosse observed the same phenomenon based using more accurate schemes (private communication and [**Gos13**])

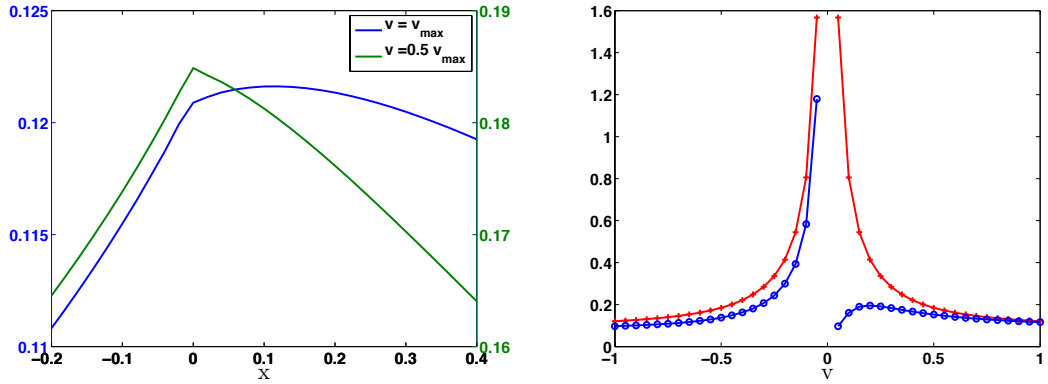

FIGURE 2.4. (Left) Spatial density profile $f(x,v)$ for two different values of v. The density does not reach its maximum value at $x=0$ when $v=\max V$. There is clearly an overshoot effect. (Right) Velocity density profile $f(x,v)$ around the transition at $x=0$: the red plot is for $x=0$, whereas the blue plot is for small $x>0$. The density is increasing for $v<0$, but it exhibits a non monotonic behaviour for $v>0$.

REMARK 2.9. *By differentiating system (2.27) with respect to x, we immediately see that it satisfies a maximum principle, ensuring negativeness of $\partial_x f^{\pm}$ provided it is nonpositive on the boundaries $x=0$ (for $v>0$) and $x=+\infty$ (for $v<0$). The latter is clearly satisfied, knowing very precisely the asymptotic profile as $x\to+\infty$ (Theorem 2.6). However, the condition at $x=0$ appears to be not satisfied for some values of the parameters (χ,V).*

Step #1. If V is "far enough from zero", then I is decreasing. Here, we assume that the velocity set is $V=(-v_0-1/2,-v_0)\cup(v_0,v_0+1/2)$ with $v_0\gg 1$. The key observation is that the equilibrium of the model with only two velocities $V=\{-v_0,+v_0\}$ can be computed explicitly. There, $I(x)$ is decreasing for $x>0$. The computations are facilitated by the fact that $\rho^+=\rho^-$ at equilibrium, since the flux $J=v_0(\rho^+-\rho^-)$ vanishes.

If V is not too far from such a discrete set, then the same result should hold, using again the fact that the flux $j(x)=\int vf(x,v)\,dv$ is identically zero at equilibrium. This is indeed the case,

$$\begin{aligned}\frac{dI}{dx}&=\int T\partial_x f\,dv=\left(\int\frac{T}{v}\,dv\right)I-\int\frac{T^2}{v}f=\left\langle\frac{T}{v}\right\rangle I-\int\frac{T^2}{v}f+\frac{\gamma}{v_0^2}J\\&=\int\left(\left\langle\frac{T}{v}\right\rangle T-\frac{T^2}{v}+\frac{\gamma}{v_0^2}v\right)f\,dv\,,\end{aligned}$$

where $\gamma\in\mathbb{R}$ is arbitrary. As $v_0\to+\infty$, we find $\int v^{-1}T\,dv=\left\langle v^{-1}T\right\rangle\sim v_0^{-1}\chi$. Thus, we get the following equivalence, uniformly with respect to $v\in V$,

$$\left\langle\frac{T}{v}\right\rangle T-\frac{T^2}{v}+\frac{\gamma}{v_0^2}v\sim\frac{\chi T^{\pm}}{v_0}-\frac{(T^{\pm})^2}{\pm v_0}+\frac{\gamma}{\pm v_0}\,,\quad\text{as } v_0\to+\infty\,,\tag{2.28}$$

where the sign $\pm$ is determined by the sign of v. For the r.h.s. of (2.28) to be always negative, we seek γ such that

$$\begin{cases}\chi(1+\chi)-(1+\chi)^2+\gamma<0\\ \chi(1-\chi)+(1-\chi)^2-\gamma<0\end{cases}$$

Such a positive γ exists if and only if

$$\chi(1-\chi)+(1-\chi)^2<-\chi(1+\chi)+(1+\chi)^2\,,$$
$$1-\chi<1+\chi\,,$$

which holds true since $\chi>0$. As a result, we get that I is globally decreasing if $V^+=(v_0,v_0+\frac{1}{2})$ for $v_0\gg 1$.

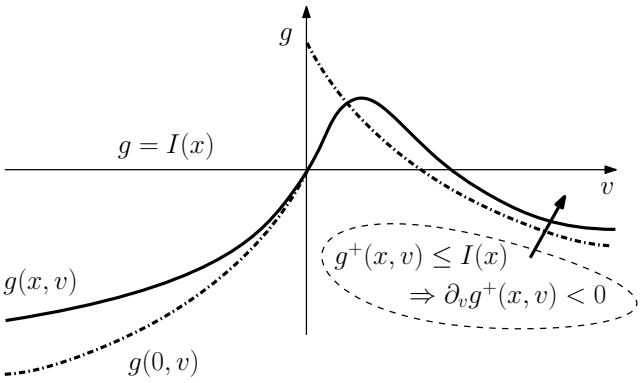

FIGURE 2.5. Typical velocity profile of $g = Tf$ for $x > 0$, close to the transition at $x = 0$ (plain line). Recall that, as $x \to +\infty$, g is globally increasing with respect to v. For the sake of comparison, $g(0, v)$ is depicted in dashed line. It is discontinuous at $v = 0$ since f is continuous, and T is not.

Step #2. If I is nonincreasing, then both ρ^+ and ρ^- are (strictly) decreasing. We prove this statement by deciphering the shape of the velocity profile $f(x, \cdot)$. Accordingly, we assume throughout this step that I is nonincreasing.

REMARK 2.10. *Several issues arise due to small velocities. We restrict to the case $v_0 > 0$ throughout this step in order to circumvent these analytical issues. We present how to derive uniform estimates with respect to $v_0 = 0$ at the end of the proof. Such estimates are useful for the proof of travelling waves (Section 2.2.4.2).*

The easiest part of the statement concerns negative velocities: by integration along the characteristics, we get that

$$(\forall v < 0) \quad f^-(x, v) = \int_0^{+\infty} I(x - sv) \exp(-T^- s)\, ds\,, \tag{2.29}$$

which is clearly increasing with respect to v, provided that I is nonincreasing, and non constant on $(x, +\infty)$ for all $x > 0$, which it is by assumption.

Let introduce the notation $g = Tf$. From (2.29) we also get the following statement:

$$(\forall v < 0) \quad g^-(x, v) = \int_0^{+\infty} I(x - sv) T^- \exp(-T^- s)\, ds < I(x)\,. \tag{2.30}$$

We deduce immediately that the density $\rho^-(x)$ is decreasing, since the combination of (2.27) and (2.30) implies that

$$(\forall v < 0) \quad \partial_x f^-(x, v) < 0 \implies \frac{d\rho^-}{dx} < 0\,.$$

The case of positive velocities requires more work. Indeed, the velocity profile $f(x, \cdot)$ does not behave as nicely for $v > 0$ as for $v < 0$ (Figure 2.4 and 2.5). However, we are able to establish the following property, which is sufficient for our purpose.

LEMMA 2.11. *Recall the definition $g = Tf$. The density g^+ is decreasing with respect to $v \in V^+$ on the set $\{g^+ \le I\}$. As a consequence, for all $x > 0$ there is at most one $v_*(x) \in V^+$ such that $g^+(x, v_*(x)) = I(x)$.*

▹ *Proof of the lemma.* The density g^+ satisfies

$$v \partial_x g^+ = T^+ \left(I - g^+ \right)\,. \tag{2.31}$$

By differentiating with respect to v, we obtain

$$v \partial_x (\partial_v g^+) + \partial_x g^+ = -T^+ \partial_v g^+\,.$$

Let introduce $h = g^+ - I$. The last identity rewrites as follows,

$$v \partial_x (\partial_v h) - \frac{T^+}{v} h + T^+ \partial_v h^+ = 0\,.$$

We deduce that

$$\partial_v h(x,v) = \partial_v h(0,v)\exp\left(-v^{-1}T^+x\right) + \int_0^x \frac{T^+}{v^2}h(y,v)\exp\left(-v^{-1}T^+(x-y)\right)\,dy\,.$$

We know from the reflection condition at $x=0$, $f(0,v)=f(0,-v)$, that $\partial_v h(0,v)<0$, since f^- is increasing with respect to v. Therefore, it remains to prove that, if $h(x,v)\le 0$, *i.e.* $(x,v)\in\{g^+\le I\}$, then $h(y,v)\le 0$ for all $0<y<x$. For this, we note that h satisfies the following transport equation,

$$v\partial_x h = v\partial_x g^+ - v\frac{dI}{dx} = -T^+h - v\frac{dI}{dx}\,.$$

Thus,

$$h(x,v) = h(y,v)\exp\left(-v^{-1}T^+(x-y)\right) - \int_y^x \frac{dI}{dx}(z)\exp\left(-v^{-1}T^+(x-z)\right)\,dz\,.$$

Then, it is immediate to see that $h(x,v)\le 0$ implies that $h(y,v)\le 0$ for $y<x$, knowing that I is nonincreasing. ◁

To conclude Step #2, we are going to show that ρ^+ is also decreasing, using compensations between lower and higher velocities. The derivative writes

$$\frac{d\rho^+}{dx}(x) = \int_{v>0}\frac{1}{v}\left(I(x)-g^+(x,v)\right)\,dv\,. \tag{2.32}$$

The key observation here is that, were we ignoring the factor $1/v$ inside the integral, the r.h.s. in (2.32) would be

$$\int_{v>0}\left(I(x)-g^+(x,v)\right)\,dv = \int_{v<0}\left(g^-(x,v)-I(x)\right)\,dv<0\,, \tag{2.33}$$

by the very definition of $I=\int g\,dv$. Indeed, it is negative since $g^-(x,v)<I(x)$ for all $v<0$ (2.30). It is sufficient to show that the right hand side of (2.32) can be handled in the same way, because lower velocities contribute more to the integral (and the bad sign contribution comes from higher velocities by Lemma 2.11). Let us denote $v_1=v_0+\frac12$. By integration by parts, we have

$$\frac{d\rho^+}{dx}(x) = \frac{1}{v_1}\int_{v_0}^{v_1}\left(I(x)-g^+(x,v)\right)\,dv + \int_{v_0}^{v_1}\frac{1}{v^2}\left(\int_{v_0}^{v}\left(I(x)-g^+(x,v')\right)\,dv'\right)\,dv\,. \tag{2.34}$$

For $x>0$, the auxiliary function $H(v)=\int_{v_0}^v\left(I(x)-g^+(x,v')\right)\,dv'$ satisfies the following properties: $H(v_0)=0$, $H(v_1)<0$ (2.33), and

- either $(\forall v>v_0)\ \frac{dH}{dv}(v)\le 0$, then $(\forall v>v_0)\ H(v)\le 0$,
- or there exists $v_*=\inf\left\{v\in(v_0,v_1)\ \frac{dH}{dv}(v)>0\right\}$, then $\frac{dH}{dv}\le 0$ on (v_0,v_*) and $\frac{dH}{dv}\ge 0$ on (v_*,v_1) by Lemma 2.11 since $\frac{dH}{dv}=I-g^+$, and therefore $\frac{d^2H}{dv^2}\ge 0$ on the set $\left\{\frac{dH}{dv}\ge 0\right\}$. We obtain also that $(\forall v>v_0)\ H(v)\le 0$ in this case, since $H(v_1)<0$.

As a consequence,

$$\frac{d\rho^+}{dx}(x) = \frac{1}{v_1}H(v_1) + \int_{v_0}^{v_1}\frac{1}{v^2}H(v)\,dv<0\,.$$

Step #3. Propagation of the monotonicity property from "large V" to any V by connectedness. Step #1 establishes the monotonicity property for sufficiently large v_0. Step #2 enables to transform a nonincreasing property into a (strict) decreasing property. On the other hand, we know two additional properties from Theorem 2.6 [**21**]:

(i) The stationary distribution is unique in the space $L^2(e^{\lambda|x|}dxdv)$ (up to a multiplicative constant). This is a consequence of the linear and irreducible structure of the kinetic equation: let (f_1,f_2) be two stationary distributions belonging to $L^2(e^{\lambda|x|}dvdx)$, and denote $h=f_2-f_1$. By integration against h/f, we obtain

$$0 = \frac12\iiint f(x,v')T(v')\left(\frac{h(x,v')}{f_1(x,v')}-\frac{h(x,v)}{f_1(x,v)}\right)^2\,dv'dvdx\,.$$

Hence, there exists a function of the variable x only $c(x)$ such that $f_2(x,v) = c(x)f_1(x,v)$. Plugging this into the stationary equation, we find $c'(x) = 0$[7].

(ii) We control explicitly the behaviour of f as $x \to +\infty$, namely (2.23) can be recast as

$$f(x,v) = \mu F_+(v)e^{-\lambda x} + \mathcal{O}(e^{-\lambda x - \beta x}), \tag{2.35}$$

where the $\mathcal{O}$ notation stands for boundedness in the $L^2(v^2dv)$ norm, which is equivalent to the L^2 norm for positive $v_0 > 0$. Recall that the constant μ (2.22) is defined as

$$\mu = \frac{\int_V f(0,v)v^2F_+(v)\,dv}{\int_V v^2F_+(v)^2\,dv} = e^{\lambda x}\frac{\int_V f(x,v)v^2F_+(v)\,dv}{\int_V v^2F_+(v)^2\,dv}.$$

We can bound μ from below using the normalization $\|f\|_{L^1(\mathbb{R}\times V)} = 1$

$$\int_{x=0}^{+\infty} \mu e^{-\lambda x}\,dx \geq \frac{\inf\left(v^2F_+(v)\right)}{\int_V v^2F_+(v)^2\,dvdx}\|f\|_{L^1(\mathbb{R}_+\times V)}, \tag{2.36}$$

$$\frac{\mu}{\lambda} \geq \frac{\inf\left(v^2F_+(v)\right)}{2\int_V v^2F_+(v)^2\,dvdx},$$

by using $\|f\|_{L^1(\mathbb{R}_+\times V)} = 1/2$, which is a consequence of the symmetry of f. From (2.35), we deduce that $I(x) = \mu e^{-\lambda x} + \mathcal{O}(e^{-\lambda x-\beta x})$ (recall that $\int_V T_+F_+\,dv = 1$ by convention). We deduce that

$$\begin{aligned}\frac{dI}{dx}(x) &= \int_V \frac{T(v)}{v}\left(I(x) - T(v)f(x,v)\right)\,dv \\ &= \mu\left(\int_V \frac{T(v)}{v}\left(1 - T(v)F_+(v)\right)\,dv\right)e^{-\lambda x} + \mathcal{O}(e^{-\lambda x-\beta x}) \\ &= \left(-\mu\lambda + \mathcal{O}(e^{-\beta x})\right)e^{-\lambda x}.\end{aligned} \tag{2.37}$$

As a conclusion, there exists $L > 0$ such that I is strictly decreasing for $x > L$. Moreover, by examining the dependency upon the parameters, we find that L is bounded locally uniformly as $v_0 \in \mathbb{R}_+^*$.

We can propagate the monotonicity property using the following lemma

LEMMA 2.12. *Let Ω be the set of $v_0 > 0$ such that $V = (-v_0 - \frac{1}{2}, -v_0) \cup (v_0, v_0 + \frac{1}{2})$ satisfies the monotonicity property. Then $\Omega = \mathbb{R}_+^*$.*

▹ *Proof of the lemma.* Essentially, Step #2 guarantees that Ω is open. On the other hand, continuity arguments show that Ω is closed. It is non empty by Step #1, therefore Ω coincides with $\mathbb{R}_+^*$.

The details are as follows.

(i) **Ω is closed.** This is a simple consequence of the continuity of I with respect to the parameters of the equation (here the velocity set V). Continuity itself results from the uniqueness of the stationary distribution. Let $V_n \to V$, in the sense that $v_{0,n} \to v_0$. The sequence (f_n) is equicontinuous (because it is Lipschitz continuous as can be directly seen on the equation (2.27)), and uniformly exponentially small as $x \gg 1$. Therefore we can extract a subsequence $(f_{n'})$ converging uniformly towards some f'. Passing to the limit into the equation, we realize that f' is indeed the unique stationary distribution with normalized unit mass, $f' = f$. Since it is unique, the whole sequence f_n converges towards f.

(ii) **Ω is open.** Some stability result in Lipschitz regularity is needed to ensure that $\frac{dI}{dx}$ can be made uniformly negative, on compact sets of $\mathbb{R}_+$ (recall that we control the asymptotic behaviour as $x \to +\infty$). In the case $v_0 > 0$, we immediately get that I is uniformly Lipschitz, since $\partial_x g$ is bounded pointwise. By iteration, $\frac{dI}{dx}$ is also uniformly Lipschitz continuous. Now, assume that for some $v_0 > 0$, we have

[7] A much more refined analysis based on hypocoercive estimates after [**DMS15**] is developped in [**21**] for the Cauchy problem. There, the goal is to capture exponential decay to the equilibrium. Of course, this ensures uniqueness as a weak corollary. Interestingly enough, this is a peculiar application of Dolbeault-Mouhot-Schmeiser's methodology where the stationary state does not lie in the intersection of the kernels of the transport and the scattering operators, on the contrary to the examples in [**DMS15**]. Dolbeault-Mouhot-Schmeiser's methodology relies on the combination of microscopic coercivity (seen on the scattering operator), and macroscopic coercivity (seen on the parabolic macroscopic limit) in order to design a suitable modified entropy which satisfies a global coercivity estimate.

$\frac{dI}{dx} < 0$. There exists $\varepsilon > 0$ and a neighbourhood $\mathcal{V}_0$ of v_0 such that for all $v_0' \in \mathcal{V}_0$, $\frac{dI'}{dx} < -\varepsilon$ on $[0, L]$, where L is defined after (2.37). Otherwise, there would exist a sequence v_n converging towards v_0 such that $\lim\left(\min \frac{dI_n}{dx}\big|_{[0,L]}\right) = 0$. By equi-continuity, we could pass to the limit, and we would obtain eventually $\min \frac{dI}{dx}\big|_{[0,L]} = 0$, which is a contradiction.

◁

Appendix: Uniform estimates with respect to v_0. The previous methodology can be adapted to include the case $V \ni 0$. Alternatively speaking, we can derive estimates that are uniform with respect to v_0 in the limit $v_0 \to 0$. Small velocities must be treated with caution, due to several occurrence of division by v in the computations. Two preliminary observations are required:

(i) For $x = 0$, we deduce from the symmetry $f(0, v) = f(0, -v)$, that f is continuous at $v = 0$. However it is immediately discontinuous at $v = 0$ for $x > 0$ (compare the red and the blue velocity profiles in Figure 2.4, see also Figure 2.5).

(ii) On the other hand, $g = Tf$ is continuous at $v = 0$, except at $x = 0$, where it is discontinuous (simply because f is). Indeed, by integration along the characteristic lines, we get

$$\begin{cases} g^+(x,v) = T^+ f(0,v) \exp\left(-v^{-1}T^+ x\right) + \int_0^{x/v} I(x - sv) T^+ \exp\left(-T^+ s\right)\, dy \\ g^-(x,v) = \int_0^{+\infty} I(x - sv) T^- \exp(-T^- s)\, ds \end{cases}$$

We deduce that for $x > 0$,

$$\lim_{v \to 0^+} g^+(x,v) = I(x) = \lim_{v \to 0^-} g^-(x,v)\,. \tag{2.38}$$

Let us examine how the previous methodology is affected by the small velocities. Firstly, we need to check that the computation (2.34) is not singular,

$$\begin{aligned} \frac{d\rho^+}{dx}(x) &= \left[\frac{1}{v}\int_0^v \left(I(x) - g^+(x,v)\right) dv\right]_0^{v_1} + \int_0^{v_1} \frac{1}{v^2}\left(\int_0^v \left(I(x) - g^+(x,v')\right) dv'\right) dv \\ &= \frac{1}{v_1}\int_0^{v_1} \left(I(x) - g^+(x,v)\right) dv - \left(I(x) - g^+(x,0^+)\right) + \int_0^{v_1} \frac{1}{v^2}\left(\int_0^v \left(I(x) - g^+(x,v')\right) dv'\right) dv\,, \end{aligned}$$

and the same conclusion as (2.34) follows from (2.38).
Secondly, the exponential decay of the renormalized density $e^{\lambda x}\left(F_+(v)\right)^{-1} f(x,v)$ towards a constant as $x \to +\infty$ is not affected by small velocities. However, the convergence is measured in the $L^2(v^2 dv)$ norm, which is not equivalent to the L^2 norm obviously. To circumvent this issue, it is fruitful to make the following observation: the velocity $v_*(x)$ above which $I > g^+$ (and troubles arise), is increasing with respect to x. Therefore, it is sufficient to estimate $v_*(0)$ in order to resume the computation (2.37) uniformly with respect to x. The former is a consequence of the following computation, provided that v_* varies regularly with x (which is a consequence of uniqueness),

$$\begin{aligned} I(x) &= g^+(x, v_*(x))\,, \\ \frac{dI}{dx}(x) &= \partial_x g^+(x, v_*(x)) + \frac{dv_*}{dx}(x)\partial_v g^+(x, v_*(x))\,, \end{aligned}$$

but $\partial_x g^+(x, v_*(x)) = 0$ by definition of v_* and (2.31). Therefore,

$$\frac{dv_*}{dx}(x) = \left(\partial_v g^+(x, v_*(x))\right)^{-1} \frac{dI}{dx}(x) > 0\,,$$

by Lemma 2.11. The estimate on $v_*(0)$ goes as follows, by using the Hölder regularity of I (see Lemma 2.7),

$$\begin{aligned} I(0) = g^+(0, v_*(0)) &= \int_0^{+\infty} I(sv_*(0))T^+ \exp(-T^- s)\, ds \\ &= \int_0^{+\infty} (I(sv_*(0)) - I(0))T^+ \exp(-T^- s)\, ds + \frac{T^+}{T^-} I(0)\,, \\ \frac{2\chi}{1-\chi} I(0) &\le C_\alpha \int_0^{+\infty} |sv^*(0)|^\alpha T^+ \exp(-T^- s)\, ds\,, \\ C_\alpha^{-1} \left(\frac{2\chi}{1-\chi} I(0)\right)^{1/\alpha} &\le v^*(0)\,. \end{aligned}$$

To conclude, it remains to bound $I(0)$ from below, by noticing for instance that $I(0) = \|I\|_\infty$. From (2.25), and the proof of Lemma 2.7, we deduce

$$\frac{1}{2} = \|f\|_{L^1(\mathbb{R}_+ \times V)} \le C \|f^+(0,\cdot)\|_{L^\infty(V^+)} \int_{x=0}^{+\infty} e^{-\lambda x}\, dx \le \frac{C}{\lambda} \|I\|_{L^\infty}\,. \tag{2.39}$$

Finally, the lower bound on μ goes in the same way as for (2.36), except that it is mandatory to control the density for small densities, basically using the bound (2.25). In fact, we have

$$\begin{aligned} \int_{x=0}^{+\infty} \mu e^{-\lambda x}\, dx &\ge \frac{\delta^2 (\inf F_+)}{\int_V v^2 F_+(v)^2\, dv dx} \iint_{|v|>\delta} f(x,v)\, dv dx \\ \frac{\mu}{\lambda} &\ge \frac{\delta^2 (\inf F_+)}{\int_V v^2 F_+(v)^2\, dv} \left(\frac{1}{2} - \iint_{|v|<\delta} f(x,v)\, dv dx\right) \\ &\ge \frac{\delta^2 (\inf F_+)}{\int_V v^2 F_+(v)^2\, dv} \left(\frac{1}{2} - C \iint_{|v|<\delta} e^{-\lambda x}\, dv dx\right) \\ &\ge \frac{\delta^2 (\inf F_+)}{\int_V v^2 F_+(v)^2\, dv} \left(\frac{1}{2} - 2\delta \frac{C}{\lambda}\right) \end{aligned} \tag{2.40}$$

We can choose δ small enough, such that the last contribution is uniformly positive, namely

$$\frac{\mu}{\lambda} \ge \frac{(\lambda/8C)^2 (\inf F_+)}{4 \int_V v^2 F_+(v)^2\, dv}\,.$$

As a conclusion, we have obtained uniform estimates with respect to $v_0 \in \mathbb{R}_+^*$, each time it was needed.

We also have to revise the proof of Lemma 2.12, concerning the regularity of I. Indeed, we cannot even show that I is Lipschitz continuous uniformly for $x > 0$. However, we are able to prove that it has the correct monotonicity for x close to 0, where it possibly diverges. We only compute the contribution having

possibly the wrong sign, *i.e.* the integral over positive velocities,

$$\begin{aligned}
\frac{d\rho^+}{dx}(x) &= \int_{v>0} \frac{1}{v}\left(I(x) - g(x,v)\right)\, dv\,,\\
&= \int_{v>0} \frac{1}{v}\left(I(x) - g(0,v)\exp(-v^{-1}T^+x) - \int_0^{x/v} I(x-sv)T^+\exp(-T^+s)\, ds\right) dv\\
&= \int_{v>0} \frac{1}{v}\left(I(x) - g(0,v)\exp(-v^{-1}T^+x) - I(x)\left(1-\exp(-v^{-1}T^+x)\right)\right) dv\\
&\le \int_{v>0} \frac{1}{v}\left(I(x) - g(0,v)\right)\exp(-v^{-1}T^+x)\, dv\\
&= \int_{v>0} \frac{1}{v}\left(I(0) - g(0,v)\right)\exp(-v^{-1}T^+x)\, dv + \left(I(x) - I(0)\right)\int_0^{1/2}\frac{1}{v}\exp(-v^{-1}T^+x)\, dv\\
&\le \int_{v>0} \frac{1}{v}\left(I(0) - \frac{T^+}{T^-}\int_0^{+\infty} I(-sv)T^-\exp(-T^-s)\, ds\right)\exp(-v^{-1}T^+x)\, dv + \mathcal{O}\left(x^\alpha|\log x|\right)\\
&\le \left(1-\frac{T^+}{T^-}\right)I(0)\int_0^{1/2}\frac{1}{v}\exp(-v^{-1}T^+x)\, dv\\
&\quad + T^+\int_{v>0}\frac{1}{v}\left(\int_0^{+\infty}\left(I(0)-I(-sv)\right)\exp(-T^-s)\, ds\right)\exp(-v^{-1}T^+x)\, dv + \mathcal{O}\left(x^\alpha|\log x|\right)\\
&\le -\frac{2\chi}{1-\chi}I(0)\int_{2x}^{+\infty}\frac{1}{s}\exp(-T^+s)\, ds + C\int_{v>0} v^{\alpha-1}\exp(-v^{-1}T^+x)\, dv + \mathcal{O}\left(x^\alpha|\log x|\right)\\
&\le -\frac{2\chi}{1-\chi}I(0)\left(-\log x + \mathcal{O}(1)\right) + C + \mathcal{O}\left(x^\alpha|\log x|\right)
\end{aligned}$$

Consequently, no stability in Lipschitz regularity seems available, uniformly with respect to v_0. However, we can restrict to $x \in [l, L]$, for some uniformly positive l, such that I is sufficiently regular on $[l, L]$, and I is uniformly decreasing outside $[l, L]$. ◂

Corollary 2.13: Existence of stationary clusters of bacteria (Calvez, not yet published)

Under the same assumptions as in Theorem 2.8, the following system of equations admits a symmetric stationary distribution $f(x,v)$, associated with a unimodal chemical signal concentration $S(x)$,

$$\begin{cases}
v\partial_x f(x,v) = \displaystyle\int_{v'\in V}(1-\chi\mathrm{sign}\left(v'\partial_x S(x)\right)f(x,v')\, dv' - (1-\chi\mathrm{sign}\left(v\partial_x S(x)\right)f(x,v)\\
-D_S\partial_x^2 S(x) + \alpha S(x) = \beta\rho(x)\,.
\end{cases}$$

▸ *Sketch of proof.* It is enough to check that the linear kinetic equation with a sign transition at $x = 0$ generates a unimodal macroscopic density ρ: this is exactly the purpose of Theorem 2.8. Hence, the unimodal distribution ρ itself generates a unimodal concentration S, and the coupling is satisfied as $\partial_x S$ changes sign at $x = 0$ only. ◂

2.2. Concentration waves of bacteria

We describe in this Section an accurate modelling of concentration waves of bacteria *E. coli* in a microchannel, following the couple of papers [**24**, **23**]. They are based on the kinetic description of the bacteria population at the mesoscopic scale developed in Section 2.1. We first present the macroscopic model, for which analytic computations are tractable. Then, we present the mesoscopic model for which the comparison with experimental data relies essentially on numerical simulations, in the absence of quantitative analysis.

We highlight that both the macro and the mesoscopic models have been validated on two different experimental settings.

We conclude this section by a rigorous proof of existence of travelling waves for the mesoscopic model[8].

2.2.1. Experimental setting. In collaboration with biophysiscists from Silberzan's lab at Institut Curie (Paris, France), we have designed and validated two models at two different scales (macro/meso) on experimental data.

The experiment is the following: The population of cells (approx. 10^5 bacteria *E. coli*) is initially located on the left side of a microchannel after centrifugation. The width of the microchannel is $500\mu m$, the height is $100\mu m$, and the length is $2cm$. The time span of the experiment is a few hours. After short time, a significant fraction of the population moves towards the right side of the channel, at constant speed, within a constant profile (see Figures 0.1 and 2.6).

The data are derived from massive tracking experiments performed by J. Saragosti during his PhD thesis. Statistics about the biases in cell trajectories, depending on the direction and the relative position with respect to the peak of the wave, were obtained by J. Saragosti. The data acquisition proceeds via recording and reconstructing individual trajectories of cells labelled by the green fluorescent protein GFP. The key point is that no invasive measurement, *e.g.* concentration of chemical signals, is available.

2.2.2. Comparison with the Fisher-KPP equation. The nature of the wave is very different from travelling waves occurring in classical reaction-diffusion equations, as the Fisher-KPP equation [**Fis37**, **KPP37**, **AW78**]. Indeed, there is no reaction term in (2.1): the total number of individuals is assumed to be constant. On the contrary to the Fisher-KPP equation where individuals experience unbiased diffusion, motion of bacteria inside chemotactic waves is biased in the direction of chemical gradients: favorable directions are subject to smaller tumbling rates (see Figure 0.1). From the mathematical viewpoint, the existence/uniqueness of travelling waves are much more difficult to establish as opposed to the Fisher-KPP equation because the maximum principle does not hold for equation (2.1) in general.

2.2.3. The macroscopic Model. After many discussions, and several attempts with variants of the classical Keller-Segel system (mainly following [**SZL+06**]), we ended up with a model consisting in a system of three coupled PDE, for the cell density ρ and for two chemical signals, a nutrient N (glucose or oxygen), and a communication signal S (some amino-acid, *e.g.* aspartate, serine or glycine). The former is consumed by the bacteria, whereas the latter is produced. The macroscopic model reads as follows in one-dimension of space,

$$\left\{\begin{array}{l} \partial_t\rho = D_\rho\partial_{xx}\rho - \partial_x\left(\rho\left(\chi_S \mathrm{sign}\left(\partial_x S\right) + \chi_N \mathrm{sign}\left(\partial_x N\right)\right)\right) \\ \partial_t S = D_S\partial_{xx}S - \alpha S + \beta\rho \\ \partial_t N = D_N\partial_{xx}N - \gamma\rho N \end{array}\right. \tag{2.41}$$

It is a superposition of (2.15) with two additive chemotactic transport speeds $\chi_S \mathrm{sign}\left(\partial_x S\right)$ and $\chi_N \mathrm{sign}\left(\partial_x N\right)$, and the reaction-diffusion equations (2.2)–(2.3). We have found evidence that removing any one of the two reaction-diffusion equations alters the propagation of the wave.

[8]This work has been achieved during the redaction of this memoir, for the sake of completeness.

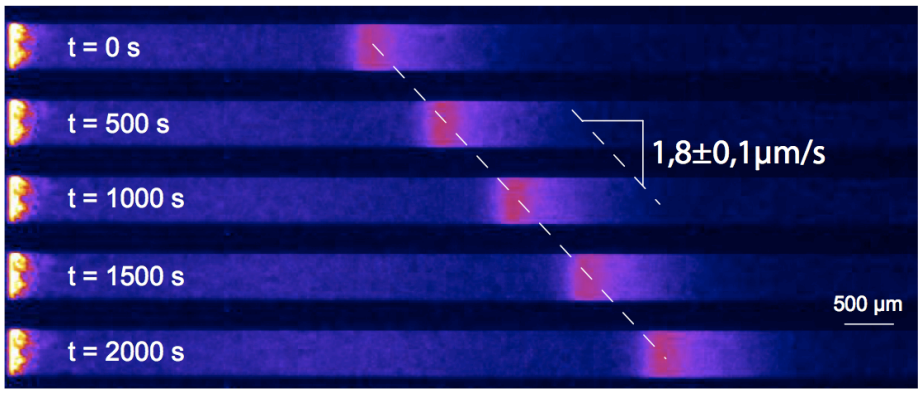

FIGURE 2.6. Concentration waves of bacteria. This will be referred to as the *slow wave* [24], as opposed to Figure 0.1 which will be referred to as the *fast wave* [23], see Section 2.2.3.3 for a discussion. Observe the difference between the profile asymmetry in the two sets of experiments. The macroscopic model (2.41) is well adapted to describe the slow wave, whereas the mesoscopic model (2.48) is better adapted to fit the fast wave.

2.2.3.1. *Travelling waves for the macroscopic model.* The intuition goes as follows. Without the nutrient, the communication signal S yields the formation of a stable cluster (see the confinement effect in Section 2.1.3). Hence, it is able to maintain the cohesion of the cell population in a band. Then, the band moves forward because the gradient of nutrient is dynamically updated via consumption by the cell population.

The following Theorem translates this intuition into a quantitative result.

Theorem 2.14: Existence of chemotactic waves at the macro scale [24]

Let $\alpha, \beta, \gamma > 0$. The system (2.41) admits travelling wave solutions $(\rho(x-ct), S(x-ct), N(x-ct))$ with the following boundary conditions:

$$\lim_{|x|\to\infty} \rho = \lim_{|x|\to\infty} S = 0\,, \quad \lim_{x\to-\infty} N = N_- < N_+ = \lim_{x\to+\infty} N\,. \tag{2.42}$$

Moreover, the speed $c > 0$ is uniquely determined by the following implicit relation,

$$\chi_N - c = \chi_S \frac{c}{\sqrt{c^2 + 4\alpha D_S}}\,. \tag{2.43}$$

It is important to make the following comments: Firstly, the wave speed c does not depend on the reaction kinetics of the diffusion-consumption of the nutrient. The reason is simple: the equation for the nutrient is coupled to the cell density only through the sign of $\partial_x N$. However, the wave is constructed such that the nutrient concentration is always increasing. Secondly, the coupling is sufficiently weak, so that the cell density ρ is explicit, up to the knowledge of the speed c. It is simply the concatenation of two exponential tails (see the sketch of proof below). Therefore, this model is very well suited to comparison with experimental data.

▸ *Sketch of proof.* The proof is based on explicit computations. Equations are written in the moving frame $z = x - ct$. The starting point consists in assuming that the communication signal S reaches a unique maximum value at $z = 0$. We shall eventually confirm that this ansatz is valid, so that $\partial_z S(0) = 0$. To do so, we first compute the cell density ρ, solution of the following equation,

$$-c\partial_z \rho = D_\rho \partial_z^2 \rho - \partial_z \left(\rho \left(\chi_S \operatorname{sign}(-z) + \chi_N\right)\right)\,.$$

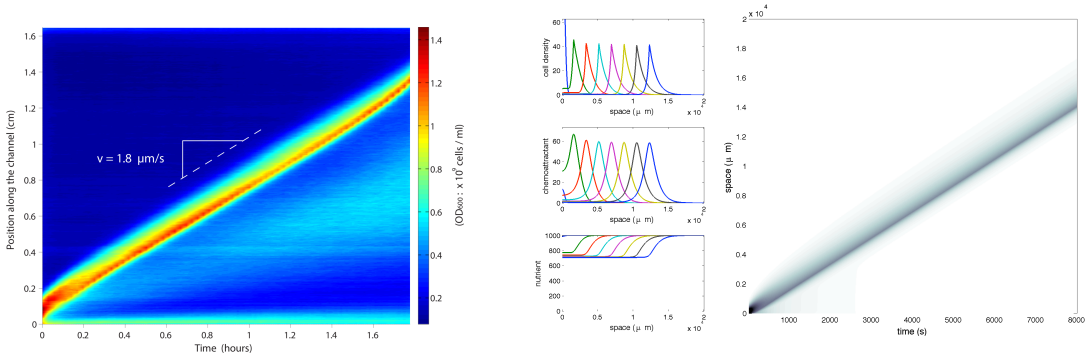

FIGURE 2.7. (Left) Experimental kymograph of the chemotactic band (in time×space coordinates) for the same experiment as in Figure 2.6. (Right) Numerical simulations of (2.41): time evolution of the cell density, the concentration of S and the concentration of N are plotted (from top to bottom), as well as the numerical kymograph of the cell density. In both cases, one can observe a remarkable solitary wave.

It is a combination of two exponential tails,

$$\rho(z) = \begin{cases} \exp\left(\dfrac{-c+\chi_S+\chi_N}{D_\rho} z\right) & \text{when } z<0, \textit{ i.e. } \text{both signals are attractive} \\ \exp\left(\dfrac{-c-\chi_S+\chi_N}{D_\rho} z\right) & \text{when } z>0, \textit{ i.e. } \text{the signals have opposite contributions} \end{cases} \tag{2.44}$$

In a second step, we compute the concentration S through the equation

$$-c\partial_z S = D_S \partial_z^2 S - \alpha S + \beta\rho\,.$$

The solution is given by $S = \mathcal{S} * (\beta\rho)$, where $\mathcal{S}$ is the Green function associated to the elliptic operator $-c\partial_z - D_S\partial_z^2 + \alpha$. We have

$$\mathcal{S}(z) = \begin{cases} \mathcal{S}_0 \exp\left(\dfrac{-c+\sqrt{c^2+4\alpha D_S}}{2D_S} z\right) & \text{when } z<0 \\ \mathcal{S}_0 \exp\left(\dfrac{-c-\sqrt{c^2+4\alpha D_S}}{2D_S} z\right) & \text{when } z>0 \end{cases} \tag{2.45}$$

The value of the renormalization constant $\mathcal{S}_0$ does not matter here. Finally, we compute the value of $\partial_z S(0)$. It should vanish according to the preliminary assumption. Denoting by $\mu_\pm > 0$ the exponential rates of decay of $\mathcal{S}$ (resp. for $z<0$ and $z>0$), and by $\lambda_\pm > 0$ the exponential rates of decay of ρ (2.44), we find eventually,

$$\begin{aligned} \partial_z S(0) &= \beta \int_{\mathbb{R}} \partial_z \mathcal{S}(-z)\rho(z)\,dz \\ &= \beta\mathcal{S}_0 \left(\frac{\mu_+}{\lambda_- - \mu_+} - \frac{\mu_-}{\lambda_+ - \mu_-}\right) \end{aligned}$$

Therefore, the dispersion relation simply reads

$$\lambda_+\mu_+ = \lambda_-\mu_-\,, \tag{2.46}$$

which is equivalent to (2.43). Finally, we notice that the relation (2.43) is decreasing (resp. increasing) with respect to c on the left hand side (resp. right hand side). Therefore, c is uniquely determined. ◂

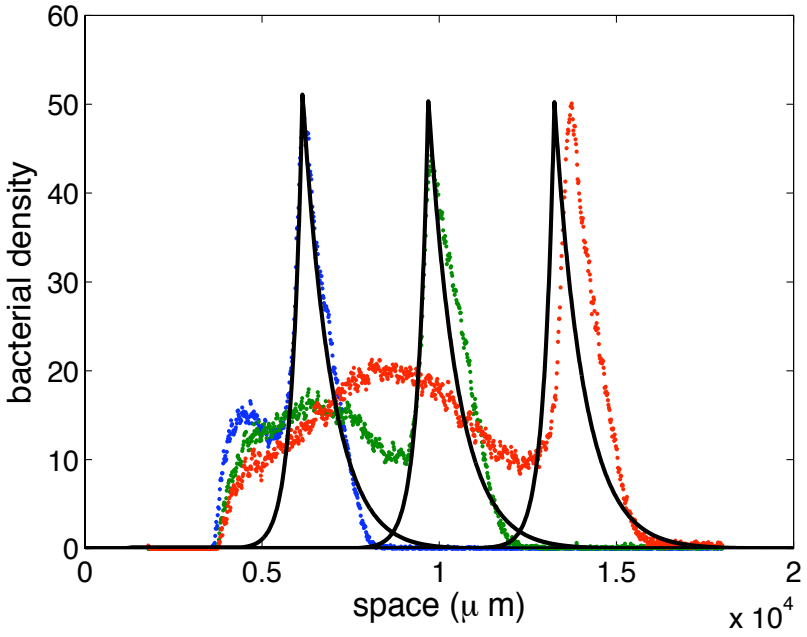

FIGURE 2.8. Same experiment as in Figures 2.6 and 2.7. Comparison of three snapshots of the cell density between the numerical simulations (black plain line), and the experimental measurements at three successive times (colored dots obtained from optical density). The experimental density is reasonably similar to the concatenation of two exponential tails, except at the back of the wave, where optical density shows a moreless constant, nonzero, background. This may correspond to non motile bacteria that have lost their flagella after cell division. Nonetheless, it seems to play no role during the wave propagation. The numerical speed is a bit slower than the experimental one as can be seen on the third snapshot, probably due to inaccuracy of the first order numerical scheme.

2.2.3.2. *Validation on experimental data (I).* Model (2.41) is interesting because it contains only few parameters that are not available in the literature, namely χ_S and χ_N. On the other hand, the wave speed c is easily measurable. In addition, measurements of the cell density profile (2.44) are also available via optical density. It can be reasonably fitted with two exponential tails, as predicted in the proof of Theorem 2.14, thus giving two additional numbers, λ_+ and λ_-. These two numbers can be used to estimate χ_S and χ_N. Thus, the wave speed can be predicted, giving a quite good agreement with the observation [**24**].

A more direct, and certainly more faithful way to validate model (2.41) is to focus on relation (2.46) which is the quantitative result that we obtained for the wave speed. Using the formulas for the exponential rates of decay $\mu_\pm$ (2.45), it reads,

$$\lambda_+\left(c+\sqrt{c^2+4\alpha D_S}\right)=\lambda_-\left(-c+\sqrt{c^2+4\alpha D_S}\right),$$

which is equivalent to

$$\alpha D_S = c^2\frac{\lambda_+\lambda_-}{\lambda_- - \lambda_+}. \tag{2.47}$$

The reaction kinetics of the communication signal are well known. We found the values of $\alpha = 5\times10^{-3}s^{-1}$ [**SZL+06**], and $D_S = 8-10\times10^{-6}cm^2.s^{-1}$ [**WAB84**] in the literature. On the other hand, the values $\lambda_- = 34cm^{-1}$ and $\lambda_+ = 13cm^{-1}$ are obtained from exponential fitting of the optical density of bacteria in the microchannel. By plugging these numerical values into (2.47), we obtain

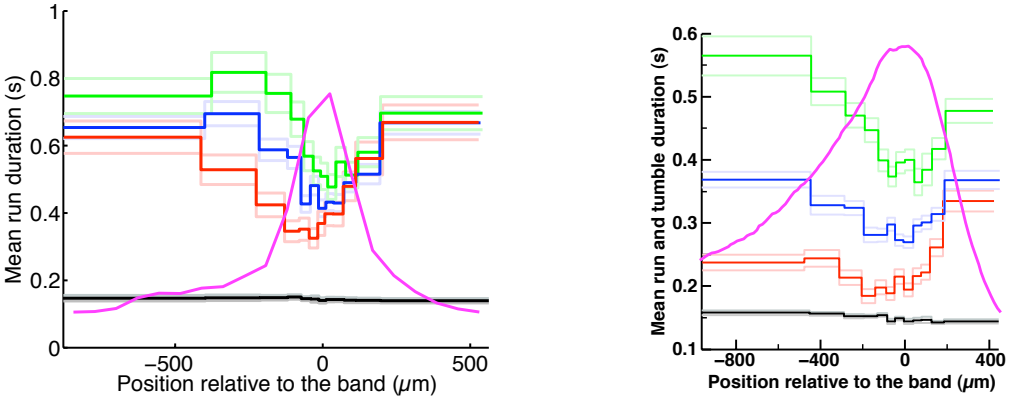

FIGURE 2.9. In both pictures, the green curve is the mean duration of runs for bacteria moving to the right, the red curve corresponds to bacteria moving to the left, and the blue curve corresponds to bacteria moving in the transverse direction. The pink curve is the cell density. (Left) For the experiments performed in [**24**], the biases are small, and we evaluate $\varepsilon \approx 0.1$ in (2.13). (Right) For the experiments performed in [**23**], the biases are large (especially at the back of the wave where both gradients of S and N are pointing in the same direction, to the right), and we evaluate $\varepsilon \approx 0.5$ in (2.13). Clearly, the macroscopic wave speed is impacted by the relative size of the biases. In fact, the wave speed in the latter case is more than twice the wave speed in the former case (compare Figures 0.1 and Figure 2.6).

eventually $c = 2\mu m.s^{-1}$, which is remarkably close to the measured value of $c = 1.8\mu m.s^{-1}$. This proves that this model is quantitatively consistent with the experimental observations.

2.2.3.3. *Is the diffusion limit relevant?* The previous analysis relies on the diffusion approximation of the run-and-tumble process that leads to the macroscopic model (2.41), see Section 2.1.3.1. Recall that the diffusion limit is a reasonably good approximation if the biases in trajectories due to chemotaxis are small, *i.e.* $\varepsilon \ll 1$ in (2.13). We have access to this information by looking on the various run durations depending on the spatial location, and the direction of cells. This is summarized in Figure 2.9. The main conclusion is the following:

Depending on the experimental setting, the diffusion limit may be valid or not.

This clearly motivates the analysis of travelling waves for the underlying kinetic model.

2.2.4. The mesoscopic (kinetic) model. The mesoscopic (kinetic) version of (2.41) writes as follows,

$$\text{(2.48)} \qquad \begin{cases} \partial_t f(t,x,v) + v\cdot\nabla_x f(t,x,v) = \displaystyle\int_{v'\in V} \mathbf{T}(t,x,v,v') f(t,x,v')\,dv' - \boldsymbol{\lambda}(t,x,v) f(t,x,v) \\ \partial_t S = D_S \partial_{xx} S - \alpha S + \beta\rho \\ \partial_t N = D_N \partial_{xx} N - \gamma\rho N \end{cases}$$

where the tumbling rate can be decomposed as $\mathbf{T}(t,x,v,v') = K(t,x,v,v')\boldsymbol{\lambda}(t,x,v')$, where the tumbling frequency reads

$$\boldsymbol{\lambda}(t,x,v') = \psi_0\left(1 + \chi_S\phi\left(\frac{D\log S}{Dt}\Big|_{v'}\right) + \chi_N\phi\left(\frac{D\log N}{Dt}\Big|_{v'}\right)\right).$$

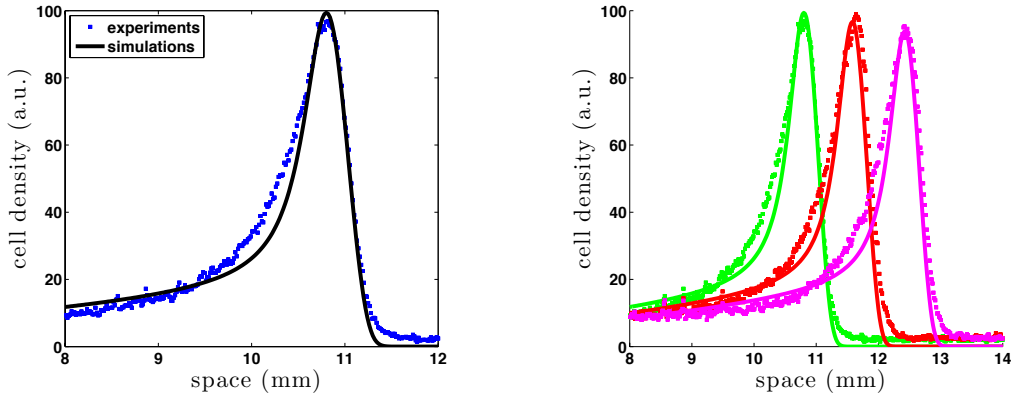

FIGURE 2.10. (Left) Agreement between numerical simulations (plain line) and experimental measurements (blue dots) of the macroscopic density ρ in the case of the fast wave (Figure 0.1 and equation (2.48)). (Right) Comparison between the simulations and the experiments for three successive times.

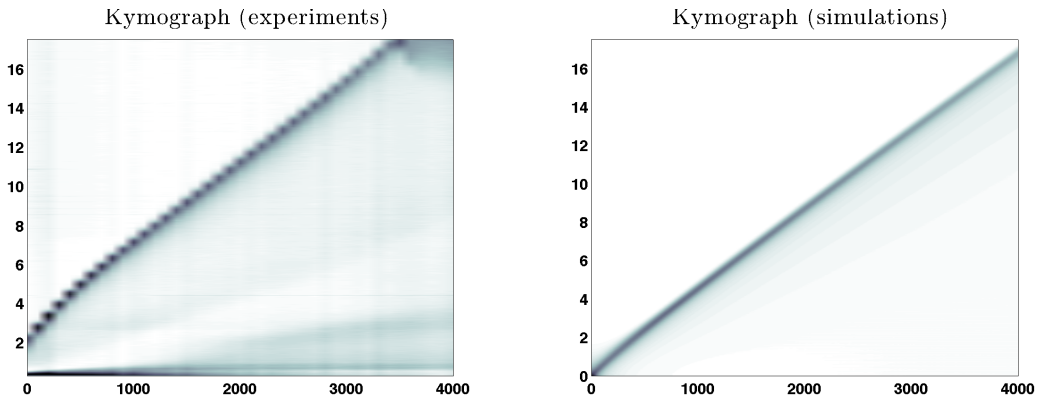

FIGURE 2.11. Same as Figure 2.10. Propagation of the wave in time (abscissa) and space (ordinate). Observe the slight dispersion effects that slow down the wave. Spatial confinement is not perfectly efficient there because $\tau < +\infty$.

It is assumed that the two chemotattractants have additive effects, and that they proceed with the same internal response function ϕ, with possibly different amplitudes χ_S, χ_N. Note that the diffusion limit of (2.48) when the biases χ_S, χ_N are small is precisely (2.41).

2.2.4.1. *Validation on experimental data (II).* The probability kernel $K(v, v')$ enables to include secondary effects, such as persistence in the tumbling angle, *i.e.* correlation between v' and v, and possible modulation of persistence. We discuss briefly these effects below, and refer to [**23**] for further details.

The post-tumbling velocity v' is not uncorrelated to the pre-tumbling velocity v[9]. The mean value of the change of direction is approx. 68° [**23**]. Bacteria presumably perform rotational diffusion

[9]Bacteria are rarely seen to make a U-turn during the tumble.

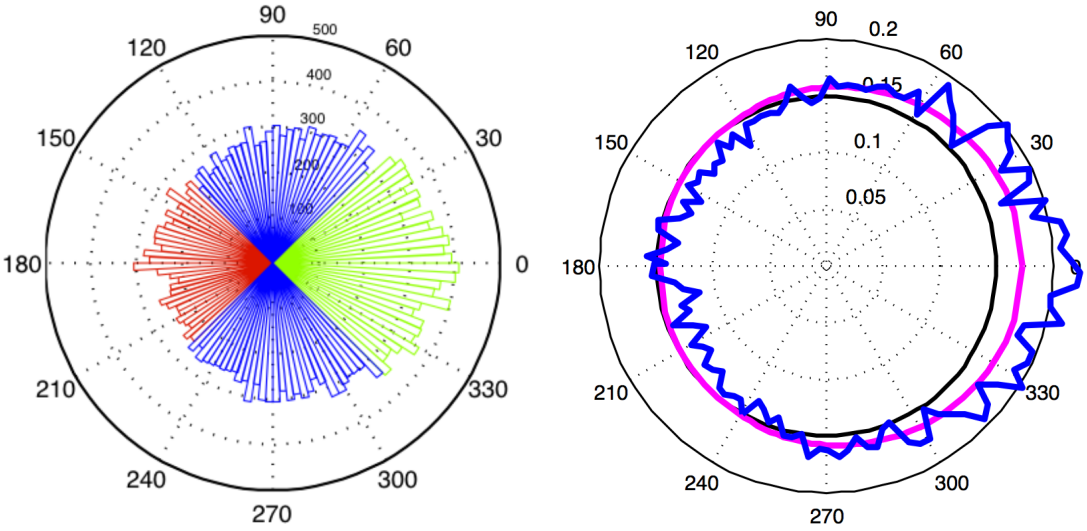

FIGURE 2.12. (Left) Distribution of the number of runs with respect to the orientation in the microchannel (same color code as in Figure 2.9). The distribution is clearly not uniform, as globally favorable directions are more frequent. (Right) The blue curve is the same as the Left picture (experumental data), and the pink curve is the numerical simulations for a nonconstant standard deviation σ having an affine dependency with respect to $\boldsymbol{\lambda}(t, x, v')$. The uniform distribution is plotted in black for the sake of comparison.

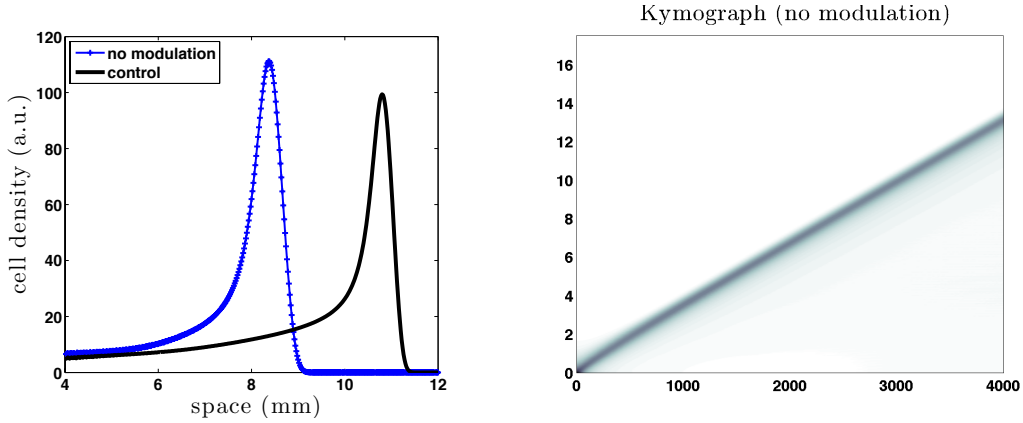

FIGURE 2.13. Comparison between the control configuration, and the configuration without modulation of the persistence angle. The density profile is not changed, whereas the wave is significantly slower.

during the tumble phase, which does not last sufficiently long to enable them to decorrelate the pre- and post-tumbling directions. In the velocity-jump model (2.48), we assumed that the tumbling phase is instantaneous for the sake of simplicity. However, we can encode this angular persistency using a Gaussian p.d.f. to distribute the post-tumbling velocity, namely

$$K(v, v') = \frac{1}{Z_\sigma} \exp\left(\frac{v \cdot v'}{\sigma^2}\right),$$

with a suitable standard deviation σ that accounts for the mean persistence angle. In [23], it has been evidenced that the standard deviation itself is modulated by the chemical gradients, as

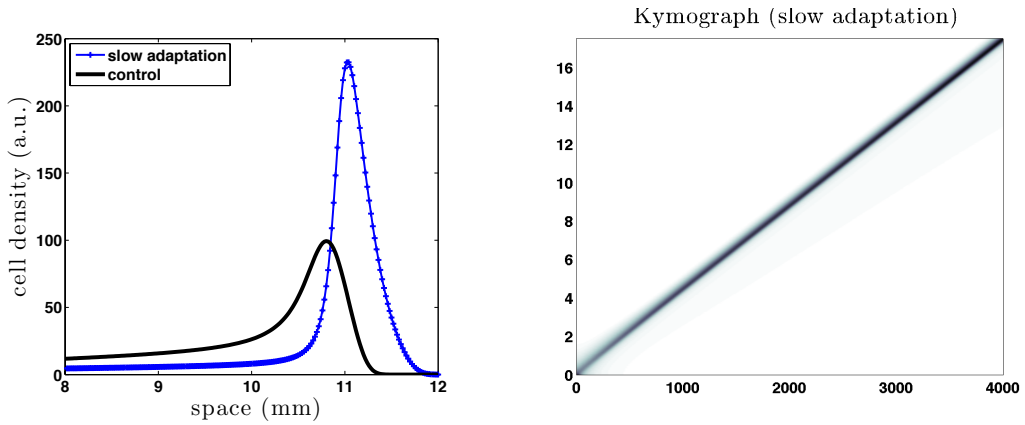

FIGURE 2.14. Comparison between the control configuration, and the case of slow adaptation (τ is twice the control value). The wave is sharper: we observe no dispersion effects. Note the inversion of asymmetry of the profile.

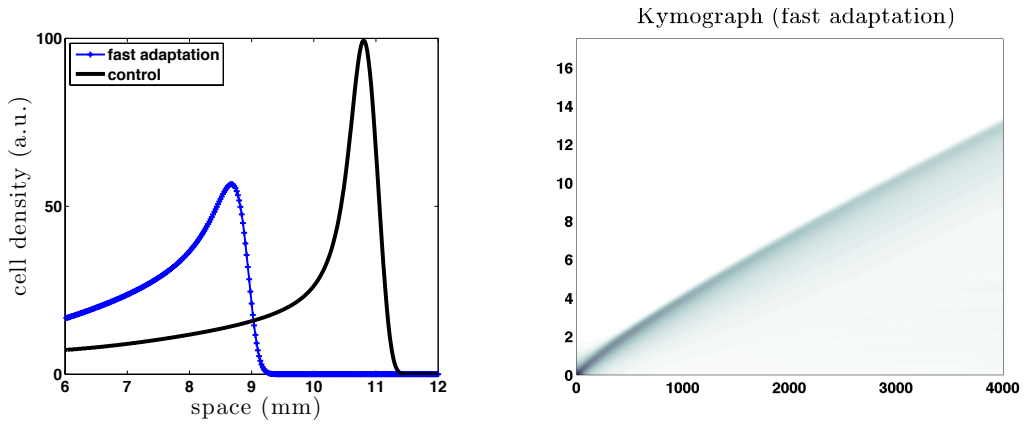

FIGURE 2.15. Comparison between the control configuration, and the case of fast adaptation (τ is half the control value). We observe more dispersion effects, which slow down the wave.

predicted in [**VLS10**]. This was put into the model via the dependency $\sigma = \sigma(t, x, v')$, where σ is an increasing function of $\boldsymbol{\lambda}(t, x, v')$: more likely is the tumble, larger the deviation between v and v' is expected.

This modulation has been evidenced by looking at the statistics of run directions. Indeed, were the standard deviation σ be constant, the distribution of *number* of runs with respect to the direction would be isotropic, as in the case of a complete decorrelation (K uniform[10]). However, this was not the case, see Figure 2.12. Hence, there is a secondary modulation effect which makes that favorable directions are not only longer, but more frequent. This secondary modulation accounts for a significant fraction of the macroscopic wave speed (25%), see Figure 2.13.

[10]If the post-tumbling velocity is chosen uniformly at random, the distribution of number of runs with respect to the direction is also uniform. Modulation of the duration of runs is the only determinant of biases in favorable directions.

The internal response function ϕ is not chosen to be the sign function, as in (2.17). It is a decreasing sigmoidal function with a transition parameter $\tau > 0$ which is a typical timescale,

$$\phi\left(\left.\frac{D\log S}{Dt}\right|_{v'}\right) = -\tanh\left(\tau\left.\frac{D\log S}{Dt}\right|_{v'}\right). \tag{2.49}$$

Time τ can be related to the adaptation timescale of individual cells [**Xue13**, **PTV15**]. Interestingly enough, this parameter is available in the literature [**BSB83**]. The experimental value $\tau \approx 20\,\text{sec}$ gave very good fits between numerical simulations and experiments.

Larger values of τ decrease dispersion and increase the wave speed (Figure 2.14). The resulting concentration profile narrows and changes its symmetry by getting wider on the right side, as for the wave in Figure 2.8.

On the contrary, smaller values of τ increase dispersion and decrease the wave speed (Figure 2.15). In fact, dispersion effects are so strong that the wave is hardly propagating: it slows down, and the profile gets broader.

Rigorously speaking, there exists a travelling wave solution only in the extremal case $\tau = +\infty$, where ϕ is the sign function[11]. The same statement holds for the confinement effect in the absence of nutrient (see Section 2.1.3.4). If the response function ϕ vanishes for shallow gradients, then bacteria which are very far from the peak of concentration experience an almost unbiased velocity-jump process, so that they do not get confined.

2.2.4.2. *Existence of travelling waves for the mesoscopic problem.* The purpose of this section is to prove the existence of travelling waves for (2.48) in the extreme case $\tau = +\infty$. For the sake of simplicity, we ignore the modulation of persistence, so that K is set to be constant.

Theorem 2.15: Existence of chemotactic waves at the meso scale (Calvez, not yet published)

Assume $d = 1$, $(\chi_S, \chi_N) \in [0,1]^2$ such that $0 \le \chi_N < \chi_S < 1$ and $\chi_S + \chi_N < 1$, and V is a symmetric combination of at most two intervals: $V = (-1/2, 1/2)$, or $V = (-v_0 - 1/2, -v_0) \cup (v_0, v_0 + 1/2)$ for some $v_0 > 0$. There exist $c \in \mathbb{R}$ and $(f, S, N) \in \left(L^1 \cap L^\infty(\mathbb{R}\times V)\right) \times \mathcal{C}^2(\mathbb{R}) \times \mathcal{C}^2(\mathbb{R})$ solutions of the following travelling wave problem,

$$\begin{cases} (v-c)\partial_x f(x,v) = \displaystyle\int_{v'\in V} \left(1 - \chi_S \operatorname{sign}\left((v'-c)\partial_x S(x)\right) - \chi_N \operatorname{sign}\left((v'-c)\partial_x N(x)\right)\right) f(x,v')\,dv' \\ \qquad\qquad - \left(1 - \chi_S \operatorname{sign}\left((v-c)\partial_x S(x)\right) - \chi_N \operatorname{sign}\left((v-c)\partial_x N(x)\right)\right) f(x,v) \\ -c\partial_x S(x) = D_S \partial_x^2 S(x) - \alpha S(x) + \beta\rho(x) \\ -c\partial_x N(x) = D_N \partial_x^2 N(x) - \gamma\rho(x) N(x) \end{cases} \tag{2.50}$$

Moreover, there exist two exponents $\lambda_\pm > 0$, and two velocity profiles $F_\pm(v)$ such that $e^{\lambda_+ x} f(x,v)$ (resp. $e^{-\lambda_- x} f(x,v)$) converges exponentially fast to $F_+(v)$ as $x \to +\infty$ (resp. to $F_-(v)$ as $x \to -\infty$).

▸ *Sketch of proof.* We describe how to extend Theorems 2.6, 2.8, and Corollary 2.13 to the asymmetric case where the cluster of bacteria is travelling at constant speed c.

We adopt the following convention: the superscripts $^+$ and $^-$ denote the relative velocity with respect to c (resp. $v > c$ and $v < c$), whereas the subscripts $_+$ and $_-$ denote the relative position with respect to the origin (resp. $x > 0$ and $x < 0$).

Firstly, we shall solve with full accuracy the linear problem, for which we assume *a priori* the following facts:

[11] Erban et al came up with the same conclusion [**XHPE10**], see also [**FXPE13**].

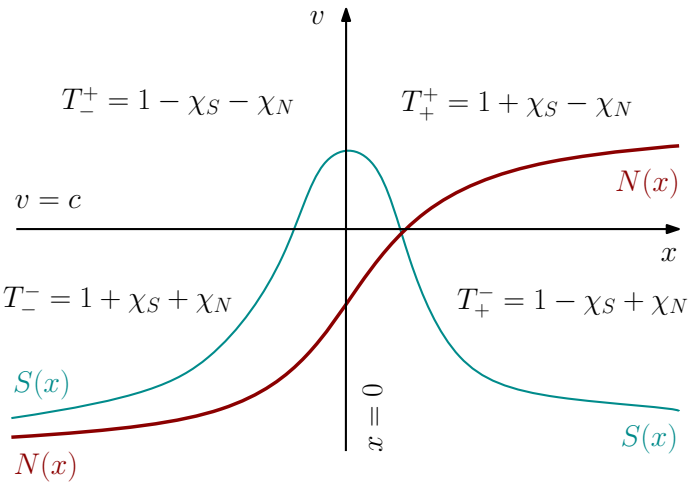

FIGURE 2.16. Expression of the tumbling kernel $T_\pm^\pm$ depending on the signs of x and $v-c$. The expected profiles of S and N are plotted in order to get the correct value of $T_\pm^\pm$ at a glance. Note the c dependency as it is the value where the sign changes from bottom to top of the (x,v) plane.

(i) c is given in a suitable interval (c_*, c^*), depending on V, χ_S, and χ_N, to be defined later,

(ii) $\partial_x S$ changes sign at $x = 0$,

(iii) $\partial_x N$ does not change sign. We assume w.l.o.g. that $\partial_x N > 0$ [12]

Then, we are reduced to examine the following linear problem,

$$(v-c)\partial_x f = \int_V T_\pm^\pm(v') f(x,v')\,dv' - T_\pm^\pm(v) f(x,v)\,, \tag{2.51}$$

where $T_\pm^\pm(v) = 1 \pm \chi_S \pm \chi_N$, with the sign convention as depicted in Figure 2.16.

We expect the following behaviour at infinity, $f(x,v) \sim e^{-\lambda_+ x} F_+(v)$, as $x \to +\infty$, where

$$F_+(v) = \frac{1}{T_+(v) - \lambda_+(v-c)}\,,$$

and $\lambda_+ > 0$ is uniquely determined by the following relation, as in the proof of Theorem 2.6,

$$\int_V \frac{T_+(v)}{T_+(v) - \lambda_+(v-c)}\,dv = 1\,,$$

provided that the mean algebraic run length is negative in the moving frame, *i.e.*

$$\int_V \frac{v-c}{T_+(v)}\,dv < 0 \quad \Leftrightarrow \quad c > c_* = \left(\int_V \frac{1}{T_+(v)}\,dv\right)^{-1} \int_V \frac{v}{T_+(v)}\,dv\,. \tag{2.52}$$

The same holds for $x \to -\infty$: we expect $f(x,v) \sim e^{\lambda_- x} F_-(v)$ as $x \to +\infty$, where

$$F_-(v) = \frac{1}{T_-(v) + \lambda_-(v-c)}\,,$$

where $\lambda_- > 0$ is uniquely determined by the following relation, as in Theorem 2.6

$$\int_V \frac{T_-(v)}{T_-(v) + \lambda_-(v-c)}\,dv = 1\,,$$

[12] This would correspond eventually to a travelling wave moving to the right, *i.e.* $c > 0$, but N, S and c are not coupled yet.

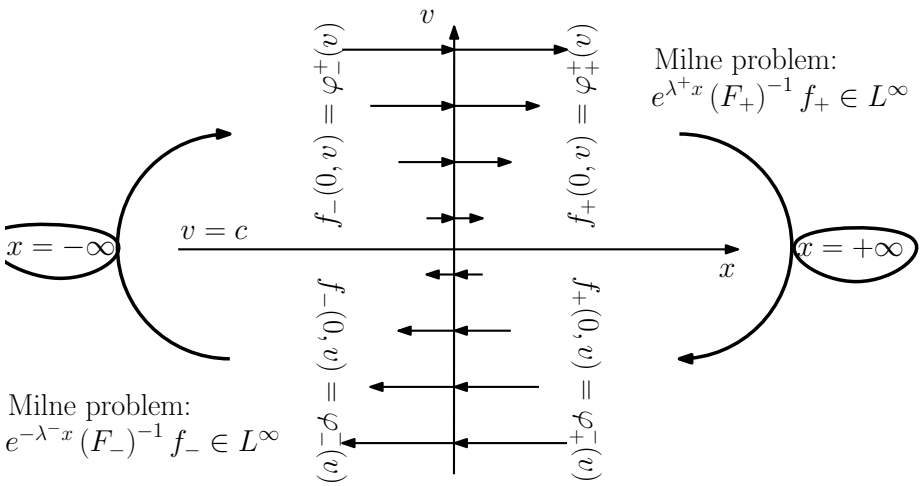

FIGURE 2.17. Cartoon of the map $\mathbf{B} : \varphi_+^+ \mapsto \varphi_-^+$ via two applications of the Milne problem at $x = \pm\infty$.

provided that the mean algebraic run length is positive in the moving frame, *i.e.*

$$\int_V \frac{v-c}{T_-(v)}\,dv > 0 \quad \Leftrightarrow \quad c < c^* = \left(\int_V \frac{1}{T_-(v)}\,dv\right)^{-1} \int_V \frac{v}{T_-(v)}\,dv\,. \tag{2.53}$$

Notice that $T_\pm, F_\pm, \lambda_\pm$ all depend on c. For the sake of clarity, we omit this dependency in the notation. From now on, we assume that the speed belongs to the interval $c \in (c_*, c^*)$, and we keep in mind the extremal behaviours,

$$\lim_{c\to c_*} \lambda_+ = 0\,, \quad \lim_{c\to c^*} \lambda_- = 0\,. \tag{2.54}$$

Alternatively speaking, the spatial density becomes flat on the far right side as the speed c decreases to c_*, whereas it becomes spatially flat on the far left side as it increases to c^*. This property will be crucial in the last step of the proof, when determining the speed c for the coupled problem.

We are now in position to set up a fixed point strategy, as in the proof of Theorem 2.6. Let $\varphi_+^+(v)$, defined for $v > c$, be an inward velocity profile which serves as a boundary condition for the following Milne problem,

$$\begin{cases} (v-c)\partial_x f_+ = \displaystyle\int_V T_+^\pm(v') f_+(x,v')\,dv' - T_+^\pm(v) f_+(x,v)\,, & x > 0\,,\ v \in V \\ f_+(0,v) = \varphi_+^+(v)\,, & v > c \\ e^{\lambda^+ x}\,(F_+(v))^{-1}\,f_+(x,v) \in L^\infty(\mathbb{R}_+ \times V) \end{cases} \tag{2.55}$$

There exists a unique f_+ satisfying the last boundedness condition, with prescribed inward values for the velocity distribution at $x = 0$, φ_+^+. This determines in a unique way an outward velocity profile at $x = 0$, denoted by $\varphi_+^-(v) = f_+(0,v)$, defined for $v < c$.

We introduce a similar Milne problem for $x < 0$, associated with the following inward velocity profile φ_-^-, that we set equal to φ_+^-,

$$(\forall v < c) \quad \varphi_-^-(v) = \varphi_+^-(v)\,.$$

This defines in a unique way a velocity profile φ_-^+, defined for $v > c$ at $x = 0$, such that $f_-(0,v) = \varphi_-^-(v)$ for $v < c$, and $e^{-\lambda^- x}\,(F_-(v))^{-1}\,f_-(x,v) \in L^\infty(\mathbb{R}_- \times V)$.

Finally, we denote by $\mathbf{B} : \mathcal{C}^0(V^+) \to \mathcal{C}^0(V^+)$ the linear map

$$\mathbf{B}\varphi_+^+ = \varphi_-^+\,.$$

By reproducing the same arguments as in Theorem 2.6, we can prove that $\mathbf{B}$ is a compact, positive operator. Therefore it admits a simple dominant eigenvalue, equal to one by conservation of mass, associated to a

positive eigenfunction φ. This velocity profile enables to define a solution to (2.51) by solving two Milne problems, as depicted in Figure 2.17.

In addition, we get several interesting quantitative properties for the stationary distribution f associated with the speed c, including the exponential decay of $e^{\pm\lambda_\pm x} f(x,v)$ towards $F_\pm(v)$, as in Theorem 2.6.

Secondly, we shall prove that the macroscopic profile $\rho(x) = \int_V f(x,v)\,dv$ is monotonic on both sides of the origin, though clearly not symmetric as in Theorem 2.8. Namely, we establish that it is increasing for $x > 0$ and decreasing for $x < 0$. We argue as in Theorem 2.8. We take $c \in (c_*, c^*)$ as a continuously varying parameter.

The case $c = 0$ has been treated in Theorem 2.8, except that T_+ and T_- are not symmetric since χ_N is not necessarily zero here. However, the proof goes exactly in the same way, with $\chi_+ = \chi_S - \chi_N \in (0,1)$ for $x > 0$, and $\chi_- = \chi_S + \chi_N \in (0,1)$ for $x < 0$. Consequently, $I_+ = \int T_+ f_+\,dv$ is decreasing, and $I_- = \int T_- f_-\,dv$ is increasing. As a by-product, both ρ_+^+ and ρ_+^- are decreasing, whereas both ρ_-^+ and ρ_-^- are increasing. Notice that the coupling from $x < 0$ to $x > 0$ goes through the velocity profile $f_+^+(0,v) = f_-^+(0,v)$, which is increasing with respect to v, provided I_- is nondecreasing, since we have

$$(\forall x < 0) \quad f_-^+(x,v) = \int_0^{+\infty} I_-(x - s(v-c)) \exp(-T_-^+ s)\,ds\,.$$

The reverse holds true for the coupling from $x > 0$ to $x < 0$, through $f_-^-(0,v) = f_+^-(0,v)$, and

$$(\forall x < 0) \quad f_+^-(x,v) = \int_0^{+\infty} I_+(x - s(v-c)) \exp(-T_+^- s)\,ds\,.$$

Remark 2.16. *In the proof of Theorem 2.8, we have used twice the identity* $\|f\|_{L^1(\mathbb{R}_+\times V)} = \frac{1}{2}\|f\|_{L^1(\mathbb{R}\times V)}$, *when estimating both* $I(0)$ *and* μ *from below. However, this identity does not hold true in the asymmetric case, when* $c \neq 0$ *or* $\chi_N > 0$. *We have more generally*

$$1 = \iint f\,dvdx = \iint_{x>0} f_+(x,v)\,dvdx + \iint_{x<0} f_-(x,v)\,dvdx = M_+ + M_-\,.$$

Therefore, we need some additional control from below on $M_\pm$. *To circumvent this issue, we can use the two conservation laws associated with* $\lambda_\pm$ *on both sides of the origin. Namely, we have for all* $x > 0$ *and* $y < 0$,

$$\left\{\begin{aligned} \mu_+ &= \frac{\int_V f_+(0,v)(v-c)^2 F_+(v)\,dv}{\int_V (v-c)^2 F_+(v)^2\,dv} = e^{\lambda_+ x}\frac{\int_V f_+(x,v)(v-c)^2 F_+(v)\,dv}{\int_V (v-c)^2 F_+(v)^2\,dv}\,,\\ \mu_- &= \frac{\int_V f_-(0,v)(v-c)^2 F_-(v)\,dv}{\int_V (v-c)^2 F_-(v)^2\,dv} = e^{-\lambda_- y}\frac{\int_V f_-(y,v)(v-c)^2 F_-(v)\,dv}{\int_V (v-c)^2 F_-(v)^2\,dv}\,. \end{aligned}\right. \tag{2.56}$$

We can couple these two identities by using the transmission condition $(\forall v \in V)\ f_+(0,v) = f_-(0,v)$. *This yields*

$$\frac{\mu_+}{\mu_-} \geq \left(\inf \frac{F_+}{F_-}\right)\frac{\int_V (v-c)^2 F_-(v)^2\,dv}{\int_V (v-c)^2 F_+(v)^2\,dv}\,.$$

On the other hand, by a similar computation as (2.40), *we get*

$$\begin{aligned} \frac{\mu_-}{\lambda_-} &\geq \frac{\delta^2\,(\inf F_-)}{\int_V (v-c)^2 F_-(v)^2\,dv}\left(M_- - \iint_{|v-c|<\delta} f_-(y,v)\,dvdy\right)\\ &\geq \frac{\delta^2\,(\inf F_-)}{\int_V (v-c)^2 F_-(v)^2\,dv}\left(M_- - 2\delta\frac{C}{\lambda_-}\right)\,, \end{aligned}$$

from which we deduce,

$$\mu_- \geq C^{-1}(\lambda_- M_-)^3\,.$$

On the other hand, we get easily that

$$\frac{\mu_+}{\lambda_+} \leq C\|f_+\|_{L^1(\mathbb{R}_+\times V)} = CM_+\,,$$

since the set of velocities is bounded. It yields the following series of estimates,

$$\lambda_+ M_+ \geq C^{-1}\mu_+ \geq C^{-1}\mu_- \geq C^{-1}(\lambda_- M_-)^3\,.$$

Therefore,

$$1 = M_+ + M_- \leq M_+ + C\frac{(\lambda_+ M_+)^{1/3}}{\lambda_-}\,.$$

As a consequence, M_+ is uniformly bounded from below. By exchanging the roles of $x > 0$ and $x < 0$, we obtain an analogous estimate for M_-.

The case $c \neq 0$ is identical to the case $c = 0$, except that the velocity sets $V^+ = \{v > c\}$ and $V^- = \{v < c\}$ are not symmetric with respect to each other[13]. The key observation is that (2.33) still holds: with the same notations as in the proof of Theorem 2.8, we have

$$(\forall x > 0) \qquad \int_{v>c} \big(I_+(x) - g_+^+(x,v)\big)\, dv = \int_{v<c} \big(g_+^-(x,v) - I_+(x)\big)\, dv < 0\,, \tag{2.57}$$

and the same holds true for $x < 0$. This enables to deal with compensations between lower and higher velocities exactly in the same way.

Consequently, for any $c \in (c_*, c^*)$, $I_+ = \int T_+ f_+\, dv$ is decreasing, resp. $I_- = \int T_- f_-\, dv$ is increasing, provided that it is nonincreasing, resp. nondecreasing. As a by-product, both ρ_+^+ and ρ_+^- are decreasing, whereas both ρ_-^+ and ρ_-^- are increasing. Moreover, the distribution f is unique, up to a multiplicative constant, and we have a good control of the asymptotic decay on both sides, $x \to \pm\infty$. Thus, we are able to prolongate the monotonicity properties to any $c \in (c_*, c^*)$, as in the proof of Theorem 2.8. There, it is more convenient to handle the case $V \ni c$ directly, *i.e.* dealing with arbitrary small velocities in the moving frame. This can be treated as in the Appendix of the proof of Theorem 2.8, by paying attention to the (singular) contribution of small velocities.

Lastly, with the monotonicity property of ρ_+ and ρ_-, we deduce that N is increasing, which is the appropriate monotonicity for our purpose. Also, we deduce that $\partial_x S$ changes sign only once. However it may not be at $x = 0$. The last step consists in varying c such as to satisfy $\partial_x S(0) = 0$ (see the proof of Theorem 2.14 in the macroscopic case). For this, we recall the extremal properties (2.54). Indeed, as $c \to c_*$, $\lambda_+ \to 0$, whereas λ_- remains uniformly strictly positive. Hence, the maximum point of S is shifted to $+\infty$. On the other hand, as $c \to c^*$, the maximum point of S is shifted to $-\infty$. By continuity, there exists $c \in (c_*, c^*)$ such that the maximum point is located at $x = 0$. This concludes the proof of Theorem 2.8. ◂

2.3. Conclusion and open problems.

We have investigated stationary states and travelling waves of chemotactic bacteria in various cases, corresponding to various sets of experiments. Interestingly, kinetic models enable to shed light on the mesoscopic structure of bacterial travelling waves. Theorems 2.14 and 2.15 are only preliminary steps of a larger research program. The success of this research program will be facilitated by the possible reduction of the problems to simple cases: from the mesoscale to the macroscale through the diffusion limit, from the propagating waves to the stationary cluster via ignoring the nutrient. Here are few open problems that may be of great interest from a mathematical and a modelling point of views.

Open Problem(s) 2.17

(1) In all previous statements, we have assumed *a priori* that $\partial_x S$ changes sign only once, and construct ρ accordingly. Prove that it is necessarily the case. Alternatively speaking, multimodal solutions are not admissible.

(2) The speed c in Theorem 2.14 is uniquely determined by the relation (2.43). Prove that the same holds true for the mesoscopic model in Theorem 2.15.

(3) Investigate the stability of clusters/travelling waves at the macroscopic and the mesoscopic levels.

[13] In fact, the case $c \neq 0$ is equivalent to considering an asymmetrical velocity set $\widetilde{V} = V - c$.

(4) One of the main drawback of the velocity-jump process (2.48) is that the transduction of a change in the signal concentraion S ranges over seconds [**SBB86**]. It is significantly longer that the mean run duration. Thus, setting the tumbling rate as a function of the instantaneous time variation of the signal as in (2.49) is not reasonable. This can be overcome by introducing internal state variables that accounts for the transduction of the external signal through some protein network. Relatively simple models are available in the literature [**EO05**, **XHPE10**, **Xue13**, **PTV15**], but they include an additional level of description. The same questions as above are completely open for this kind of multiscale models (existence of clusters/travelling waves, etc.).

CHAPTER 3

Propagation phenomena at the mesoscale

This chapter presents the contents of articles [4], [2], [5], [3], [6], written in collaboration with E. Bouin, N. Meunier, S. Mirrahimi, B. Perthame, G. Raoul, R. Voituriez, and G. Nadin.

Sections 3.1, 3.2 and 3.3 are part of E. Bouin's PhD thesis.

Summary

{3.1} Reaction-transport equations are analysed as a model for investigating kinetic travelling waves, in analogy with reaction-diffusion travelling waves. {3.1.1} Trajectories are not biased, but logistic growth of the population is included. The diffusive limit yields the Fisher-KPP equation. {3.1.2} In the case of bounded velocities, existence of travelling waves, together with stability and spreading properties, are proven for the mesoscopic model, without any perturbative argument. {3.1.3} The front accelerates in the case of unbounded velocities. Quantitative spreading is established in the Gaussian case.

{3.2} The analogy between reaction-transport equations and dynamics of populations structured by dispersal motivates the study of mutation-selection-diffusion equations. {3.2.1} A minimal model accounting for mutation-selection in an invasion front where the phenotypical trait influences dispersal is presented. {3.2.2} In the case of bounded dispersal, existence of travelling waves is established, despite the lack of maximum principle. {3.2.3} The front is expected to accelerate when dispersal can take arbitrarily large values.

{3.3} The approximation of geometric optics is a powerful tool to derive quantitative informations about spreading, {3.3.1} as shown for the Fisher-KPP equation. {3.3.2} This methodology is applied to the reaction-transport equation in the case of bounded velocities. It involves homogenization with respect to velocity. {3.3.3} On the contrary, there is no such homogenization in the case of unbounded velocities. Appropriate rescaling yields a non local kinetic Hamilton-Jacobi equation in the limit. Computation of the fundamental solution permits to capture quantitative features of the acceleration mechanism. {3.3.4} The same methodology cannot be directly transferred to mutation-selection-diffusion problems, because of the lack of maximum principle. Heuristics, together with spatially heterogeneous adaptive dynamics are presented formally.

{3.4} Two future directions of research are depicted: {3.4.1} the analysis of subdiffusive processes using models structured with respect to residence time; {3.4.2} evolution in age-structured populations, with a focus on maladaptation to a changing environment.

3.1. Reaction-transport equations

During the course of my research, I faced the difficulty of proving the existence of travelling waves for the kinetic model (2.48), now Theorem 2.15. At that time, it was natural to investigate a similar

problem, that involves the analysis of travelling waves in a multiscale problem of kinetic type. This was the main subject of E. Bouin's PhD thesis. The hope was to gain some insight about the analysis of chemotactic travelling bands. Meanwhile, we realized that the kinetic model we were studying may drastically differ from its diffusion limit, especially concerning the propagation of travelling waves. This was subject to a new direction of investigation.

3.1.1. Model. Reaction-diffusion equations, as the celebrated Fisher-KPP equation, have been extensively studied in mathematical biology. They have remarkable spreading properties, characterized by the particular travelling wave solutions. Hence, it was natural to analyse a kinetic substitute for the Fisher-KPP equation. As opposed to the chemotaxis equation (2.1), the velocity-jump process is unbiased, *i.e.* all directions are equally favorable. However, the population is assumed to increase by cell division, following a logistic growth law[1].

$$\underbrace{\partial_t f(t,x,v) + v\partial_x f(t,x,v)}_{run} = \underbrace{\rho(t,x)M(v) - f(t,x,v)}_{tumbling} + \underbrace{r\left(\rho(t,x)M(v) - \rho(t,x)f(t,x,v)\right)}_{saturated\ growth}, \tag{3.1}$$

where $\rho(t,x) = \int_V f(t,x,v')\,dv'$ denotes the macroscopic density of individuals. The reorientation process is much simpler than in the previous chapter: the tumbling rate is constant (renormalized to one), and post-tumbling velocities are chosen randomly following a given symmetrical distribution $M(v)\,dv$. New individuals are created with rate $r > 0$, and choose their velocity at random following the same distribution $M(v)\,dv$. Finally, there is a quadratic saturation term, mimicking the classical logistic saturation of growth. The stationary state of the reaction part is $f \equiv M(v)$. It is worth noticing that the diffusion limit $(t,x,r) \to (t/\varepsilon^2, x/\varepsilon, r\varepsilon^2)$ yields the classical Fisher-KPP equation for the macroscopic density ρ as $\varepsilon \to 0$, provided the variance of M is finite,

$$\partial_t \rho = \theta\partial_x^2\rho + r\rho(1-\rho)\,, \quad \theta = \int v^2 M(v)\,dv\,. \tag{3.2}$$

A key quantity in the forthcoming analysis is the support of the distribution M. We define $V = \operatorname{supp} M$. We assume henceforth that, either V is a symmetric interval, or $V = \mathbb{R}$.

3.1.2. Existence of travelling waves and spreading properties in the case of bounded velocities. The existence of travelling waves for reaction-transport equations as (3.1) was addressed in [**Sch00**] for a slightly different problem[2]. More recently, in [**CHS12**], the authors used a perturbative argument, called micro-macro decomposition, in order to construct travelling waves for (3.1) close to the diffusive regime. The following result is contained in [**6**]. It resolves the problem of linear spreading for solutions of (3.1) in a nonperturbative setting.

Theorem 3.1: Existence of travelling waves for bounded velocities [6]

Assume that $d = 1$. Assume that the velocity set V is compact, and that $M \in \mathcal{C}^0(V)$. There exists a travelling wave solution $f(t,x,v) = g(x - c_* t, v)$ of (3.1). The speed is given by $c_* = \min\{c(\lambda) : \lambda \in \mathbb{R}_+^*\}$, where $c(\lambda)$ is implicitly given as a solution of the dispersion relation

$$(1+r)\int_V \frac{M(v)}{1+\lambda(c(\lambda)-v)}\,dv = 1\,. \tag{3.3}$$

Moreover, take any initial datum f_0 which satisfies $(\forall (x,v) \in \mathbb{R}\times V)\ 0 \le f_0(x,v) \le M(v)$, $(\forall x \ge R)\ f_0(x,v) = 0$ and $(\forall x \le -R)\ f_0(x,v) \ge \delta M(v)$ for $\delta, R > 0$ resp. small and large enough. Then the solution of (3.1) with initial datum f_0 spreads asymptotically linearly with speed c_*, in a weak sense.
In addition the travelling wave solution is stable in some weighted L^2 space.

[1] Other choices are possible, but we will restrict here to the logistic growth for the sake of simplicity.

[2] Notice that Equation (1) in [**Sch00**] coincides with (3.1). However the author performs some solution-dependent change of time which makes Equation (4) not equivalent to (3.1).

A similar result was obtained previously in [5], in the case of two velocities $M = \frac{1}{2}(\delta_{-\nu} + \delta_\nu)$[3]. However, there is some discrepancy between the result stated in Theorem 3.1 and those contained in [5], due to the singularity of the distribution M. In the latter, two regimes have to be distinguished, namely $r < 1$ (parabolic regime) and $r \geq 1$ (hyperbolic regime). In the case $r \geq 1$ the travelling wave with minimal speed vanishes on a half-line. There, the speed of the wave is not characterized by the linearized problem for $f \ll 1$, on the contrary to Theorem 3.1. Note that this case is not contained in the statement of Theorem 3.1 since it is assumed that $M \in \mathcal{C}^0(V)$. This makes a clear difference between the case of a measure M which is absolutely continuous with respect to the Lebesgue measure, and the case of a measure with atoms.

▸ *Sketch of proof.* The main observation is the following: as in the Fisher-KPP equation, the travelling front is of *pulled* type. The dynamics are driven by the linearized problem in the asymptotic regime $f \ll 1$ (after removal of the quadratic term in (3.1)). As in the proof of Theorem 2.15, we make the following ansatz for the linearized problem: $f(t,x,v) = e^{-\lambda(x-c(\lambda)t)}F_\lambda(v)$. Then F_λ is solution of the following spectral problem

$$\left\{ \begin{array}{l} \lambda c(\lambda) F_\lambda(v) - v\lambda F_\lambda(v) + F_\lambda(v) = M(v) \displaystyle\int_{v'\in V} F_\lambda(v')\,dv', \\ F_\lambda \in L^1(V), \quad (\forall v \in V)\ F_\lambda(v) \geq 0. \end{array} \right. \tag{3.4}$$

This is explicitly solvable. In particular the eigenvalue $\lambda c(\lambda)$ is given as a solution of the implicit relation (3.3). It is worth noticing that the condition $F_\lambda \geq 0$ rules out the case of unbounded velocities, because of the nonlinear dependency on velocity v.

Then, we proceed as for the Fisher-KPP equation, using monotonicity properties and the maximum principle which holds true for (3.1) provided that $0 \leq f \leq M$. Let $c > c_*$. The function $\overline{f}(x,v) = \min\{M(v), e^{-\lambda x}F_\lambda(v)\}$ is clearly a supersolution of (3.1) provided that F_λ solves the spectral problem (3.4). On the other hand there exist $\gamma, A > 0$, resp. small and large enough such that $\underline{f}(x,v) = \max\{0, e^{-\lambda x}F_\lambda(v) - Ae^{-(\lambda+\gamma)x}F_{\lambda+\gamma}(v)\}$ is a subsolution.

Consider the solution of (3.1) with the initial datum $f_0 = \overline{f}$. The maximum principle guarantees that $f(t, x-ct, v)$ is sandwiched between $\overline{f}(x,v)$ and $\underline{f}(x,v)$. Moreover it is nonincreasing with respect to space and time. Finally it is uniformly Lipschitz continuous with respect to space, and velocity. Spatial regularity is obtained by propagating the log-Lipschitz regularity of the initial datum $\overline{f}$ through time $t > 0$ using a comparison argument. Velocity regularity is obtained by differentiating (3.1) with respect to v, and multiplying by $\mathrm{sign}(\partial_v f)$ as follows,

$$\partial_t|\partial_v f| + v\partial_x|\partial_v f| + (1+r\rho)|\partial_v f| \leq (1+r)|\partial_v M|\rho + |\partial_x f|.$$

Clearly the constant $(1+r)\sup_V |\partial_v M| + \sup_{\mathbb{R}_+\times\mathbb{R}\times V}|\partial_x g|$ is a supersolution of this inequality, therefore it enables to bound $|\partial_v f|$ from above.

Finally, passing to the limit as $t \to +\infty$, the existence of a travelling wave $g_c(x,v) = \lim_{t\to+\infty} f(t, x-ct, v)$ is proven. Then, passing to the limit $c \to c_*$ enables to prove existence of a travelling wave with minimal speed c_*. ◂

3.1.3. Acceleration in the case of unbounded velocities. The restriction to compact velocity sets in Theorem 3.1 is not a technical condition. In [6] we also proved infinite spreading speed under the condition $(\forall v \in \mathbb{R})\ M(v) > 0$. As a corollary there cannot exist travelling waves in the case of unbounded velocities. Clearly, the rate of propagation depends on the tail of the velocity distribution M. We prove that the front spreads as $X(t) = \mathcal{O}(t^{3/2})$ in the case of a Gaussian function. This was announced independently in [MCGP10] using formal analysis.

Theorem 3.2: Superlinear propagation for a Gaussian distribution [6]

[3] The so-called reaction-telegraph equation, see [Had88, GR97, Had99, MFF99, Fed99, FM99, MFH10]

Let $M(v) = \frac{1}{\sqrt{2\pi}} \exp\left(-\frac{v^2}{2}\right)$, defined for $v \in \mathbb{R}$. Let $f_0 \in L^\infty(\mathbb{R}\times V)$ such that $0 \le f_0(x,v) \le M(v)$ for all $(x,v) \in \mathbb{R}\times V$. The two following statements hold true.

(1) Assume that there exist $1 \le b \le a$ such that

$$(\forall (x,v) \in \mathbb{R}\times V) \quad f_0(x,v) \le \frac{1}{b} M\left(\frac{x}{b}\right) M(v) e^{ra}\,.$$

Let f be the solution of the Cauchy problem (3.1). Then for all $\varepsilon > 0$, one has

$$\lim_{t\to+\infty} \left(\sup_{|x| \ge (1+\varepsilon)(2r)^{1/2} t^{3/2}} \rho(t,x) \right) = 0\,.$$

(2) Assume that there exists $\gamma \in (0,1)$, and $R \in \mathbb{R}$ such that

$$(\forall x < -R)\ (\forall v \in V) \quad f_0(x,v) \ge \gamma M(v)\,.$$

Let f be the solution of the Cauchy problem (3.1). Then for all $\varepsilon > 0$, one has

$$\lim_{t\to+\infty} \left(\inf_{x \le (1-\varepsilon)\left(\frac{r}{r+2}t\right)^{3/2}} \rho(t,x) \right) \ge 1-\gamma\,.$$

REMARK 3.3. *Remarkably, Theorem 3.2 seems to be in contradiction with the diffusion limit of (3.1). Indeed, the Fisher-KPP equation (3.2) for which there is finite speed of spreading. In fact, the diffusion limit and the long time asymptotics do not commute: if ε denotes some small parameter that yields the diffusion limit as $\varepsilon \to 0$, then the solution spreads asymptotically as $\mathcal{O}(t^{3/2})$ for any $\varepsilon > 0$, but it spreads as $\mathcal{O}(t)$ "at $\varepsilon = 0$". This is an obstacle to using a perturbative approach in order to investigate travelling waves for (3.1) in the case of unbounded velocities. The reason is that the spreading is driven by the exponentially small densities that are not captured in the diffusion limit.*

▸ *Sketch of proof.* The first item is proven via calculations of convolutions of gaussian functions. The main motivation comes from the classical Fisher-KPP equation, for which the function

$$\overline{\rho}(t,x) = \exp\left(-\frac{x^2}{4t}\right) e^{rt}\,,$$

is the fundamental solution of the linearized equation. Thus it is a good candidate for being a supersolution of the nonlinear problem, since a nonpositive quadratic term has been removed. In our case, we make a similar guess for the macroscopic density

$$\rho(t,x) \le M\left(\frac{x}{t+a}\right) e^{r(t+a)}\,. \tag{3.5}$$

Then we plug the right hand side of (3.5) into the Duhamel formula corresponding to the linearized problem,

$$\overline{f}(t,x,v) = f_0(x-vt,v)e^{-t} + \int_0^t (1+r) M(v) \left(M\left(\frac{x-v(t-s)}{s+a}\right) e^{r(s+a)} \right) e^{-(t-s)} ds\,.$$

To conclude, it is sufficient to prove that the macroscopic density $\overline{\rho}(t,x) = \int_{\mathbb{R}} \overline{f}(t,x,v)\,dv$ verifies the initial guess (3.5). We see immediately that this technical estimate relies on the calculation of convolutions of gaussian functions, and more precisely on the following bound,

$$(\forall x \in \mathbb{R})\ (\forall s \in (0,t)) \quad \int_V M(v) M\left(\frac{x-v(t-s)}{s+a}\right) dv \le M\left(\frac{x}{t+a}\right)\,. \tag{3.6}$$

The second item is very much inspired from [**Gar11**]. There, the author investigated the nonlocal Fisher-KPP equation,

$$\partial_t \rho = J * \rho - \rho + r\rho(1-\rho)\,, \tag{3.7}$$

where J is some fat-tailed convolution kernel that replaces the diffusion operator. There, the accelerating behaviour of the front is under-estimated using some ad-hoc subsolution which behaves asymptotically as $J(x)e^{(r-\varepsilon)t}$ (roughly speaking).

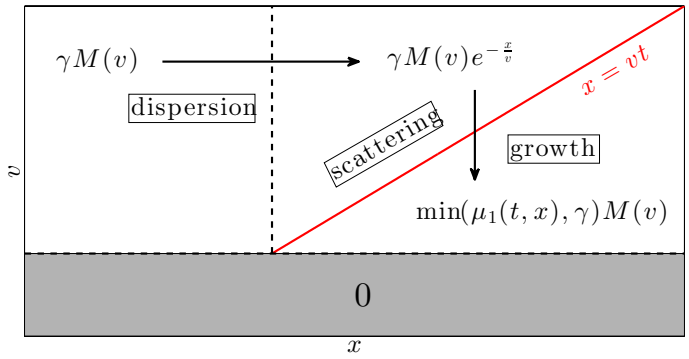

FIGURE 3.1. Schematic view of the construction of the subsolution as in the proof of Theorem 3.2. It is defined piecewise. The mechanism which drives the subsolution can be described as follows. The free transport operator sends very few particles with very high velocity at the edge of the front. They are redistributed to lower velocities, while the local mass grows exponentially fast. The mass in the lower branch $\{v < x/t\}$, $\mu_1(t,x)$, is computed analytically.

In our case, we expect that the solution will grow at least as $\exp(-C|x|^{2/3})e^{rt}$ (roughly speaking). More precisely, we distinguish between large velocities $v > x/t$ and small velocities $v < x/t$. Large velocities have a density of at least $\gamma M(v)e^{-x/v}$, provided that the solution is sustained at a density above $\gamma M(v)$ at $x = 0$, for some arbitrary $\gamma \in (0,1)$. This is a consequence of the fast spreading of large velocities far away. Then the small density of large velocities scatters. Accordingly, the density is redistributed to smaller velocities. It also grows exponentially fast due to the linear growth term. When estimating the macroscopic density of the subsolution, we distinguish between the partial mass of large velocities,

$$\mu_2(t,x) = \gamma \int_{\{v>x/t\}} M(v)e^{-x/v}\,dv \approx \exp\left(-\min_{\{v>x/t\}}\left(\frac{v^2}{2}+\frac{x}{v}\right)\right), \tag{3.8}$$

and the partial mass of small velocities,

$$\partial_t \mu_1 + \mu_1 = (1+r)(\mu_1+\mu_2), \tag{3.9}$$

The former contains the spatial dispersion $\exp(-C|x|^{2/3})$, as the minimum of $\frac{v^2}{2}+\frac{x}{v}$ over $v > 0$ is $\frac{3}{2}x^{2/3}$. The latter takes into account the exponential growth that levels up the macroscopic density. Note that μ_2 acts as a source term in (3.9), so as to initiate the spreading. ◂

The extension to more general distributions $M(v)$ has not been done yet. Clearly, the Gaussian distribution facilitates the technical estimates.

This result should be compared to similar results obtained in variants of the macroscopic Fisher-KPP equations, where accelerating phenomena occur. We refer to [**Gar11**] for the analysis of (3.7). Also, the fractional Fisher-KPP equation has raised a lot of interest recently, see [**CR09**, **CR12**, **CR13**, **MM15**],

$$\partial_t \rho + (-\partial_x^2)^\alpha \rho = r\rho(1-\rho).$$

There, propagation occurs exponentially fast, whatever is the exponent of fractional diffusion.

Open Problem(s) 3.4

(1) It is not very difficult to deduce heuristically the rate of spreading from the tail of the distribution M. To which extent the behaviour at infinity is enough to drive the propagation, rather than the exact form of M?

(2) Does there exist a particular accelerating wave solution, *e.g.* in some self-similar variables? A weaker result would consist in characterizing the typical length scales of the front, as it is expected to widen as $t \to +\infty$ [**RT15**].

(3) The Brunet-Derrida conjecture concerns the spreading speed of a finite system of particles which is a discrete stochastic version of the Fisher-KPP equation [**BD97**, **BD01**]. Alternatively, it concerns the influence of an additive noise term on the Fisher-KPP equation. The conjecture says that the correction of the spreading speed due to the stochasticity is surprisingly big, of the order of $(\log N)^{-2}$ (or $(\log \varepsilon)^{-2}$ if ε denotes the amplitude of the noise). It was proven rigorously in [**MMQ11**] and in [**BG10**]. What about a similar result for branching velocity-jump processes? Let me refer to recent results by J. Bérard and P. Maillard who deal with a finite system of branching particles that makes spatial jumps according to some distribution kernel with regularly varying tails (fat tailed) [**BM14**]. This elucidates the finite (noisy) counterpart of the fractional diffusion Fisher-KPP equation.

3.2. Selection-mutation-diffusion waves for the evolution of dispersion

The interplay between evolutionary processes and spatial heterogeneities has a long history in theoretical biology. In this section, we provide some mathematical contribution to the analysis of dispersal evolution, a major topic in evolutionary biology [**LMLNC03**, **Ron07**, **TMB+12**, **CBBB12**]. There, the relevant phenotypic trait to consider is the dispersal ability of individuals. We will focus on the refined analysis of the phenotypic structure of an invasion front, subjet to dispersal evolution. This clearly mixes ecological and evolutionary processes. We shall not model sophisticated dispersal strategies, nor complex ecological interactions. However, we shall keep as far as possible the multiscale nature of the problem, without separating timescales. Indeed, it has been reported that both ecological and evolutionary processes can arise over similar time scales [**TBW+01**, **PBWS06**, **Le13**].

An evolutionary spatial sorting process was described in [**SBP11**]. It is specific to dispersal evolution during species' invasion. Intuitively, individuals with higher dispersal reach farther area where they produce offsprings having possibly higher dispersal abilities. Based on numerical simulations of an individual-based model, it was predicted that this process generates biased phenotypic distributions towards higher dispersive phenotypes at the expanding margin [**TD02**, **SBP11**]. As a by-product, the front accelerates. This happens at least transiently, before the evolutionary process stabilizes. Biological evidence of biased distributions and accelerating fronts have been reported in the literature [**TBW+01**, **PBWS06**].

From the mathematical viewpoint, the framework is quite similar to the reaction-transport problem presented in Section 3.1. Indeed, the wave of invasion is structured with respect to dispersal ability, whereas it is structured with respect to velocity in (3.1). Changing of velocity after tumbling is replaced with a possible change in phenotype (dispersal ability) through mutations after each generation. The main disparity is the lack of heritability in (3.1) with respect to the structure variable v: the velocity of offsprings is not correlated with the velocity of the parents. An important mathematical difference is the lack of maximum principle for the forthcoming model.

3.2.1. Model. A minimal mathematical model was proposed in [**1**], based on previous works [**DFP04**, **CM07**, **PDA11**]. The density of individuals $f(t, x, \theta)$ is structured by space x and

dispersal ability $\theta > 0$[4],

(3.10)
$$\frac{\partial f}{\partial t}(t,x,\theta) - \theta \frac{\partial^2 f}{\partial x^2}(t,x,\theta) = r\alpha \frac{\partial^2 f}{\partial \theta^2}(t,x,\theta) + r f(t,x,\theta)(1-\rho(t,x))\,, \quad t>0\,,\ x\in\mathbb{R}\,,\ \theta\in(\theta_{\min},\theta_{\max})\,,$$

where $\rho(t,x) = \int f(t,x,\theta')\,d\theta'$ is the macroscopic density. The model is supplemented with Neumann boundary conditions in θ.

Asexual reproduction is considered here for the sake of simplicity. As compared to (3.2) the additional term $r\alpha\partial_\theta^2 f$ represents mutations, *i.e.* unbiased "displacement" in the phenotypic space. At each generation, offsprings inherit the trait of their parents up to a small symmetric variation due to mutations: in the limit where the variance of the mutation kernel vanishes variance, one gets a diffusion process.

The analogy with the kinetic equation (3.1) is illuminating: the free transport operator $\partial_t f + v\partial_x f$ is replaced with the "free diffusion operator" $\partial_t f - \theta\partial_x^2 f$; tumbling (change of the velocity) is analogous to mutation (change of the dispersal ability). One noticeable difference however is the lack of a comparison principle for (3.10) as opposed to (3.1). This makes a huge difference in the mathematical analysis since the toolbox developed for the Fisher-KPP equation (3.2) very much relies on comparison arguments.

Existence of travelling waves for reaction-diffusion equations lacking the maximum principle due to the presence of nonlocal terms has raised a lot of interest recently [**BNPR09**, **ACR13**]. I emphasize that (3.10) has an additional level of difficulty since the mesoscopic variable θ acts on higher-order derivatives, exactly as for kinetic equations.

Equation (3.10) belongs to a larger class of problems in spatial dynamics of a structured populations [**LMP13**]. Such problems have raised a lot of interest in the past decade. They arise naturally when modelling the niche expansion of a species, or, on the contrary, the maintenance of a species' range; the adaptation of a population to a shifting environment [**KB97**, **MR13**, **CB13**, **ACR13**, **BJS14**]; the evolution of an invasive population structured by dispersal ability [**DFP04**, **CM07**, **OGB13**], [**1**, **4**]; propagation of an epidemic when individuals are structured with respect to their age of infection [**DM09**, **DMR10**]; drug resistance in a spatially heterogeneous environment [**LLC+15**].

A research program for analysing the dynamics of (3.10) was outlined in [**4**]. The remainder of this section, together with the next one, aim to present the main features of this program.

3.2.2. Existence of travelling waves for bounded dispersion. In [**4**] it was postulated that in the case of bounded θ ($\theta_{\max} < +\infty$), there exists a travelling wave solution to (3.10). The minimal speed c_* is given by an associated spectral problem in the diffusion variable θ, as in the proof of Theorem 3.1. This statement was rigorously established in [**3**].

Theorem 3.5: Existence of travelling waves [3]

Assume $\theta \in (\theta_{\min},\theta_{\max})$, $0 < \theta_{\min} < \theta_{max} < +\infty$. There exists a travelling wave solution $f(t,x,\theta) = g(x - c_* t,\theta)$ of (3.10). The speed is given by $c_* = \min\{c(\lambda) : \lambda \in \mathbb{R}_+^*\}$, where $\lambda c(\lambda)$ is the dominant eigenvalue of the following spectral problem

(3.11)
$$\begin{cases} \left(-\lambda c(\lambda) + \theta\lambda^2 + r\right) Q_\lambda(\theta) + r\alpha\partial_{\theta\theta}^2 Q_\lambda(\theta) = 0\,, \\ \partial_\theta Q_\lambda(\theta_{\min}) = \partial_\theta Q_\lambda(\theta_{\max}) = 0\,, \quad (\forall\theta)\ Q_\lambda(\theta) \geq 0\,. \end{cases}$$

[4]Here, dispersal ability is simply modelled as a diffusion coefficient which encodes the features of individual dispersal.

▸ *Sketch of proof.* The proof is very much inspired from [**BNPR09**] and [**ACR13**]. It is based on a topological degree argument, in order to circumvent the lack of comparison principle. A simplifying observation is that one can easily reduce to the classical Fisher-KPP equation by continuously transforming the spatial diffusion coefficient $(\tau,\theta)\mapsto(1-\tau)\theta+\tau\theta_{\min}$, for $\tau\in[0,1]$, without affecting the main estimates.

The key *a priori* estimate reads as follows: let $g(z,\theta)$ be a solution of the stationary problem (3.10) in the moving frame $z=x-ct$,

$$-c\partial_z g-\theta\partial_{zz}g=\alpha\partial_{\theta\theta}g+rg(1-\mu)\,,\quad \mu(z)=\int g(z,\theta')\,d\theta'\,. \tag{3.12}$$

Assume that c is a given parameter (some *a priori* bound of c is required, but this is another story). Then $g\in L^\infty(\mathbb{R}\times(\theta_{\min},\theta_{\max}))$. The argument invokes a partial maximum principle in combination with elliptic Sobolev regularity. Assume that g attains its maximum at (z_0,θ_0). Denote by $K_0=g(z_0,\theta_0)$ the maximum value. Then the maximum principle for (3.12) implies that $\mu(z_0)=\int g(z_0,\theta')\,d\theta'\le 1$. Hence, we get automatically a L^1_θ estimate (with respect to θ), but we are seeking a L^∞_θ estimate. Therefore, it is sufficient to get some partial regularity with respect to the variable θ only, in order to control the L^∞_θ norm with the L^1_θ norm using a suitable interpolation inequality.

Partial regularity with respect to θ is obtained thanks to a trace inequality. Firstly, we test a localized version of (3.12) against g. Using the negative sign of the quadratic saturation term, we deduce that

$$\|g\|_{H^1}\le C(\theta_{\min},\theta_{\max})K_0\,.$$

Secondly, we test a localized version of (3.12) against $(-\partial^2_\theta g)$. Integrating by part, and using that μ is independent on θ[5] and nonnegative, we obtain that

$$\|\partial_\theta g\|_{H^1}\le C(\theta_{\min},\theta_{\max})K_0\,.$$

Therefore the partial function $g(z_0,\cdot)$ belongs to $H^{3/2}(\theta_{\min},\theta_{\max})$ by the trace inequality. We conclude by using interpolation of $L^\infty(\theta_{\min},\theta_{\max})$ between $L^1(\theta_{\min},\theta_{\max})$ and $H^{3/2}(\theta_{\min},\theta_{\max})$,

$$\|g(z_0,\cdot)\|^3_{L^\infty_\theta}\lesssim\|g(z_0,\cdot)\|_{L^1_\theta}\|g(z_0,\cdot)\|^2_{H^{3/2}_\theta}\,,$$
$$K_0^3\lesssim\times 1\times K_0^2\,.$$

This proves uniform boundedness of g. We refer to [**3**] for a complete proof of Theorem 3.1. As in the proof of Theorem 3.1, the spectral problem (3.11) arises when plugging the ansatz $f(t,x,\theta)=e^{-\lambda(x-c(\lambda)t)}Q_\lambda(\theta)$ into (3.10). Thus, $Q_\lambda(\theta)$ represents the distribution of phenotypes at the edge of the front. ◂

The previous result presents some interesting qualitative conclusions. Interestingly, the sorting effect at the edge of the front predicted in [**SBP11**] is rigorously proven for this equation. Indeed, the phenotypical distribution of individuals at the edge of the front, $Q_{\lambda^*}(\theta)$, is increasing with respect to θ. In addition it converges towards a dirac mass at $\theta_{\max}$ as the mutation rate $\alpha\to 0$ (see [**4, 3**]).

A more comprehensive analysis was performed by Turanova in [**Tur15**]. Using a different approach based on Schauder elliptic regularity estimates, she was able to prove uniform L^∞ bound for the Cauchy problem.

3.2.3. Acceleration in the case of unbounded dispersal. An intuitive consequence of selection of higher dispersal by spatial sorting at the edge of the front , is that the front should accelerate when θ can be arbitrarily large. This statement is motivated by formal quantitative computations in [**4**], see Section 3.3.3.5 for a sketchy presentation. The front is expected to spread as $\mathcal{O}(t^{3/2})$. The rigorous proof was announced by N. Berestycki, C. Mouhot and G. Raoul [**BMR15**], but for a different saturation term.

[5]This crucial observation enables to integrate by parts with respect to θ only, without impacting the sign of the negative quadratic saturation term.

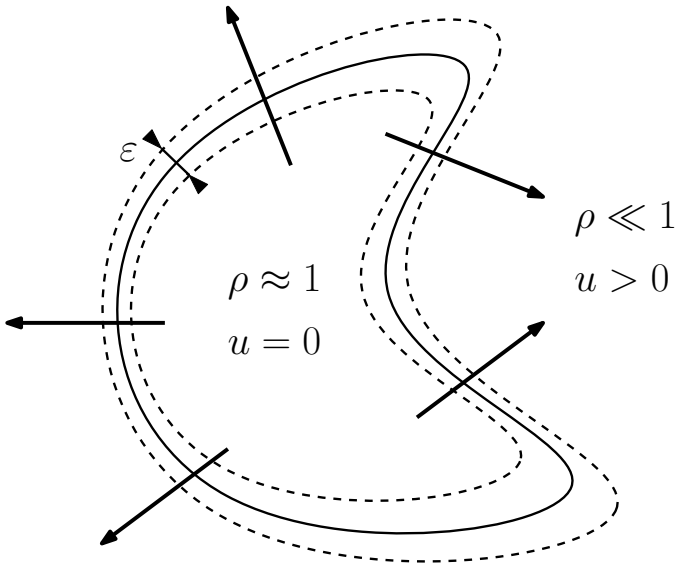

FIGURE 3.2. Approximation of geometric optics. After a wide spatial rescaling, the typical size of the transition front becomes of order ε. Front propagation is encoded in the dynamics of a level set function u.

3.3. The approximation of geometric optics

The results in the previous two sections guarantee the existence of multiscale travelling waves. Furthermore, they provide some quantitative features such as the minimal speed of propagation, and the distribution with respect to the mesoscopic variable (velocity, dispersal) at the edge of the front. Beyond these theoretical results, it is challenging to perform some asymptotic analysis in order to catch the dynamics of the Cauchy problem. This is particularly interesting when travelling wave solutions do not exist, as it is the case when the front is accelerating. This asymptotic analysis enables to gain more insight that can be transferred back to the analysis of the full models.

The approximation of geometric optics is a powerful tool for studying of propagation phenomena in reaction-diffusion equations [**Fre86**, **ES89**, **Xin00**]. The goal is to analyse the propagation in the limit of long time and large space scales, where the typical length scale of the front vanishes. Thus, the location of the front is reduced to a level set function (Figure 3.2). The dynamics of this level set function are given by a Hamilton-Jacobi equation that has to be solved in the viscosity sense. Obviously, the time/space rescaling must be adapted to the spreading features of the problem.

Extending this toolbox to multiscale models of structured populations can bring quantitative answers to some theoretical biology problems.

3.3.1. Asymptotic analysis of the Fisher-KPP equation. It is well-known that the propagation dynamics in *pulled fronts* is driven by the dynamics of low density populations at the edge of the front. Accordingly, the minimal speed of propagation is determined by the linearized problem, as in Theorems 3.1 and 3.5. This was systematized by Freidlin who used the probabilistic theory of large deviations to characterize the propagation in the asymptotic scaling limit $(t, x) = (t'/\varepsilon, x'\varepsilon)$ as $\varepsilon \to 0$ [**Fre86**]. This approach was reformulated with PDE tools by Evans and Souganidis based on

the theory of viscosity solutions [ES89]. The Fisher-KPP equation writes after rescaling[6],

$$\varepsilon\partial_t\rho^\varepsilon = \varepsilon^2\theta\partial_x^2\rho^\varepsilon + r\rho^\varepsilon(1-\rho^\varepsilon)\,, \tag{3.13}$$

where $\theta, r > 0$ are resp. the diffusion coefficient of individuals and the reproduction rate. It was proven in [ES89] that the function $u^\varepsilon(t,x) = -\varepsilon\log\rho^\varepsilon(t,x)$ converges uniformly, as $\varepsilon\to 0$, towards the viscosity solution of the following Hamilton-Jacobi equation

$$\min\left(\partial_t u + \theta|\partial_x u|^2 + r\,,\, u\right) = 0\,. \tag{3.14}$$

The constraint $u \geq 0$ comes from the saturation effect of the logistic growth in (3.2) that ensures $\rho \leq 1$ by the maximum principle. The contribution $\partial_t u + \theta|\partial_x u|^2 + r = 0$ is the transcription of the linear problem in the vanishing viscosity limit $\varepsilon \to 0$.

Then, the location of the front is determined by the level set function $u(t,x)$. More precisely, we have $\rho^\varepsilon \to 0$ uniformly on the compact subsets of $\{u > 0\}$; and $\rho^\varepsilon \to 1$ uniformly on the compact subsets of $\mathrm{Int}\{u = 0\}$, as $\varepsilon \to 0$.

From the mathematical point of view, Hamilton-Jacobi equations such as (3.14) enables to derive quantitative results as they contain only first-order derivatives. For instance, they can be handled with the method of characteristics. This is one of the main purpose of this asymptotic analysis.

3.3.2. Asymptotic analysis of reaction-transport equations: bounded velocities. Together with E. Bouin, we have extended the previous methodology to (3.1), using the PDE toolbox of [ES89], together with techniques coming from the homogenization of Hamilton-Jacobi equations. It should be possible to perform the very same analysis using probabilistic tools from the theory of large deviations, but we did not follow this direction.

We set temporarily $r = 0$, so that we focus on spatial dispersion only. We make the hyperbolic scaling $(t,x) = (t'/\varepsilon, x'/\varepsilon)$, in accordance with the linear speed of propagation (Theorem 3.1) when $r > 0$. The new equation after rescaling reads:

$$\varepsilon\partial_t f^\varepsilon + \varepsilon v\cdot\nabla_x f^\varepsilon = \rho^\varepsilon(t,x)M(v) - f^\varepsilon(t,x,v)\,. \tag{3.15}$$

This is the so-called BGK equation in kinetic theory of gases.

Theorem 3.6: The approximation of geometric optics for bounded velocities [2]

Assume that $d = 1$. Assume that the velocity set V is compact, and $M \in \mathcal{C}^0(V)$. Assume the initial datum f_0^ε is well prepared in the following sense: $-\varepsilon\log\left(f_0^\varepsilon(x,v)/M(v)\right)$ converges uniformly towards some function $u_0(x)$ not depending on the velocity v as $\varepsilon\to 0$. Then $u^\varepsilon(t,x,v) = -\varepsilon\log\left(f^\varepsilon(t,x,v)/M(v)\right)$ converges (locally) uniformly towards a function $u(t,x)$ which does not depend on v. It is the viscosity solution of the following Hamilton-Jacobi equation,

$$\int_V \frac{M(v)}{1-\partial_t u(t,x) - v\partial_x u(t,x)}dv = 1\,, \tag{3.16}$$

under the condition that the denominator in (3.16) is nonnegative for all $v \in V$.

We refer to [2] for a complete proof of this Theorem. The proof relies on the perturbed test function method of Evans to deal with the loss of the velocity variable in the limit [Eva89]. This result can be interpreted as homogenization with respect to velocity which acts as the fast variable here. The spectral problem that leads to (3.16) is analogous to a cell problem. Compactness of V yields ergodicity with respect to velocity, and thus, velocity averaging. This is the reason why $u(t,x)$ does

[6] We drop the $'$ by a slight abuse of notations.

not depend on v in the limit. This will cease to be the case for unbounded velocities, see Section 3.3.3.

Notice that the left-hand-side of (3.16) is nondecreasing with respect to $\partial_t u$. Thus the Hamilton-Jacobi equation (3.16) can be recast into

$$\partial_t u(t,x) + H(\partial_x u(t,x)) = 0\,,$$

where the hamiltonian $H(p)$ is defined implicitly as

$$\int_V \frac{M(v)}{1+H(p)-pv}dv = 1\,. \tag{3.17}$$

It is convex and it grows linearly as $|p| \to +\infty$, namely $\|\nabla H\|_{L^\infty} \le \max V$. Equation (3.16) is the analogous of the quadratic Hamilton-Jacobi equation $\partial_t u(t,x) + \theta\,|\partial_x u(t,x)|^2 = 0$ derived from the diffusion equation after the same rescaling (Section 3.3.1).

REMARK 3.7. *It was noticed by J. Vovelle that the multidimensional version of* (3.16)*, where the term $v\partial_x u(t,x)$ is replaced with $v\cdot\nabla_x u(t,x)$ might not be well-posed, as there might not exist a real $H(p)$ solution of* (3.17) *under the condition $1+H(p)-p\cdot v \ge 0$. The correct limiting equation is under current investigation.*

The asymptotic limit for $r>0$ can be deduced from the previous analysis, as shown by Bouin in [**Bou15**][7]. It reads as follows,

$$\min\left(\partial_t u + H_r(\partial_x u), u\right) = 0\,,$$

where the Hamiltonian $H_r(p)$ is implicitly defined by

$$(1+r)\int_V \frac{M(v)}{1+H_r(p)-vp}dv = 1\,.$$

REMARK 3.8. *This result emphasizes the disparity between front propagation in reaction-transport equations, as compared to their diffusive counterparts. Indeed, the rescaling $(t,x) = (t'/\varepsilon, x'/\varepsilon)$ is not the same as for the diffusion limit*[8]*. It captures the dynamics of exponentially low densities, or equivalently the behaviour of exponentially small probabilities of moving at a certain distance starting from the origin, as in the theory of large deviations. These exponential tails of distributions dramatically differs from the diffusion limit. The discrepancy will even be stronger in the next section.*

3.3.3. Asymptotic analysis of reaction-transport equations: unbounded velocities. As in Section 3.1.3, the nonnegativity condition in (3.16) immediately rules out unbounded velocities, due to the linear dependency with respect to v. There are two main discrepancies: firstly the appropriate rescaling is not $(t,x) = (t'/\varepsilon, x'/\varepsilon)$ anymore, but it depends on the tails of the velocity distribution M. Secondly, the limiting function $u(t,x,v)$ keeps the velocity dependence, *i.e.* there is no averaging with respect to velocity.

3.3.3.1. *Appropriate rescaling in the Gaussian case.* Together with E. Bouin, E. Grenier and G. Nadin, we investigated thoroughly the case of a Gaussian velocity distribution, as in Theorem 3.2. As in Section 3.3.2, we begin with the case $r=0$. There, the appropriate rescaling is $(t,x,v) = \left(t'/\varepsilon, x'/\varepsilon^{3/2}, v'/\varepsilon^{1/2}\right)$, in accordance with the spreading rate of Theorem 3.2. The equation becomes

$$\partial_t f^\varepsilon(t,x,v) + v\partial_x f^\varepsilon(t,x,v) = \frac{1}{\epsilon}\left(M_\varepsilon(v)\rho^\varepsilon(t,x) - f^\varepsilon(t,x,v)\right), \quad t>0\,,\ x\in\mathbb{R}\,,\ v\in\mathbb{R}\,, \tag{3.18}$$

where M_ε is the Gaussian distribution function with variance ε, $M_\varepsilon(v) = \frac{1}{\sqrt{2\pi\varepsilon}}\exp\left(-\frac{v^2}{2\varepsilon}\right)$.

[7] Among many other results dealing with more general forms of the equation (3.1)

[8] The diffusion scaling would be $(t,x) = (t'/\varepsilon^2, x'/\varepsilon)$.

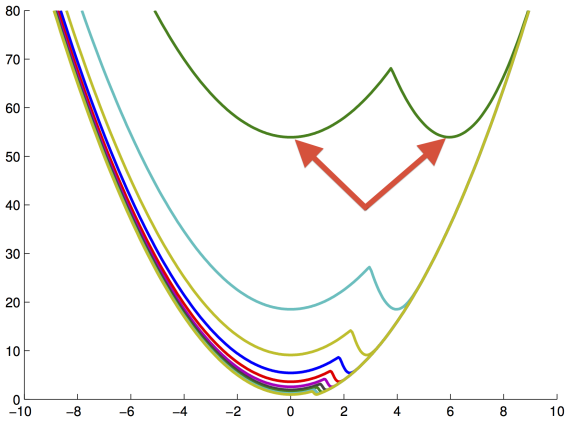

FIGURE 3.3. Time snapshots of the velocity profile for a given $x \in \mathbb{R}$. There are clearly two minimal points: the zero velocity, and a nonzero velocity that belongs to the unsaturated area, where $u < \min u + v^2/2$.

In order to catch the dynamics of exponentially small tails, the same logarithmic transformation as in (3.6) is useful, $u^\varepsilon(t,x,v) = -\varepsilon \log f^\varepsilon(t,x,v)$. The function u^ε satisfies

$$\partial_t u^\varepsilon(t,x,v) + v\partial_x u^\varepsilon(t,x,v) = 1 - \frac{1}{\sqrt{2\pi\varepsilon}} \int_{\mathbb{R}} \exp\left(\frac{u^\varepsilon(t,x,v) - u^\varepsilon(t,x,v') - v^2/2}{\varepsilon}\right) dv' . \tag{3.19}$$

3.3.3.2. *A non local Hamilton-Jacobi equation.* We were able to prove that u^ε converges locally uniformly towards the unique viscosity solution of the following non local Hamilton-Jacobi equation,

$$\begin{cases} \max\left(\partial_t u(t,x,v) + v\partial_x u(t,x,v) - 1, u(t,x,v) - \min\limits_{w\in\mathbb{R}} u(t,x,w) - \dfrac{v^2}{2}\right) = 0 , \\ \partial_t\left(\min\limits_{w\in\mathbb{R}} u(t,x,w)\right) \le 0 , \\ \partial_t\left(\min\limits_{w\in\mathbb{R}} u(t,x,w)\right) = 0 , \qquad \text{if } \operatorname*{argmin}\limits_{w\in\mathbb{R}} u(t,x,w) = \{0\} . \end{cases} \tag{3.20}$$

In fact, defining properly viscosity subsolutions and viscosity supersolutions of (3.20), and then proving the comparison principle that ensures uniqueness of the viscosity solution are not straightforward tasks[9].

It is worth making some comments concerning the structure of the system (3.20). First of all, it seems not to be a standard Hamilton-Jacobi equation as the one obtained in the case of bounded velocities [**2**]. Moreover, we notice that the first equation of (3.20) does not contain enough information due to the apparition of the non local term $\min_w u$ for which extra dynamics are required. Although it seems somehow sparse, the two additional (in)equations $\partial_t(\min_w u) \le 0$ $(= 0)$ are sufficient to determine the viscosity solution of the Cauchy problem in a unique way.

In order to understand the dynamics of system (3.20), we shall distinguish between the staurated area where $u = \min u + v^2/2$, and the unsaturated area, where $u < \min u + v^2/2$. The zero velocity $v = 0$ belongs to the saturated area (see Section 3.3.3.3). There, the knowledge of $\min u$ is sufficient to reconstruct the solution. However, the dynamics of $\min u$ are driven by the unsaturated area,

[9]This is joint work with E. Bouin, E. Grenier and G. Nadin.

in the sense that $\partial_t \min u < 0$ only if there is a nonzero velocity, say $v^*(t,x) \neq 0$ that realizes the minimum value of $u(t,x,\cdot)$. Note that $v^*(t,x)$ necessarily belongs to the unsaturated area. A typical representation of the solution is plotted in Figure 3.3.

Finally, it is fruitful to notice that $\min_w u(t,x,w)$ encodes the dynamics of the exponential tails of the macroscopic distribution ρ^ε, as the following convergence holds true,

$$\lim_{\varepsilon\to 0}\left(-\varepsilon\log\rho^\varepsilon(t,x)\right) = \lim_{\varepsilon\to 0}\left(-\varepsilon\log\left(\int_{\mathbb{R}}\exp\left(-\frac{u^\varepsilon(t,x,v')}{\varepsilon}\right)dv'\right)\right) = \min_{w\in\mathbb{R}} u(t,x,w)\,.$$

3.3.3.3. *Heuristics.* The following heuristics sheds some light on the structure of the system (3.20). In particular, we aim to understand how the supplementary condition

$$\partial_t\left(\min_{w\in\mathbb{R}} u(t,x,w)\right) \leq 0 \ (=0)\,,$$

pops up in the limit $\varepsilon\to 0$.

Firstly, let us notice that the constraint

$$(\forall (v,v')) \quad u(t,x,v) - u(t,x,v') - \frac{v^2}{2} \leq 0 \quad \Leftrightarrow \quad u(t,x,v) \leq \min_w u(t,x,w) + \frac{v^2}{2}\,, \tag{3.21}$$

immediately follows from (3.19) when the left-hand-side is bounded uniformly with respect to ε. The latter is usually derived from standard Lipschitz *a priori* estimates, uniformly with respect to ε. As a consequence, the minimum of u with respect to velocity is necessarily attained at $v=0$. Then, integrating (3.19) against the probability measure

$$d\mu_\varepsilon = \left(\int_{\mathbb{R}}\exp\left(-\frac{u^\varepsilon}{\varepsilon}\right)dv\right)^{-1}\exp\left(-\frac{u^\varepsilon}{\varepsilon}\right)dv = \frac{f^\varepsilon}{\rho^\varepsilon}\,dv\,,$$

we obtain the following continuity equation,

$$\int_{\mathbb{R}} \partial_t u^\varepsilon\, d\mu_\varepsilon + \int_{\mathbb{R}} v\partial u^\varepsilon\, d\mu_\varepsilon = 0\,. \tag{3.22}$$

The probability measure $d\mu_\varepsilon$ is expected to concentrate on the set of minimum points of u as $\varepsilon\to 0$. Let assume that we do have

$$d\mu_\varepsilon \rightharpoonup \sum_{w\in\mathcal{S}(u)(t,x)} p_w\delta_{v=w} \;=\; p_0\delta_{v=0} + \sum_{w\in\mathcal{S}(u)(t,x)\setminus\{0\}} p_w\delta_w\,, \tag{3.23}$$

where $\sum p_w = 1$, and $\mathcal{S}(u)(t,x)$ denotes the set of minimum points of u with respect to v. We notice that the constraint (3.21) at each $w\in\mathcal{S}(u)(t,x)\setminus\{0\}$ is clearly unsaturated, in the sense that $u < \min_w u + w^2/2$. Therefore, we expect to have there $\partial_t u(t,x,w) + w\partial_x u(t,x,w) = 1$, as the right-hand-side of (3.19) vanishes. Plugging this into (3.22), and using (3.23), we obtain successively,

$$\begin{aligned}
\sum_{w\in\mathcal{S}(u)(t,x)} p_w\left(\partial_t u + w\partial_x u\right) &= 0\,,\\
p_0\partial_t u(t,x,0) + \sum_{w\in\mathcal{S}(u)(t,x)\setminus\{0\}} p_w &= 0\,,\\
p_0\partial_t u(t,x,0) + 1 - p_0 &= 0\,.
\end{aligned}$$

We deduce formally from the chain rule that $\partial_t u(t,x,0) = \partial_t\left(\min_w u(t,x,w)\right)$. Thus, we expect eventually that $\partial_t \min_w u \leq 0$ and even $\partial_t \min_w u = 0$ if $p_0 = 1$, that is loosely speaking, $\mathcal{S}(u)(t,x) = \{0\}$. Obviously, all this reasoning is formal, but it can be made rigorous.

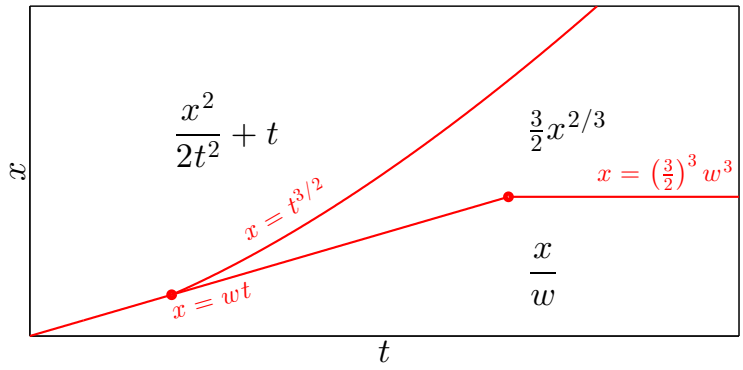

FIGURE 3.4. The macroscopic fundamental solution $\mu(t, x; w)$ (3.24) has three possible expressions, depending on the relative values of t, x and w.

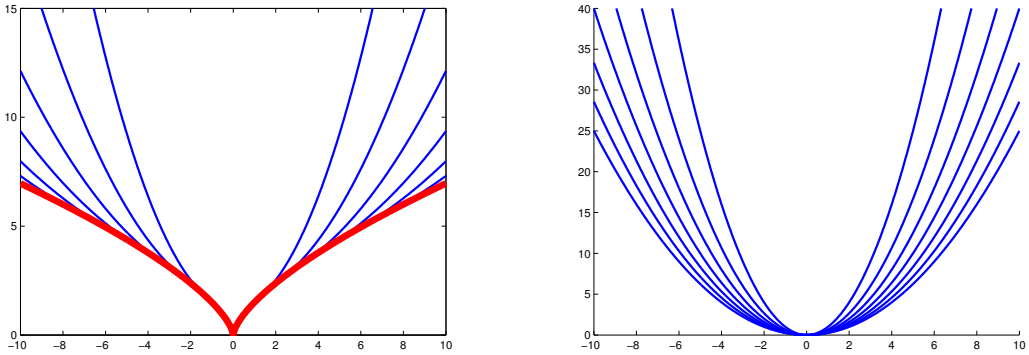

FIGURE 3.5. (Left) To illustrate the behaviour of the fundamental solution of (3.20), the minimum value $\mu(t, \cdot\,; 0)$ is plotted for successive values of time; The red curve is the limiting envelop of the blue curves. It is a multiple of $|x|^{2/3}$, see Section 3.3.3.4. (Right) For the sake of comparison, the fundamental solution corresponding to the diffusion limit $\partial_t u + \theta|\partial_x u|^2 = 0$, *i.e.* $u(t, x) = \frac{x^2}{4\theta t}$ is plotted for successive values of time.

3.3.3.4. *The fundamental solution.* We computed explicitly the fundamental solution of the nonlocal Hamilton-Jacobi equation (3.20). We followed a time discrete iteration scheme based on the Duhamel formulation of (3.1) to guess the formula. Since the problem is not translation invariant with respect to velocity, it is necessary to compute the solution for all initial data of the form

$$u(0, x, v) = \mathbf{0}_{x=0} + \mathbf{0}_{v=w}\,,$$

for which the mass is initially concentrated at the origin $x = 0$, with the velocity $w \in \mathbb{R}$. We have obtained the following expression for the solution (see also Figure 3.4),

(3.24)

$$\phi(t, x, v; w) = \min\left(\mathbf{0}_{x=tv} + \min\left(\mathbf{0}_{v=w}, \frac{v^2}{2}\right) + t, \frac{v^2}{2} + \min_{\substack{(s_1,s_2,s_3):\\ 0\le s_1+s_2+s_3\le t}} \left(\frac{(x - s_1 w - s_3 v)^2}{2s_2^2} + s_1 + s_2 + s_3\right)\right).$$

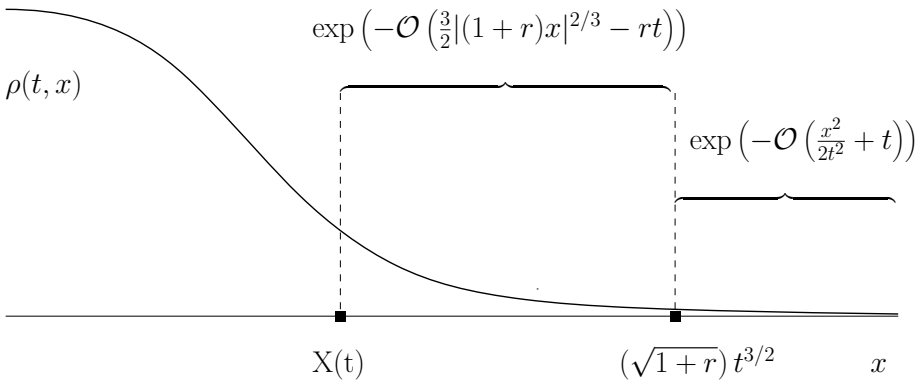

FIGURE 3.6. Asymptotic behaviour of the macroscopic density at the edge of the front

In particular, the minimum value with respect to velocity is given by

$$\mu(t,x;w)=\min_{v\in V}\phi(t,x,v;w)=\min_{\substack{(s_1,s_2):\\ 0\le s_1+s_2\le t}}\left(\frac{(x-s_1w)^2}{2s_2^2}+s_1+s_2\right)=\begin{cases}\dfrac{x}{w} & \text{if } 0\le x\le tw\\ \dfrac{3}{2}|x|^{2/3} & \text{if } |x|\le t^{3/2}\\ \dfrac{x^2}{2t^2}+t & \text{if } |x|\ge t^{3/2}\end{cases}.$$

The function $\mu(t,\cdot\,;0)$ is plotted in Figure 3.5 for successive values of time. A striking feature is that the solution does not converge to zero as $t\to+\infty$, as compared to the fundamental solution of the Hamilton-Jacobi equation associated with the diffusion equation $\partial_t u+\theta|\partial_x u|^2=0$.

3.3.3.5. *Quantitative front acceleration.* The previous quantitative analysis enables to describe precisely the dynamics of accelerating fronts in the asymptotic regime. In fact the fundamental solution in the case $r>0$ can be deduced from the case $r=0$ as follows,

$$\mu_r(t,x;w)=\mu\left((1+r)t,(1+r)x;w\right)-rt\,.$$

We can compute accordingly the location of the front, for a localized initial data (both in space and velocity)[10]. Indeed, for $w=0$, the fundamental solution simply writes

$$\mu_r(t,x;0)=\begin{cases}\dfrac{3}{2}|(1+r)x|^{2/3}-rt & \text{if } |x|\le(1+r)^{1/2}t^{3/2}\\ \dfrac{x^2}{2t^2}+t & \text{if } |x|\ge(1+r)^{1/2}t^{3/2}\end{cases}$$

As a consequence, the density of individuals becomes significantly large, as soon as $\mu_r(t,X(t);0)=0$, *i.e.*

$$X(t)=\left(\frac{\left(\frac{2}{3}r\right)^{\frac{3}{2}}}{1+r}\right)t^{\frac{3}{2}}\,.$$

This gives precisely the location of the front in the asymptotic regime, after tedious and technical justifications, taking into account the quadratic saturation term $-r\rho f$ in (3.1). As a by-product, we realize that the macroscopic front exhibits quite complicated dynamics at the edge of the front. For very large x, the front is exponentially uniformly small, with a hyperbolic scales as a function of x/t. For intermediate values of x, there is a transient region where the macroscopic profile is stationary with respect to x, and increases globally exponentially fast (as in [**Gar11**]). This is summarized in Figure 3.6.

[10]For instance, compactly supported initial data are localized in the sense that the support converges to $(0,0)$ in the rescaling limit $(x,v)=\left(x'/\varepsilon^{3/2},v'/\varepsilon^{1/2}\right)$ as $\varepsilon\to0$.

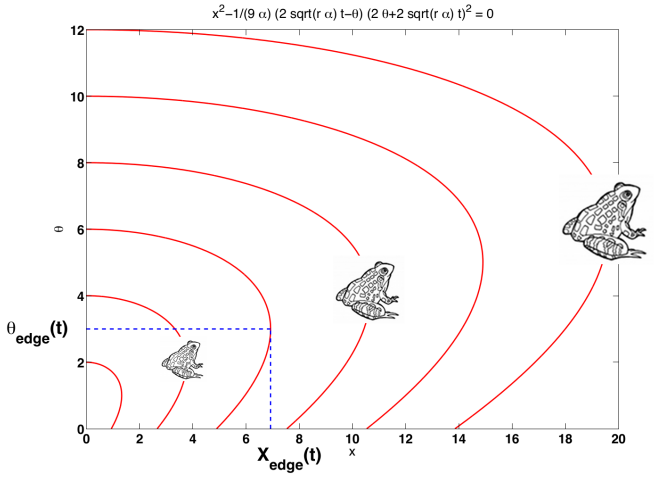

FIGURE 3.7. Zero-level set of u (3.26), the fundamental solution of the unconstrained equation (3.25).

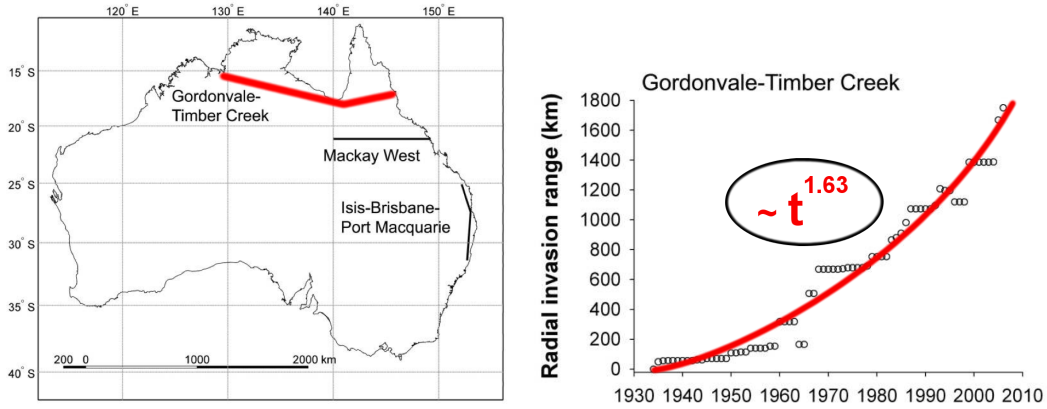

FIGURE 3.8. Data of the propagation of cane toads in North-Western Australia, in a East-West cross-section of approx. $2000km$ (red line on the map) [**UPSS08**]. The spreading follows a power law, with exponent 1.63 ± 0.13 [**UPSS08**, Table 1].

3.3.4. Asymptotic analysis of mutation-selection-diffusion equations.

3.3.4.1. *Approximation of geometric optics for bounded dispersal.* In [**Tur15**], Turanova performed the asymptotic analysis of (3.10), as a continuation of the crucial L^∞ bound she obtained for the Cauchy problem. The formal computations were provided in [**4**]. This result is analogous to a previous work by Bouin and Mirrahimi about the asymptotic analysis of reaction-diffusion equations structured by a phenotypical trait, but for which the trait influences the growth rate rather than the dispersal ability [**BM13**]. In the latter case, *a priori* estimates are easier to derive since the trait does not affect the higher-order derivatives. However, the lack of maximum principle still makes the analysis quite involved.

3.3.4.2. *Accelerating front for unbounded dispersal (formal computations).* Unsurprisingly, (3.10) exhibits accelerating waves when $\theta \in (0,+\infty)$, due to constant sorting of individuals. Formal computations suggest that the front is located around $X(t) = \mathcal{O}(t^{3/2})$. However, no rigorous result has been published so far due to deep technical obstacles[11].

Formal computations are based on the approximation of geometric optics, by removing the saturation term $-r\rho f$. This yields a Hamilton-Jacobi equation:

$$\frac{\partial u}{\partial t}(t,x,\theta) + \theta \left|\frac{\partial u}{\partial x}(t,x,\theta)\right|^2 + r\alpha \left|\frac{\partial u}{\partial \theta}(t,x,\theta)\right|^2 + r = 0\,, \tag{3.25}$$

for which the fundamental solution can be computed analytically by the method of characteristics,

$$u(t,x,\theta) = \frac{1}{4t}(\theta + r\alpha Z(x,\theta)^2)^2 - rt\,, \tag{3.26}$$

where $Z(x,\theta)$ is the positive root of $x = \theta Z(x,\theta) + \frac{r\alpha}{3} Z(x,\theta)^3$. In this framework, the front emerges when $\min_\theta u(t,X(t),\theta) = 0$. This yields a front which is localized around $\Theta(t) = \sqrt{r^2\alpha}\, t$ and $X(t) = (4/3) r\alpha^{1/4} t^{3/2}$.

Intuitively, the solution of (3.25) combines linear propagation in the trait variable θ (due to the sorting of faster individuals), and accordingly an accelerating wave in the spatial direction x. This is emphasized in Figure 3.7 where the zero-level sets of the fundamental solution u (3.26) are drawn for successive times. The far-right point of the level-set corresponds to the location of the front.

The complete Hamilton-Jacobi equation taking into account nonlocal saturation effects should read as follows,

$$\min\left(\frac{\partial u}{\partial t}(t,x,\theta) + \theta \left|\frac{\partial u}{\partial x}(t,x,\theta)\right|^2 + r\alpha \left|\frac{\partial u}{\partial \theta}(t,x,\theta)\right|^2 + r, \min_\theta u(t,x,\theta)\right) = 0\,. \tag{3.27}$$

It deserves a rigorous justification since it contains many quantitative features of the front acceleration.

3.3.4.3. *Adaptive dynamics at the edge of the front (formal computations).* In [4], we sketched formally the evolutionary dynamics evolutionary dynamics at the edge of the front, based on the theory of adaptive dynamics, following [**DJMP05**, **Per07**]. The theory of adaptive dynamics [**DL96**, **GMMo98**, **CFM06**] is widely accepted as a powerful tool to investigate evolutionary dynamics and equilibria. We refer to [**Die03**] for a comprehensive introduction to the theory. Apart from the classification of evolutionary equilibrium states, one of the main outcome is the so-called *canonical equation* that gives the dynamics of the dominant trait in the population. It has been derived from microscopic trait-substitution sequences [**DL96**] and individual-based models [**CFM08**].

An alternative continuous framework has been developed in [**DJMP05**, **Per07**, **LMP11**, **Mir13**], based on some asymptotic limit of PDE models, as in the present section.

Let me introduce the canonical equation by a simple example, without the spatial structure, following [**Per07**]. Let $f(t,\theta)$ denote the density of individuals with respect to some phenotypic trait θ, that is solution to a nonlocal mutation-selection PDE:

$$\varepsilon \partial_t f^\varepsilon(t,\theta) = \underbrace{\varepsilon^2 \partial_\theta^2 f^\varepsilon(t,\theta)}_{\text{small mutations}} + \underbrace{R(\theta) f^\varepsilon(t,\theta) - f^\varepsilon(t,\theta)\rho^\varepsilon(t)}_{\text{selection of individuals}}\,, \quad \rho^\varepsilon(t) = \int f^\varepsilon(t,\theta)\, d\theta\,.$$

[11] Some result was announced recently by N. Berestycki, C. Mouhot and G. Raoul [**BMR15**], but for a slightly different choice of the saturation term. They derived regularity estimates in order to reduce to a local reaction term $f(1-f)$. Then, they applied a probabilistic argument in order to prove the exact rate of spreading.

Selection of the fittest individuals occurs due to the non constant growth rate $R(\theta)$. There, the long time asymptotics $t = t'/\varepsilon$ has already been done, where ε represents the typical size of mutations. Again, the logarithmic transformation enables to catch the behaviour of exponentially small tails $u^\varepsilon(t,\theta) = -\varepsilon \log(f^\varepsilon(t,\theta))$, as $\varepsilon \to 0$. In the limit $\varepsilon \to 0$, u^ε converges towards the viscosity solution of the following constrained Hamilton-Jacobi equation,

$$\begin{cases} \partial_t u(t,\theta) + |\partial_\theta u(t,\theta)|^2 + R(\theta) = \rho(t)\,, \\ \min_\theta u(t,\theta) = 0\,. \end{cases} \tag{3.28}$$

where the scalar $\rho(t)$ is formally the limit of $\rho^\varepsilon(t)$. However, this limit is not quite well defined in general, and $\rho(t)$ should be viewed as a Lagrange multiplier associated with the constraint $\min_\theta u(t,\theta) = 0$ that guarantees the persistence of the population.

The dynamics of a trait $\Theta(t)$ which is dominant in the population, can be computed analytically. It is defined as the local minima of u with respect to θ, such that

$$u\left(t,\Theta(t)\right) = \min_\theta u(t,\theta)\,. \tag{3.29}$$

By differentiating the first order condition $\partial_\theta u\left(t,\Theta(t)\right) = 0$ with respect to t, and by differentiating (3.28) with respect to θ, the canonical equation for $\Theta(t)$ is obtained,

$$\frac{d\Theta}{dt}(t) = \frac{\partial_\theta R\left(\Theta(t)\right)}{\partial_\theta^2 u\left(t,\Theta(t)\right)}\,. \tag{3.30}$$

It is valid as soon as $\Theta(t)$ is not a degenerate minimum. The term $\partial_\theta R\left(\Theta(t)\right)$ is the gradient of the growth rate that drives the dominant trait in the population up to the fittest possible traits. The term $\partial_\theta^2 u\left(t,\Theta(t)\right)$ accounts for the phenotypic diversity around the dominant trait[12]: the more diversity, the faster the dynamics.

A similar analysis can be formally performed taking into account the spatial structure. We seek an equation for the locally fittest trait $\Theta(t,x)$ such that

$$u\left(t,x,\Theta(t,x)\right) = \min_\theta u^0(t,x,\theta)\,.$$

The canonical equation for $\Theta(t,x)$ can be derived formally as previously [4]. It writes

$$\partial_t\Theta(t,x) + 2\left(\Theta(t,x)\partial_x u(t,x,\Theta(t,x))\right)\partial_x\Theta(t,x) = \frac{|\partial_x u(t,x,\Theta(t,x))|^2}{\partial_\theta^2 u(t,x,\Theta(t,x))}\,.$$

This looks like a nonlinear transport equation, like the Burgers equation, with a nonnegative source term. The transport accounts for the motion of the front, whereas the source term accounts for the spatial sorting of individuals with higher dispersal. Shocks have been observed numerically, when individuals with higher dispersal are initially located behind individuals with lower dispersal.

Open Problem(s) 3.9

(1) Prove the acceleration with the expected rate $\mathcal{O}(t^{3/2})$ for the model (3.10) when $\theta_{\max} = +\infty$.

(2) Derive rigorously the approximation of geometric optics (3.27).

(3) Develop the theory of adaptive dynamics in a spatially heterogeneous environment. Two recent preprints [**PS15, LL15**] tackle this problem in a slightly different setting. They study dispersal evolution on a bounded domain, with heterogeneous, but fixed, resources. Classical theory in the case of a finite number of traits predicts that

[12] It is in fact analogous to the inverse of the variance of the population, since $f^\varepsilon = \exp(-u^\varepsilon/\varepsilon)$ and Θ is a local minimum.

evolutionary dynamics leads to smaller dispersal abilities [**Has83**, **DHMP98**]. In [**PS15**, **LL15**], the authors perform the rare mutation limit of the steady state problem, thus extending partially the results of [**Has83**, **DHMP98**] to a continuum of traits.

3.4. Future directions of research

The approximation of geometric optics is a powerful tool for quantitative analysis in theoretical biology. I aim to develop this methodology for age-structured models in various contexts.

3.4.1. Intra-cellular subdiffusive processes. A current view in molecular biology is that small particles experience a intracellular diffusion hindrance due to macromolecular crowding. This was reported in several experiments in the past decade, see [**HF13**] for a review. Interestingly enough, different cell compartments (nucleus, cytoplasm) show various patterns of anomalous diffusion [**WWL00**, **KIH+11**]. This suggests that mathematical models for anomalous diffusion should take into account strong spatial heterogeneities.

In collaboration with H. Berry, P. Gabriel, A.M. González and Th. Lepoutre, we have started to analyse subdiffusive processes in a synthetic manner. We base our analysis on continuous time random walks (CTRW) which exhibit a subdiffusive scaling, $\langle x(t)^2 \rangle \sim Ct^\gamma$, $\gamma \in (0,1)$ [**MFH10**]. Subdiffusive CTRW are usually non-markovian, since particles can be trapped for a while at some location[13]. Alternatively, we study a markovian version which accounts for aging of particles at a given position, through the p.d.f. $f(t,x,a)$,

$$\begin{cases} \partial_t f(t,x,a) + \partial_a f(t,x,a) + \beta(a,x) f(t,x,a) = 0 \\ f(t,x,0) = \displaystyle\int_{\mathbb{R}} w(x-x') \left(\int_0^\infty \beta(a,x') f(t,x',a)\, da \right) dx' . \end{cases} \tag{3.31}$$

The homogeneous version of (3.31) is simply a renewal equation [**Fel66**]. Subdiffusion occurs when the age-dependent rate of jump $\beta(a)$ decreases with age with the particular scaling $\beta(a) \sim \gamma/a$ as $a \to +\infty$. It is exactly the critical case where the renewal equation does not admit a stationary distribution, but $f(t,a)$ converges towards the Dynkin-Lamperti arcsine law in self-similar variables $(\tau, b) = (\log t, a/t)$.

The entropy/entropy dissipation method[**Kam90**, **MMP05**, **Per07**] enables to obtain rates of convergence in self-similar variables for the homogeneous model [**BLG15**]. If $u(\tau,b)$ denotes the density in self-similar variables, then it satisfies the following transport equation[14],

$$\begin{cases} \partial_\tau u + \partial_b((1-b)u) + \dfrac{\gamma}{e^{-\tau}+b} u = 0 \\ u(\tau,0) = \int_0^\infty \gamma e^{-\tau} + b u(\tau,b)\, db . \end{cases}$$

The intermediate asymptotics are captured more accurately with the quasi-stationary state,

$$U(\tau,b) = \frac{C(\tau) e^{-\gamma\tau}}{(e^{-\tau}+b)^\gamma (1-b)^{1-\gamma}} .$$

The following convergence holds true [**BLG15**],

$$\| u(\tau,\cdot) - U(\tau,\cdot) \|_{L^1} \lesssim e^{-\min(\gamma,1-\gamma)\tau} , \tag{3.32}$$

except in the case $\gamma = 1/2$, where the r.h.s. is be replaced by $\tau e^{-(1/2)\tau}$. The novelty from a mathematical viewpoint is that the limit of $U(\tau,b)$ as $\tau \to +\infty$ (*i.e.* , the arcsine law) is singular at

[13] More precisely, times between jumps do not have a Poissonian distribution. Furthermore, the mean time between jumps is assumed to be infinite.

[14] This is for the case $\beta(a) = \gamma/(1+a)$

both $b = 0$ and $b = 1$. In particular, the rate of jump is infinite in the limit $\tau \to +\infty$. Therefore the relative entropy is not straightforward to define.

The rate of convergence seems to be new, even in the large literature of renewal processes. There exist connections with ergodic theory for dynamical systems with an infinite measure, see [**MT12**] where the authors obtain non-optimal rates of convergence (rates of mixing). This connection has yet to be explored.

We aim to perform asymptotic limits of (3.31), as in Section 3.3, in order to investigate propagation phenomena in subdiffusive processes, taking into account nonlinear reaction terms in the model [**GC06**, **GW08**, **SLM12**]. Since the underlying CTRW is non-markovian, it is of paramount importance to properly set when the reaction takes place, *e.g.* during the aging phase, and/or during the jump step. The markovian version (3.31) has enough flexibility for such purposes. The long time behaviour (linear or sublinear propagation) depends on these modelling details [**VNN13**].

3.4.2. Evolution in age-structured populations. In collaboration with biologists at ISEM (Montpellier), O. Cotto and O. Ronce, and together with E. Bouin and J. Garnier, we have obtained some contributions to the evolution of life history traits with a special focus on aging. In [**CR14**], the authors propose a minimal model for the adaptation of an age-structured population to a changing environment. More precisely, they study the effect of an age-specific quantitative trait. The deviation from the optimal trait affects the mortality rate at a given age, say a^*, which is a parameter of the model. The authors derive very interesting conclusions depending on the age threshold a^*. For instance, in a linearly changing environment, selection is more efficient at younger ages than at older ages, meaning that the predominant trait deviates less from the optimal one when a^* is smaller. Their conclusions are derived from various heuristical simplifications, and also numerical simulations. Our main contribution consists in the quantification of their observations.

Evolutionary biology of aging, and particularly, the apparent paradox of senescence has a long history [**Le09**, Chap. I.10], [**Le13**, Chap. III.11], [**Ros94**], [**Cha94**], [**Cha00**]. It was hypothesized in the mid 20th century by Haldane, Medawar and Williams that aging does not evolve for the benefit of the group or species[15], but because natural selection is not efficient to wash out deleterious mutations, and to maintain physiological functions at old age. This theory was formalized later by Hamilton, based on his indicator of the force of selection H [**Ham66**, **Bau05**].

3.4.2.1. *Hamilton's indicator of the force of selection.* In order to define H, let $(\beta(a), \mu(a))$ be respectively the age-dependent birth rate and the age-dependent death rate of a population. The rate of growth of the whole population, r, is uniquely determined by the following implicit formula,

$$\int_0^\infty \beta(a) \exp\left(-ra - \int_0^a \mu(a')\, da'\right) da = 1\,. \tag{3.33}$$

Now, consider the effect of an age-specific perturbation at a single age a^*, *e.g.* on the death rate μ,

$$\mu(a, m) = \mu(a) + m\delta_{a=a*}\,. \tag{3.34}$$

Alternatively speaking, the survivorship function has a discontinuity at age a^*. Hamilton's indicator is the derivative of the fitness with respect to the increment of mortality m,

$$H = -\frac{dr}{dm} = \frac{\int_{a*}^\infty \beta(a) \exp\left(-ra - \int_0^a \mu(a')\, da'\right) da}{\int_0^\infty a\beta(a) \exp\left(-ra - \int_0^a \mu(a')\right) da}\,.$$

It is decreasing with respect to the threshold a^*. Therefore, the force of selection diminishes in late age classes. As a consequence, the mutation/selection balance yields larger mortality rates at

[15] *e.g.* by making space for younger, better reproductive individuals.

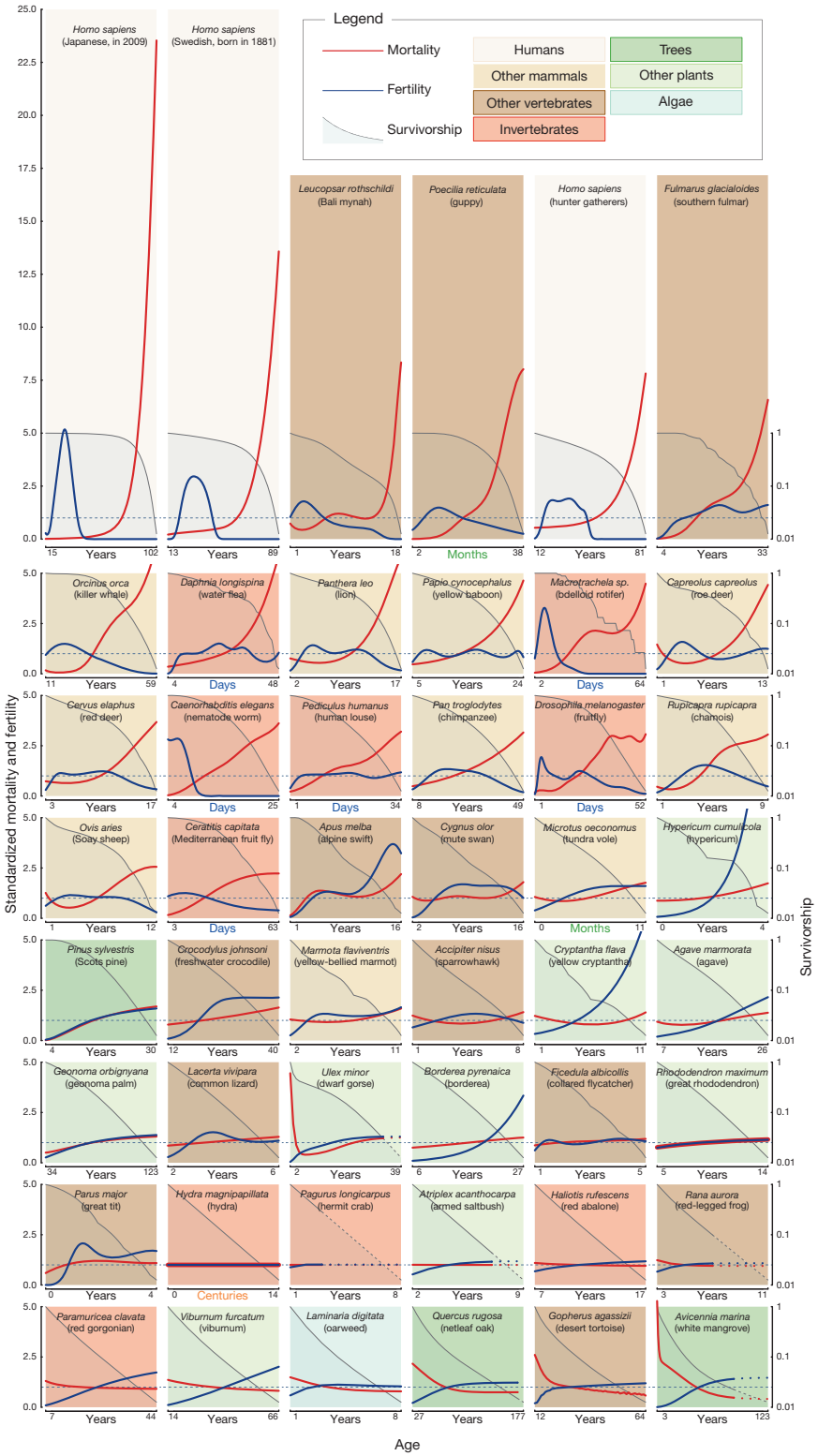

FIGURE 3.9. Diversity of ageing patterns, from [JSSG+14].

late ages. This linear, simple but quantitative, theory predicts that mortality rates should follow a Gompertz law [**Cha01**].

3.4.2.2. *Maladaptation in a changing environment (no age structure).* In order to introduce the mathematical formalism, we present briefly the results contained in [**LGW91**, **LL93**, **BL95**, **Bür00**] that concerns maladaptation without the age structure. Let $f(t,x)$ be the density of individuals with respect to a quantitative trait x that affects mortality of individuals. The following model contains the minimal ingredients for mutations, and selection of individuals.

$$\partial_t f(t,x) + (\mu + m(x) + \rho(t))\, f(t,x) = \int_{\mathbb{R}} K(x-x')\,(\beta f(t,x'))\, dx'\,. \tag{3.35}$$

The mutation kernel K describes the possible changes in phenotype at each generation. It is a symmetric probability distribution. For the sake of simplicity, we assume that the birth rate β is constant. The additional mortality rate $m(x)$ is a nonnegative function such that $m(0) = 0$, *i.e.* the fittest trait is located at $x = 0$. For the sake of clarity, we assume henceforth that $m(x) = \alpha|x|^2$, where $\alpha > 0$ is related to the intensity of selection. Finally, the scalar $\rho(t) = \int_{\mathbb{R}} f(t,x)\,dx$ accounts for the global competition among individuals.

Mutation/selection equilibria are stationary states of (3.35). They are solutions of the following spectral problem,

$$\rho_0 F_0(x) = -(\mu + m(x))F_0(x) + \int_{\mathbb{R}} K(x-x')\,(\beta F_0(x'))\, dx'\,, \tag{3.36}$$

with the constraint $\rho_0 \geq 0$. If this constraint is not satisfied, the Cauchy problem (3.35) goes to extinction.

The influence of a changing environment may be taken into account within this framework, by replacing the mortality rate $m(x)$ with $m(x-ct)$[16]. This modifies the spectral problem (3.36) as follows,

$$\rho_c F_c(y) = c\partial_y F_c(y) - (\mu + m(y))F_c(y) + \int_{\mathbb{R}} K(y-y')\,(\beta F_c(y'))\, dy'\,. \tag{3.37}$$

Two quantities arise naturally in order to measure the ability of the population to adapt to a lineary changing environment:

(1) The **load** $\delta\rho = \rho_0 - \rho_c$, which measures the impact of the change on the global fitness.

(2) The **lag** y_c which is the dominant trait in the population,*i.e.* the maximal point of F_c[17].

When the mutational increments are infinitesimal, *i.e.* the mutation operator is a diffusion operator, $\beta\left(\mathrm{Id} + \sigma^2\partial_x^2\right)$, then everything is explicit, because the eigenfunctions are Gaussian functions with variance $(\beta/\alpha)^{1/2}\sigma$. In particular, we have

$$\delta\rho = \frac{c^2}{4\beta\sigma^2}\,, \quad y_c = -\frac{c}{2(\alpha\beta)^{1/2}\sigma}\,. \tag{3.38}$$

Notice that the lag is linear with respect to the forcing speed c.

The equation $\rho_{c^*} = 0$ defines a critical speed c^*, above which the population goes extinct [**LGW91**].

Analogous results can be derived for a general mutation kernel K, in the asymptotic limit of small mutations. We introduce a small parameter $\varepsilon \ll 1$ in (3.37), as follows,

$$\rho_c F_c(y) = c\partial_y F_c(y) - (\mu + m(y))F_c(y) + \int_{\mathbb{R}} \frac{1}{\varepsilon} K\left(\frac{y-y'}{\varepsilon}\right)(\beta F_c(y'))\, dy'\,. \tag{3.39}$$

[16]It means that the optimal trait is shifted at a constant speed c.

[17]Clearly, $y_0 = 0$ holds by symmetry.

As for the semi-classical analysis of the Schrödinger equation, the limit $\varepsilon \to 0$ yields a Hamilton-Jacobi equation for the WKB expansion $U^\varepsilon = -\varepsilon \log F^\varepsilon$. When $c = 0$, the equation of the mutation/selection equilibria for U, in the limit $\varepsilon \to 0$, reads

$$\rho_0 + \mu + m(x) = \beta \hat{K}(\partial_x U_0(x)) \,, \tag{3.40}$$

where $\hat{K}$ is the bilateral Laplace transform of the kernel K. Clearly, $\rho_0 = \beta - \mu$, as expected, since the population concentrates around the dominant trait, which is the fittest trait in a static environment. In the case of a changing environment, it reads

$$\rho_c + c\partial_y U_c(y) + \mu + m(y) = \beta \hat{K}(\partial_y U_c(y)) \,. \tag{3.41}$$

The lag y_c is defined accordingly as the minimal point of U_c. In addition, let introduce the auxiliary quantity $p_c = \partial_y U(0)$. The following relations are easy to derive from (3.40)–(3.41),

$$\begin{cases} \rho_c = \beta - \mu - m(y_c) \\ (\rho_0 - \rho_c) = \beta \left(\hat{K}(0) - \hat{K}(p_c) \right) + c p_c \\ \beta \hat{K}'(p_c) = c \end{cases}$$

This provides two different ways to compute the load $\delta\rho$,

$$\begin{cases} \delta\rho = m(y_c) & \text{(mutation free relation)} \\ \delta\rho = \beta \left(1 - \hat{K}(\hat{K}'^{-1}(c/\beta)) \right) + c \hat{K}'^{-1}(c/\beta) & \text{(selection free relation)} \end{cases} \tag{3.42}$$

The second relation is explicit. The first relation enables to derive the lag y_c from the load δ_c.

Again, the equation $\rho_{c^*} = 0$ defines a critical speed c^*, above which the population goes extinct.

Remark 3.10. *An important observation to keep in mind is that the load does not depend on the selection intensity α. This was already the case in the fully explicit case* (3.38).

3.4.2.3. *Maladaptation in a changing environment (with the age structure).* We have transcribed the discrete stage-structured model of [**CR14**] into a continous setting. It is a quantitative genetics model based on the formalism of Lande [**Lan82**], Charlesworth [**Cha94**], see also Barfield for a more general presentation of stage-structured models [**BHG11**]. Interestingly, it is very similar to the model (3.31) for subdiffusive processes, although the outcomes are quite different. The model reads as follows,

$$\begin{cases} \partial_t f(t,a,x) + \partial_a f(t,a,x) + (\mu(a, m(x-ct)) + \rho(t))\, f(t,a,x) = 0 \,, \quad \rho(t) = \int_{\mathbb{R}} \int_0^\infty f(t,a,x)\, da dx \\ f(t,0,x) = \displaystyle\int_{\mathbb{R}} \frac{1}{\varepsilon} K\left(\frac{x - x'}{\varepsilon} \right) \left(\int_0^\infty \beta(a) f(t,a,x')\, da \right) dx' \,. \end{cases} \tag{3.43}$$

The mortality rate is chosen as in (3.34). We assume as above that there exists an optimal phenotype, located at the origin $x = 0$. We set $m(x) = \alpha |x|^2 \geq 0$. Finally, intraspecific competition is global, via the total number of individuals $\rho(t)$.

The goal is to investigate the mutation/selection balance at the demographic equilibrium. Accordingly, we seek a nonnegative solution (ρ_c, F_c) to the following spectral problem,

$$\begin{cases} -c\partial_y F_c(a,y) + \partial_a F_c(a,y) + (\mu(a, m(y)) + \rho_c)\, F_c(a,y) = 0 \,, \\ F_c(0,y) = \displaystyle\int_{\mathbb{R}} \frac{1}{\varepsilon} K\left(\frac{y - y'}{\varepsilon} \right) \left(\int_0^\infty \beta(a) F_c(a,y')\, da \right) dy' \,. \end{cases}$$

The renormalized density

$$U^\varepsilon(a,y) = -\varepsilon \log \left(F_c(a,y) \right) \,.$$

converges towards a viscosity solution of the following stationary Hamilton-Jacobi equation,

$$\rho_c + c\partial_y U_c(y) = R(m(y), \partial_y U_c(y)), \tag{3.44}$$

where the Hamiltonian $R(m,p)$ is given implicitly by the following relation:

$$\int_0^\infty \beta(a) \exp\left(-aR(m,p) - \int_0^a \mu(a',m)\, da'\right) da = \frac{1}{\widehat{K}(p)}.$$

The following properties hold true,

$$\begin{cases} R(m,0) = r(m) & \text{where } r(m) \text{ is defined as in (3.33)} \\ R(0,p) = \beta\hat{K}(p) - \mu \end{cases}$$

The former property captures the features of selection in the absence of mutations, whereas the latter property captures the features of mutations in the absence of selection.

We can perform the very same analysis as without the age structure (Section 3.4.2.2). We deduce the two alternative formulations of the load, as in (3.42):

$$\begin{cases} \delta\rho = R(0,0) - R(m(y_c),0) & \text{(mutation free relation)} \\ \delta\rho = R(0,0) - R(0,p_c) + cp_c & \text{(selection free relation)} \end{cases} \tag{3.45}$$

As a consequence, the load $\delta\rho$ coincides with the load obtained in the model without the age structure, since it depends only on the function $R(0,p)$. Alternatively speaking, the load does not depend on selection (Remark 3.10), which depends specifically on the age structure. Therefore, the load does not depend on the age structure. Only the lag y_c depends on the way of selection.

3.4.2.4. *Wall of death (the dramatic effect of the age structure).* In [**CR14**], the authors observed numerically that the lag may not converge to a stationary value when the mutations impact old age classes. This is confirmed by the following quantitative analysis.

Recall that for the age free model (Section 3.4.2.2), in the simple Gaussian case, the lag y_c is linear with respect to the speed c (3.38). The relation is more complicated in the case of a general mutation kernel, but it is qualitatively similar. We have

$$y_c = -\left(\frac{\beta\left(1 - \hat{K}(\hat{K}'^{-1}(c/\beta))\right) + c\hat{K}'^{-1}(c/\beta)}{\alpha}\right)^{1/2}.$$

Under reasonable assumptions on K, we deduce that $\lim_{c\to\infty} y_c = \infty$.

In the age-structured model, there may exist a critical speed c^{**} such that the lag diverges as $c \to c^{**}$,

$$\lim_{c\to c^{**}} y_c = \infty.$$

Such a speed exists if $\beta a^* > 1$[18]. An interesting situation arises when $c^{**} < c^*$, *i.e.* the lag diverges, but the population is not globally extinct. The condition $c^{**} < c^*$ is not void. In this case, the individuals older than a^* suffer severe maladaptation, as the survivorship function of the dominant trait y_c gets arbitrarily small in the age classes $a > a^*$.

This result can be easily understood from the following heuristics. Firstly, we analyse the first relation of (3.45) in the limit $y_c \to \infty$,

$$\delta\rho = R(0,0) - R(\infty,0). \tag{3.46}$$

On the contrary to the case without the age structure, it is possible to get a finite load with an infinite lag. This is because the individuals with age $a < a^*$ are not affected by the arbitrarily

[18]It means that the threshold a^* is greater than the mean age at the first reproduction event β^{-1}.

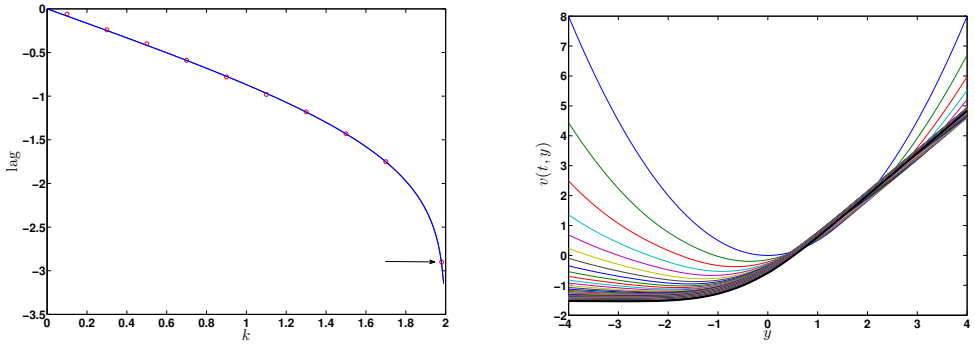

FIGURE 3.10. (Left) The lag y_c: red dots are obtained after numerical integration of the Hamilton-Jacobi equation (3.44); blue line is the plot of the formula (3.48), for the sake of comparison. Here, the critical value is $c^{**} = 2$. (Right) Shape of the stationary profile U_c, for $c < c^{**}$. Clearly, it gets flatter and flatter as $c \to c^{**}$. As a by-product, the minimal point y_c is shifted to the left infinity.

large mortality at age a^*. Hence, they still contribute significantly to the next generations. More precisely, (3.46) reads as follows after simple computations,

$$\delta\rho a^* \exp\left(-\delta\rho a^*\right) = \beta a^* \exp\left(-\beta a^*\right) . \tag{3.47}$$

Only the case $\delta\rho = \rho_0 - \rho_c < \beta$ makes sense, because $\rho_0 = \beta - \mu \leq \beta$, and we have the constraint $\rho_c \geq 0$. Equation (3.47) admits a nontrivial solution with $\delta\rho < \beta$ if $\beta a* > 1$: $\delta\rho a^*$ is conjugate to βa^* with respect to the function $X\exp(-X)$.

This heuristics is confirmed by the explicit formula for the lag (see also Figure 3.10),

$$y_c = -\left(-\frac{1}{\alpha}\log\left(1 - \frac{\delta\rho e^{-\delta\rho a^*}}{\beta e^{-\beta a^*}}\right)\right)^{1/2} . \tag{3.48}$$

These conclusions are summarized in the following Theorem.

Theorem 3.11: Maladaptation in age-structured populations (Bouin, Calvez, Garnier, not yet published)

In the case $\beta a^* > 1$, there exists a critical speed c^{**} such that the population is globally persistent if $c < c^*$, but the fraction of population with age $a > a^*$ goes extinct as $t \to \infty$ when $c^{**} < c < c^*$.
The two critical speeds c^{**} and c^* are not in specific order, but $c^{**} < c^*$ when $\beta a* \gg 1$.

Open Problem(s) 3.12

(1) Perform the same analysis in the case of diploid reproduction, with the infinitesimal model [**Bul80**, **MR13**, **CR14**]. The first step would consist in proving the existence of a mutation-selection equilibrium.

(2) Compare these results with the comprehensive study of Evans, Steinsaltz and Wachter [**SEW05**, **ESW13**, **WES13**]. The authors follow a population genetics approach, where the mutations are always considered deleterious.

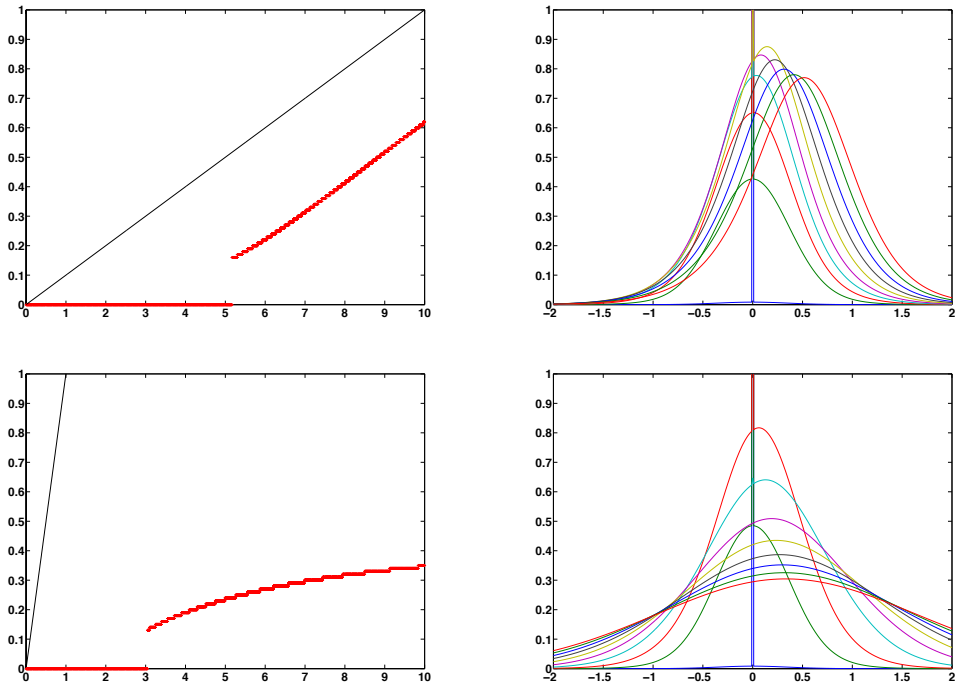

FIGURE 3.11. Numerical simulation of the Cauchy problem (3.43) in the case of slow change $c < c^{**}$ (top), and fast change $c > c^{**}$ (bottom). In the former case, the dominant trait follows the linear shift of the optimum (red line), whereas it fails to follow in the latter case. There, the trait distribution gets wider.

CHAPTER 4

Optimization of growth-fragmentation processes

This chapter presents the contents of articles [**20**], [**14**], [**15**], [**16**], written in collaboration with N. Lenuzza, D. Oelz, J.-P. Deslys, P. Laurent, F. Mouthon, B. Perthame, M. Doumic, P. Gabriel, and S. Gaubert.

Summary

{4.1} Amyloid diseases such as Prion diseases are modelled by means of biophysical processes, according to the "protein-only hypothesis". {4.1.1} The Masel-Jansen-Novak is a simple version of a general elongation-fragmentation model for polymer aggregation. {4.1.2} It predicts a unimodal distribution of polymer sizes, whereas a bimodal distribution was observed in some experimental data. {4.1.3} This discrepancy can be rectified using a heterogeneous elongation rate. {4.1.4} In vitro amplification of Prions (PMCA) is described. It is based on purely biophysical hypotheses on polymer dynamics. The main ingredient is controlled sonication, that enhances polymer fragmentation. Model writes as a linear growth-fragmentation equation. Dependency of the dominant eigenvalue with respect to extremal values of the control parameters is established.

{4.2} Optimization of the exponential growth rate, *i.e.* the Lyapunov exponent, is an infinite horizon optimal control problem. {4.2.1} A baby model is provided by a low-dimensional reduction to the full growth-fragmentation equation, with only three possible sizes of polymers. Interestingly, an optimal Lyapunov exponent can be achieved for intermediate constant sonication rates. However, there is room for possibly better rates in the class of time-varying controls. {4.2.2} The existence of the best Lyapunov exponent of the optimal control problem is established in a general setting, but still finite dimensional. The existence of a companion potential function is also proven. {4.2.3} The problem can be reformulated as a fixed point problem for a suitable Lax-Oleinik operator, or as a solution of a stationary (ergodic) Hamilton-Jacobi equation. The proof of existence involves contraction estimates of the flow with respect to Hilbert's metric, giving Lipschitz estimates, thus compactness. An alternative proof using Lagrangian estimates is sketched. {4.2.4} Links with other theories are discussed, including the Perron-Frobenius theory, the weak KAM theory, and the stability of linear inclusion systems.

{4.3} Qualitative behaviours of optimal trajectories are investigated. {4.3.1} The ergodic set, which is positively invariant, attractant, and controllable, is described for the baby model, using ad-hoc monotonicity formulas. {4.3.2} Pursuing the analogy with the weak KAM theory, the Aubry set is characterized through the Peierls barrier. The latter must be defined with caution due to the lack of controllability. {4.3.3} The optimal sonication strategy happened to be constant in all numerical tests for the baby model, but we found an optimal periodic strategy in a larger class of monotone systems. {4.3.4} A simple criterion is introduced to characterize (local) optimality of constant controls. It is connected to the generalized Legendre condition for local optimality of controls on short time horizons.

4.1. Modelling prion dynamics

I present in this Chapter several contributions to the modelling of polymer dynamics. The central model is a size-structured equation describing a population of polymers $u(t,x)$, possibly coupled to a bath of monomers $V(t)$. The main motivation is the modelling of amyloid diseases, such as Prion proliferation.

According to the "protein-only hypothesis", the infectious agent in Prion diseases consists in a misfolded protein (called PrPsc), without any nucleic acid. It is hypothesized that PrPsc self-replicates, by converting the normal form of PrP (called PrPc for Prion Protein cellular) into PrPsc (for Prion Protein scrappie) [**PSDC98**]. Many evidences are in favor of an autocatalytic replication of PrPsc, as the generation of infectivity from recombinant proteins [**LBN+04**] or the success of in vitro PrPsc conversion systems, such as the protein misfolding cyclic amplification (PMCA) technique [**CSHS05**].

Several mathematical models of prion replication have been proposed in the literature [**Eig96**, **MJN99**, **MCS+03**, **PK98**]. They contribute to demonstrating that essential features of prion diseases can be explained by purely physico-chemical mechanisms, as supposed by the protein-only hypothesis.

The early proposed model is based on the conformational change of PrPc into PrPsc after the formation of a heterodimeric complex

$$\mathrm{PrPc} + \mathrm{PrPsc} \longrightarrow 2\mathrm{PrPsc}\,.$$

This model does not account for the aggregation of PrPsc in a polymerized state. Some other mechanisms have been proposed. They deal with PrP fibrilar aggregation [**JL93**, **CPH+94**, **MJN99**, **KSS+03**, **MCS+03**]. We refer to N. Lenuzza's PhD thesis for a comprehensive review of prion modelling [**Len09**].

We have opted for the model of nucleated polymerization, introduced by Masel et al [**MJN99**, **GPMW06**, **EPW06**]. PrPsc is considered to be a polymeric form of PrPc. Polymers can lengthen by addition of PrPc monomers, and they can replicate by splitting into smaller fragments. The continuous version of the full biophysical model reads as follows [**GPMW06**],

$$\left\{\begin{array}{l} V'(t) = \lambda - \left(\gamma + \displaystyle\int_0^\infty \tau(x)u(t,x)\,dx\right)V(t) \\ \partial_t u(t,x) + V(t)\partial_x(\tau(x)u(t,x)) + (\mu(x)+\beta(x))\,u(t,x) = 2\displaystyle\int_x^\infty \beta(y)\kappa(x,y)u(t,y)\,dy\,, \end{array}\right. \tag{4.1}$$

where $V(t)$ is the concentration of monomers (PrPc), and $u(t,x)$ is the size-distribution of polymers (PrPsc). It is complemented with the influx boundary condition $u(t,0) = 0$. Monomers are renewed with a constant input λ, whereas they are degraded at rate γ. In addition, they are incorporated into polymers at rate $\tau(x)$, where x denotes the length. Accordingly, polymers elongate at speed $V(t)\tau(x)$, whereas they break into smaller fragments at rate $\beta(y)$, $y > x$. The size of the two resulting fragments are x and $y-x$. The size distribution of the two daughter fragments is encoded in the kernel $\kappa(x,y)$. It is generally assumed that $\kappa(x,y) = y^{-1}\kappa_0(y^{-1}x)$, where κ_0 is a probability measure, symmetrical with respect to $1/2$.

There exist more realistic models describing oligomers with intermediate sizes, and accounting for more complex reaction kinetics before the nucleation size is attained, see *e.g.* [**PBC+12**]. I will not comment further on that.

There is an extended literature about linear growth-fragmentation equations (4.1) when $V(t)$ is set to a constant value [**MMP05**, **Mic06**, **LP09**, **DJG10**, **MS13**]. Under rather general assumptions, it was proven that the solution behaves asymptotically as an exponentially growing profile: $e^{-\lambda t}u(t,x) \to \mathcal{U}(x)$ in some weigthed L^1 space. Furthermore, some rate of convergence was obtained in [**CCM11**, **BCG13**]. The coupled system is more complicated to analyse, and more

complex behaviours are to be expected [Gab12]. I will not discuss the analysis of the coupled system here.

There is also an extended literature dealing with nonlinear size- or age-structured population dynamics, where the growth rate (here, the elongation rate) depends on some environmental state variables (here, the concentration of monomers), see for instance the celebrated *Daphnia*-algae model. It is a size-structured consumer-resource model, which has served as a reference model to elucidate the long time behaviour of size-strutured equations. We refer to [DGM+10] for an overview on the modelling and the associated mathematical theory. However, we shall focus on the linear problem hereafter.

4.1.1. The Masel-Jansen-Nowak model. In Masel et al [MJN99], and also in the continuous version of Greer et al [GPMW06], the coefficients are chosen in the following way: both the polymerization rate $\tau(x)$, and the degradation rate $\mu(x)$ are constants, say $\tau(x) \equiv \tau_0$, and $\mu(x) \equiv \mu_0$, whereas the fragmentation rate is proportional to polymer length, $\beta(x) = \beta_1 x$. Finally the fragments are homogeneously distributed with $\kappa_0(z) \equiv 1$. We will refer to this particular choice of coefficients as *the MJN model*.

Mathematical analysis of the MJN model has been performed in [MJN99, GPMW06]. The coupled ODE-PDE system can be reduced to a closed system of three ODE for the monomer concentration $V(t)$, the number of polymers $U(t) = \int u(t,x)\,dx$, and the total mass of polymers $P(t) = \int xu(t,x)\,dx$. By constructing a suitable Lyapunov function, it was proven that the infectious state is globally stable when it exists, and the disease free steady state is globally stable otherwise.

4.1.2. Criticism of the MJN model. In the MJN model, each aggregate has the same replicative behaviour regardless to its size. However, some indirect evidences suggest that this hypothesis should be relaxed. Indeed, PrPsc aggregates are very heterogeneous in morphology: in several preparation conditions, either amorphous, spherical or fibrillar aggregates have been observed [JGB+97, SRH+05, EMPS+08]. It seems unlikely that differently structured aggregates possess the same biological or biophysical properties. Experimental investigation of the relation between infectivity and size distribution of PrPsc aggregates (for PrPsc purified from infected brain [SRH+05] or for PrPsc produced by PMCA [WGP+06, WGP+07]) are in favor of a heterogeneous behaviour of PrPsc aggregates. For instance, Weber et al. found a bell-shaped-like dependence of infectivity on particle size [WGP+07, WRM+08]. These considerations suggest that the infectivity of PrPsc aggregates could be dependent on its aggregation state, i.e. the size in model (4.1).

Together with N. Lenuzza, D. Oelz, M. Doumic, F. Mouthon, and B. Perthame, we have generalized previous theoretical studies to take into account the size-dependency of prion infectivity. In the biophysical models, infectivity is a balance between three elementary processes (fragmentation, degradation/sequestration and polymerization). Although we cannot exclude a size-dependent stability (assumed via a heterogeneous degradation rate $\mu(x)$ or a heterogeneous fragmentation factor $\beta(x)$), we have opted for a non uniform elongation rate $\tau(x)$. Indeed, conversion activity, which is the most direct measure of the elongation rate, was shown to be size-dependent [CKRL95, SRH+05].

4.1.3. The MJN model with heterogeneous rate of elongation. In [SRH+05], the size-distribution of prion aggregates was measured experimentally. The distribution was bimodal, with a relatively small amount of polymers having intermediate sizes. However, the MJN model with homogeneous coefficients predicts a unimodel distribution. In [SRH+05], the smaller amount of intermediate size polymers was correlated to a higher converting activity. We have hypothesized that a bimodal distribution could be the consequence of a size-dependent polymerization rate $\tau(x)$.

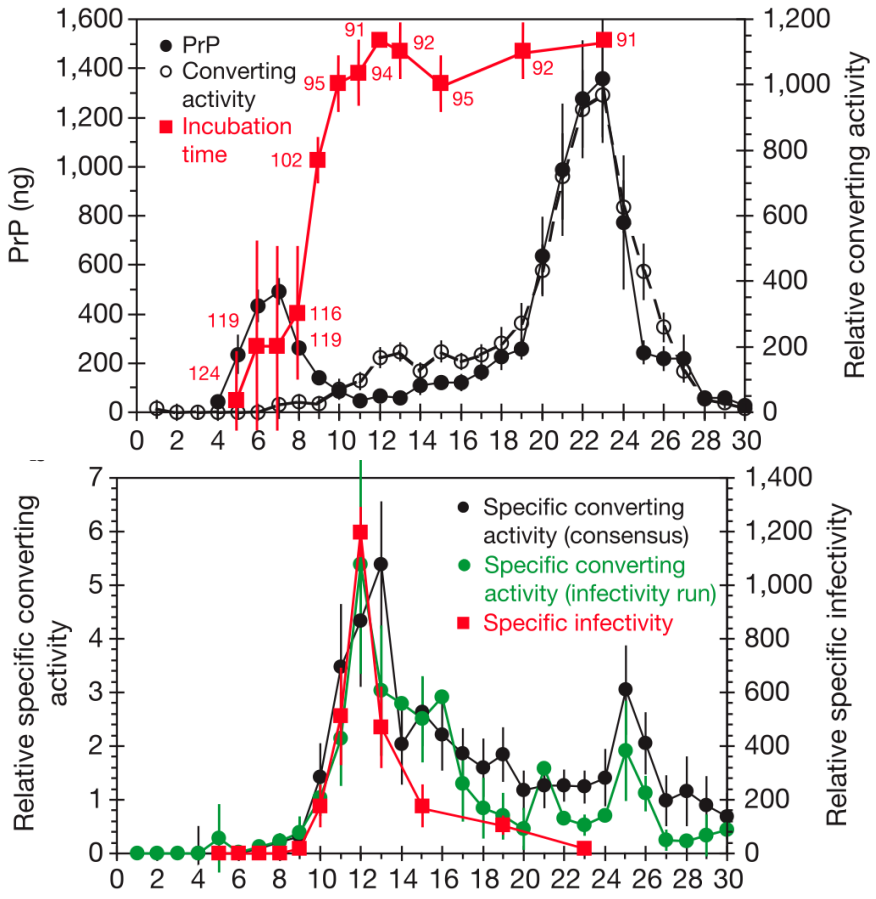

FIGURE 4.1. Experimental data from Silveira et al. [SRH+05] (Top) The measured distribution of polymers was bimodal (black dots), with two peaks located at small and large polymers. The authors made the connection to the concept of Prion infectivity: the incubation time is relatively shorter for intermediate size polymers. (Bottom) Relative converting activity exhibited a higher rate for intermediate size polymers.

Intuitively, if $\tau(x)$ increases at some intermediate size x, this results in faster elongation. Hence the density must drop for this size.

We have tested this hypothesis on the continuous model (4.1). Unsurprisingly, we found that the equilibrium density of polymers in the infectious state is bimodal, provided the variation of $\tau(x)$ has sufficiently large amplitude [20]. We also proved the stability of the disease free state, or the persistence of the infectious state, depending on the parameters. However, we imposed more stringent conditions than [GPMW06].

Then, we checked using numerical simulations that intermediate size polymers do have a higher level of infection, as it is defined experimentally in Silveira et al. as the incubation time of a secondary infection (time to reach a given amount of polymers) [20].

As a partial conclusion, a simple but relevant modification of the MJN model accounts for experimental observations. This work opened several interesting mathematical and biological problems.

The asymptotic analysis of the nonlinear size-structured model is more complicated than for the MJN model. In [20], we have only considered perturbations of the disease-free state using basic

weighted L^1 estimates. This work has been continued in Pierre Gabriel's thesis for particular nonlinearities involving some moments of the size distribution. I will not discuss further the nonlinear case. I shall rather focus on the linear problem.

An interesting linear problem is obtained by assuming that the quantity of monomers $V(t)$ remains at a constant value $V(t) \equiv V_0$. This is reasonable at the early stage of infection, or when the quantity of monomers is artificially sustained, for instance during the PMCA protocol.

4.1.4. Description of PMCA. According to [GMSM08] the development of a blood test is a major priority in prion disease diagnosis (particularly to early detects TSE in cattle with confidence, as well as to ensure the safety of blood transfusion within humans). Indeed, up to date, Transmissible Spongiform Encephalopathies (TSE) are to be detected post-mortem via analysis of tissues collected from dead animals (e.g. brain extracts which contain very large amounts of infectious prion agent PrPsc whereas blood or urin samples contain poor levels). A very promising approach, the protocol PMCA (Protein Misfolding Cyclic Amplification) has been proposed by Soto *et al.* [SSA02, CSHS05, CSS05]. It aims to quickly generate *in vitro* detectable quantities of PrPsc being given minute quantities of it (*e.g.* issued from a blood sample). This technique has been experimentally optimized.

PMCA follows the protein-only hypothesis, which postulates auto-catalytic transconformation, nucleation and aggregation of PrPsc. In fact, it confirms the autocatalytic propagation of PrP misfolding *a posteriori* [BWS+04].

PMCA consists in successive alternations between (i) incubation phases, during which aggregates are expected to grow following a seeding-nucleation scenario alimented by purified PrPc, and (ii) sonication phases, during which fragmentation of aggregates is enhanced in order to increase the number of nucleation sites. It is worth noticing that sonication phases were shown to be necessary [PWGK05].

The control parameter in the PMCA protocol is naturally the rate of fragmentation β, which can be tuned during sonication phases. Efficiency is measured by the exponential growth of the number (or mass) of aggregates. This yields an interesting optimization problem on the Lyapunov exponent.

The Lyapunov exponent is defined as the dominant eigenvalue of the linear growth-fragmentation operator. We assume no degradation, *i.e.* $\mu_0 = 0$, w.l.o.g. The spectral problem writes as follows: find $(\Lambda, \mathcal{U})$ solution of

$$\begin{cases} \Lambda \mathcal{U}(x) + v \dfrac{\partial}{\partial x}\left(\tau(x)\mathcal{U}(x)\right) = \alpha\left(-\beta(x)\mathcal{U}(x) + 2\displaystyle\int_x^\infty \beta(y)\kappa(x,y)\mathcal{U}(y)\,dy\right), \\ \mathcal{U}(x) \geq 0\,, \quad \displaystyle\int \mathcal{U}(x)\,dx = 1\,, \end{cases} \tag{4.2}$$

where v is the constant level of monomer concentration, and α is the intensity of fragmentation, *i.e.* the sonication rate.

The existence of eigenelements for (4.2) has been established in a series of works, with increasing generality [Per07, Mic06, Dou07]. We refer to [DJG10] for the more general conditions up to date, including a discussion about the critical cases. The proof of existence of eigenelements is based on the Krein-Rutman theorem. The key point is to avoid the formation of dust (elongation should overcome fragmentation for small sizes $x \ll 1$), and the escape of mass at $x \to +\infty$ (fragmentation should dominate elongation for large sizes $x \gg 1$). In the case of power-like coefficients: $\tau(x) = \tau_1 x^\nu$ and $\beta(x) = \beta_1 x^\gamma$, these two commitments boil down to the condition $\nu < 1 + \gamma$ [Mic06, DJG10].

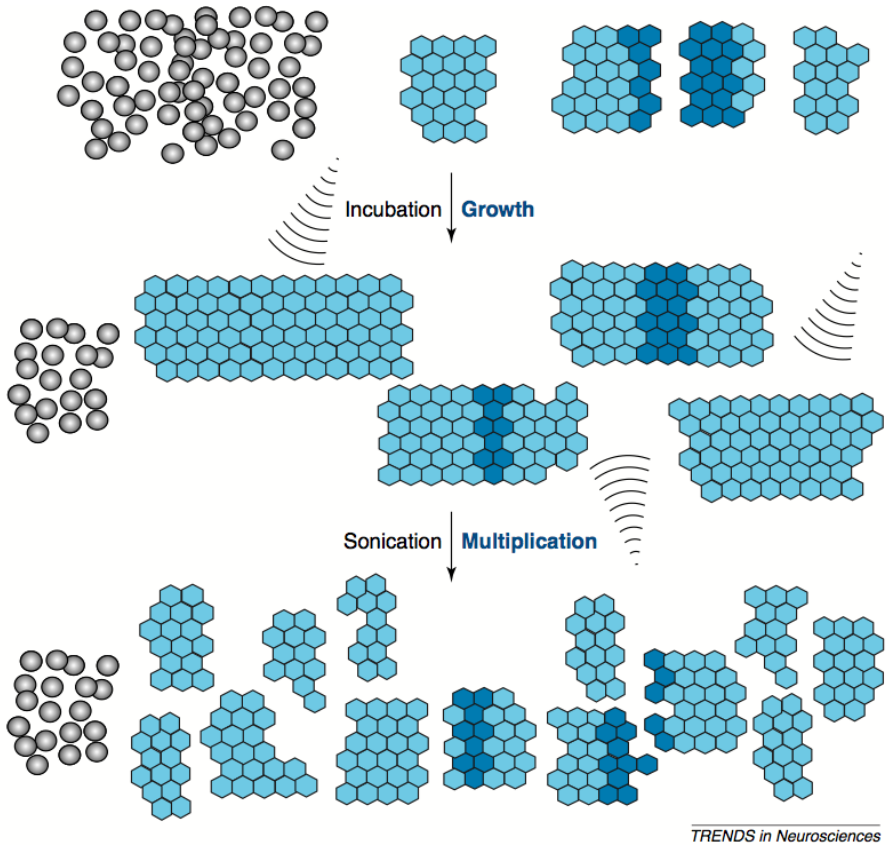

FIGURE 4.2. Sketch of the PMCA protocol: short sonication phases alternate with longer incubation phases. During the sonication phase, the polymers are broken into smaller pieces, thus increasing the number of nucleation units, and enhancing the efficiency of polymer elongation. [SSA02]

Together with M. Doumic and P. Gabriel, we have investigated the dependency of the eigenvalue Λ with respect to the parameters. Clearly, Λ is an increasing function of α, when τ is constant. Indeed, the more units of polymers created by fragmentation, the more efficient is the addition of new monomers. There is an explicit formula in the case of the MJN model: $\Lambda = (\tau_0 \alpha \beta_1 v)^{1/2}$ [GPMW06], [20]. However, this is not the case anymore when τ is not a constant function. If τ is increasing, meaning that larger polymers have a higher converting activity, then a very high level of fragmentation is not efficient because it generates too small aggregates. On the other hand, the absence of fragmentation is clearly not efficient. There should be some trade-off. We formalized this issue in [14], and proved the following result.

Theorem 4.1: Asymptotic dependency of the dominant eigenvalue [14]

Assume that τ and β have power-like behaviours as $x \to 0$ and $x \to +\infty$, ensuring the existence of eigenelements. Then the eigenvalue Λ behaves as follows when the monomer concentration v takes extremal values,

$$\lim_{v\to 0} \Lambda(v) = \lim_{x\to 0} \beta(x)\,, \qquad \lim_{v\to +\infty} \Lambda(v) = \lim_{x\to +\infty} \beta(x)\,. \tag{4.3}$$

A similar result holds true when the sonication rate α takes extremal values,

$$\lim_{\alpha\to 0}\Lambda(\alpha)=\lim_{x\to+\infty}\frac{\tau(x)}{x}\,,\qquad \lim_{\alpha\to+\infty}\Lambda(\alpha)=\lim_{x\to 0}\frac{\tau(x)}{x}\,. \tag{4.4}$$

REMARK 4.2. *Results (4.3) and (4.4) seem independent since they involve the behaviours of β and τ respectively. However they are linked by the fact that τ and β are assumed to behave like power functions for small and large x, and the exponents should satisfy some inequality condition in order to get existence of eigenelements, see* [14] *for more details.*

We derived qualitative conclusions from the non-monotonicity of Λ.

(1) Let the degradation rate $\mu(x)\equiv\mu_0$ be constant. There could exist multiple steady states (V_∞,u_∞) of the nonlinear problem. In fact, those steady states are characterized by the condition $\Lambda(V_\infty)=\mu_0$. We refer to [14] for examples and discussion.

(2) There could exist some rate of sonication α^* maximizing $\Lambda(\alpha)$.

We shall discuss this last issue quantitatively in the next two sections on a finite dimensional version of (4.2).

4.2. Optimal control of sonication and related problems

Together with P. Gabriel and S. Gaubert, we have investigated the optimal control problem associated to a finite dimensional reduction of (4.2), in the general case where $\alpha(t)$ is a time dependent control.

4.2.1. Trade-off between growth and fragmentation results in optimal sonication rate. Before I present the general optimal control problem, let me describe the finite dimensional reduction we had in mind. Further, it will serve as a running example for the presentation of the forthcoming results. Polymers can have three possible states relative to their sizes: small (size 1), medium (size 2), and large (size 3). We denote by x_i, $i=1,2,3$ the number of polymers in each compartment[1]. Transition rates due to elongation of polymers from smaller to larger sizes (polymerization) are denoted by τ_i, $i=1,2$. Transition rates due to fragmentation from larger to smaller sizes are denoted by β_i, $i=2,3$. The corresponding matrices are

$$\begin{cases} G=\begin{pmatrix}-\tau_1 & 0 & 0\\ \tau_1 & -\tau_2 & 0\\ 0 & \tau_2 & 0\end{pmatrix} & \textit{(Growth by elongation)}\\ F=\begin{pmatrix}0 & 2\beta_2 & \beta_3\\ 0 & -\beta_2 & \beta_3\\ 0 & 0 & -\beta_3\end{pmatrix} & \textit{(Fragmentation)}\ . \end{cases} \tag{4.5}$$

Again, the sonication rate is denoted by α. Hence, the dynamics of the system are given by

$$\dot{x}(t)=(G+\alpha F)x(t)=M(\alpha)x(t)\,,$$

where $M(\alpha)=G+\alpha F$ is the growth-fragmentation matrix, and α is the control parameter. This example can be obviously extended to a larger number of compartments. However, the three-dimensional case already exhibits interesting behaviours.

The following proposition gives a qualitative description of the Lyapunov exponent $\lambda(\alpha)$ of the discrete growth-fragmentation linear system $G+\alpha F$ (see also Figure 4.3).

[1]It should denoted by u_i to be consistent with the notations of the two previous sections.

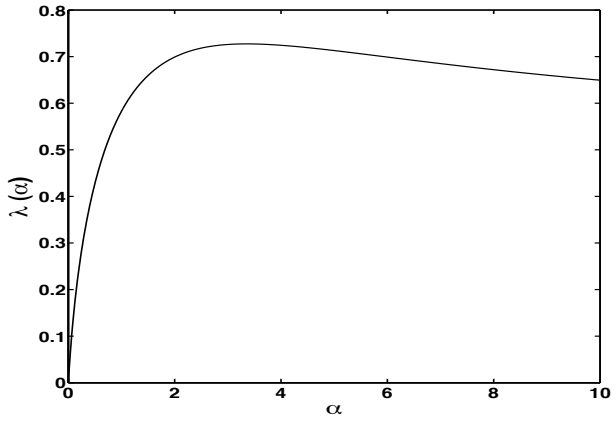

FIGURE 4.3. Dominant eigenvalue $\lambda(\alpha)$ of the matrix $G+\alpha F$ as a function of the control parameter α. It achieves its maximum at some intermediate $\alpha = \alpha^* \in (0, +\infty)$.

Proposition 4.3

The Perron eigenvalue $\lambda(\alpha)$ of $G+\alpha F$ reaches a maximum value for some $\alpha^* \in (0, +\infty)$ if, and only if $\tau_2 > 2\tau_1$. Furthermore the following alternative holds:

- either $\tau_2 \le 2\tau_1$ and $\lambda(\alpha)$ increases from 0 to τ_1,
- or $\tau_2 > 2\tau_1$ and $\lambda(\alpha)$ increases from 0 to $\lambda(\alpha^*)$ and then decreases from $\lambda(\alpha^*)$ to τ_1.

Clearly, if a strategy of constant sonication is followed, $\alpha(t) \equiv \alpha$, this excessively simple model predicts that the sonication rate should be adjusted to a finite value α^* when $\tau_2 > 2\tau_1$.

The following question arises naturally:

> *Can we find a better strategy,* i.e. *yielding a larger Lyapunov exponent, than constant sonication?*

P. Gabriel and I investigated this question numerically and theoretically on the finite-dimensional caricature of the MJN model (4.5), see [**15**] and Section 4.3.1. After the preprint was released, S. Gaubert realized that our preliminary results could be greatly generalized, using ideas and techniques from max-plus linear algebra. In fact, they could be extended to any linear monotone finite-dimensional system, under some irreducibility condition, as described below.

4.2.2. The Lyapunov exponent of a monotone linear controlled system. Let $\mathcal{M}$ be a compact set of irreducible Metzler matrices[2]. Let $K = (\mathbb{R}_+)^n$ be the nonnegative orthant in $\mathbb{R}^n$, K_+ the positive orthant, and $K_0 = K \setminus \{0\}$. For $t > 0$, $x \in K$ and a bounded measurable control function $M \in L^\infty((0,t), \mathcal{M})$, we define $x_M \in W^{1,\infty}((0,t), \mathbb{R}^n)$ as the solution of the following linear system with control function M:

$$\begin{cases} \dot{x}_M(s) = M(s)x_M(s)\,, \quad s \in (0,t) \\ x_M(0) = x \end{cases} \tag{4.6}$$

[2]Recall that Metzler matrices are such that $(\forall i \neq j)\ m_{ij} \ge 0$. Irreducible Metzler matrices are such that for every partition of indices $\{1 \dots n\} = I \cup J$ one can pick $i \in I$ and $j \in J$ such that $m_{ij} > 0$

The optimal asymptotic growth $\lambda(\mathcal{M})$ is defined as the maximal possible growth rate realized by the trajectories of (4.6),

$$(\forall x \in K_0) \quad \lim_{t\to+\infty} \frac{1}{t}\left(\sup_{M\in L^\infty(0,t)} \log\|x_M(t)\|\right) = \lambda(\mathcal{M})\,, \tag{4.7}$$

where $\|\cdot\|$ is an arbitrary norm on $\mathbb{R}^n$. The fact that the limit (4.7) does not depend on the initial condition x is in fact a Corollary of the following Theorem. The Lyapunov exponent is also called the joint spectral radius of $\mathcal{M}$, after Rotta and Strang.

Theorem 4.4: Existence of nonlinear eigenelements [16]

For any compact set of irreducible Metzler matrices $\mathcal{M}$, there exist a real $\lambda(\mathcal{M})$ and a function $\overline{v} : K \to \mathbb{R}_+$, homogeneous of degree 1, positive on K_0, Lipschitz continuous, satisfying the following identity

$$(\forall t \in \mathbb{R}_+)\,(\forall x \in K) \quad e^{\lambda(\mathcal{M})t}\overline{v}(x) = \sup_{M\in L^\infty(0,t)} \overline{v}(x_M(t))\,, \tag{4.8}$$

Moreover the "eigenvalue" $\lambda(\mathcal{M})$ is unique with respect to the class of homogeneous functions of degree 1 which are locally bounded on K.

Identity (4.8) reads as follows: the potential $\overline{v}$ is such that the extremal trajectories with respect to $\overline{v}$ grows exponentially, exactly with rate $\lambda(\mathcal{M})$.

The infinitesimal version of (4.8) is a Hamilton-Jacobi equation in the viscosity sense [**BCD13**],

$$\lambda(\mathcal{M})\overline{v}(x) = \max_{m\in\mathcal{M}} \langle D_x\overline{v}(x), mx\rangle\,. \tag{4.9}$$

Further, using the presumed homogenity of $\overline{v}$, we can define $\mathring{v}$ such that

$$(\forall x \in K_0) \quad \overline{v}(x) = \langle \mathbf{1}, x\rangle \mathring{v}\,(x)\,,$$

where $\mathring{v}$ is a zero-homogeneous function, naturally defined on the projective space PK_0 denoted by $\mathcal{S}$, *i.e.* $\mathcal{S} = K_0/\sim$, where $\sim$ is the equivalence relation induced by colinearity of vectors. Accordingly, $\mathcal{S}_+$ denotes the projective space PK_+.

Remark 4.5. *The projective space $\mathcal{S}$ can be identified with the simplex $\{y \in K \mid \langle \mathbf{1}, y\rangle = 1\}$, and $\mathcal{S}_+$ can be identified with the interior of the simplex.*

Then, problem (4.9) is equivalent to finding $(\lambda(\mathcal{M}), \mathring{v})$ such that

$$\lambda(\mathcal{M})\mathring{v}(x) = \max_{m\in\mathcal{M}} \left(L(x,m)\mathring{v}(x) + \langle D_x\mathring{v}(x), mx\rangle\right)\,, \tag{4.10}$$

where the pay-off L is defined as

$$L(x,m) = \frac{\langle \mathbf{1}, mx\rangle}{\langle \mathbf{1}, x\rangle}\,. \tag{4.11}$$

Remark 4.6. *The identification with the simplex yields the following self-consistent equation in the variable y,*

$$\lambda(\mathcal{M})\mathring{v}(y) = \max_{m\in\mathcal{M}} \left(L(y,m)\mathring{v}(y) + \langle D_y\mathring{v}(y), b(y,m)\rangle\right)\,,$$

where the pay-off L and the vector fields $b(\cdot, m)$ are given by

$$L(y,m) = \langle \mathbf{1}, my\rangle\,, \quad b(y,m) = my - L(y,m)y\,. \tag{4.12}$$

Note that each vector field $b(\cdot, m)$ is tangent to the simplex. Indeed, it gives the projected dynamics on the simplex: if x_M is solution to (4.6) then $y_M = \frac{x_M}{\langle \mathbf{1}, x_M\rangle}$ is solution to the ODE

$$\begin{cases} \dot{y}_M(s) = b(y_M(s), M(s)) \\ y_M(0) = y \end{cases} \tag{4.13}$$

4.2.3. Sketch of proof of Theorem 4.4. In order to capture the exponential growth, it is useful to make the logarithmic transformation

$$\mathring{u} = \log \mathring{v}\,.$$

The original problem (4.8) writes equivalently: find a real $\lambda(\mathcal{M})$ and a zero-homogeneous function $\mathring{u}$, such that

$$\lambda(\mathcal{M})t + \mathring{u}(x) = \sup_{M\in L^\infty(0,t)} \left\{ \int_0^t L(x_M(s), M(s))\, ds + \mathring{u}(x_M(t)) \right\}, \tag{4.14}$$

where the Lagrangian (or running pay-off) L coincides with (4.11). The infinitesimal version reads as follows: find a real $\lambda(\mathcal{M})$ and a zero-homogeneous function $\mathring{u}$ viscosity solution of the ergodic Hamilton-Jacobi equation

$$-\lambda(\mathcal{M}) + H(x, D_x\mathring{u}(x)) = 0\,, \tag{4.15}$$

where the Hamiltonian is defined as

$$H(x,p) = \max_{m\in\mathcal{M}} \left(L(x,m) + \langle p, mx\rangle \right)\,. \tag{4.16}$$

The so-called *ergodic Hamilton-Jacobi equation* (4.15) has been largely studied in the past three decades. It arises in the homogenization of Hamilton-Jacobi equations [**LPV88, EG01, BR03**]. In the context of long time behaviour of Lagrangian dynamics, the existence of a viscosity solution to (4.15) is known as the weak KAM theorem [**Fat97, FS04**], see [**Fat12, Eva04**] for an introduction.

In both settings, the methodology rely either on some regularizing effect of the Lax-Oleinik semi-group (when the Lagrangian is Tonelli), or on some coercivity conditions on the Hamiltonian[3]. It is worth noticing that the coercivity of the Hamiltonian (4.16) is equivalent to uniform controllability of the vector fields $b(\cdot, m)$ for $m \in \mathcal{M}$.

However, uniform controllability is far from being satisfied in our case, since the trajectories flow into smaller and smaller cones of the positive orthant K_+, due to monotonicity of the system. Therefore, one should rely on long time behaviour of (4.6) rather than short time effects, *e.g.* contractivity with respect to the Hilbert distance.

4.2.3.1. *The time-discrete case.* For the sake of simplicity, I present the proof in the discrete time setting firstly. With some abuse of notation, we assume that $\mathcal{M}$ is a compact set of irreducible matrices with nonnegative coefficients. The time-discrete analog of (4.8) reads as follows: find $\lambda(\mathcal{M})$ and $\overline{v}$ such that[4]

$$\lambda(\mathcal{M}) + \log \overline{v}(x) = \sup_{M\in\mathcal{M}} \log \overline{v}(Mx)\,.$$

After reduction by homogeneity, we seek a fixed point of the following time-discrete semi-group,

$$\left(T\mathring{u}\right)(x) = \max_{M\in\mathcal{M}} \left(\mathring{u}\left(Mx\right) + \log\left(\frac{\langle \mathbf{1}, Mx\rangle}{\langle \mathbf{1}, x\rangle} \right) \right)\,.$$

Here, by a fixed point we mean a fixed point in the quotient space $\mathcal{C}^0(\mathcal{S},\mathbb{R})/\mathbb{R}$ in order to eliminate the unknown constant $\lambda(\mathcal{M})$.

The key point is to notice that each flow associated to a given control $M \in \mathcal{M}$ is non-expansive for the Hilbert metric defined in the projective space $\mathcal{S}$ by

$$d(x,y) = \max_{1\le i\le n} \left(\log \frac{x_i}{y_i} \right) - \min_{1\le j\le n} \left(\log \frac{x_j}{y_j} \right)\,. \tag{4.17}$$

[3] With one noticeable exception in [**BCD13**, Proposition].

[4] The underlying dynamics are given by the iterations $x_{n+1} = Mx_n$.

Furthermore, Birkhoff's theorem asserts that it is even a contraction if the matrix M is irreducible: there exists $k(M) < 1$ such that

$$\forall (x,y) \in \mathcal{S} \times \mathcal{S} \quad d(Mx, My) \leq k(M) d(x,y)\,. \tag{4.18}$$

In fact the contractivity ratio is given explicitely by $k(M) = \tanh((\operatorname{diam} M)/4)$, where $\operatorname{diam} M$ is the diameter of the image $M(K)$ with respect to Hilbert's metric d. Therefore, if M is irreducible, then $M(K)$ is a compact set of $\mathcal{S}$ for the Hilbert's metric. Accordingly, it has a finite diameter, and thus $k(M) < 1$.

It is not difficult to show that the discrete time Lagrangian $\tilde{L}(x,M) = \log\left(\frac{\langle \mathbf{1}, Mx\rangle}{\langle \mathbf{1}, x\rangle}\right)$ is Lipschitz continuous from $(\mathcal{S}, d)$ to $(\mathbb{R}, |\cdot|)$.

LEMMA 4.7. *The operator T preserves a compact subset of the quotient $\mathcal{C}^0(\mathcal{S},\mathbb{R})/\mathbb{R}$.*

▸ *Sketch of proof.* The compact subset of $\mathcal{C}^0(\mathcal{S},\mathbb{R})/\mathbb{R}$ that we are looking for is characterized by an *a priori* bound on the Lipschitz constant. More precisely, we have for any $(x,y) \in \mathcal{S} \times \mathcal{S}$,

$$(T\mathring{u})(x) - (T\mathring{u})(y) \leq \mathring{u}\left(M^* x\right) + \tilde{L}(x, M^*) - \mathring{u}\left(M^* y\right) - \tilde{L}(y, M^*)\,, \tag{4.19}$$

for some $M^* \in \mathcal{M}$ (the optimal control associated to x). Therefore,

$$\begin{aligned}(T\mathring{u})(x) - (T\mathring{u})(y) &\leq (\operatorname{Lip}\mathring{u}) d(M^* x, M^* y) + (\operatorname{Lip}\tilde{L}) d(x,y)\\ &\leq \left(\left(\sup_{M\in\mathcal{M}} k(M)\right)(\operatorname{Lip}\mathring{u}) + \operatorname{Lip}\tilde{L}\right) d(x,y)\,.\end{aligned}$$

Therefore, $\operatorname{Lip}(T\mathring{u}) \leq k(\mathcal{M})\operatorname{Lip}\mathring{u} + \operatorname{Lip}\tilde{L}$. Hence, the set of Lipschitz continuous functions such that

$$\operatorname{Lip}\mathring{u} \leq \frac{\operatorname{Lip}\tilde{L}}{1 - k(\mathcal{M})}\,,$$

is invariant by the operator T. ◂

From Schauder's theorem, there exists a fixed point $\mathring{u}$ in the quotient space $\mathcal{C}^0(\mathcal{S},\mathbb{R})/\mathbb{R}$. It means that there exists a constant $-\lambda$ such that $T\mathring{u} = \mathring{u} + \lambda$, *i.e.*

$$\lambda + \mathring{u}(x) = \max_{M\in\mathcal{M}} \left(\mathring{u}(Mx) + \log\frac{\langle \mathbf{1}, Mx\rangle}{\langle \mathbf{1}, x\rangle}\right).$$

4.2.3.2. *The time-continous case.* I briefly sketch the proof of Theorem 4.4 in the time-continuous setting. Following (4.14), let T_t^+ be the forward Lax-Oleinik semi-group

$$(T_t^+ \mathring{u})(x) = \sup_{M\in L^\infty(0,t)} \left\{\int_0^t L(x_M(s), M(s))\, ds + \mathring{u}(x_M(t))\right\}, \quad t > 0\,. \tag{4.20}$$

By exploiting the Finsler structure of the projective space $\mathcal{S}$ endowed with the Hilbert projective metric [**No94**], we can establish the following claim: The Lagrangian $L(x,m) = \frac{\langle \mathbf{1}, mx\rangle}{\langle \mathbf{1}, x\rangle}$ is Lipschitz continuous from $(\mathcal{S}, d)$ to $(\mathbb{R}, |\cdot|)$. More precisely, the Lipschitz constant is bounded above by

$$\operatorname{Lip} L(\cdot, m) \leq \sup_{x\in\mathcal{S}} \inf_{\gamma\in\mathbb{R}} \left(\frac{\langle \mathbf{1}, |m - \gamma.\mathrm{Id}|x\rangle}{\langle \mathbf{1}, x\rangle}\right).$$

The analog of statement (4.18) in the continuous setting is slightly more difficult to establish. For the sake of simplicity we restrict here to matrices with positive coefficients off the diagonal. In this case, we have the following uniform contraction estimate, providing that the same control is applied at each time for two trajectories starting from x and y respectively,

$$(\forall t \geq 0)\ (\forall M \in L^\infty(0,t))\ (\forall (x,y) \in \mathcal{S} \times \mathcal{S}) \quad d(x_M(t), y_M(t)) \leq e^{-\mu t} d(x,y)\,, \tag{4.21}$$

where the contraction exponent μ is given by

$$\mu = \inf_{m \in \mathcal{M}} \left(\min_{i \neq j} \left(2(m_{ij} m_{ji})^{1/2} \right) \right) > 0 \,. \tag{4.22}$$

It is possible to define a weaker contraction exponent based on the irreducibility assumption only, and sub-additivity. Then, for any discount rate $\varepsilon > 0$, the infinite-horizon problem is defined as follows,

$$u_\varepsilon(x) = \sup_{M \in L^\infty(0,\infty)} \left\{ \int_0^\infty e^{-\varepsilon t} L(x_M(t), M(t))\, dt \right\} . \tag{4.23}$$

It is clearly zero-homogeneous. Furthermore, it is a viscosity solution of the following stationary Hamilton-Jacobi equation,

$$-\varepsilon u_\varepsilon(x) + H(x, D_x u_\varepsilon(x)) = 0 \,. \tag{4.24}$$

Clearly, $\varepsilon u_\varepsilon$ is uniformly bounded by $\|L\|_\infty$. Similarly as in the discrete time problem, exponential contraction of trajectories yields an *a priori* Lipschitz estimate, uniformly with respect to ε. Indeed, for any pair (x, y), we can choose a close-to-optimal control function $M : [0, \infty) \to \mathcal{M}$, associated with the initial point $x \in \mathcal{S}$. We choose the same control function for the initial point $y \in \mathcal{S}$. Then, we have

$$\begin{aligned} u_\varepsilon(x) - u_\varepsilon(y) &\leq \delta + \int_0^\infty e^{-\varepsilon t} \left(L(x_M(t), M(t)) - L(y_M(t), M(t)) \right) dt \\ &\leq \delta + \left(\sup_m \operatorname{Lip} L(\cdot, m) \right) \int_0^\infty e^{-\varepsilon t} d(x_M(t), y_M(t))\, dt \\ &\leq \delta + \left(\sup_m \operatorname{Lip} L(\cdot, m) \right) \int_0^\infty e^{-(\varepsilon+\mu)t} d(x, y)\, dt \\ &\leq \delta + \left(\sup_m \operatorname{Lip} L(\cdot, m) \right) \frac{1}{\varepsilon + \mu} d(x, y) \,. \end{aligned} \tag{4.25}$$

As δ is arbitrary, we deduce

$$\operatorname{Lip} u_\varepsilon \leq \frac{\operatorname{Lip} L}{\mu} \,. \tag{4.26}$$

Hence, up to extraction, $\varepsilon u_\varepsilon$ converges towards a constant $\lambda(\mathcal{M})$, locally uniformly on $\mathcal{S}$. In addition, we can extract a subsequence $(u_{\varepsilon'})$, which converges towards some Lipschitz function $\mathring{u}$, up to the subtraction of a (possibly large) constant, say $\min u_{\varepsilon'}$. It can be proven that $\mathring{u}$ is globally Lipschitz on $\mathcal{S}$, up to the boundary ∂S.

Finally, passing to the limit in (4.24) in the viscosity sense, the limit function $\mathring{u}$ is a viscosity solution of the ergodic equation (4.15). Equivalently, it is a fixed point of the semi-group T_t^+, in the following sense,

$$(\forall t > 0) \quad \lambda t + \mathring{u}(x) = \sup_{M \in L^\infty(0,t)} \left\{ \int_0^t L(x_M(s), M(s))\, ds + \mathring{u}(x_M(t)) \right\} , \tag{4.27}$$

This concludes the proof of Theorem 4.4.

4.2.3.3. *Connection with the Pontryagin Maximum Principle.* As a side remark, let me draw preliminary connections between the previous analysis and the Pontryagin Maximum Principle (PMP). Recall that the PMP provides a necessary condition for optimal trajectories [**Tré05**]. In our context, it reads as follows.

Theorem 4.8: Pontryagin Maximum Principle (PMP)

If $x(s)$ is an optimal trajectory of the controlled problem (4.13) associated with the running pay-off $L(x,m)$, then there exists a costate $p(s)$, solution of the adjoint problem

$$\dot{p}(s) = -p(s)^T M(s) - D_x L(x(s), M(s))\,. \tag{4.28}$$

Moreover, we have

$$\lambda(\mathcal{M}) = H(x(s),p(s)) = \max_{m\in\mathcal{M}} \left(L(x(s),m) + \langle p(s), mx\rangle\right)\,,$$

where the maximum value in the latter expression is attained at $m = M(s)$.

The costate $p(s)$ is related to the solution $\mathring{u}$ by the relation $p(s) = D_x\mathring{u}(x(s))$, obtained by the integration of the Hamilton-Jacobi equation along the characteristic curves. Therefore, a Lipschitz estimate on u should naturally translate into a L^∞ bound on $p(s)$. Such a bound is established below in the appropriate norm. The projective space $\mathcal{S}$ endowed with the Hilbert projective metric (4.17) is endowed with a Finsler structure [**No94**]. Hence, the tangent space (here, the velocity space) is equipped with the semi-norm

$$\|v\|_x = \max_{1\le i\le n} \frac{v_i}{x_i} - \min_{1\le j\le n} \frac{v_j}{x_j}\,, \tag{4.29}$$

such that $\|v\|_x = 0$ if and only if v is a colinear to x. This semi-norm pops up when looking at the infinitesimal variation

$$d(x+h,x) = \max_{1\le i\le n} \log\left(1+\frac{h_i}{x_i}\right) - \min_{1\le j\le n} \log\left(1+\frac{h_j}{x_j}\right) = \max_{1\le i\le n} \frac{h_i}{x_i} - \min_{1\le j\le n} \log\frac{h_j}{x_j} + o(h)\,.$$

Then, the costate $p(s)$ (4.28) lies naturally on the cotangent space $T_x^*\mathcal{S}$, defined as

$$T_x^*\mathcal{S} = \{p \mid \langle p, x\rangle = 0\}\,, \quad \|p\|_x = \frac{1}{2}\langle |p|, x\rangle = \frac{1}{2}\sum_{k=1}^n |p_k| x_k\,. \tag{4.30}$$

Proposition 4.9: Lagrangian estimates

(i) The following duality inequality holds true

$$\forall (p,v) \in T_x^*\mathcal{S} \times T_x\mathcal{S}\,, \quad \langle p, v\rangle \le \|p\|_x \|v\|_x\,.$$

(ii) As we seek eventually a zero-homogeneous function $\mathring{u}$ verifying $\langle D_x\mathring{u}(x), x\rangle = 0$, it is natural to require $\langle p, x\rangle = 0$, as in the definition (4.30). In fact, it is immediate to check that the identity $\langle p(s), x(s)\rangle$ is conserved along the Pontryagin flow,

$$\begin{cases} \dot{x}(s) = M(s)x(s) \\ \dot{p}(s) = -p(s)^T M(s) - D_x L(x(s), M(s)) \end{cases} \tag{4.31}$$

(iii) The main Lagrangian type *a priori* estimate is a backward in time estimate on the costate $p(s)$,

$$\frac{d}{ds}\|p(s)\|_{x(s)} \ge \mu \|p(s)\|_{x(s)} - \|D_x L(x(s), M(s))\|_{x(s)}\,, \tag{4.32}$$

where μ is defined in (4.22).

Corollary 4.10: Existence of nonlinear eigenelements (alternative proof)

The semi-group T^+ (4.20) stabilizes the set of Lipschitz continous functions with the same estimate as in (4.26).

▸ *Sketch of proof.* Let $w(s,x)$ be the value function,

$$w(s,x) = \sup_{M\in L^\infty(s,t)} \left\{ \int_s^t L(x_M(s), M(s))\, ds + \mathring{u}(x_M(t)) \right\},$$

The Pontryagin maximum principle can be applied to this equation, known as the Mayer problem in optimal control theory [**CS04**, **Tré05**]. The equation on the costate $p(s)$ has to be understood as a backward in time equation, with the final datum $p(t) = D_x w(t, x(t)) = D_x \mathring{u}(x(t))$. Moreover, we have $p(0) = D_x w(0,x) = D_x(T_t^+ \mathring{u})(x)$ by the classical Hamilton-Jacobi transformation. Then, we deduce from (4.32), and the Gronwall lemma, that

$$\|D_x(T_t^+\mathring{u})(x)\|_x = \|p(0)\|_{x(0)} \le \|p(t)\|_{x(t)} e^{-\mu t} + \sup_{s\in(0,t)} \frac{\|D_x L(x(s), M(s)\|_{x(s)}}{\mu} \left(1 - e^{-\mu t}\right) \le \frac{\operatorname{Lip} L}{\mu},$$

when $\|p(t)\|_{x(t)} = \|D_x \mathring{u}(x(t))\|_{x(t)} \le (\operatorname{Lip} L)/\mu$. ◂

4.2.4. Links with other theories. It is instructive to make the parallel between Theorem 4.4 and three other theories, old and new.

4.2.4.1. *The Perron-Frobenius theory.* For a constant control $M(s) \equiv m$ we have $x_M(t) = e^{tm}x$. It is an immediate consequence of the Perron-Frobenius Theorem that, being $\phi_m \in K_+$ the left Perron eigenvector of m, the linear function $\overline{v}(x) = \langle \phi, x\rangle$ satisfies the following identity,

$$(\forall t \in \mathbb{R}_+)\ (\forall x \in K) \quad e^{\lambda(m)t}\overline{v}(x) = \overline{v}(x_m(t)),$$

where $\lambda(m) \in \mathbb{R}$ is the dominant eigenvalue of m. Therefore, Theorem 4.4 can be seen as a generalization of the Perron-Frobenius theorem to a compact set of irreducible matrices. Note that the infinitesimal problem (4.9) simply reduces to the dual eigenproblem $\lambda(m)\phi^T = \phi^T m$.

4.2.4.2. *The weak KAM theory: homogenization and Lagrangian dynamics.* In [**LPV88**], the authors analyse a homogenization problem for a Hamilton-Jacobi equation in a periodic setting,

$$\partial_t u^\varepsilon(t,x) + H\left(\frac{x}{\varepsilon}, D_x u^\varepsilon(t,x)\right),$$

where $H(x,p)$ is periodic with respect to the spatial variable. In this context, the *cell problem* boils down to solving the so-called ergodic Hamilton-Jacobi equation on the torus

$$-\overline{H}(P) + H(y, P + D_y u(y)) = 0, \quad y \in \mathbb{T}^n, \tag{4.33}$$

where P is a constant vector (accounting for the variations of the solution at a macroscopic scale), and u is the corrector of the homogenization problem. The homogenized Hamiltonian $\overline{H}(P)$ is uniquely defined, and it is convex when H is convex with respect to p. It is analogous to the *eigenvalue* $\lambda(\mathcal{M})$ in our setting. Lions, Papanicolaou and Varadhan solved the cell problem under the assumption that the Hamiltonian is coercive,

$$\lim_{|p|\to+\infty} H(y,p) = +\infty, \quad \text{uniformly with respect to } y \in \mathbb{T}^n. \tag{4.34}$$

Theorem 4.11: Existence for the ergodic Hamilton-Jacobi equation [LPV88]

Under assumption (4.34), for each $P \in \mathbb{R}^n$ there exists a unique $\overline{H}(P)$ such that there exists a continuous periodic viscosity solution u of (4.33).

▸ *Sketch of proof.* The original proof is based on the approximation by the discounted equation (4.24). As compared to the proof of Theorem 4.4 above, the Lipschitz estimate comes directly from (4.34), the equation, and the immediate bound $\|\varepsilon u_\varepsilon\|_\infty \le \|L\|_\infty$. ◂

There are two main discrepancies between the context of Theorem 4.4, and the cell problem (4.33). Firstly, as opposed to $\mathbb{T}^n$, our problem is naturally set on the simplex $\mathcal{S}$ which is not compact for

the Hilbert metric. Therefore, one should pay attention to the behaviour of the family of vector fields at the boundary $\partial\mathcal{S}$. Irreducibility plays of course a crucial role here.

A related but more intricated issue is that the Hamiltonian (4.16) does not satisfy the condition (4.34). In the context of optimal control, the coercivity of H is a consequence of the uniform local controllability of the system. For instance, $|H(x,p)| \gtrsim \mu|p|$ for $\mu > 0$ is equivalent to the following controllability condition [**CDL90**, Hyp. (115)]

$$\forall y \in \mathbb{T}^n \quad B(0,\mu) \subset \text{convex hull}\{b(y,m) \mid \alpha \in \mathcal{M}\}\,, \tag{4.35}$$

Alternatively speaking, the set of control enables to follow any direction in space at a speed uniformly bounded below. On the contrary, system (4.13) fails to be locally uniformly controllable due to the monotonicity of the system which rules out some directions of the state space. In fact, there exist cones strictly included in K_+, that are invariant by the dynamics.

Independently, in the context of Lagrangian dynamics, Fathi obtained an analogous result as Theorem 4.11, in any compact manifold, but for Tonelli Lagrangians[5] [**Fat97**]. In particular, the corresponding Hamiltonian is assumed to be superlinear with respect to p, which is a stronger assumption than coercivity (4.34). Superlinearity ensures that the forward semi-group

$$T_t^+ u(y) = \sup\left\{ \int_0^t L(y(s), \dot{y}(s))\, ds + u(y(t)) \mid y(0) = y \right\}, \quad t > 0\,,$$

where the supremum is taken over any $\mathcal{C}^1$ curve $y(s)$ starting from y at time $s = 0$, has an instantaneous regularizing effect: the image of a continuous function is Lipschitz continuous for $t > 0$, with a Lipschitz constant depending on L and t. This provides enough compactness to prove the existence of a common fixed point of the semi-group, up to a constant $-\lambda t$, like for (4.14).

Fathi's weak KAM theory goes further. It makes the connection between viscosity solutions of Hamilton-Jacobi equations and the theory of Aubry-Mather in Lagrangian dynamics. It aims to investigate the long time behaviour of extremal trajectories of Lagrangian dynamics, *i.e.* minimizing curves[6]. We will discuss further connections in Section 4.3.2.

4.2.4.3. *The theory of linear inclusion systems.* Let $\mathcal{A}$ be a compact set of matrices, non necessarily of Metzler type. Following Rotta and Strang, the generalized spectral radius $\rho(\mathcal{A})$ is the maximal spectral radius generated by products of arbitrarily large number of matrices,

$$\rho(\mathcal{A}) = \sup\left(\lim_{N\to+\infty} \{\|A_{i_1} \dots A_{i_N}\|^{1/N}\} \right) = \sup\left(\inf_{N\geq 1} \{\|A_{i_1} \dots A_{i_N}\|^{1/N}\} \right), \tag{4.36}$$

where $\|\cdot\|$ is any operator norm. The identity between the last two terms holds by a classical subadditivity argument. This generalized spectral radius is important for studying linear inclusion systems,

$$x(k+1) \in \mathcal{A}x(k)\,.$$

In particular, the condition $\rho(\mathcal{A}) < 1$ guarantees the stability of the inclusion.

Observe the correspondence between (4.36) (discrete time) and (4.7) (continuous time).

In the early 1980's, Barabanov introduced a very powerful tool to investigate further stability of linear inclusions, the so-called Barabanov norms. A Barabanov norm V is a norm on $\mathbb{R}^n$ such that for all x,

$$\max_{A\in\mathcal{A}} V(Ax) = \rho(A)V(x)\,. \tag{4.37}$$

[5] *i.e.* superlinear and strictly convex in the fibers.

[6] Extremal curves are generally minimizing curves in the theory of Lagrangian dynamics, and maximizing curves in optimal control theory, as in our context. One can easily switch from one framework to the other by changing the sign of the Lagrangian, and reversing time.

Hence, a Barabanov norm measures in an optimal way the growth of the semi-group associated to the linear inclusion. Alternatively, we can interpret N as a nonlinear eigenvector associated to the eigenvalue $\rho(A)$ for the tropical Perron-Frobenius-Ruelle operator $v \mapsto \max_{A\in\mathcal{A}} v(Ax)$.

The existence of a Barabanov norm (4.37) is guaranteed under compactness, and some irreducibility property of the set $\mathcal{A}$. However, irreducibility here is different from irreducibility of Metzler matrices as above (recall that $A \in \mathcal{A}$ are not assumed to be Metzler matrices here). Here, irreducibility means that the set of matrices $\mathcal{A}$ does not have any invariant subspace, but the trivial ones $\{0\}$ and $\mathbb{R}^n$.

There is a wide class of problems (already solved, or still open), following the works of Rotta and Strang, and Barabanov. One of the problem is the practical computation of the generalized spectral radius. Another type of problem is the uiqueness of the Barabanov norm. Also, many authors have investigated the regularity of the generalized spectral radius in the space of matrix sets endowed with the Hausdorff metric.

Clearly, Barabanov norms and the potential $\overline{v}$ defined in Theorem 4.4, are similar objects.

I refer to [**Mor13**] for the study of Barabanov norms using Mather theory. See also [**MW14**] for recent work on extremal norms in the context of monotone systems. Up to our knowledge, Theorem 4.4, as it is stated in full generality, seems to be new.

4.3. Qualitative behaviour of optimal trajectories

4.3.1. The ergodic set: dynamics of the running example (4.5). I briefly present some qualitative results obtained together with P. Gabriel [**15**] on the three-dimensional problem (4.5)[7],

$$\begin{cases} \dot{x}_\alpha(s) = (G + \alpha(s)F)x_\alpha(s) \\ x_\alpha(0) = x \end{cases} \tag{4.38}$$

associated with the scalar control function $\alpha \in L^\infty(0,\infty)$. Recall that the goal is to maximize the asymptotic exponential growth of x_α.

As emphasized by Arisawa in a couple of papers [**Ari97, Ari98**], a particular set, called the *ergodic set* $\mathcal{Z} \subset \mathcal{S}$, plays an important role in the study of the ergodic Hamilton-Jacobi equation (4.15), when uniform controllability is lacking. It is characterized by the following properties:

(i) $\mathcal{Z}$ is non empty, closed and positively invariant by the flows,

(ii) $\mathcal{Z}$ is globally attractant,

(iii) $\mathcal{Z}$ is globally controllable.

We refer to [**Ari97, Ari98**] for the precise meaning of each of these properties.

Together with P. Gabriel, we have characterized the ergodic set $\mathcal{Z}$ for the growth-fragmentation controlled problem (4.5) in dimension $d = 3$, under some suitable conditions which are valid for a large set of parameters τ_i, β_j.

In order to define the set $\mathcal{Z}$, let me introduce some notations: we assume that α can take values in $[a, A]$, with $0 < a < A < \infty$. Moreover, we denote by $e(\alpha) \in \mathcal{S}$ the dominant eigenvector associated with the eigenvalue $\lambda(\alpha)$ (see Proposition 4.3). We denote by $\mathcal{E} \subset \mathcal{S}$ the curve of eigenvectors: $(e(\alpha))_{\alpha\in[0,\infty]}$. The curve $\mathcal{E}_a^A \subset \mathcal{S}$ denotes the restriction to the admissible controls $\alpha \in [a, A]$:

$$\mathcal{E}_a^A = \{e(\alpha) \mid \alpha \in [a, A]\}.$$

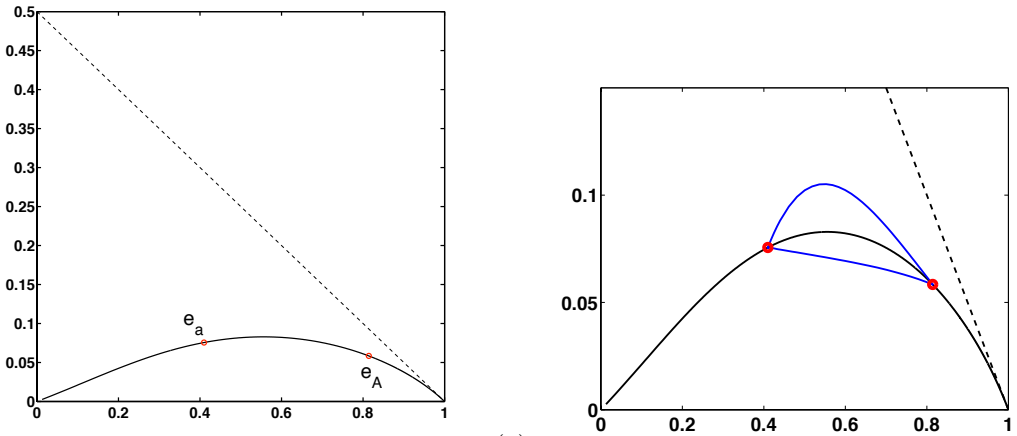

(a) (b)

FIGURE 4.4. (a) The curve of eigenvectors $\mathcal{E}$ in the simplex $\mathcal{S}$. Here, the simplex is paramatrized by the first two coordinates. The particular eigenvectors $e(a)$ and $e(\alpha)$ are depicted in red dots. (b) The blue curves delimit the ergodic set $\mathcal{Z}$. The dashed line represents the boundary of the simplex.

The ergodic set $\mathcal{Z}$ is the compact set enclosed by the two following curves,

$$\gamma_a^A \begin{cases} \dot\gamma(s) = b(\gamma(s), a) \\ \gamma(0) = e(A) \end{cases}, \quad \gamma_A^a \begin{cases} \dot\gamma(s) = b(\gamma(s), A) \\ \gamma(0) = e(a) \end{cases}. \tag{4.39}$$

Recall that b stands for the projected dynamics (4.6) on the two-dimensional simplex (Remark 4.6). Alternatively speaking, $\mathcal{Z}$ is delimited by the two following infinite horizon trajectories:

- the first trajectory starts from the first eigenvector $e(a)$ with the maximal intensity $\alpha(t) \equiv A$,
- the second trajectory starts from the last eigenvector $e(A)$ with the minimal intensity $\alpha(t) \equiv a$.

Using a suitable parametrization of the simplex by specific trajectories, and a dedicated monotonicity formula, we were able to prove that all trajectories enter eventually any larger approximation of the ergodic set. Moreover we could prove that the ergodic set is controllable.

The parametrization of the simplex goes as follows. We cover partially[8] the simplex with trajectories $\Gamma(\beta, s)$, parametrized by their starting point $e(\beta)$, for $\beta \in [0, a) \cup (A, \infty]$, and time $s > 0$, see Figure 4.5:

$$(\forall \beta \in [0, a)) \quad \Gamma_A : \begin{cases} \partial_s \Gamma_A(\beta, s) = b(\Gamma_A(\beta, s), A) \\ \Gamma_A(\beta, 0) = e(\beta) \in \mathcal{E} \end{cases} \tag{4.40}$$

$$(\forall \beta \in (A, \infty]) \quad \Gamma_a : \begin{cases} \partial_s \Gamma_a(\beta, s) = b(\Gamma_a(\beta, s), a) \\ \Gamma_a(\beta, 0) = e(\beta) \in \mathcal{E} \end{cases}.$$

[7] The two-dimensional case was investigated thoroughly in [CGS14]

[8] Another set of charts is used to cover the rest of the simplex. However it provides only transient informations about the trajectories. In short, it guarantees that any trajectory will enter the area covered by the charts $\Gamma_A \cup \Gamma_a$ after some time.

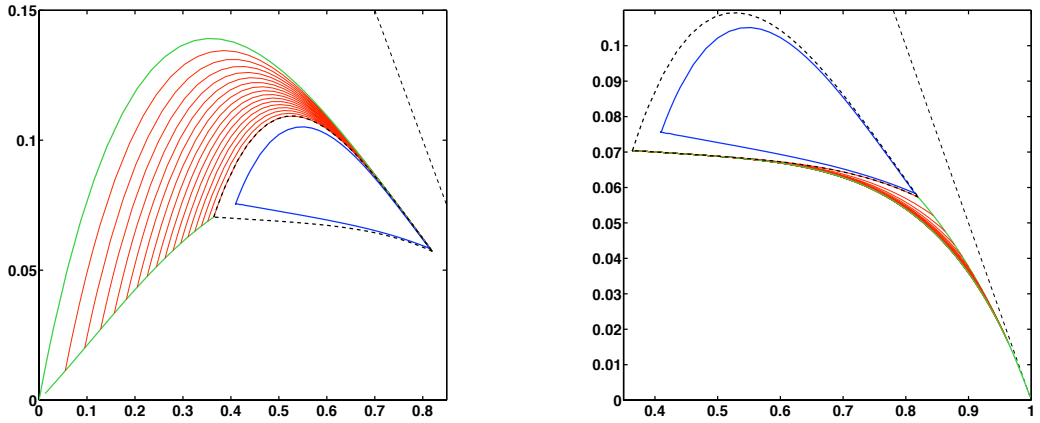

(Γ_A) (Γ_a)

FIGURE 4.5. Tunneling effect: the trajectories are trapped in the areas delimited by the green curves. They are forced to enter the ergodic set $\mathcal{Z}$ due to the monotonicity formulas (4.41)-(4.42), as they cross monotonically the red trajectories towards $\mathcal{Z}$.

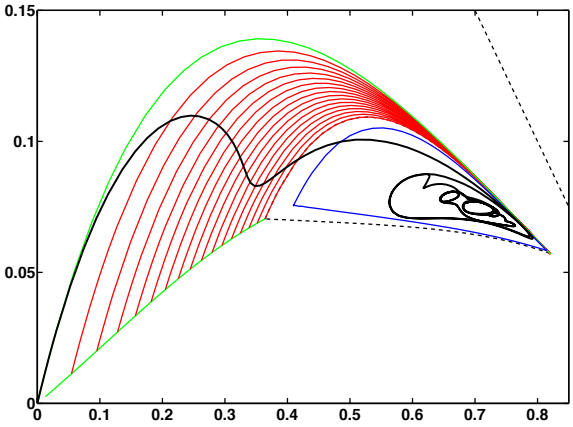

FIGURE 4.6. Any trajectory enters the ergodic set in a monotonic way (black line).

We derived monotonicity formulas which enable to drive the trajectories towards the ergodic set. They rely on the affine structure of the control system, namely $G + \alpha F$, where α is a scalar control parameter. Let $x_\alpha(t)$ be any trajectory of the control system (4.38). Let $\beta_A(t) \in [0, a)$ denotes the first coordinate of the trajectory $x_\alpha(t)$ in the chart system Γ_A which covers partially the upper side of $\mathcal{E}$ (as in Figure 4.5–left), then we have:

(4.41)

$$\dot{\beta}_A(t) = \operatorname{sign}(A - \beta_A(t))(A - \alpha(t))\varphi(x_\alpha(t)) \exp\left(-\int_0^{s(t)} \omega_A'(\beta_A(t), s')\, ds'\right) \left\langle \frac{de}{d\beta}(\beta_A), \frac{\Theta Fe(\beta_A)}{|\Theta Fe(\beta_A)|} \right\rangle^{-1},$$

where $\varphi(x_\alpha(t)) \leq 0$ as $x_\alpha(t)$ lies in the upper side of $\mathcal{E}$. Also, Θ denotes the direct orthogonal rotation on the tangent space of $\mathcal{S}$. On the other hand, for the chart system Γ_a which covers partially the lower side of $\mathcal{E}$, if $\beta_a(t) \in (A, \infty]$ denotes the first coordinate of the trajectory $x_\alpha(t)$

(as in Figure 4.5–right), we have

(4.42)
$$\dot\beta_a(t) = \operatorname{sign}(a-\beta_a(t))(a-\alpha(t))\varphi(x_\alpha(t))\exp\left(-\int_0^{s(t)}\omega_a'(\beta_a(t),s')\,ds'\right)\left\langle \frac{de}{d\beta}(\beta_a), \frac{\Theta Fe(\beta_a)}{|\Theta Fe(\beta_a)|}\right\rangle^{-1},$$

where $\varphi(x_\alpha(t)) \geq 0$ as $x_\alpha(t)$ lies in the lower side of $\mathcal{E}$. We make the technical hypothesis that $\left\langle \frac{de}{d\beta}, \Theta Fe\right\rangle < 0$ is negative everywhere on $\mathcal{E}$[9]. Using this assumption, we could prove that β_A is increasing, and β_a is decreasing. This is enough to prove that trajectories are moving monotonically towards the ergodic set $\mathcal{Z}$. Here, monotonicity means that they cross the red curves in a forward way, see Figure 4.6.

Such geometrical characterization of the ergodic set, as the enclosure of two extremal trajectories, is complementary to the analytical results presented in Section 4.2.2. The existence of the ergodic set is sufficient to prove the existence of an ergodic constant $\lambda(\mathcal{M})$, but it is not enough to get the existence of an *eigenfunction*, *i.e.* a critical viscocity solution $\mathring{u}$ of the ergodic Hamilton-Jacobi equation (4.15). However, it brings interesting qualitative informations about the long time behaviour of maximizing curves.

4.3.2. The Aubry set: asymptotics of maximizing curves. Here, we continue the analysis of Section 4.2, by deriving some consequences of the existence of a critical viscosity solution of the ergodic problem $\mathring{u}$ (4.14). The objective is to define the Aubry set, which encodes the long time behaviour of maximizing trajectories.

4.3.2.1. *Calibrated trajectories.* An important notion in the weak KAM theory is the definition of calibrated trajectories. From now on, we allow relaxed controls, which are obtained as weak limits of control sequences. Alternatively speaking, we suppose that the control $M(s)$ is allowed to take values in the convex closure of $\mathcal{M}$, such that the set of control functions, $L^\infty((0,t);\overline{\text{co}}(\mathcal{M}))$, is closed by weak$-*$ convergence.

Definition 4.12: Calibrated curves

Let $\mathring{u}$ be a solution of (4.14). A Lipschitz curve $\gamma : I \to \mathcal{S}$ defined on the interval $I \subset \mathbb{R}_+$, associated to some relaxed control $M \in \mathcal{C}(I)$, $\gamma = x_M$, is calibrated if for every $t \leq t' \in I$, we have

$$\mathring{u}(\gamma(t')) - \mathring{u}(\gamma(t)) = \int_t^{t'} (L(x_M(s),M(s)) - \lambda(\mathcal{M}))\,ds\,.$$

In other words, the supremum identity (4.14) is saturated along γ.

Calibrated curves are the extremal trajectories associated to the optimal control problem. The existence of calibrated trajectories on a bounded interval is a consequence of the weak$-*$ compactness of $L^\infty(I;\overline{\text{co}}(\mathcal{M}))$. It enables to extract a subsequence out of a sequence of maximizing trajectories. Then, the existence of calibrated curves on $[0,+\infty)$ is obtained by a diagonal argument from calibrated curves defined on $[0,n]$ with a fixed origin $\gamma_n(0) = x$. This argument yields the following proposition.

Proposition 4.13: Existence of calibrated curves

For any $x \in K_+$ there exists a calibrated curve $\gamma : [0,+\infty) \to K_+$ such that $\gamma(0) = x$.

We present below some aspects of the Aubry-Mather theory. The purpose of this theory is to describe some special subsets, the so-called Mather, and Aubry sets. Here, we will focus on the

[9]It is related to the way ho the vector fields $b(y,\alpha)$ cross the curve $\mathcal{E}$ at $e = e(\beta)$. This condition has been checked numerically in the particular case (4.5) for a large set of paramaters.

Aubry set, also known as the *minimal Martin space* in potential theory. We essentially transcribe the lines of Akian, Gaubert and Walsch [**AGW09**], where they defined the Aubry set in the context of the max-plus spectral theory. In particular, [**AGW06**] deals with the time-continuous case, as in our case. There are discrepancies between our optimal control problem, and the classical Aubry-Mather theory in Lagrangian dynamics, because the system is not controllable. Indeed, it is not generally possible to connect two given points x and y by a controlled trajectory.

Below, we endow the metric space $\mathcal{S}$ with some structure related to optimal curves. Firstly, the renormalized maximal pay-off between two points $(x,y) \in \mathcal{S}\times\mathcal{S}$ is defined as follows,

(4.43)
$$h_t(x,y) = \sup\left\{ \int_0^t \left(L(\gamma(s),M(s)) - \lambda(\mathcal{M})\right) ds \mid \gamma \text{ is a controlled curve}\,,\ \gamma(0)=x\,,\ \gamma(t)=y \right\}$$

Notice that $h_t(x,y)$ may take the value $-\infty$ if no control enables to connect x to y. We have the following characterization which comes from the very definition (4.43): A function u is a critical viscosity subsolution of the stationary Hamilton-Jacobi equation

$$-\lambda(\mathcal{M}) + H(D_x u, x) \le 0\,, \quad x\in\mathcal{S}\,, \tag{4.44}$$

if, and only if, u satisfies

$$(\forall t>0) \quad (\forall (x,y)\in\mathcal{S}\times\mathcal{S}) \quad u(x)-u(y) \ge h_t(x,y)\,. \tag{4.45}$$

Moreover, it is a critical viscosity solution if for every $x \in K_+$, there exists a calibrated curve $\gamma:[0,\infty)\to\mathcal{S}$ such that $\gamma(0)=x$, and the inequality (4.45) is saturated along γ, *i.e.*

$$(\forall t>0) \quad u(x)-u(\gamma(t)) = h_t(x,\gamma(t))\,. \tag{4.46}$$

It is immediate to see that the equality is saturated for all intermediate times,

$$(\forall 0\le s\le t) \quad u(\gamma(s))-u(\gamma(t)) = h_{t-s}(\gamma(s),\gamma(t))\,. \tag{4.47}$$

The following Lemma provides a characterization of the critical value λ.

LEMMA 4.14. *The critical value is realized as the following maximization problem,*

$$\lambda(\mathcal{M}) = \lim_{t\to+\infty}\left(\frac{1}{t}\sup\left\{\int_0^t L(\gamma(s),M(s))\,ds \mid \gamma \text{ is a controlled curve}\right\}\right). \tag{4.48}$$

REMARK 4.15. *By sub-additivity, we have the equivalent formulation*

$$\lambda(\mathcal{M}) = \inf_{t>0}\left(\frac{1}{t}\sup\left\{\int_0^t L(\gamma(s),M(s))\,ds \mid \gamma \text{ is a controlled curve}\right\}\right). \tag{4.49}$$

4.3.2.2. *The Peierls barrier.* In Lagrangian dynamics, the Peierls barrier h is defined as follows,

$$h(x,y) = \limsup_{t\to+\infty} h_t(x,y) \tag{4.50}$$

In our case, due to the lack of controllability, an alternative definition is required.

Definition 4.16: The Peierls barrier

The Peierls barrier h is defined as follows,

$$h(x,y) = \lim_{t\to+\infty}\left(\limsup_{y'\to y}\left(\sup_{s>t} h_s(x,y')\right)\right). \tag{4.51}$$

This definition is motivated by the following configuration: assume $y = e(m)$ is an eigenvector associated with the (constant) control m. It might happen that $e(m)$ is not reachable in finite time starting from x[10]. However, we would like to define properly $h(x, e(m))$. Therefore, we cannot handle (4.50), but we should rather rely on some approximation argument, as in (4.51).

The Peierls barrier may take the value $-\infty$ when y is not reachable from x in infinite horizon. It can be interpreted as a correction of the characterization (4.48). It brings the desired structure on $\mathcal{S}$ as described in the following lemma.

LEMMA 4.17. *The Peierls barrier satisfies the following properties*[11]*:*

(i) (Nonpositivity on the diagonal) For all $x \in \mathcal{S}$, $h(x,x) \le 0$.

(ii) For all (x,y,z), and for all time $T > 0$, $h(x,z) \ge h_T(x,y) + h(y,z)$.

(iii) The function h is Lipschitz continuous with respect to the first variable, where it is finite.

(iv) (Reverse triangle inequality) For all (x,y,z), $h(x,z) \ge h(x,y) + h(y,z)$.

▸ *Sketch of proof.* The first item is a consequence of the existence of a critical viscosity solution $\mathring{u}$[12]. In fact, we deduce immediately from (4.45)

$$h_t(x,y') \le \mathring{u}(x) - \mathring{u}(y')\,,$$

that

$$(\forall t > 0) \quad \sup_{s>t} h_s(x,y') \le \mathring{u}(x) - \mathring{u}(y')\,.$$

Then, passing to the lim sup as $y' \to y$, we obtain (i).

The proof of the second item is immediate. Indeed, for all $(s > 0)$ and $z' \in \mathcal{S}$, we get the following inequality by concatenation of trajectories, and optimality in (4.43),

$$h_T(x,y) + h_s(y,z') \le h_{T+s}(x,z')\,.$$

As a consequence, for any $t > 0$, we have

$$h_T(x,y) + \sup_{s>t} h_s(y,z') \le \sup_{s>t} h_s(x,z')\,.$$

Passing to the lim sup $z' \to z$, we obtain

$$h_T(x,y) + h(y,z) \le h(x,z)\,.$$

The proof of the third item is similar to the proof of the main *a priori* estimate (4.25). Let (x,z) such that $h(x,z) > -\infty$. We aim to prove that

$$(\forall (x,y,z)) \quad |h(x,z) - h(y,z)| \le \frac{\operatorname{Lip} L}{\mu} d(x,y)\,. \tag{4.52}$$

Let us choose a pair of maximizing sequences $s_n \to +\infty$ and $z_n \to z$ associated to the value $h(x,z) = \lim h_{s_n}(s; z_n)$. Let M_n be the controlled function such that $z_n = R(s_n, M_n)x$, where $R(s,M)$ denotes the flow of (4.6) with the control function M (in short, $R(s,M)x = x_M(s)$). Let $z'_n = R(s_n, M_n)y$. Then the two following inequalities hold true,

$$d(z_n, z'_n) \le e^{-\mu s_n} d(x,y)\,.$$

$$h_{s_n}(x,z_n) - h_{s_n}(y,z'_n) \le \frac{\operatorname{Lip} L}{\mu} d(x,y)\,.$$

We deduce from the former that $z'_n \to z$. Then, passing to the limit in the latter, we obtain (4.52).

[10] It is the case when $\mathcal{M} = \{m\}$ and $x \neq e(m)$

[11] The Peierls barrier usually defined in Lagrangian dynamics correspond to the opposite $-h$. Thus, it is non-negative on the diagonal, and it verifies the triangle inequality with the correct sign.

[12] In fact, the existence of a viscosity subsolution is enough.

Finally, we deduce the reverse triangle inequality as a corollary of items (ii)-(iii). Indeed, we have for all (x, y', z), and $t > 0$,

$$h(x,z) \geq \sup_{s>t} h_s(x,y') + h(y',z)\,.$$

Passing to the $\limsup$ $y' \to y$ in the right-hand-side, and using the continuity of h with respect to the first variable, we obtain the result. ◂

The following corollary is a consequence of the continuity with respect to the first variable.

Corollary 4.18

We have the equivalent formulation for the Peierls barrier,

$$h(x,y) = \lim_{t\to+\infty} \left(\limsup_{(x',y')\to(x,y)} \left(\sup_{s>t} h_s(x,y') \right) \right). \tag{4.53}$$

REMARK 4.19. *As a by-product of the proof of Lemma 4.17, we observe that if $h(x,z) > -\infty$ for some $(x,z) \in S \times S$, then $h(y,z) > -\infty$ for all $y \in S$. More precisely, this can occur only if z belongs to the ergodic set $\mathcal{Z}$.*

4.3.2.3. *The Aubry set.* The property contained in Lemma 4.17(i) expresses that a point cannot return back to itself with a positive pay-off in the infinite horizon.

Definition 4.20: The Aubry set

The Aubry set is defined as the set of points which can return back to themselves in the infinite horizon with zero pay-off,

$$\mathcal{A} = \{a \in \mathcal{S} \mid h(a,a) = 0\}\,. \tag{4.54}$$

The Aubry set is not empty, as stated in the following proposition.

Proposition 4.21: The Aubry set is not empty

If a is an accumulation point of a calibrated trajectory, then $a \in \mathcal{A}$.

▸ *Sketch of proof.* From (4.47) we deduce that there exists a sequence of increasing times $t_n \to +\infty$ such that $t_n \to +\infty$, $\lim \gamma(t_n) = a$, and

$$u(\gamma(t_n)) - u(\gamma(t_{n+1}) = h_{s_n}(\gamma(t_n), \gamma(t_{n+1}))\,.$$

Passing to the limit $n \to +\infty$, and using the formulation (4.53), and also item (i) in Lemma 4.17 we obtain

$$0 \leq h(a,a) \leq 0\,.$$

◂

We deduce from the preceding analysis the following representation formula (see [**AGW09**], [**Fat12**]), and references therein.

Theorem 4.22: The representation formula

Any critical viscosity solution u of (4.15) can be represented as

$$u(x) = \sup_{a\in\mathcal{A}} \left(h(x,a) + u(a) \right)\,. \tag{4.55}$$

Reciprocally, being given the values $u(a)$ for $a \in \mathcal{A}$, formula (4.55) defines a critical viscosity solution.

▸ *Sketch of proof.* The first implication is immediate: from (4.45), we deduce that forall (x, y), $u(x) - u(y) \geq h(x, y)$, and *a fortiori*,

$$u(x) \geq \sup_{a \in \mathcal{A}} \left(h(x, a) + u(a) \right) .$$

On the other hand, using a calibrated curve γ, as in (4.46), we obtain, up to extracting a subsequence such that $\gamma(t_n) \to a \in \mathcal{A}$, the following inequality

$$u(x) - u(a) \leq h(x, a) .$$

On the other hand, it is not difficult to prove that $h(\cdot, a)$ is a viscosity solution, and accordingly that (4.55) defines a viscosity solution. ◂

There are many more important properties making the connection between viscosity solutions and the Aubry set, see [**Fat12, Ber12**] for a review. In particular, it is expected that

(1) The Peierls barrier $h(x, a)$ coincides with the so-called Mañé critical potential[13] if, and only if, $a \in \mathcal{A}$.

(2) The Mañé potential is a global viscosity solution if, and only if, a belongs to the Aubru set.

(3) Viscosity solutions of (4.15) are differentiable on the Aubry set.

(4) Uniqueness of viscosity solutions to (4.15) (up to an additive constant) is guaranteed when the Aubry set is connected. More generally, the number of connected components of $\mathcal{A}$ determines the number of degrees of freedom for u, in accordance with Theorem 4.22.

4.3.3. Optimality of the maximal Perron eigenvalue? In our preliminary study of the PMCA optimal control problem [**15**], Gabriel and I were puzzled by the fact that intensive numerical simulations of the running example (4.5) showed that optimal trajectories converge towards a unique equilibrium. We could not find any counter-example. This equilibrium is necessarily an eigenvector associated to the maximal constant control, say α^*. Alternatively speaking, we found numerically that

$$\lambda = \lambda(\alpha^*) = \max\{\lambda(\alpha) , \alpha \in [a, A]\} , \quad \mathcal{A} = \{e(\alpha^*)\} , \tag{4.56}$$

for a large set of parameters. Accordingly, the asymptotic optimal control $\alpha(t)$ is constant, and we observe $\alpha(t) \rightharpoonup \alpha^*$ as $t \to +\infty$. Actually, the numerical outcomes are quite interesting, since our numerical algorithm[14]. naturally follows a BANG-BANG procedure. It generates a highly oscillating sequence of controls that weakly converges asymptotically towards the optimal constant control α^* as the time step vanishes.

The following question arises naturally:

Under which conditions do we have $\lambda = \lambda(\alpha^*)$?

[13] Mañé's potential is defined by replacing the lim sup in (4.50) with a sup with respect to time $t > 0$. As elements of the Aubry set are recurrent in the sense of Definition 4.20, then it is intuitively clear that the supremum of the pay-off from x to a can be attained in arbitrary large times, simply by concatenating arbitrarily long trajectories with almost zero pay-off.

[14] The resolution of the two-dimensional Hamilton-Jacobi equation on the simplex $\mathcal{S}$, using the Lax-Friedrichs scheme.

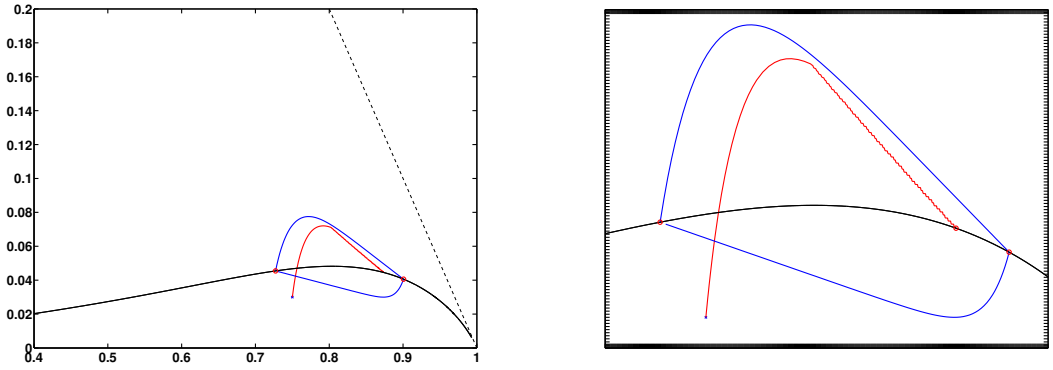

FIGURE 4.7. Illustration of convergence of optimal trajectories towards the optimal Perron eigenvector for the three-dimensional growth-fragmentation process (4.5) with typical parameters. We have plotted the curve of Perron eigenvectors (black line), the boundary of the ergodic set (blue line), and some optimal trajectory (red line). The optimal trajectory enters the ergodic set and then converges towards a limit cycle. Right picture is a zoom. The numerical grid is plotted on the axes: the space step is $\Delta x = 5\text{E}{-4}$ to fall much below the width of the ergodic set. Parameters are $\tau_1 = 2\text{E}{-2}, \tau_2 = 1, \beta = 4\text{E}{-2}$, and $a = 2, A = 8$.

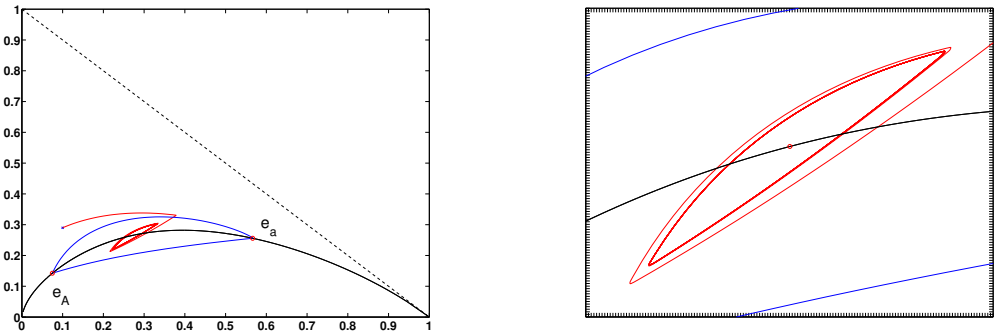

(a) (b)

FIGURE 4.8. Illustration of the optimal limit cycle for our counter-example (matrices not shown). We have plotted the curve of Perron eigenvectors (black line), the boundary of the ergodic set (blue line), and some optimal trajectory (red line). The optimal trajectory enters the ergodic set and then converges towards a limit cycle. Right picture is a zoom. The numerical grid is plotted on the axes: the space step is $\Delta x = 10^{-3}$ to fall much below the width of the limit cycle.

Together with P. Gabriel and S. Gaubert, we proved that (4.56) holds true when $n = 2$ in full generality [**16**]. This is a consequence of the fact that the simplex is a segment, and that dynamical systems on segments have a simple asymptotic behaviour, although they behave quite singularly since the control paramater can switch.

We also found a counter-example which does not belong to the class of examples (4.5), for which (4.56) fails. More precisely, we found two Metzler matrices G, F in dimension 3, such that the optimal trajectories accumulate on limit cycles (see Figure 4.8). In order to find a counter-example, we addressed the problem of optimality of the optimal constant control in the larger class of periodic controls. We derived some analytical criterion ensuring that the best constant control is not optimal

in the class of periodic controls. This criterion allowed us to test a large number of random Metzler matrices chose at random.

Meanwhile, we realized that the optimality of constant controls in dimension $n = 2$ was already proven by a different approach in [**GSM07**]. Also, a three-dimensional counter-example was described in [**FMC09**], thus answering a question raised in [**GSM07**]. These two works deal with more general linear inclusion systems, without the monotonicity property.

4.3.4. Non optimality of the constant control. Finally, we investigate second-order conditions for the optimality of the best constant control. For the sake of simplicity, we restrict to the case of an affine control set parametrized by the scalar control α, $M(\alpha) = G + \alpha F$. Similar results hold in a more general setting. We assume that there exists $\alpha^* \in (a, A)$ such that $\lambda(\alpha^*)$ is a local maximum of $\lambda(\alpha)$.

We assume for the sake of simplicity that the matrix $G + \alpha^* F$ is diagonalizable. We denote by $(e_1^*, e_2^*, \dots, e_n^*)$ and $(\phi_1^*, \phi_2^*, \dots, \phi_n^*)$ the bases of right- and left- eigenvectors associated to the eigenvalues $(\lambda_1^*, \lambda_2^*, \dots, \lambda_n^*)$ at the the best constant control α^*, where $\lambda_1^* = \lambda(\alpha^*)$ is the Perron eigenvalue The first order condition for $\lambda(\alpha^*)$ being a local maximum of $\lambda(\alpha)$ is: $\phi_1^* F e_1^* = 0$.

We consider small periodic perturbations of the best constant control: $\alpha(t) = \alpha^* + \epsilon\gamma(t)$, where γ is a given T-periodic function. There exists a periodic eigenfunction $e_{\alpha^*+\epsilon\gamma}(t)$ associated to the Floquet eigenvalue $\lambda_F(\alpha^* + \epsilon\gamma)$ such that

$$\partial_t e_{\alpha^*+\epsilon\gamma}(t) + \lambda_F(\alpha^* + \epsilon\gamma) e_{\alpha^*+\epsilon\gamma}(t) = (G + (\alpha^* + \epsilon\gamma(t))F) e_{\alpha^*+\epsilon\gamma}(t)\,.$$

The following proposition provides a second order necessary condition for $\lambda(\alpha^*)$ to be a local maximum relatively to periodic perturbations of the control. We denote by $\langle f \rangle_T$ the time average over one period,

$$\langle f \rangle_T = \frac{1}{T}\int_0^T f(t)\,dt\,.$$

Proposition 4.23: Second-order variation of the Floquet eigenvalue

The directional derivative of the Floquet eigenvalue vanishes at $\epsilon = 0$:

$$\left.\frac{d\lambda_F(\alpha^* + \epsilon\gamma)}{d\epsilon}\right|_{\epsilon=0} = 0\,. \tag{4.57}$$

Hence, α^* is also a critical point in the class of periodic controls. The second directional derivative of the Floquet eigenvalue writes at $\epsilon = 0$:

$$\left.\frac{d^2\lambda_F(\alpha^* + \epsilon\gamma)}{d\epsilon^2}\right|_{\epsilon=0} = 2\sum_{i=2}^{n} \langle |\gamma_i|^2 \rangle_T \frac{(\phi_1^* F e_i^*)(\overline{\phi_i^*} F e_1^*)}{\lambda_1^* - \lambda_i^*}\,, \tag{4.58}$$

where $\gamma_i(t)$ is the unique T-periodic solution of the following relaxation equation,

$$\frac{\dot\gamma_i(t)}{\lambda_1^* - \lambda_i^*} + \gamma_i(t) = \gamma(t)\,.$$

Taking $\gamma \equiv 1$ in Equation (4.58), we get the second derivative of the Perron eigenvalue at α^*,

$$\frac{d^2\lambda}{d\alpha^2}(\alpha^*) = 2\sum_{i=2}^{n} \frac{(\phi_1^* F e_i^*)(\overline{\phi_i^*} F e_1^*)}{\lambda_1^* - \lambda_i^*}\,, \tag{4.59}$$

which is nonpositive since α^* is a maximum point. Therefore we are led to the following question: is it possible to construct counter-examples such that the sum (4.58) is positive for some periodic control γ, whereas the sum (4.59) is nonpositive? This is clearly not possible in dimension $n = 2$ because the sum in (4.58) is reduced to a single nonpositive term by (4.58).

By considering periodic perturbations of the form $\gamma(t) = e^{i\omega t}$ we get the formula

$$\left.\frac{d^2\lambda_F(\alpha^* + \epsilon\gamma)}{d\epsilon^2}\right|_{\epsilon=0} = 2\sum_{j=2}^{n} \frac{\lambda_1^* - \overline{\lambda_j^*}}{|(\lambda_1^* - \lambda_j^*) + i\omega|^2}(\phi_1^* F e_j^*)(\overline{\phi_j^*} F e_1^*)\,.$$

An asymptotic expansion when $\omega \to +\infty$ yields the following corollary.

Corollary 4.24: Non-optimality of the best constant control

Assume that $G + \alpha^* F$ is diagonalizable. If the following condition holds,

$$\sum_{i=2}^{n} (\lambda_1^* - \overline{\lambda_i^*})(\phi_1^* F e_i^*)(\overline{\phi_i^*} F e_1^*) > 0\,, \tag{4.60}$$

then the best constant control does not realize the maximum value $\lambda(\mathcal{M})$.

We found by chance[15] some example for which the Perron eigenvalue is not optimal. However, we have very few insights on the underlying mechanisms that yields non-optimality.

Interestingly, there is a link between the basic computations of Proposition 4.23 and the more general framework of Legendre type conditions for local optimality on short times. The goal in this framework is to derive second order conditions for the optimality of the end point mapping, $X_T : \alpha \mapsto x_\alpha(T)$, for a fixed time $T > 0$. For a given constant control α, the Fréchet derivative of X_T at α in the direction γ is:

$$(D_\alpha X_T)\gamma = \int_0^T \beta(t) e^{(G+\alpha F)(T-t)} F x_\alpha(t)\, dt\,.$$

The best constant control α^* is a critical point of X_T, since the costate $p_\alpha^*(t) = e^{\lambda^*(T-t)}\phi^*$ satisfies the condition

$$(\forall t \in (0,T)) \quad p_\alpha^*(t) F x_\alpha^*(t) = 0\,.$$

The second order differential of the end point mapping X_T at the critical control α^* reads as follows,

$$(D^2_{\alpha^*} X_T)(\gamma,\gamma) = 2\int_0^T \int_0^t \gamma(t)\gamma(s) e^{(G+\alpha^* F)(T-t)} F e^{(G+\alpha^* F)(t-s)} F x(s)\, ds\, dt.$$

A quadratic form is obtained by testing again $e^{-\lambda^* T}\phi^*$, namely

$$\begin{aligned} Q^*(\gamma) &= \phi^*(D^2_{\alpha^*} X_T)(\gamma,\gamma) \\ &= 2e^{\lambda^* T}\int_0^T \int_0^t \gamma(t)\gamma(s)\, \phi^* F e^{(G+\alpha^* F-\lambda^* I)(t-s)} F e_1^*\, ds\, dt\,. \end{aligned}$$

By computing the leading order terms in Q^* when time T is small, we get a sufficient condition for α^* to be locally optimal for small times with respect to variations with zero meanvalue. By denoting $L_0^\infty = \{\gamma \in L^\infty \mid \langle\gamma\rangle_T = 0\}$, we obtain the following statement.

Proposition 4.25: Generalized Legendre condition

If the condition

$$\phi^* F(G + \alpha^* F - \lambda^* I) F e_1^* > 0. \tag{4.61}$$

is satisfied, then there exists a time $T_0 > 0$ such that the quadratic form $Q^*|_{L_0^\infty}$ is negative with respect to the Sobolev norm H^{-1} for short time,

$$(\exists \delta > 0) \quad (\forall T \in (0,T_0)) \quad Q^*|_{L_0^\infty}(\gamma,\gamma) \le -\delta\|\gamma\|^2_{H^{-1}}\,.$$

[15] More precisely, by drawing randomly pairs of matrices (G,F) in a suitable subclass of Metzler matrices, until criterion (4.60) is satisfied.

Condition (4.61) is the so-called *generalized Legendre condition* of our problem. The generalized Legendre condition appears in the study of optimality for totally singular extremals, i.e. when the second derivative of the Hamiltonian is identically zero along the trajectory. A typical example is provided by the single-input affine control systems, namely, $\dot{x}(t) = f_0(x(t)) + \alpha(t) f_1(x(t))$, where $\alpha(t) \in \mathbb{R}$, and f_0, f_1 are smooth vector fields. In this case the generalized Legendre condition writes

$$\langle p(\cdot)[f_1,[f_0,f_1]]x(\cdot)\rangle > 0\,.$$

where $[\cdot,\cdot]$ is the Lie bracket of vector fields. The control system (4.38) belongs to this class of problems, and straightforward computations show that for $x(t) = e^{\lambda^* t} e_1^*$ and $p(t) = e^{-\lambda^* t}\phi_1^*$, we have $p(\cdot)[F,[G,F]]x(\cdot) = \phi^* F(G + \alpha^* F - \lambda^* I)Fe_1^*$. The generalized Legendre condition allows to deduce that the trajectory $x(\cdot)$ is locally optimal for short final times T in the C^0 topology [**AS04**, **BCT07**].

The following observation makes the link between Proposition 4.25 and Corollary 4.24:

$$\phi^* F(G + \alpha^* F - \lambda^* I)Fe_1^* = -\sum_{i=2}^{n} (\lambda_1^* - \lambda_i^*)(\phi_1^* F e_i^*)(\phi_i^* F e_1^*)\,.$$

Alternatively speaking, the generalized Legendre condition coincides with the criterion (4.60) obtained in the high frequency limit. This is intuitive, as the generalized Legendre condition deals with short time dynamics.

4.4. Open problems

Open Problem(s) 4.26

(1) Prove the existence of Barabanov norms using PDE methods as above. Article [**Wir02**] is a good starting point, but the link with Lipschitz bounds of solutions to Hamilton-Jacobi equations is not so clear. However, these estimates are crucial in our approach.

(2) Prove that maximizing trajectories converge to points or cycles in dimension three, as in Figures 4.7 and 4.8. This should involve some version of the Poincaré-Bendixon theorem for switched systems [**GCM13**, **dCBE13**].

(3) Prove the existence of a fixed point to the forward Lax-Oleinik operator (4.14) when the ambient space is an infinite dimensional Banach space. This should include the infinite-hoizon optimal problem for the linear growth-fragmentation equation (4.2).

CHAPTER 5

Cell polarization viewed as an instability

This chapter presents the contents of articles [10], [18], written in collaboration with R. Hawkins, N. Meunier, R. Voituriez, and L. Giraldi.

Summary

{5.1} Mating yeast is able to polarize spontaneously in absence of external pheromone gradients. {5.1.1} A model based on active transport along actin filaments is described. {5.1.2} The one-dimensional case is analysed comprehensively. It exhibits a similar dichotomy as the two-dimensional Keller-Segel equation. {5.1.3} A more realistic model with exchange of polarity markers at the cell membrane is also analysed, still in the one-dimensional case. {5.1.4} The higher-dimensional case is discussed.

{5.2} Fission yeast is a rod-like unicellular organism, for which growth is localized at the cell tip. {5.2.1} A biomechanical model is described. It accounts for heterogeneous cell wall expansion, coupled to cell geometry. {5.2.2} Previous modelling works are reviewed, {5.2.3} and results of linear stability analysis are presented together with numerical simulations. {5.2.4} An alternative model is proposed in the two-dimensional case. It is based on a simple description of microtubule sliding dynamics along the cell membrane. Numerical simulations show the emergence of a rod-like shape.

5.1. Spontaneous cell polarization in budding yeast

Cell polarisation refers generically to a process that enables a cell to switch from a spherically symmetric shape to a state with a prefered axis. It is always characterised in early stages by an inhomogeneous distribution of specific molecular markers, which in turn induces a mechanical deformation of the cell shape.

Cell polarisation can be driven by an external asymmetric signal as in the example of chemotaxis, where a chemical gradient imposes the direction of migration of cells [**Alb08**]. Another example is given by budding yeast (*Saccharomyces cerevisiae*), for which the external signal is a pheromone gradient, which causes the cell to grow an elongation in the direction of the mating partner [**Alb08**, **MS98**, **SSL09**]. On starvation, yeast switch from haploid to diploid phenotype by fusion of two cells having opposite sexual types (A or α). On the contrary to budding, polarisation is determined by pheromone gradients during the mating phase (A or α factors). Interestingly, some mutants of *S. cerevisiae* can polarise independently of any external pheromone gradient [**WSAWL03**, **IGL03**, **WSWSL04**].

Molecular pathways involved in yeast cell polarisation have been studied extensively over the past decade. It was proposed that symmetry breaking is based on Turing instability, involving the protein Bem1 [**LKR06**, **OR07**, **ID08**, **GP08**]. This presumably combines small diffusion of some activator on the membrane, and large diffusion of some inhibitor in the cytoplasm. Together with Meunier

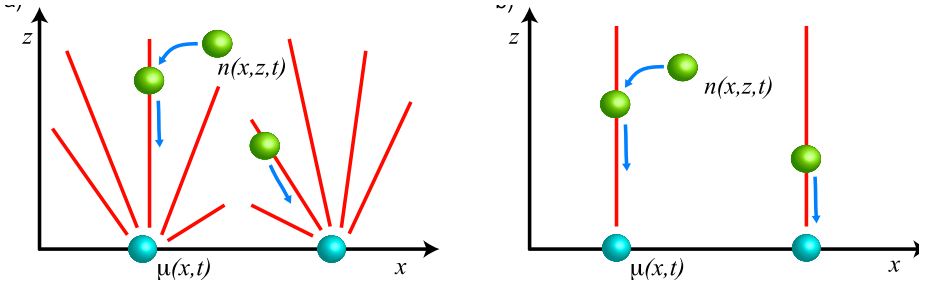

FIGURE 5.1. Schematic representation of the orientation of the cytoskeleton network with respect to the cell membrane. (left) Actin filaments: filaments are distributed in several directions from nucleation sites. The resultant field derives from a harmonic potential with source located on the cell boundary. (right) Microtubules: filaments are growing from the center of the cell. The resultant field is normal to the cell boundary. (From [HBPV09]).

and Voituriez, we focused on an alternative mechanism which involves the transport of polarity markers (Cdc42 proteins) along actin filaments. Active transport towards enriched Cdc42 regions is enhanced, as the binding of Cdc42 on the membrane triggers assembly of new actin filaments. This mechanism was suggested initially in [WSAWL03]. It was observed in experiments that the formation of polar caps is reduced when actin transport is disrupted, and that the polar caps formed are unstable [WSAWL03, WSWSL04, IHTL05], indicating that actin plays a prominent role in the process. We refer to [OR09] for a review, and [SSL09] for a discussion of the different possible feedback loops from a biological viewpoint.

5.1.1. The model. The concentration of polarity markers (Cdc42 proteins) is denoted by $n(t,x)$. It is assumed to diffuse in the cytoplasm and to be actively transported along the actin filaments. Polarity markers activate the nucleation of actin filaments when they bind to the cell membrane. Motion across the actin network is described by advection at the macroscopic scale. The advection field is denoted by $\mathbf{u}(t,x)$. The source term of the advection field is supported on the cell boundary. It was proposed in [HBPV09] that the field $\mathbf{u}(t,x)$ derives from a harmonic potential, in order to model nucleation of actin filaments at the cell membrane (the *potential case*, see Figure 5.1–left). For the sake of comparison, the case of a parallel vector field was also considered (the *transversal case*, see Figure 5.1–right). The latter corresponds schematically to the case of active transport along microtubules, which are very rigid filaments growing from the cell nucleus towards the membrane. We refer to [HBPV09] for a thorough presentation of the modelling assumptions.

The cell is schematically described by the half-space $\mathcal{H} = \mathbb{R}^{N-1} \times (0, +\infty)$. Moreover, the space variable is denoted by $x = (y, z)$. The advection-diffusion equation for the evolution of molecular markers reads as follows in adimensional form,

$$\begin{cases} \partial_t n(t,x) = \Delta n(t,x) - \nabla \cdot (n(t,x)\mathbf{u}(t,x)) \,, & t > 0 \,, \quad x \in \mathcal{H} \,, \\ n(0,x) = n_0(x) \,, \end{cases} \tag{5.1}$$

together with the zero-flux boundary condition:

$$\partial_z n(t,y,0) - n(t,y,0)\mathbf{u}(t,y,0) \cdot \mathbf{e}_z = 0 \,, \quad y \in \mathbb{R}^{N-1} \,. \tag{5.2}$$

The total amount of proteins is a conserved quantity, so it is a parameter of the problem. We define accordingly,

$$M = \int_{\mathcal{H}} n_0(x) \, \mathrm{d}x = \int_{\mathcal{H}} n(t,x) \, \mathrm{d}x \,.$$

Following [**HBPV09**], we distinguish between the *transversal case*, where the field $\mathbf{u}$ is normal to the boundary:

$$\mathbf{u}(t,y,z) = -n(t,y,0)\mathbf{e}_z\,, \tag{5.3}$$

and the *potential case*, where the field $\mathbf{u}$ derives from a harmonic potential,

$$\mathbf{u}(t,x) = \nabla c(t,x)\,, \quad \text{where} \quad \begin{cases} -\Delta c(t,x) = 0\,, \\ -\partial_z c(t,y,0) = n(t,y,0)\,. \end{cases} \tag{5.4}$$

In dimension $N = 1$, the two choices (5.3) and (5.4) coincide.

Together with Meunier and Voituriez, we analysed the long time asymptotics of the models, beyond the linear stability analysis performed in [**HBPV09**].

The positive feedback loop behind (5.1)–(5.4) is very similar to the chemotactic instability described by the Keller-Segel model (Chapter 1). Cell movement up the chemotactic gradient is replaced by trafficking of molecules in the cell cytoplasm. The main discrepancy is the source of the advection potential: it is distributed everywhere in the domain for the Keller-Segel model, whereas it is supported on the boundary for the polarization model.

Mathematical analysis of the one-dimensional problem appeared to be very interesting, but of limited interest for the symmetry breaking issue, because the boundary is reduced to a single point[1]. However, no mathematical result could be derived in the higher-dimensional case, apart from heuristical results. The latter suggest that symmetry breaking may occur, or not, depending on the parameters.

5.1.2. The one-dimensional problem. In the case of the half-line $\mathcal{H} = (0,+\infty)$, the advection field is spatially constant, $\mathbf{u}(t,z) = -n(t,0)$.

The model is reduced to the following equation,

$$\partial_t n(t,z) = \partial_z^2 n(t,z) + n(t,0)\partial_z n(t,z)\,, \quad t>0\,,\ z\in(0,+\infty)\,, \tag{5.5}$$

together with the zero-flux boundary condition at $z = 0$:

$$\partial_z n(t,0) + n(t,0)^2 = 0\,. \tag{5.6}$$

This model is similar to the two-dimensional Keller-Segel system regarding the behaviour of solutions (Section 1.1.1).

Theorem 5.1: Long-time asymptotics in the subcritical regime [10]

Assume that $M \le 1$. Assume that the initial data $n_0 \in L^1((1+z)\,\mathrm{d}z)$ satisfies $\int n_0(z)(\log n_0(z))_+\,\mathrm{d}z < +\infty$. There exists a unique global weak solution of (5.5).
In the subcritical case $M < 1$, the solution converges in L^1 towards the self-similar profile $G_\alpha(y) = \alpha\exp\left(-\alpha y - y^2/2\right)$, where α is uniquely determined by conservation of mass $\int_{y>0} G_\alpha(y)\,dy = M$:

$$\lim_{t\to+\infty} \left\| n(t,z) - \frac{1}{\sqrt{1+2t}} G_\alpha\left(\frac{z}{\sqrt{1+2t}}\right)\right\|_{L^1} = 0\,.$$

In the critical case $M = 1$, assume in addition that the second moment is finite $\int_{z>0} z^2 n_0(z)\,\mathrm{d}z < +\infty$. Then, the solution converges in L^1 towards the stationary state $\alpha\exp(-\alpha z)$, where $\alpha^{-1} = \int_{z>0} z n_0(z)\,\mathrm{d}z$.

[1] Except if one considers the cell as a finite interval. In that case, symmetry breaking makes sense.

REMARK 5.2. *Equation (5.5) shares analogous features with the integrate-and-fire model analysed in* [**CCP11**]. *In the latter, variable z represents the membrane potential of neurons. It also combines diffusion and a drift coupled to some boundary value of the neuron density. The main discrepancy is that the coupling goes through the derivative of the density at the boundary, since the firing rate is proportional to the flux of neurons that overcome a given voltage threshold. The authors investigate the following problems, similar to ours: steady states, blow-up, long-time asymptotics. There, blow-up can be interpreted as strong partial synchronization of the population of excitatory neurons, as the firing rate diverges.*

▸ *Sketch of proof.* Global existence is a consequence of the following computation,

$$\begin{aligned}\frac{\mathrm{d}}{\mathrm{d}t}\int_{z>0} n(t,z)\log n(t,z)\,\mathrm{d}z &= \int_{z>0}\partial_t n(t,z)\log n(t,z)\,\mathrm{d}z\\ &= -\int_{z>0}\left(\partial_z n(t,z)+n(t,0)n(t,z)\right)\frac{\partial_z n(t,z)}{n(t,z)}\,\mathrm{d}z\\ &= -\int_{z>0} n(t,z)\left(\partial_z\log n(t,z)\right)^2\,\mathrm{d}z + n(t,0)^2\,.\end{aligned}$$

The two contributions have opposite signs. We can estimate the balance using the following trace-type inequality,

$$n(t,0)^2 = \left(\int_{z>0}\partial_z n(t,z)\,\mathrm{d}z\right)^2 \le \left(\int_{z>0} n(t,z)\,\mathrm{d}z\right)\left(\int_{z>0} n(t,z)\left(\partial_z\log n(t,z)\right)^2\,\mathrm{d}z\right). \tag{5.7}$$

This enables to prove dissipation of the entropy in the case $M \le 1$,

$$\frac{\mathrm{d}}{\mathrm{d}t}\int_{z>0} n(t,z)\log n(t,z)\,\mathrm{d}z \le (M-1)\int_{z>0} n(t,z)\left(\partial_z\log n(t,z)\right)^2\,\mathrm{d}z\,. \tag{5.8}$$

Surprisingly, dissipation of entropy gives the sharp criterion on the mass. In fact, stationary states $\alpha\exp(-\alpha z)$ saturate inequality (5.7). Besides, there is apparently no free energy for (5.5), on the contrary to the Keller-Segel system (Section 1.1.1).

It is even more surprising that entropy methods enable to catch the long-time behaviour in a very precise way. Below, we distinguish between the critical and the subcritical case.

The critical case: there is no need to rescale variables in this case. We introduce the relative entropy:

$$\mathbf{H}(t) = \int_{z>0}\frac{n(t,z)}{h_\alpha(z)}\log\left(\frac{n(t,z)}{h_\alpha(z)}\right)h_\alpha(z)\,\mathrm{d}z = \int_{z>0} n(t,z)\log n(t,z)\,\mathrm{d}z + \alpha\mathbf{J}(t) - \log\alpha\,,$$

where α is defined as in Theorem 5.1, and $\mathbf{J}(t)$ denotes the first moment. The latter is conserved in the critical case $M=1$: $\mathbf{J}(t)=\mathbf{J}(0)=\alpha^{-1}$. Hence, inequality (5.8) is equivalent to

$$\frac{\mathrm{d}}{\mathrm{d}t}\mathbf{H}(t) \le 0\,, \tag{5.9}$$

with equality if and only if $n(t,z)$ is a stationary state. Classical methods as in [**BDP06**] enable to conclude that the solution converges to the unique stationary state having the same first moment.

The subcritical case: variables must be rescaled in order to catch the decay of the solution to zero,

$$n(t,z) = \frac{1}{\sqrt{1+2t}}\,u\left(\log\sqrt{1+2t}, \frac{z}{\sqrt{1+2t}}\right).$$

The rescaled density $u(\tau,y)$ satisfies the following equation in self-similar variables:

$$\partial_\tau u(\tau,y) = \partial_y^2 u(\tau,y) + \partial_y\left(yu(\tau,y)\right) + u(\tau,0)\partial_y u(\tau,y)\,, \tag{5.10}$$

The unique stationary state can be computed explicitly: $G_\alpha(y) = \alpha\exp\left(-\alpha y - y^2/2\right)$, where α is uniquely determined by mass conservation. We define accordingly the relative entropy and the first momentum in the rescaled frame:

$$\mathbf{H}(\tau) = \int_{y>0}\frac{u(\tau,y)}{G_\alpha(y)}\log\left(\frac{u(\tau,y)}{G_\alpha(y)}\right)G_\alpha(y)\,\mathrm{d}y\,,\quad \mathbf{J}(\tau) = \int_{y>0} yu(\tau,y)\,\mathrm{d}y\,. \tag{5.11}$$

The problem (5.10) admits a Lyapunov functional, defined as follows,

$$\mathbf{L}(\tau) = \mathbf{H}(\tau) + \frac{1}{2(1-M)} \left(\mathbf{J}(\tau) - \alpha(1-M)\right)^2 .$$

Indeed, we have

$$\frac{\mathrm{d}}{\mathrm{d}t}\mathbf{L}(\tau) = -\int_{y>0} u(\tau,y) \left(\partial_y \log u(\tau,y) + y + u(\tau,0)\right)^2 \mathrm{d}y - \frac{1}{(1-M)} \left(\frac{\mathrm{d}}{\mathrm{d}\tau}\mathbf{J}(\tau)\right)^2 \le 0 . \tag{5.12}$$

Again, classical methods enable to prove convergence towards the unique stationary state. ◂

In [LMM14], Lepoutre, Meunier and Muller obtained a rate of convergence in the subcritical case, using the logarithmic Sobolev inequality. The rate of convergence does not depend on the mass M. Remarkably, they also obtained a rate of convergence in the critical case using the so-called HWI inequality.

Theorem 5.3: Blow-up in the supercritical regime [10]

Assume $M > 1$. Assume that the initial data n_0 is non-increasing. Then the solution of the Cauchy problem blows up in finite time.

▸ *Sketch of proof.* The argument is the same as for the two-dimensional Keller-Segel system, but it involves the first momentum of $n(t,z)$, as opposed to the second momentum for the former. Monotonicity of n_0 guarantees that $n(t,\cdot)$ is also non-increasing for $t > 0$ due to the maximum principle. Therefore $-\partial_z n(t,z)/n(t,0)$ is a probability density. We deduce from Jensen's inequality the following estimate:

$$\left(\int_{z>0} z \frac{-\partial_z n(t,z)}{n(t,0)}\,\mathrm{d}z\right)^2 \le \int_{z>0} z^2 \frac{-\partial_z n(t,z)}{n(t,0)}\,\mathrm{d}z ,$$

which is in fact equivalent to an interpolation inequality,

$$M^2 \le 2n(t,0) \int_{z>0} z n(t,z)\,\mathrm{d}z . \tag{5.13}$$

The evolution of the first momentum $\mathbf{J}(t) = \int_{z>0} z n(t,z)\,\mathrm{d}z$ is computed as follows,

$$\mathbf{J}(t) = \mathbf{J}(0) + (1-M)\int_0^t n(s,0)\,\mathrm{d}s \le \mathbf{J}(0) + \frac{(1-M)M^2}{2}\int_0^t \frac{1}{\mathbf{J}(s)}\,\mathrm{d}s . \tag{5.14}$$

We introduce the auxiliary function $\mathbf{K}(t) = \mathbf{J}(0) + (1-M)M^2 \int_0^t \mathbf{J}(s)^{-1}\,\mathrm{d}s$. It is positive and it satisfies the following differential inequality:

$$\frac{\mathrm{d}}{\mathrm{d}t}\mathbf{K}(t) = \frac{(1-M)M^2}{2}\frac{1}{\mathbf{J}(t)} \le \frac{(1-M)M^2}{2}\frac{1}{\mathbf{K}(t)} ,$$
$$\frac{\mathrm{d}}{\mathrm{d}t}\mathbf{K}(t)^2 \le (1-M)M^2 .$$

We obtain a contradiction: the maximal time of existence is necessarily finite when $M > 1$. ◂

In [LMM14], Lepoutre, Meunier and Muller removed the monotonicity assumption on the initial data. They worked with cumulative densities, which have more fruitful properties.

5.1.3. The one-dimensional model with exchange of markers at the boundary. The boundary condition (5.6) is not realistic from a biophysical viewpoint. This claim is emphasized by the possible occurence of blow-up in finite time. In [MWSL+07, HBPV09], the authors distinguished between cytoplasmic content $n(t,z)$, and the concentration of molecules that are trapped on the boundary, say at $z = 0$, denoted by $\mu(t)$. The exchange of markers at the boundary follows very simple kinetics of binding/unbinding,

$$\frac{\mathrm{d}}{\mathrm{d}t}\mu(t) = n(t,0) - \gamma\mu(t) ,$$

where γ is the inverse of a typical length. The transport speed is modified accordingly: $\mathbf{u}(t,z) = -\mu(t)$. The model writes:

$$\begin{cases} \partial_t n(t,z) = \partial_z^2 n(t,z) + \mu(t)\partial_z n(t,z)\,, \quad t>0\,,\ z\in(0,+\infty) \\ \partial_z n(t,0) + \mu(t) n(t,0) = \frac{d}{dt}\mu(t)\,. \end{cases}$$

The flux condition on the boundary ensures the conservation of total molecular content (cytoplasmic and membranous markers). Denoting by $m(t) = \int_{z>0} n(t,z)\,\mathrm{d}z$ the partial mass of cytoplasmic markers, we have:

$$M = \mu_0 + m_0 = \mu(t) + m(t)\,.$$

Since the transport speed is bounded, $\mu(t) \le M$, solutions exist globally for any mass. The following result describes the asymptotic behaviour in the super-critical case $M > 1$.

Theorem 5.4: Long-time asymptotics in the supercritical regime [10]

Assume $M > 1$. Assume that the initial data n_0 is as in Theorem 5.1. Then, the partial mass $m(t)$ converges to 1 and the density $n(t,z)$ converges in L^1 towards the stationary profile $(M-1)e^{-(M-1)z}$.

▸ *Sketch of proof.* The proof relies on entropy techniques, as previously. The definition of the relative entropy takes into account the variable mass of the cytoplasmic content,

$$\mathbf{H}(t) = \int_{z>0} \frac{n(t,z)}{m(t)h(z)} \log\left(\frac{n(t,z)}{m(t)h(z)}\right) h(z)\,\mathrm{d}z\,,$$

where the asymptotic profile h is given by:

$$h(z) = \nu \exp\left(-\nu z\right)\,, \quad \nu = M-1\,.$$

The following quantity is a Lyapunov function, as in (5.12),

$$\mathbf{L}(t) = m(t)\mathbf{H}(t) + \frac{1}{2}\left(\mu(t)-\nu\right)^2 + \mu(t)\log\left(\frac{\mu(t)}{\nu}\right) + m(t)\log m(t)\,.$$

Indeed, we have

$$\frac{\mathrm{d}}{\mathrm{d}t}\mathbf{L}(t) = -\int_{z>0} n(t,z)\left(\partial_z \log n(t,z) + \frac{n(t,0)}{m(t)}\right)^2 \mathrm{d}z - m(t)\left(\frac{n(t,0)}{m(t)} - \mu(t)\right)^2 - \left(n(t,0)-\mu(t)\right)\log\left(\frac{n(t,0)}{\mu(t)}\right) - \mu(t)\left(\mu(t)-\nu\right)^2 \le 0\,.$$

◂

We were not able to find a Lyapunov function in the subcritical case $M < 1$, for which global decay of the solution is expected, as well as convergence in self-similar variables. This shows the limits of our methodology for analysing this problem.

5.1.4. The higher-dimensional case. In the higher dimensional case $N \ge 2$ we only analysed simplified models such as (5.5) where the transport speed is directly obtained from the trace value $n(t,y,0)$, without exchange of markers. We proved global existence for small initial data in the Lebesgue L^N, similarly to the Keller-Segel system in dimension $N \ge 3$ (for wich the critical space is $L^{N/2}$). The smallness criterion does not depend on the form of the advection field, either (5.3) or (5.4). This is so because both fields are divergence free and possess the same normal component at the boundary.

Theorem 5.5: Global existence for small initial data in dimension $N \ge 2$ [10]

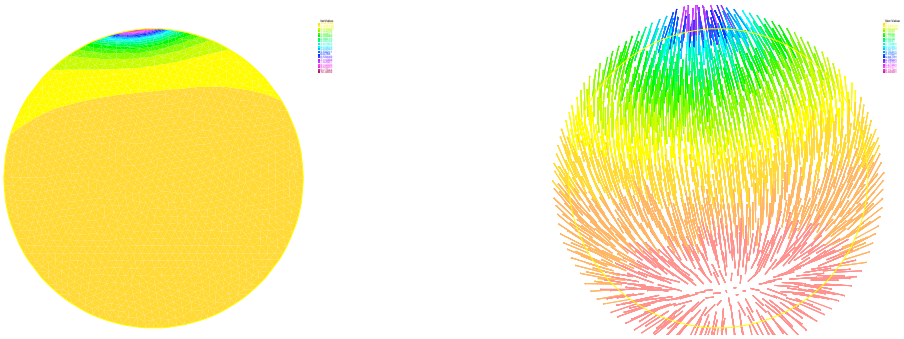

FIGURE 5.2. Numerical simulation of spontaneous polarization in a circular domain. (Left) Molecular concentration $n(t,x)$. (Right) Active transport field $\mathbf{u}(t,x)$. The active transport field is harmonic in the disc, with Neumann boundary condition, as in (5.4). So far, no rigorous result can explain these numerical observations.

Assume that the advection field satisfies the two following conditions: $\nabla\cdot\mathbf{u}\geq 0$ and $\mathbf{u}(t,y,0)\cdot\mathbf{e}_z = n(t,y,0)$. There exists $c_N>0$ such that for any initial data $n_0\in L^1((1+|x|^2)\,\mathrm{d}x)$ satisfying $\|n_0\|_{L^N}<c_N$, the solution is global in time.

This result is not quite satisfactory, as it does not capture the geometry of the advection field. Indeed, linear stability analysis clearly indicates that the transversal case (5.3) does not lead to symmetry breaking, on the contrary to the potential case (5.4). Numerical simulations on a circular shape support this statement.

The following heuristics gives some insights about the potential case. Assume that the advection potential is given by the following harmonic extension, as in (5.4),

$$\mathbf{u}(t,x) = \nabla c(t,x)\,, \quad \text{where} \quad \begin{cases} -\Delta c(t,x) = 0\,, \\ -\partial_z c(t,y,0) = n(t,y,0)\,. \end{cases} \tag{5.15}$$

Then, the tangential part of the field $\mathbf{u}$ is given by the (nonlocal) normal-to-tangential operator. In dimension $N=2$, it coincides with the Hilbert transform on the line, *i.e.* $\mathbf{u}_y(t,\cdot,0) = Hn(t,\cdot,0)$. On the other hand, we know from [**CPSt07**] that the combination of diffusion and mean field advection through the Hilbert transform yields a critical mass phenomenon in dimension 1. Above a certain mass, there should be spontaneous breaking of symmetry leading to the concentration of markers on the membrane. However, we were not able to transform these heuristics into a rigorous statement.

5.1.5. Future directions of research.

5.1.5.1. *Analysis of the higher-dimensional case beyond linear stability analysis.* Despite significant efforts, there is still some hope to obtain interesting results on the long time dynamics of the system in dimension higher than two. We focused on the simple model, but we failed to derive conditions that ensure blow-up of solutions. However, the model with exchange of markers at the boundary is of greater interest. There, the heuristics makes sense, assuming that most proteins are already concentrated on the boundary, as captured in the one-dimensional problem.

5.1.5.2. *Mating.* Competition for partnership in a population of yeast cells is of considerable interest. The model must be extended to include external pheromone gradients. In his thesis, N. Muller designed a promising models, together with very interesting numerical simulations in the two-dimensional case. One of the relevant biological question is the following: when a cell with type A is surrounded by many cells with type α, how can the A cell select a partner in order to

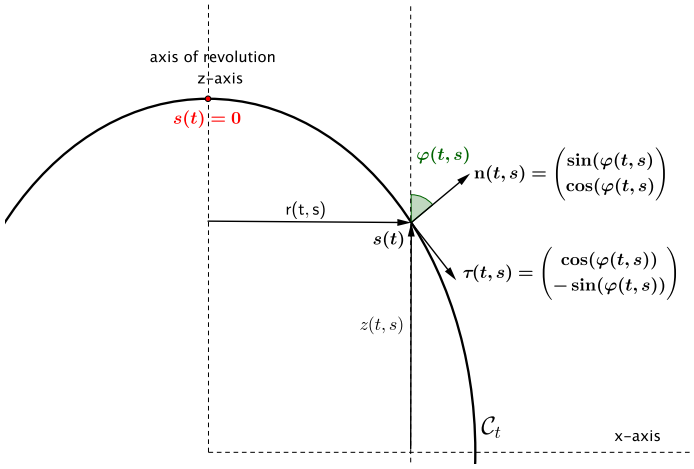

FIGURE 5.3. Generatrix curve of the surface of revolution in the xz–plane. Cell boundary is parametrized by $\varphi(t,s)$, or alternatively by $r(t,s)$.

align his polar cap with it, as for a private conversation. To answer this question, one-dimensional models where the A cell is a finite interval surrounded by two half-lines (α cells) is already quite informative. This is work in progress with Th. Lepoutre and N. Meunier.

5.2. Polar growth of the fission yeast (and other walled cells)

The physical features that account for the acquisition and maintenance of cellular shape is a current problem in experimental and theoretical biology [**Dum13**, **CH14**].

Together with L. Giraldi, we investigated a generic biomechanical model for the growth of walled cells, such as plant cells, fungal hyphae, or fission yeast (*Schizosaccharomyces pombe*). Cell wall can be described as a thin shell subject to a high internal pressure, called the turgor pressure, that can reach up to 10 atmospheres [**CM09**, **MBC09**]. It is commonly admitted that a good representation of an expanding cell wall is provided by an inflating balloon [**BRD07**, **CH14**].

Several attempts were made in the past decade to understand the growth dynamics of walled cells, and in particular rod-like cells and pollen tubes, from a physical and geometrical viewpoint [**DSS+06**, **CM09**, **RHD11**, **DV13**]. Our goal was to further analyse the coupling between the mechanics of cell wall expansion, and the pattern of growth, the latter being determined by cell geometry. For this purpose we studied a minimal model accounting for the mechanics of wall expansion, and heterogeneous distribution of growth along the wall as a function of its geometry.

Fission yeast is a rod-shaped unicellular organism. It grows by tip extension and divides by medial fission creating two daughter cells of equal sizes [HN01, M09, PT09]. It is well-established that the cytoskeleton controls cell polarity and cell shape [**TMVC+08**]. In normal conditions, microtubules align preferentially in the axis of growth. Thus, they deliver a group of proteins (the +TIP complex) to the cell tip. The delivery of polarity factors occurs during the catastrophe events (*i.e.* sudden shrinkage of the tubules). Polarity factors enhance nucleation of actin, as in budding yeast. Rich-actin sites subsequently drive the transport of cell wall material toward cell tips (see [**MC05**] and references therein). Interestingly enough, it is possible to redirect the location of the growth zone by mechanically acting on the cytoskeleton [**MBC09**, **TMVC+08**]. These experiments show evidence of a feedback loop between cytoskeleton organization and cell shape.

5.2.1. Model.

5.2.1.1. *Geometry of the cell wall.* We restrict to the case of an axisymmetric cell. This choice obviously rules out many possible shapes, but it is compatible with the acquisition and maintenance of the rod shape, which is already a challenging problem [**CH14**]. Cell boundary is described by angular deviation of the normal vector $\mathbf{n}$ from the axis of symmetry, $\varphi(t,s)$, or equivalently by the radius of the cell, $r(t,s)$, where s is the curvilinear abscissa (see Figure 5.3). We denote by $L(t)$ the length of the generatrix curve at time $t>0$.

The two principal curvatures are denote by κ_s and κ_θ ,

$$\kappa_s = \frac{\sqrt{1-(\partial_s r)^2}}{r(t,s)}\,, \quad \kappa_\theta(t,s) = \frac{-\partial_s r}{\sqrt{1-(\partial_s r)^2}}\,. \tag{5.16}$$

5.2.1.2. *Cell wall expansion: Kinematics.* We denote by $\mathbf{v}$ the vector field that governs the displacement (growth) of the cell wall. The equation governing the evolution of the membrane generatrix curve reads as follows

$$\frac{\partial}{\partial t}\left(\frac{\partial r(t,s)}{\partial s}\right) = \frac{\partial}{\partial s}\left(-\left(\int_0^s \frac{\partial \mathbf{v}(t,s')}{\partial s}\cdot\boldsymbol{\tau}(t,s')\mathrm{d}s'\right)\frac{\partial r(t,s)}{\partial s}\right) + \frac{\partial \mathbf{v}(t,s)}{\partial s}\cdot\mathbf{e}_1\,. \tag{5.17}$$

5.2.1.3. *Cell wall expansion: Mechanics.* The biomechanical part of the model follows the works of Dumais et al [**DSS+06**], and Drake and Vavylonis [**DV13**]. In the latter article, the wall is described as an elastic membrane under pressure, and subject to local remodeling. The biomechanical characteristics[2] are heterogeneous accross the membrane. We denote by Ψ the pattern of growth which yields heterogeneity on the membrane[3].

The following constitutive equations relate the strain rates and the stresses,

$$\begin{cases} \dot\epsilon_s = \Psi\,(\sigma_s - \nu\,\sigma_\theta)\,, \\ \dot\epsilon_\theta = \Psi\,(\sigma_\theta - \nu\,\sigma_s)\,, \end{cases} \tag{5.18}$$

where σ_s (resp. σ_θ) is the meridional stress (resp. the circumferential stress). Parameters are: ν, which is analogous to the Poisson ratio in linear elasticity, and Ψ, the rate of remodeling. Kinematic relations for axisymmetric shells link the strain rates and the velocity. The vector field $\mathbf{v}$ can be decomposed as $\mathbf{v} = v_n\mathbf{n} + v_\tau\boldsymbol{\tau}$, so that

$$\begin{cases} \dot\epsilon_s = v_n\kappa_s + \dfrac{\partial v_\tau}{\partial s}\,, \\ \dot\epsilon_\theta = v_n\kappa_\theta + \dfrac{v_\tau\cos(\phi)}{r}\,. \end{cases} \tag{5.19}$$

The assumption of axial symmetry enables to relate the stresses σ_s and σ_θ to the principal curvatures κ_s and κ_θ

$$\sigma_s = \frac{P}{2\kappa_\theta}\,, \quad \sigma_\theta = \frac{P}{2\delta\kappa_\theta}\left(2-\frac{\kappa_s}{\kappa_\theta}\right)\,, \tag{5.20}$$

where δ is the thickness of the wall, which is assumed to be constant. Thus, by substituting equation (5.18) into (5.19) and by using the relations (5.20), we deduce that v_n and v_τ are solutions to the following system,

$$\kappa_\theta v_n + \frac{v_\tau\cos(\phi)}{r} - \Psi(\sigma_\theta - \nu\sigma_s) = 0\,, \tag{5.21a}$$

$$\frac{\partial v_\tau}{\partial s} - \left(\frac{\kappa_s}{\kappa_\theta}\frac{\cos(\phi)}{r}\right)v_\tau + \frac{\kappa_s}{\kappa_\theta}\Psi\,(\sigma_\theta - \nu\sigma_s) - \Psi\,(\sigma_s - \nu\sigma_\theta) = 0\,. \tag{5.21b}$$

[2]Either the viscosity in Dumais et al, or the rate of remodeling in Drake and Vavylonis.

[3]This heterogeneous pattern results from a non-uniform concentration of some growth factor at the membrane, *e.g.* Cdc42 for the fission yeast, or cell wall loosening enzymes for plant cells.

5.2.1.4. *Cell wall expansion: growth pattern.* The experiments contained in [**MBC09**, **TMVC+08**] show evidence of a feedback loop between cytoskeleton organization and the cell shape. Thus, we consider a minimal coupling accounting for this loop.

We assume that $\Psi = F(\mu)$, where F is a certain nonlinear function, and μ represents the distribution of some growth factor which is released at the cell wall [**DV13**]. We assume that the dynamics of release occurs faster than growth, thereby the following reaction-diffusion equation is at quasi-stationary equilibrium,

$$-\gamma\Delta_{\mathcal{S}}\mu(t,s) + \alpha\mu(t,s) = \beta K(t,s)\,, \tag{5.22}$$

where $K = \kappa_s\kappa_\theta$ is the Gaussian curvature, and α, β, γ are positive constants.

The choice of the source term K is motivated as follows: i) growth material is delivered preferentially in regions of higher curvature, due to the accumulation of microtubule plus-ends; ii) the whole quantity $\int_{\text{wall}} K$ is constant. Thus, $\mu(t,s)$ can be viewed as the result of redistributing a limited amount of growth material according to the local geometry, together with lateral diffusion on the surface.

5.2.1.5. *A simplified 2D model.* In this subsection, we derive the dynamics which governs a thin elastic string under pressure. More precisely, we assume that the cell wall is a closed curve which is symmetric with respect to the z-axis.

The Hooke law reads $\varepsilon = \Psi\sigma$, where ε is the strain rate and σ is the stress acting on the curve. The latter is determined by the Laplace law, $\sigma = P/\kappa$, where κ is the curvature. Moreover, by geometrical consideration, the strain rate is also equal to $\varepsilon = v_n\kappa$, where v_n is the normal component of the velocity vector field. All in all, the normal velocity of the curve is given by the relation

$$v_n = \Psi\,\frac{P}{\kappa^2}\,. \tag{5.23}$$

We use the same notations as for the 3D axysimmetric case. In particular, we have $\kappa = -\partial_s\phi$. By analogy with the 3D case, the evolution of the curve obeys the following equation

$$\frac{\partial}{\partial t}\left(\frac{\partial r(t,s)}{\partial s}\right) = -\frac{\partial}{\partial s}\left(\left(\int_0^s P\,\frac{\Psi(t,u)}{\partial_s\phi(t,s')}\,\mathrm{d}s'\right)\frac{\partial r(t,s)}{\partial s}\right) + \frac{\partial}{\partial s}\left(P\frac{\Psi(t,s)}{\left(\partial_s\phi(t,s)\right)^2}\sin(\phi(t,s))\right). \tag{5.24}$$

Again, the coefficient Ψ depends on some growth material which is released proportionally to the curvature, and diffuses along the curve,

$$-\gamma\frac{\partial^2\mu(t,s)}{\partial s^2} + \alpha\mu(t,s) = \beta\frac{\partial\phi(t,s)}{\partial s}\,. \tag{5.25}$$

5.2.2. State of the art. Previous works studied the maintenance of rod-like cell shape. Generally, the growth pattern is prescribed as a function of the distance to the growing tip of the cell [**CM09**], *e.g.* via a Gaussian distribution of the growth material along the cell wall. In [**DV13**], the variance of the Gaussian distribution could depend on macroscopic quantities such as the length and the mean radius of the cell. Here, on the contrary, we do not assume that the cell is rod-shaped initially. Moreover, the distribution of the growth material intrinsically depends on the local geometry of the cell wall, *e.g.* through its curvature. We focus on the possible initiation of a rod shape from a spherical one, as observed experimentally [**KN11**]. We address mathematically the following morphogenesis question: starting from a small perturbation of a growing radially symmetrical shape, can the model evolves towards a rod shape? We answer this question using refined linear stability analysis of the radially symmetrical growing shape.

Other studies investigated the dynamics of cell growth in prokaryotic actinomycetes. On the contrary to eukaryotic fungi, such as fission yeast, the cytoskeleton plays certainly a minor role in the establishment of the growth pattern: wall building material is likely to be transported to the tip by diffusion. Goriely and Tabor proposed two models to investigate self-similar growth of the

tip. In [GT03a, GT03b], they developed a model based on large-deformation elasticity theory. The membrane was described as an axisymmetric elastic shell far from the reference configuration. Similarly to the models discussed above [DV13, DSS+06], the inhomogenous elastic modulus was given *a priori*, being assumed that the wall gets stiffer far from the tip.

In [GKT05], the same authors developed a purely geometrical model for tip growth, thus neglecting biomechanical effects. The models followed previous studies on the morphogenesis of unicellular algae [PP92, PS93]. In this model, surface evolution was determined by purely kinematical considerations, and local deposit of material, yielding areal growth. The rate of areal growth was a function of the local geometry (*e.g.* the Gaussian curvature). The authors derived analytically various shapes of self-similar growth in the 2D and in the 3D case.

5.2.3. Results. We can summarize our results as follows. As a preliminary observation, without any mechanical effects, wall expansion in the normal direction proportionally to μ (or $F(\mu)$) leads to highly singular pattern. In fact, the system is likely to be ill-posed. Unsurprisingly, taking into account mechanical effects has a stabilizing effect. We are able to measure quantitatively this effect in the linear regime. The range of parameters for which the system undergoes symmetry breaking is surprisingly narrow. For instance, it is required that F is strongly nonlinear. In addition, γ, the diffusion coefficient of μ, has to be relatively small. Then, the morphogenetic instability arises as a competition between the mechanical smoothing effects, and the redistribution of material according to the geometry.

Our analytical work is complemented with numerical simulations far from the radially symmetric shape. Interestingly enough, when it is unstable, the system selects various anisotropic shapes, including the rod-like shape.

We define the degree of a function f as follows,

$$\deg(F;\mu) = \frac{f'(\mu)\mu}{f(\mu)} = \frac{d\log f(\mu)}{d\log(\mu)}\,.$$

In particular, $\deg(\mu^p;\mu) = p$.

5.2.3.1. *Stability results for the 2D model.*

Theorem 5.6: Linear stability analysis, the 2D case [18]

Let $(a_k)_{k\geq 1}$ be the Fourier modes of the linearized version of (5.24)-(5.25) around the circular expanding shape. They are solutions to the following uncoupled linear system

$$\frac{da_k}{dt}(t) = M(t,k)a_k(t)\,,$$

where the sign of $M(t,k)$ is the same as the following polynomial,

$$N(t,k) = \Big[1-\deg(F;\mu^c(t))\Big] + \Big[\sigma^c(t) - 2 + \deg(F;\mu^c(t))\Big]k^2 - \Big[2\sigma^c(t)\Big]k^4\,,$$

where $\mu^c(t) = \frac{\beta\pi}{\alpha L^c(t)}$, $\sigma^c(t) = \frac{\gamma\pi^2}{\alpha L^c(t)^2}$, and the length of the circular expanding shape is given by $\frac{dL^c(t)}{dt} = \frac{P}{\pi}F\left(\frac{\beta\pi}{\alpha L^c(t)}\right)L^c(t)^2$.

When expansion is so slow that we can make a quasi-stationnary hypothesis on μ and σ, we get the following necessary condition for instability,

$$\deg(F;\mu^c(t)) \geq 2 + 3\sigma^c(t)\,.$$

In particular, it is mandatory that the degree of nonlinearity d is larger than 2. This could have been guessed from the expression of the velocity (5.23). In fact, when $\Psi = \kappa^2$, the velocity is constant, and the geometric coupling disappears.

On the other hand, a simple asymptotic analysis in the two cases i) $d \to +\infty$, and ii) $\sigma \to 0$ together with the condition $(d > 2)$, shows that either a high degree of nonlinearity, or a small lateral diffusion on the cell wall, guarantee instability.

5.2.3.2. *Stability results for the 3D model.*

Theorem 5.7: Linear stability analysis, the 3D case [18]

Let $A = (a_k)_{k\geq 2}$ be the Fourier modes of the linearized version of (5.17)-(5.22) around the spherical expanding shape. They are solutions to the following triangular linear system

$$\frac{dA}{dt}(t) = M(t)A(t)\,, \tag{5.26}$$

where the signs of the diagonal coefficients of M are determined by the signs of the following polynomials,

$$N(t,k) = n_0(t) + n_1(t)k + n_2(t)k^2 + n_3(t)k^3 + n_4(t)k^4\,, \quad \forall t > 0\,, \tag{5.27}$$

where

$$\begin{aligned} n_0(t) &= (1-\nu)\left[1 - 2\deg(F;\mu^c(t))\right]\,,\\ n_1(t) &= -(1-\nu)\left[\sigma^c(t) + \deg(F;\mu^c(t))\right] + 1\,,\\ n_2(t) &= -\nu\sigma^c(t) - 1 + (1-\nu)\deg(F;\mu^c(t))\,,\\ n_3(t) &= 2\sigma^c(t)\,,\\ n_4(t) &= -\sigma^c(t)\,. \end{aligned}$$

Expressions for μ^c, σ^c and L^c are similar to the 2D case.

When expansion is so slow that we can make a quasi-stationnary hypothesis on μ and σ, we get the following necessary condition for instability,

$$\deg(F;\mu^c(t)) \geq \frac{1 + (3+\nu)\sigma^c(t)}{1-\nu}\,. \tag{5.28}$$

The same asymptotic analysis as in the two-dimensional case can be done, provided $(1-\nu)d - 1 > 0$, which is compatible with the above necessary condition. The same conclusion holds true.

Unsurprisingly, the instability region in the (d,σ) space lies below a curve which is increasing with respect to d (Figure 5.4(a)). Therefore, the instability is favoured as d increases or σ decreases. As a by-product, instability is enhanced as the cell is expanding, since σ scales as the inverse of $L(t)^2$. On the other hand, for a given (d,σ), the instability region gets larger when ν increases (Figure 5.4(b)).

We present in Figure 5.5 two numerical simulations for the same set of unstable parameters, but with different initial conditions. This is to illustrate various possible behaviours in the nonlinear regime. We observed at least two possible profiles, both in the two-dimensional case and the three-dimensional case: i) $\partial_x\phi$ is above the mean for intermediate x (Figure 5.5(a)), or ii) $\partial_x\phi$ is above the mean at the extremities (Figure 5.5(b)).

5.2.4. An alternative model accounting for the dynamics of microtubules in fission yeast. We present a variant of our model within the same framework. We keep the same biomechanical equations (5.24). However, we replace the reaction-diffusion process for the deposit of the growth material by a transport-diffusion equation governing the dynamics of microtubule plus-ends along the cell wall.

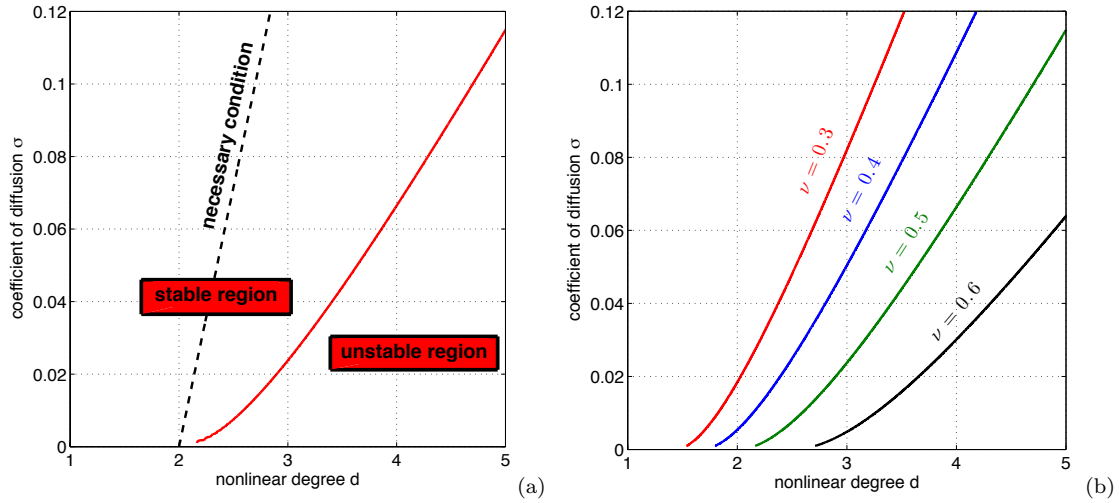

FIGURE 5.4. (a) Stability region in the space (d, σ) for $\nu = 0.5$. The red curve is the set of points such as the difference between the two greatest roots of polynomial (5.27) are equal to 1. For the sake of comparison, the necessary condition derived in (5.28) is plotted in dashed line. (b) Influence of the Poisson's ratio ν.

We restrict to the two-dimensional case. We describe the distribution of microtubules by a membrane density $\rho(t, s)$. We assume their minus ends are attached to the nucleus of the cell (see [**HN01**] for more biological details). For the sake of simplicity, we consider that the nucleus is reduced to a point. The plus-ends undergo a dynamical process of growth and shrinkage, allowing them *to explore the shape of the cell* [**HN01**].

To describe this exploration process, we assume that the plus-ends slide along the cell wall [**FMBN09**], with some possible fluctuations. The direction of a microtubule is encoded by the vector $e_r(t, s) = (r(t, s), z(t, s))^T$ (see Figure 5.3). The sliding velocity is the projection of the direction e_r on the tangential vector τ, up to some constant factor $\chi > 0$, $P_\tau(e_r) = \chi \left(\frac{e_r}{\|\mathbf{e}_r\|} \cdot \tau \right) \tau$. The fluctuations are described by a membrane diffusion with coefficient $D > 0$. This leads to the following Fokker-Planck equation,

$$\frac{\partial \rho}{\partial t} + \frac{\partial}{\partial s}(\rho u) = D \frac{\partial^2 \rho}{\partial s^2}, \tag{5.29}$$

where $u = \chi \frac{e_r}{\|\mathbf{e}_r\|} \cdot \tau$ is the modulus of the sliding velocity. We introduce $V(t, s) = \chi \|\mathbf{e}_r\|$, so that u can be expressed in potential form as $u = \partial_s V(t, s)$. As before, we assume that the timescale of the dynamics of microtubules is faster than growth, thereby the distribution of (5.29) is at quasi-stationary equilibrium for a given shape *i.e.*

$$\frac{\partial}{\partial s}(\partial_s V \, \overline{\rho}) = D \frac{\partial^2 \overline{\rho}}{\partial s^2}, \quad \overline{\rho}(t, s) = \frac{\exp(D^{-1} V(t, s))}{\int \exp(D^{-1} V(t, s)) \, ds}. \tag{5.30}$$

Under the assumption of quasi-stationary expansion, the condition to get unstable modes for the system reads as follows

$$\frac{\chi L^c \deg(F; \mu^c)}{D} \geq 7\pi.$$

The latter is satisfied when $\deg(F; \mu^c)$ is sufficiently large or when the diffusion coefficient is sufficiently small.

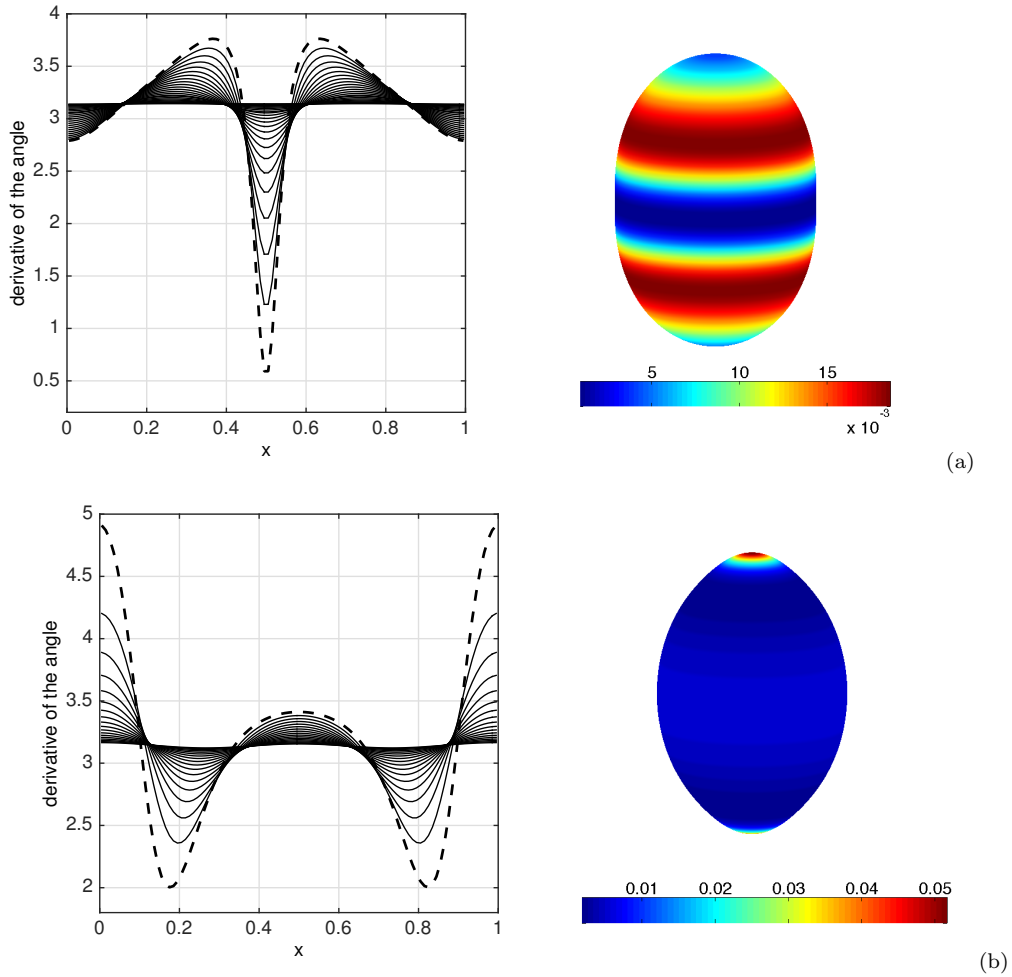

FIGURE 5.5. Evolution of function $\partial_x \phi$ for an unstable set of parameters $\sigma = 5.10^{-2}$ and $d = 4$, and two different initial conditions. Final shape plotted in dash line on the left corresponds to the surface plotted on the right. The color (online) represents the quantity of the density of materials available on the membrane.

Figure 5.6 shows an instability pattern obtained in the nonlinear regime. We observe clearly the emergence of the rod shape when the cell is growing.

5.2.5. Perspectives.

5.2.5.1. *Nonlinear analysis.* So far, we restricted the mathematical analysis to the linear regime, close to the spherical (resp. circular) shape. However, global existence of solutions is not clear. Also, existence of nontrivial shapes, possibly in self-similar variables, would be of great interest.

5.2.5.2. *Other feedback loops between mechanics, geometry and growth.* An insightful feedback loop has been unravelled recently in plant biology, both at the tissue level [**HHJ+08**], and at the cellular level [**SKW+14**]. It involves orientation of the cytoskeleton (here, microtubules). In fact, they align preferentially with the mechanical stress. It yields synthesis of cellulose fibers with the same orientation. In turn, this constrains the growth of the tissue (resp. the cell) in preferred directions, enhancing heterogeneous mechanical stresses, and complex forms.

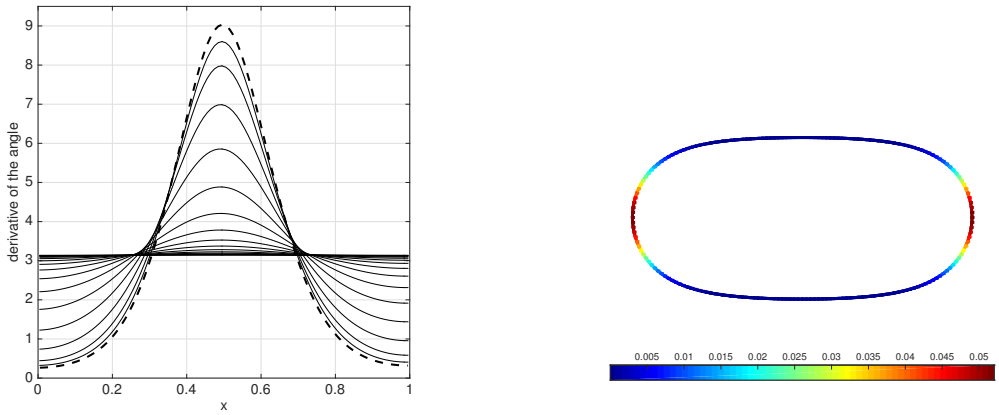

FIGURE 5.6. Evolution of function $\partial_x \phi$ for an unstable set of parameters $\deg(F; \mu^c) = 3$ and $D = 0.1$. Final shape plotted in dash line on the left corresponds to the curve plotted on the right. The color (online) represents the quantity of microtubules.

Following our collaborative work [22] on the biomechanical modelling of cranial suture growth, we aim to model this biomechanical feedback loop, and to analyse emergence of biomechanical patterns.

Bibliography

[ACR13] M. Alfaro, J. Coville, and G. Raoul. Travelling waves in a nonlocal reaction-diffusion equation as a model for a population structured by a space variable and a phenotypic trait. *Comm. PDE*, 2013.

[Adl66] J. Adler. Chemotaxis in Bacteria. *Science*, 1966.

[AGS08] L. Ambrosio, N. Gigli, and G. Savaré. *Gradient flows in metric spaces and in the space of probability measures*. Lectures in Mathematics ETH Zürich. Birkhäuser Verlag, Basel, second edition, 2008.

[AGW06] M. Akian, S. Gaubert, and C. Walsh. How to find horizon-independent optimal strategies leading off to infinity: a max-plus approach. In *2006 45th IEEE Conference on Decision and Control*, pages 5024–5029, 2006.

[AGW09] M. Akian, S. Gaubert, and C. Walsh. The max-plus Martin boundary. *Documenta Mathematica*, 2009.

[Alb08] B. Alberts, editor. *Molecular biology of the cell*. Garland Science, New York, 5th ed edition, 2008.

[Alt80] W. Alt. Biased random walk models for chemotaxis and related diffusion approximations. *J. Math. Biol.*, 1980.

[Ari97] M. Arisawa. Ergodic problem for the Hamilton-Jacobi-Bellman equation. I. Existence of the ergodic attractor. *Annales de l'Institut Henri Poincare (C) Non Linear Analysis*, 1997.

[Ari98] M. Arisawa. Ergodic problem for the Hamilton-Jacobi-Bellman equation. II. *Annales de l'Institut Henri Poincare (C) Non Linear Analysis*, 1998.

[AS04] A. A. Agrachev and Y. L. Sachkov. *Control theory from the geometric viewpoint*. Number v. 87. 2 in Encyclopaedia of mathematical sciences, Control theory and optimization. Springer, Berlin ; New York, 2004.

[AW78] D. G. Aronson and H. F. Weinberger. Multidimensional nonlinear diffusion arising in population genetics. *Adv. Math.*, 1978.

[Bau05] A. Baudisch. Hamilton's indicators of the force of selection. *PNAS*, 2005.

[BB72] H. C. Berg and D. A. Brown. Chemotaxis in Escherichia coli analysed by three-dimensional tracking. *Nature*, 1972.

[BCC08] A. Blanchet, V. Calvez, and J. Carrillo. Convergence of the Mass-Transport Steepest Descent Scheme for the Subcritical Patlak–Keller–Segel Model. *SIAM J. Numer. Anal.*, 2008.

[BCC12] A. Blanchet, E. A. Carlen, and J. A. Carrillo. Functional inequalities, thick tails and asymptotics for the critical mass Patlak-Keller-Segel model. *J. Funct. Anal.*, 2012.

[BCD13] M. Bardi and I. Capuzzo Dolcetta. *Optimal control and viscosity solutions of Hamilton-Jacobi-Bellman equations*. Systems & control Foundations & applications. Springer, New York, NY, 2013.

[BCG13] D. Balagué, J. A. Cañizo, and P. Gabriel. Fine asymptotics of profiles and relaxation to equilibrium for growth-fragmentation equations with variable drift rates. *Kinetic and Related Models*, 2013.

[BCGP08] N. Bournaveas, V. Calvez, S. Gutiérrez, and B. Perthame. Global Existence for a Kinetic Model of Chemotaxis via Dispersion and Strichartz Estimates. *Communications in Partial Differential Equations*, 2008.

[BCK+14] A. Blanchet, J. A. Carrillo, D. Kinderlehrer, M. Kowalczyk, P. Laurençot, and S. Lisini. A hybrid variational principle for the Keller-Segel system in $\mathbb{R}^2$. *arXiv:1407.5562 [math]*, 2014.

[BCL08] A. Blanchet, J. A. Carrillo, and P. Laurençot. Critical mass for a Patlak–Keller–Segel model with degenerate diffusion in higher dimensions. *Calc. Var.*, 2008.

[BCM08] A. Blanchet, J. A. Carrillo, and N. Masmoudi. Infinite time aggregation for the critical Patlak-Keller-Segel model in $\mathbb{R}^2$. *Comm. Pure Appl. Math.*, 2008.

[BCT07] B. Bonnard, J.-B. Caillau, and E. Trélat. Second order optimality conditions in the smooth case and applications in optimal control. *ESAIM: Control, Optimisation and Calculus of Variations*, 2007.

[BD85] C. Bardos and P. Degond. Global existence for the Vlasov-Poisson equation in 3 space variables with small initial data. *Annales de l'I.H.P. Analyse non linéaire*, 1985.

[BD97] E. Brunet and B. Derrida. Shift in the velocity of a front due to a cutoff. *Phys. Rev. E*, 1997.

[BD01] É. Brunet and B. Derrida. Effect of microscopic noise on front propagation. *Journal of Statistical Physics*, 2001.

[BDEF10] A. Blanchet, J. Dolbeault, M. Escobedo, and J. Fernández. Asymptotic behaviour for small mass in the two-dimensional parabolic–elliptic Keller–Segel model. *Journal of Mathematical Analysis and Applications*, 2010.

[BDP06] A. Blanchet, J. Dolbeault, and B. Perthame. Two-dimensional Keller-Segel model: optimal critical mass and qualitative properties of the solutions. *Electron. J. Differential Equations*, 2006.

[Bec93] W. Beckner. Sharp Sobolev Inequalities on the Sphere and the Moser–Trudinger Inequality. *Annals of Mathematics*, 1993.

[Bed11a] J. Bedrossian. Global minimizers for free energies of subcritical aggregation equations with degenerate diffusion. *Applied Mathematics Letters*, 2011.

[Bed11b] J. Bedrossian. Intermediate asymptotics for critical and supercritical aggregation equations and patlak-keller-segel models. *Communications in Mathematical Sciences*, 2011.

[Ber04] H. C. Berg. *E. coli in motion*. Springer, 2004.

[Ber12] P. Bernard. The Lax–Oleinik semi-group: a Hamiltonian point of view. *Proceedings of the Royal Society of Edinburgh: Section A Mathematics*, 2012.

[BG10] J. Bérard and J.-B. Gouéré. Brunet-Derrida Behavior of Branching-Selection Particle Systems on the Line. *Communications in Mathematical Physics*, 2010.

[BHG11] M. Barfield, R. D. Holt, and R. Gomulkiewicz. Evolution in stage-structured populations. *Am. Nat.*, 2011.

[BJS14] H. Berestycki, T. Jin, and L. Silvestre. Propagation in a non local reaction diffusion equation with spatial and genetic trait structure. *arXiv:1411.2019 [math]*, 2014.

[BK13] J. Bedrossian and I. C. Kim. Global Existence and Finite Time Blow-Up for Critical Patlak–Keller–Segel Models with Inhomogeneous Diffusion. *SIAM Journal on Mathematical Analysis*, 2013.

[BL95] R. Burger and M. Lynch. Evolution and Extinction in a Changing Environment: A Quantitative-Genetic Analysis. *Evolution*, 1995.

[Bla11] A. Blanchet. On the parabolic-elliptic Patlak-Keller-Segel system in dimension 2 and higher. *arXiv:1109.1543 [math]*, 2011.

[BLG15] H. Berry, T. Lepoutre, and Á. M. González. Quantitative convergence towards a self similar profile in an age-structured renewal equation for subdiffusion. *arXiv:1503.08552 [math]*, 2015.

[BM13] E. Bouin and S. Mirrahimi. A Hamilton-Jacobi approach for a model of population structured by space and trait. *arXiv:1307.8332*, 2013.

[BM14] J. Bérard and P. Maillard. The limiting process of N-particle branching random walk with polynomial tails. *Electronic Journal of Probability*, 2014.

[BMR15] N. Berestycki, C. Mouhot, and G. Raoul. Existence de fronts auto-accélérés pour des équations de réaction-diffusion non-locales. In *ReaDi workshop (11th session)*, 2015.

[BN94] P. Biler and T. Nadzieja. Existence and nonexistence of solutions for a model of gravitational interaction of particles. I. *Colloq. Math.*, 1994.

[BNPR09] H. Berestycki, G. Nadin, B. Perthame, and L. Ryzhik. The non-local Fisher–KPP equation: travelling waves and steady states. *Nonlinearity*, 2009.

[Bou15] E. Bouin. A Hamilton-Jacobi approach for front propagation in kinetic equations. *Kinetic and Related Models*, 2015.

[BPS14] G. P. Brown, B. L. Phillips, and R. Shine. The straight and narrow path: the evolution of straight-line dispersal at a cane toad invasion front. *Proc. R. Soc. B*, 2014.

[BR03] G. Barles and J.-M. Roquejoffre. Large time behavior of fronts governed by eikonal equations. *Interfaces and Free Boundaries*, 2003.

[Bra01] D. Bray. *Cell movements: from molecules to motility*. Garland Pub, New York, 2nd ed edition, 2001.

[BRD07] R. Bernal, E. Rojas, and J. Dumais. The mechanics of tip growth morphogenesis: what we have learned from rubber balloons. *Journal of Mechanics of Materials and Structures*, 2007.

[Bre91] Y. Brenier. Polar factorization and monotone rearrangement of vector-valued functions. *Comm. Pure Appl. Math.*, 1991.

[BSB83] S. M. Block, J. E. Segall, and H. C. Berg. Adaptation kinetics in bacterial chemotaxis. *J Bacteriol*, 1983.

[BSS84] C. Bardos, R. Santos, and R. Sentis. Diffusion approximation and computation of the critical size. *Trans. AMS*, 1984.

[Bul80] M. G. Bulmer. *The mathematical theory of quantitative genetics*. Oxford University Press, 1980.

[Bür00] R. Bürger. *The mathematical theory of selection, recombination, and mutation*. Wiley, Chichester; New York, 2000.

[BWS+04] J. Bieschke, P. Weber, N. Sarafoff, M. Beekes, A. Giese, and H. Kretzschmar. Autocatalytic self-propagation of misfolded prion protein. *Proc. Natl. Acad. Sci. U.S.A.*, 2004.

[CB13] G. Chapuisat and H. Berestycki. Traveling fronts guided by the environment for reaction-diffusion equations. *Networks and Heterogeneous Media*, 2013.

[CBBB12] J. Clobert, M. Baguette, T. G. Benton, and J. M. Bullock. *Dispersal ecology and evolution*. Oxford University Press, 2012.

[CC08] V. Calvez and L. Corrias. The parabolic-parabolic Keller-Segel model in $\mathbb{R}^2$. *Commun. Math. Sci.*, 2008.

[CCL10] E. A. Carlen, J. A. Carrillo, and M. Loss. Hardy-Littlewood-Sobolev inequalities via fast diffusion flows. *PNAS*, 2010.

[CCM11] M. J. Cáceres, J. A. Cañizo, and S. Mischler. Rate of convergence to an asymptotic profile for the self-similar fragmentation and growth-fragmentation equations. *Journal de Mathématiques Pures et Appliquées*, 2011.

[CCP11] M. J. Cáceres, J. A. Carrillo, and B. Perthame. Analysis of Nonlinear Noisy Integrate and Fire Neuron Models: blow-up and steady states. *The Journal of Mathematical Neuroscience*, 2011.

[CCV15] J. A. Carrillo, D. Castorina, and B. Volzone. Ground States for Diffusion Dominated Free Energies with Logarithmic Interaction. *SIAM Journal on Mathematical Analysis*, 2015.

[CD14] J. F. Campos and J. Dolbeault. Asymptotic Estimates for the Parabolic-Elliptic Keller-Segel Model in the Plane. *Communications in Partial Differential Equations*, 2014.

[CDL90] I. Capuzzo-Dolcetta and P.-L. Lions. Hamilton-Jacobi equations with state constraints. *Transactions of the American Mathematical Society*, 1990.

[CDSM+06] F. Chalub, Y. Dolak-Struss, P. Markowich, D. Oelz, C. Schmeiser, and A. Soreff. Model Hierarchies for cell aggregation by chemotaxis. *Mathematical Models and Methods in Applied Sciences*, 2006.

[CF13] E. A. Carlen and A. Figalli. Stability for a GNS inequality and the Log-HLS inequality, with application to the critical mass Keller–Segel equation. *Duke Math. J.*, 2013.

[CFM06] N. Champagnat, R. Ferrière, and S. Méléard. Unifying evolutionary dynamics: From individual stochastic processes to macroscopic models. *Theoretical Population Biology*, 2006.

[CFM08] N. Champagnat, R. Ferrière, and S. Méléard. From Individual Stochastic Processes to Macroscopic Models in Adaptive Evolution. *Stochastic Models*, 2008.

[CG05] D. A. Clark and L. C. Grant. The bacterial chemotactic response reflects a compromise between transient and steady-state behavior. *PNAS*, 2005.

[CGS14] J.-M. Coron, P. Gabriel, and P. Shang. Optimization of an amplification protocol for misfolded proteins by using relaxed control. *J. Math. Biol.*, 2014.

[CH14] F. Chang and K. C. Huang. How and why cells grow as rods. *BMC Biology*, 2014.

[Cha94] B. Charlesworth. *Evolution in age-structured populations*. Cambridge University Press, 1994.

[Cha00] B. Charlesworth. Fisher, Medawar, Hamilton and the evolution of aging. *Genetics*, 2000.

[Cha01] B. Charlesworth. Patterns of Age-specific Means and Genetic Variances of Mortality Rates Predicted by the Mutation-Accumulation Theory of Ageing. *Journal of Theoretical Biology*, 2001.

[CHS12] C. M. Cuesta, S. Hittmeir, and C. Schmeiser. Traveling Waves of a Kinetic Transport Model for the KPP-Fisher Equation. *SIAM J. Math. Anal.*, 2012.

[CKRL95] B. Caughey, D. A. Kocisko, G. J. Raymond, and P. T. Lansbury. Aggregates of scrapie-associated prion protein induce the cell-free conversion of protease-sensitive prion protein to the protease-resistant state. *Chemistry & biology*, 1995.

[CL92] E. Carlen and M. Loss. Competing symmetries, the logarithmic HLS inequality and Onofri's inequality ons n. *Geometric and Functional Analysis*, 1992.

[CM07] N. Champagnat and S. Méléard. Invasion and adaptive evolution for individual-based spatially structured populations. *J. Math. Biol.*, 2007.

[CM09] O. Campàs and L. Mahadevan. Shape and Dynamics of Tip-Growing Cells. *Current Biology*, 2009.

[CMPS04] F. A. C. C. Chalub, P. A. Markowich, B. Perthame, and C. Schmeiser. Kinetic Models for Chemotaxis and their Drift-Diffusion Limits. *Monatshefte fur Mathematik*, 2004.

[CP81] S. Childress and J. Percus. Nonlinear aspects of chemotaxis. *Mathematical Biosciences*, 1981.

[CP96] F. Castella and B. Perthame. Estimations de Strichartz pour les équations de transport cinétique. *CR Acad. Sci. Paris Sér. I Math*, 1996.

[CPH+94] F. E. Cohen, K. M. Pan, Z. Huang, M. Baldwin, R. J. Fletterick, and S. B. Prusiner. Structural clues to prion replication. *Science*, 1994.

[CPSt07] V. Calvez, B. Perthame, and M. Sharifi tabar. Modified Keller-Segel system and critical mass for the log interaction kernel. In *Stochastic analysis and partial differential equations*, volume 429 of *Contemp. Math.*, pages 45–62. Amer. Math. Soc., Providence, RI, 2007.

[CPZ04] L. Corrias, B. Perthame, and H. Zaag. Global Solutions of Some Chemotaxis and Angiogenesis Systems in High Space Dimensions. *Milan j. math.*, 2004.

[CR09] X. Cabré and J.-M. Roquejoffre. Propagation de fronts dans les équations de Fisher–KPP avec diffusion fractionnaire. *Comptes Rendus Mathematique*, 2009.

[CR12] A.-C. Coulon and J.-M. Roquejoffre. Transition Between Linear and Exponential Propagation in Fisher-KPP Type Reaction-Diffusion Equations. *Communications in Partial Differential Equations*, 2012.

[CR13] X. Cabré and J.-M. Roquejoffre. The Influence of Fractional Diffusion in Fisher-KPP Equations. *Communications in Mathematical Physics*, 2013.

[CR14] O. Cotto and O. Ronce. Maladaptation as a Source of Senescence in Habitats Variable in Space and Time. *Evolution*, 2014.

[CS04] P. Cannarsa and C. Sinestrari. Semiconcave Functions. In *Semiconcave Functions, Hamilton—Jacobi Equations, and Optimal Control*, volume 58, pages 29–47. Birkhäuser Boston, Boston, MA, 2004.

[CSHS05] J. Castilla, P. Saá, C. Hetz, and C. Soto. In Vitro Generation of Infectious Scrapie Prions. *Cell*, 2005.

[CSS05] J. Castilla, P. Saá, and C. Soto. Detection of prions in blood. *Nat. Med.*, 2005.

[CV10] A. Celani and M. Vergassola. Bacterial strategies for chemotaxis response. *PNAS*, 2010.

[DC12] J. Dolbeault and J. Campos. A functional framework for the Keller–Segel system: Logarithmic Hardy–Littlewood–Sobolev and related spectral gap inequalities. *Comptes Rendus Mathematique*, 2012.

[dCBE13] T. de Carvalho, C. A. Buzzi, and R. D. Euzébio. On Poincaré-Bendixson Theorem and Non-Trivial Minimal Sets in Planar Nonsmooth Vector Fields. *arXiv:1307.6825 [math]*, 2013.

[DFP04] L. Desvillettes, R. Ferrière, and C. Prévost. Infinite dimensional reaction- diffusion for population dynamics. 2004.

[dG04] P.-G. de Gennes. Chemotaxis: the role of internal delays. *European Biophysics Journal*, 2004.

[DGM+10] O. Diekmann, M. Gyllenberg, J. a. J. Metz, S. Nakaoka, and A. M. d. Roos. Daphnia revisited: local stability and bifurcation theory for physiologically structured population models explained by way of an example. *J. Math. Biol.*, 2010.

[DHMP98] J. Dockery, V. Hutson, K. Mischaikow, and M. Pernarowski. The evolution of slow dispersal rates: a reaction diffusion model. *Journal of Mathematical Biology*, 1998.

[Die03] O. Diekmann. A beginner's guide to adaptive dynamics. pages 47–86. Institute of Mathematics Polish Academy of Sciences, 2003.

[DJG10] M. Doumic Jauffret and P. Gabriel. Eigenelements of a general aggregation-fragmentation model. *Mathematical Models and Methods in Applied Sciences*, 2010.

[DJMP05] O. Diekmann, P.-E. Jabin, S. Mischler, and B. Perthame. The dynamics of adaptation: An illuminating example and a Hamilton–Jacobi approach. *Theoretical Population Biology*, 2005.

[DL96] U. Dieckmann and R. Law. The dynamical theory of coevolution: a derivation from stochastic ecological processes. *J. Math. Biol.*, 1996.

[DM09] A. Ducrot and P. Magal. Travelling wave solutions for an infection-age structured model with diffusion. *Proceedings of the Royal Society of Edinburgh: Section A Mathematics*, 2009.

[DMR10] A. Ducrot, P. Magal, and S. Ruan. Travelling Wave Solutions in Multigroup Age-Structured Epidemic Models. *Archive for Rational Mechanics and Analysis*, 2010.

[DMS15] J. Dolbeault, C. Mouhot, and C. Schmeiser. Hypocoercivity for linear kinetic equations conserving mass. *Transactions of the American Mathematical Society*, 2015.

[Dou07] M. Doumic. Analysis of a Population Model Structured by the Cells Molecular Content. *Mathematical Modelling of Natural Phenomena*, 2007.

[DP04] J. Dolbeault and B. Perthame. Optimal critical mass in the two dimensional Keller–Segel model in. *Comptes Rendus Mathematique*, 2004.

[DS05] Y. Dolak and C. Schmeiser. Kinetic models for chemotaxis: Hydrodynamic limits and spatio-temporal mechanisms. *Journal of Mathematical Biology*, 2005.

[DSS+06] J. Dumais, S. L. Shaw, C. R. Steele, S. R. Long, and P. M. Ray. An anisotropic-viscoplastic model of plant cell morphogenesis by tip growth. *The International Journal of Developmental Biology*, 2006.

[Dum13] J. Dumais. Modes of deformation of walled cells. *J. Exp. Bot.*, 2013.

[DV13] T. Drake and D. Vavylonis. Model of Fission Yeast Cell Shape Driven by Membrane-Bound Growth Factors and the Cytoskeleton. *PLoS Comput Biol*, 2013.

[EG01] L. C. Evans and D. Gomes. Effective Hamiltonians and Averaging for Hamiltonian Dynamics I. *Arch. Rational Mech. Anal.*, 2001.

[Eig96] M. Eigen. Prionics or the kinetic basis of prion diseases. *Biophys. Chem.*, 1996.

[EM13] F. G. Egana and S. Mischler. Uniqueness and long time asymptotic for the Keller-Segel equation: The parabolic-elliptic case. *arXiv:1310.7771 [math]*, 2013.

[EMPS+08] D. El Moustaine, V. Perrier, L. Smeller, R. Lange, and J. Torrent. Full-length prion protein aggregates to amyloid fibrils and spherical particles by distinct pathways. *FEBS journal*, 2008.

[EO04] R. Erban and H. G. Othmer. From Individual to Collective Behavior in Bacterial Chemotaxis. *SIAM J. Appl. Math.*, 2004.

[EO05] R. Erban and H. G. Othmer. From Signal Transduction to Spatial Pattern Formation in *E. coli* : A Paradigm for Multiscale Modeling in Biology. *Multiscale Modeling & Simulation*, 2005.

[EPW06] H. Engler, J. Prüss, and G. F. Webb. Analysis of a model for the dynamics of prions II. *Journal of mathematical analysis and applications*, 2006.

[ES89] L. C. Evans and P. E. Souganidis. A PDE approach to geometric optics for certain semilinear parabolic equations. *Indiana Univ. Math. J.*, 1989.

[ESW13] S. N. Evans, D. Steinsaltz, and K. W. Wachter. A mutation-selection model with recombination for general genotypes. *Mem. Amer. Math. Soc.*, 2013.

[Eva89] L. C. Evans. The perturbed test function method for viscosity solutions of nonlinear PDE. *Proc. Roy. Soc. Edinburgh Sect. A*, 1989.

[Eva04] L. C. Evans. A survey of partial differential equations methods in weak KAM theory. *Communications on pure and applied mathematics*, 2004.

[Fat97] A. Fathi. Théorème KAM faible et théorie de Mather sur les systèmes lagrangiens. *Comptes Rendus de l'Académie des Sciences - Series I - Mathematics*, 1997.

[Fat12] A. Fathi. Weak KAM from a PDE point of view: viscosity solutions of the Hamilton–Jacobi equation and Aubry set. *Proceedings of the Royal Society of Edinburgh: Section A Mathematics*, 2012.

[Fed99] S. Fedotov. Wave front for a reaction-diffusion system and relativistic Hamilton-Jacobi dynamics. *Phys. Rev. E*, 1999.

[Fel66] W. Feller. *An introduction to probability theory and its applications. Vol. II.* John Wiley & Sons Inc., 1966.

[Fil06] F. Filbet. A finite volume scheme for the Patlak–Keller–Segel chemotaxis model. *Numer. Math.*, 2006.

[Fis37] R. A. Fisher. The Wave of Advance of Advantageous Genes. *Annals of Eugenics*, 1937.

[FLP05] F. Filbet, P. Laurençot, and B. Perthame. Derivation of hyperbolic models for chemosensitive movement. *Journal of Mathematical Biology*, 2005.

[FM99] J. Fort and V. Méndez. Time-Delayed Theory of the Neolithic Transition in Europe. *Phys. Rev. Lett.*, 1999.

[FMBN09] D. Foethke, T. Makushok, D. Brunner, and F. Nédélec. Force- and length-dependent catastrophe activities explain interphase microtubule organization in fission yeast. *Mol Syst Biol*, 2009.

[FMC09] L. Fainshil, M. Margaliot, and P. Chigansky. On the Stability of Positive Linear Switched Systems Under Arbitrary Switching Laws. *IEEE Transactions on Automatic Control*, 2009.

[Fre86] M. I. Freidlin. Geometric Optics Approach to Reaction-Diffusion Equations. *SIAM J. Appl. Math.*, 1986.

[FS04] A. Fathi and A. Siconolfi. Existence of C 1 critical subsolutions of the Hamilton-Jacobi equation. *Inventiones Mathematicae*, 2004.

[FXPE13] B. Franz, C. Xue, K. J. Painter, and R. Erban. Travelling Waves in Hybrid Chemotaxis Models. *Bull Math Biol*, 2013.

[Gab12] P. Gabriel. Long-time asymptotics for nonlinear growth-fragmentation equations. *Communications in Mathematical Sciences*, 2012.

[Gar11] J. Garnier. Accelerating Solutions in Integro-Differential Equations. *SIAM J. Math. Anal.*, 2011.

[GC06] I. Golding and E. C. Cox. Physical Nature of Bacterial Cytoplasm. *Phys. Rev. Lett.*, 2006.

[GCM13] M. Gaye, Y. Chitour, and P. Mason. Properties of Barabanov norms and extremal trajectories associated with continuous-time linear switched systems. In *Proceedings of the 52nd IEEE Conference on Decision and Control*, pages 716–721, Florence, Italie, 2013.

[GKT05] A. Goriely, G. Károlyi, and M. Tabor. Growth induced curve dynamics for filamentary micro-organisms. *Journal of Mathematical Biology*, 2005.

[GLPS88] F. Golse, P.-L. Lions, B. Perthame, and R. Sentis. Regularity of the moments of the solution of a Transport Equation. *Journal of Functional Analysis*, 1988.

[GMMo98] S. A. Geritz, G. Mesze, J. A. Metz, and others. Evolutionarily singular strategies and the adaptive growth and branching of the evolutionary tree. *Evolutionary ecology*, 1998.

[GMSM08] J. Grassi, S. Maillet, S. Simon, and N. Morel. Progress and limits of TSE diagnostic tools. *Vet. Res.*, 2008.

[Gos13] L. Gosse. A well-balanced scheme for kinetic models of chemotaxis derived from one-dimensional local forward–backward problems. *Mathematical Biosciences*, 2013.

[GP08] A. B. Goryachev and A. V. Pokhilko. Dynamics of Cdc42 network embodies a Turing-type mechanism of yeast cell polarity. *FEBS letters*, 2008.

[GPMW06] M. L. Greer, L. Pujo-Menjouet, and G. F. Webb. A mathematical analysis of the dynamics of prion proliferation. *Journal of theoretical biology*, 2006.

[GR97] T. Gallay and G. Raugel. Stability of travelling waves for a damped hyperbolic equation. *Z. Angew. Math. Phys.*, 1997.

[GSM07] L. Gurvits, R. Shorten, and O. Mason. On the Stability of Switched Positive Linear Systems. *IEEE Transactions on Automatic Control*, 2007.

[GT03a] A. Goriely and M. Tabor. Biomechanical models of hyphal growth in actinomycetes. *Journal of Theoretical Biology*, 2003.

[GT03b] A. Goriely and M. Tabor. Self-Similar Tip Growth in Filamentary Organisms. *Phys. Rev. Lett.*, 2003.

[GT06] L. Gosse and G. Toscani. Lagrangian Numerical Approximations to One-Dimensional Convolution-Diffusion Equations. *SIAM J. Sci. Comput.*, 2006.

[GW08] G. Guigas and M. Weiss. Sampling the Cell with Anomalous Diffusion—The Discovery of Slowness. *Biophys. J.*, 2008.

[Had88] K. P. Hadeler. Hyperbolic travelling fronts. *Proceedings of the Edinburgh Mathematical Society. Series II*, 1988.

[Had99] K. P. Hadeler. Reaction transport systems in biological modelling. volume 1714 of *Lecture Notes in Math.*, pages 95–150. Springer, 1999.

[Ham66] W. D. Hamilton. The moulding of senescence by natural selection. *Journal of Theoretical Biology*, 1966.

[Has83] A. Hastings. Can spatial variation alone lead to selection for dispersal? *Theor. Pop. Biol.*, 1983.

[HBPV09] R. J. Hawkins, O. Benichou, M. Piel, and R. Voituriez. Rebuilding cytoskeleton roads: Active-transport-induced polarization of cells. *Physical Review E*, 2009.

[HF13] F. Höfling and T. Franosch. Anomalous transport in the crowded world of biological cells. *Rep. Prog. Phys.*, 2013.

[HHJ+08] O. Hamant, M. G. Heisler, H. Jönsson, P. Krupinski, M. Uyttewaal, P. Bokov, F. Corson, P. Sahlin, A. Boudaoud, E. M. Meyerowitz, Y. Couder, and J. Traas. Developmental Patterning by Mechanical Signals in Arabidopsis. *Science*, 2008.

[HKS05] H. J. Hwang, K. Kang, and A. Stevens. Global Solutions of Nonlinear Transport Equations for Chemosensitive Movement. *SIAM Journal on Mathematical Analysis*, 2005.

[HN01] J. Hayles and P. Nurse. A journey into space. *Nat Rev Mol Cell Biol*, 2001.

[HP09] T. Hillen and K. J. Painter. A user's guide to PDE models for chemotaxis. *J. Math. Biol.*, 2009.

[HV96] M. A. Herrero and J. J. L. Velázquez. Singularity patterns in a chemotaxis model. *Math. Ann.*, 1996.

[ID08] P. A. Iglesias and P. N. Devreotes. Navigating through models of chemotaxis. *Current opinion in cell biology*, 2008.

[IGL03] J. E. Irazoqui, A. S. Gladfelter, and D. J. Lew. Scaffold-mediated symmetry breaking by Cdc42p. *Nature cell biology*, 2003.

[IHTL05] J. E. Irazoqui, A. S. Howell, C. L. Theesfeld, and D. J. Lew. Opposing roles for actin in Cdc42p polarization. *Molecular biology of the cell*, 2005.

[JGB+97] M. Jeffrey, C. M. Goodsir, M. E. Bruce, P. A. McBride, and J. R. Fraser. In vivo toxicity of prion protein in murine scrapie: ultrastructural and immunogold studies. *Neuropathology and applied neurobiology*, 1997.

[JKO98] R. Jordan, D. Kinderlehrer, and F. Otto. The Variational Formulation of the Fokker–Planck Equation. *SIAM Journal on Mathematical Analysis*, 1998.

[JL93] J. T. Jarrett and P. T. Lansbury. Seeding "one-dimensional crystallization" of amyloid: a pathogenic mechanism in Alzheimer's disease and scrapie? *Cell*, 1993.

[JSSG+14] O. R. Jones, A. Scheuerlein, R. Salguero-Gómez, C. G. Camarda, R. Schaible, B. B. Casper, J. P. Dahlgren, J. Ehrlén, M. B. García, E. S. Menges, P. F. Quintana-Ascencio, H. Caswell, A. Baudisch, and J. W. Vaupel. Diversity of ageing across the tree of life. *Nature*, 2014.

[Kam90] N. G. v. Kampen. *Stochastic processes in physics and chemistry*. North-Holland, Amsterdam, 6. print edition, 1990.

[KB97] M. Kirkpatrick and N. H. Barton. Evolution of a species' range. *Am. Nat.*, 1997.

[KIH+11] T. Kühn, T. O. Ihalainen, J. Hyväluoma, N. Dross, S. F. Willman, J. Langowski, M. Vihinen-Ranta, and J. Timonen. Protein Diffusion in Mammalian Cell Cytoplasm. *PLoS ONE*, 2011.

[KN11] F. D. Kelly and P. Nurse. De Novo Growth Zone Formation from Fission Yeast Spheroplasts. *PLoS ONE*, 2011.

[KPP37] A. Kolmogorov, I. Petrovsky, and N. Piskunov. Etude de l'équation de la diffusion avec croissance de la quantité de matière et son application à un problème biologique. *Mosc. Univ. Bull. Math*, 1937.

[KS70a] E. F. Keller and L. A. Segel. Conflict between Positive and Negative Feedback as an Explanation for the Initiation of Aggregation in Slime Mould Amoebae. *Nature*, 1970.

[KS70b] E. F. Keller and L. A. Segel. Initiation of slime mold aggregation viewed as an instability. *Journal of Theoretical Biology*, 1970.

[KS71] E. F. Keller and L. A. Segel. Traveling bands of chemotactic bacteria: A theoretical analysis. *J. Theor. Biol.*, 1971.

[KS10] H. Kozono and Y. Sugiyama. Strong solutions to the Keller-Segel system with the weak Ln /2 initial data and its application to the blow-up rate. *Math. Nachr.*, 2010.

[KSS+03] R. V. Kulkarni, A. Slepoy, R. R. P. Singh, D. L. Cox, and F. Pázmándi. Theoretical Modeling of Prion Disease Incubation. *Biophys J*, 2003.

[KY12] I. Kim and Y. Yao. The Patlak–Keller–Segel Model and Its Variations: Properties of Solutions via Maximum Principle. *SIAM Journal on Mathematical Analysis*, 2012.

[Lan82] R. Lande. A Quantitative Genetic Theory of Life History Evolution. *Ecology*, 1982.

[LBN+04] G. Legname, I. V. Baskakov, H.-O. B. Nguyen, D. Riesner, F. E. Cohen, S. J. DeArmond, and S. B. Prusiner. Synthetic Mammalian Prions. *Science*, 2004.

[LBS+13] T. Lindström, G. P. Brown, S. A. Sisson, B. L. Phillips, and R. Shine. Rapid shifts in dispersal behavior on an expanding range edge. *PNAS*, 2013.

[Le09] S. A. Levin (edt). *The Princeton guide to ecology*. Princeton University Press, Princeton, 2009.

[Le13] J. B. Losos (edt). *The Princeton guide to evolution*. Princeton University Press, Princeton, 2013.

[Len09] N. Lenuzza. *Modélisation de la réplications des Prions : Implication de la dépendance en taille des agrégats de PrP et de l'hétérogénéité des populations cellulaires.* phdthesis, Ecole Centrale Paris, 2009.

[LGW91] M. Lynch, W. Gabriel, and A. M. Wood. Adaptive and demographic responses of plankton populations to environmental change. *Limnol. Oceanogr.*, 1991.

[LKR06] H. Levine, D. A. Kessler, and W.-J. Rappel. Directional sensing in eukaryotic chemotaxis: a balanced inactivation model. *Proceedings of the National Academy of Sciences*, 2006.

[LL93] M. Lynch and R. Lande. Evolution and extinction in response to environmental change. *Biotic interactions and global change*, 1993.

[LL15] K.-Y. Lam and Y. Lou. A mutation-selection model for evolution of random dispersal. *arXiv:1506.00662 [math]*, 2015.

[LLC+15] A. Lorz, T. Lorenzi, J. Clairambault, A. Escargueil, and B. Perthame. Modeling the Effects of Space Structure and Combination Therapies on Phenotypic Heterogeneity and Drug Resistance in Solid Tumors. *Bulletin of Mathematical Biology*, 2015.

[LMLNC03] S. A. Levin, H. C. Muller-Landau, R. Nathan, and J. Chave. The Ecology and Evolution of Seed Dispersal: A Theoretical Perspective. *Annual Review of Ecology, Evolution, and Systematics*, 2003.

[LMM14] T. Lepoutre, N. Meunier, and N. Muller. Cell polarisation model: The 1d case. *Journal de Mathématiques Pures et Appliquées*, 2014.

[LMP11] A. Lorz, S. Mirrahimi, and B. Perthame. Dirac Mass Dynamics in Multidimensional Nonlocal Parabolic Equations. *Comm. PDE*, 2011.

[LMP13] M. A. Lewis, P. K. Maini, and S. V. Petrovskii, editors. *Dispersal, Individual Movement and Spatial Ecology*, volume 2071 of *Lecture Notes in Mathematics*. Springer Berlin Heidelberg, Berlin, Heidelberg, 2013.

[Loc07] J. T. Locsei. Persistence of direction increases the drift velocity of run and tumble chemotaxis. *J. Math. Biol.*, 2007.

[LP09] P. Laurençot and B. Perthame. Exponential decay for the growth-fragmentation/cell-division equations. *Communications in Mathematical Sciences*, 2009.

[LPV88] P.-L. Lions, G. Papanicolaou, and S. R. S. Varadhan. Homogenization of hamilton-jacobi equations. Unpublished preprint, 1988.

[MBBO03] N. Mittal, E. O. Budrene, M. P. Brenner, and A. v. Oudenaarden. Motility of Escherichia coli cells in clusters formed by chemotactic aggregation. *PNAS*, 2003.

[MBC09] N. Minc, A. Boudaoud, and F. Chang. Mechanical Forces of Fission Yeast Growth. *Current Biology*, 2009.

[MC05] S. G. Martin and F. Chang. New End Take Off: Regulating Cell Polarity during the Fission. *Cell Cycle*, 2005.

[McC97] R. J. McCann. A Convexity Principle for Interacting Gases. *Advances in Mathematics*, 1997.

[MCGP10] V. Méndez, D. Campos, and I. Gómez-Portillo. Traveling fronts in systems of particles with random velocities. *Phys. Rev. E*, 2010.

[MCS+03] D. L. Mobley, D. L. Cox, R. R. Singh, R. V. Kulkarni, and A. Slepoy. Simulations of oligomeric intermediates in prion diseases. *Biophysical journal*, 2003.

[MFF99] V. Méndez, J. Fort, and J. Farjas. Speed of wave-front solutions to hyperbolic reaction-diffusion equations. *Physical Review E*, 1999.

[MFH10] V. Mendez, S. Fedotov, and W. Horsthemke. *Reaction-transport systems mesoscopic foundations, fronts, and spatial instabilities*. Springer, 2010.

[Mic06] P. Michel. Existence of a solution to the cell division eigenproblem. *Mathematical Models and Methods in Applied Sciences*, 2006.

[Mir13] S. Mirrahimi. Adaptation and migration of a population between patches. *Discrete Contin. Dyn. Syst. Ser. B*, 2013.

[MJN99] J. Masel, V. A. Jansen, and M. A. Nowak. Quantifying the kinetic parameters of prion replication. *Biophysical chemistry*, 1999.

[MK72] R. M. Macnab and D. E. Koshland. The gradient-sensing mechanism in bacterial chemotaxis. *Proceedings of the National Academy of Sciences*, 1972.

[MM15] S. Méléard and S. Mirrahimi. Singular Limits for Reaction-Diffusion Equations with Fractional Laplacian and Local or Nonlocal Nonlinearity. *Communications in Partial Differential Equations*, 2015.

[MMP05] P. Michel, S. Mischler, and B. Perthame. General relative entropy inequality: an illustration on growth models. *Journal de Mathématiques Pures et Appliquées*, 2005.

[MMQ11] C. Mueller, L. Mytnik, and J. Quastel. Effect of noise on front propagation in reaction-diffusion equations of KPP type. *Inventiones mathematicae*, 2011.

[Mon15] A. Montaru. Exponential speed of uniform convergence of the cell density toward equilibrium for subcritical mass in a Patlak–Keller–Segel model. *Journal of Differential Equations*, 2015.

[Mor13] I. D. Morris. Mather sets for sequences of matrices and applications to the study of joint spectral radii. *Proc. London Math. Soc.*, 2013.

[MR13] S. Mirrahimi and G. Raoul. Dynamics of sexual populations structured by a space variable and a phenotypical trait. *Theoretical Population Biology*, 2013.

[MS98] K. Madden and M. Snyder. Cell polarity and morphogenesis in budding yeast. *Annual Reviews in Microbiology*, 1998.

[MS13] S. Mischler and J. Scher. Spectral analysis of semigroups and growth-fragmentation equations. *arXiv:1310.7773 [math]*, 2013.

[MT12] I. Melbourne and D. Terhesiu. Operator renewal theory and mixing rates for dynamical systems with infinite measure. *Invent. Math.*, 2012.

[MW14] O. Mason and F. Wirth. Extremal norms for positive linear inclusions. *Linear Algebra and its Applications*, 2014.

[MWSL+07] E. Marco, R. Wedlich-Soldner, R. Li, S. J. Altschuler, and L. F. Wu. Endocytosis optimizes the dynamic localization of membrane proteins that regulate cortical polarity. *Cell*, 2007.

[No94] R. D. Nussbaum and others. Finsler structures for the part metric and Hilbert's projective metric and applications to ordinary differential equations. *Differential and Integral Equations*, 1994.

[ODA88] H. G. Othmer, S. R. Dunbar, and W. Alt. Models of dispersal in biological systems. *J. Math. Biol.*, 1988.

[OGB13] P. A. Orlando, R. A. Gatenby, and J. S. Brown. Tumor evolution in space: the effects of competition colonization tradeoffs on tumor invasion dynamics. *Front. Oncol.*, 2013.

[OH02] H. G. Othmer and T. Hillen. The Diffusion Limit of Transport Equations II: Chemotaxis Equations. *SIAM Journal on Applied Mathematics*, 2002.

[OR07] M. Onsum and C. V. Rao. A Mathematical Model for Neutrophil Gradient Sensing and Polarization. *PLoS Comput Biol*, 2007.

[OR09] M. D. Onsum and C. V. Rao. Calling heads from tails: the role of mathematical modeling in understanding cell polarization. *Current opinion in cell biology*, 2009.

[Ott01] F. Otto. The Geometry of Dissipative Evolution Equations: The Porous Medium Equation. *Communications in Partial Differential Equations*, 2001.

[PBC+12] S. Prigent, A. Ballesta, F. Charles, N. Lenuzza, P. Gabriel, L. M. Tine, H. Rezaei, and M. Doumic. An Efficient Kinetic Model for Assemblies of Amyloid Fibrils and Its Application to Polyglutamine Aggregation. *PLoS ONE*, 2012.

[PBWS06] B. L. Phillips, G. P. Brown, J. K. Webb, and R. Shine. Invasion and the evolution of speed in toads. *Nature*, 2006.

[PDA11] C. Prévost, L. Desvillettes, and A. Arnold. Existence of nontrivial steady states for populations structured with respect to space and a continuous trait. *Comm. Pures Appl. Math.*, 2011.

[Per07] B. Perthame. *Transport equations in biology.* Frontiers in Mathematics. Birkhäuser Verlag, 2007.

[PK98] R. J. Payne and D. C. Krakauer. The paradoxical dynamics of prion disease latency. *Journal of theoretical biology*, 1998.

[PP92] P. Pelce and A. Pocheau. Geometrical approach to the morphogenesis of unicellular algae. *Journal of Theoretical Biology*, 1992.

[PS93] P. Pelce and J. Sun. Geometrical Models for the Growth of Unicellular Algae. *Journal of Theoretical Biology*, 1993.

[PS15] B. Perthame and P. E. Souganidis. Rare mutations limit of a steady state dispersion trait model. *arXiv:1505.03420 [math]*, 2015.

[PSDC98] S. B. Prusiner, M. R. Scott, S. J. DeArmond, and F. E. Cohen. Prion Protein Biology. *Cell*, 1998.

[PTV15] B. Perthame, M. Tang, and N. Vauchelet. Derivation of the bacterial run-and-tumble kinetic equation from a model with biochemical pathway. *arXiv:1503.03979 [math]*, 2015.

[PWGK05] N. Piening, P. Weber, A. Giese, and H. Kretzschmar. Breakage of PrP aggregates is essential for efficient autocatalytic propagation of misfolded prion protein. *Biochem. Biophys. Res. Commun.*, 2005.

[RHD11] E. R. Rojas, S. Hotton, and J. Dumais. Chemically Mediated Mechanical Expansion of the Pollen Tube Cell Wall. *Biophys J*, 2011.

[Ron07] O. Ronce. How Does It Feel to Be Like a Rolling Stone? Ten Questions About Dispersal Evolution. *Annu. Rev. Ecol. Evol. Syst.*, 2007.

[Ros94] M. R. Rose. *Evolutionary Biology of Aging.* Oxford University Press, 1994.

[RS13] P. Raphaël and R. Schweyer. On the stability of critical chemotactic aggregation. *Math. Ann.*, 2013.

[RT15] J.-M. Roquejoffre and A. Tarfulea. Gradient estimates and symmetrization for Fisher-KPP front propagation with fractional diffusion. *arXiv:1502.06304 [math]*, 2015.

[SBB86] J. E. Segall, S. M. Block, and H. C. Berg. Temporal comparisons in bacterial chemotaxis. *PNAS*, 1986.

[SBP11] R. Shine, G. P. Brown, and B. L. Phillips. An evolutionary process that assembles phenotypes through space rather than through time. *PNAS*, 2011.

[Sch93] M. J. Schnitzer. Theory of continuum random walks and application to chemotaxis. *Physical Review E. Statistical, Nonlinear, and Soft Matter Physics*, 1993.

[Sch00] H. R. Schwetlick. Travelling fronts for multidimensional nonlinear transport equations. *Ann. Inst. H. Poincaré Anal. Non Linéaire*, 2000.

[Ser02] D. Serre. L^1-stability of nonlinear waves in scalar conservation laws. In *Handbook of Differential Equations: Evolutionary Equations*, volume 1, pages 473–553. North-Holland, 2002.

[SEW05] D. Steinsaltz, S. N. Evans, and K. W. Wachter. A generalized model of mutation–selection balance with applications to aging. *Advances in Applied Mathematics*, 2005.

[SKW+14] A. Sampathkumar, P. Krupinski, R. Wightman, P. Milani, A. Berquand, A. Boudaoud, O. Hamant, H. Jönsson, and E. M. Meyerowitz. Subcellular and supracellular mechanical stress prescribes cytoskeleton behavior in Arabidopsis cotyledon pavement cells. *eLife Sciences*, 2014.

[SLM12] L. E. Sereshki, M. A. Lomholt, and R. Metzler. A solution to the subdiffusion-efficiency paradox: Inactive states enhance reaction efficiency at subdiffusion conditions in living cells. *EPL*, 2012.

[SRH+05] J. R. Silveira, G. J. Raymond, A. G. Hughson, R. E. Race, V. L. Sim, S. F. Hayes, and B. Caughey. The most infectious prion protein particles. *Nature*, 2005.

[SSA02] C. Soto, G. P. Saborio, and L. Anderes. Cyclic amplification of protein misfolding: application to prion-related disorders and beyond. *Trends Neurosci.*, 2002.

[SSL09] B. D. Slaughter, S. E. Smith, and R. Li. Symmetry breaking in the life cycle of the budding yeast. *Cold Spring Harbor perspectives in biology*, 2009.

[St11] M. Sharifi tabar. One-dimensional chemotaxis kinetic model. *Nonlinear Differential Equations and Applications NoDEA*, 2011.

[Str74] D. W. Stroock. Some stochastic processes which arise from a model of the motion of a bacterium. *Z. Wahrscheinlichkeitstheorie verw Gebiete*, 1974.

[Suz05] T. Suzuki. *Free energy and self-interacting particles*. Number v. 62 in Progress in nonlinear differential equations and their applications. Birkhäuser, Boston, 2005.

[SZL+06] H. Salman, A. Zilman, C. Loverdo, M. Jeffroy, and A. Libchaber. Solitary Modes of Bacterial Culture in a Temperature Gradient. *Phys. Rev. Lett.*, 2006.

[TBW+01] C. D. Thomas, E. J. Bodsworth, R. J. Wilson, A. D. Simmons, Z. G. Davies, M. Musche, and L. Conradt. Ecological and evolutionary processes at expanding range margins. *Nature*, 2001.

[TD02] J. M. J. Travis and C. Dytham. Dispersal evolution during invasions. *Evol Ecol Res*, 2002.

[TMB+12] J. M. J. Travis, K. Mustin, K. A. Bartoń, T. G. Benton, J. Clobert, M. M. Delgado, C. Dytham, T. Hovestadt, S. C. F. Palmer, H. Van Dyck, and D. Bonte. Modelling dispersal: an eco-evolutionary framework incorporating emigration, movement, settlement behaviour and the multiple costs involved. *Methods in Ecology and Evolution*, 2012.

[TMPA08] M. J. Tindall, P. K. Maini, S. L. Porter, and J. P. Armitage. Overview of Mathematical Approaches Used to Model Bacterial Chemotaxis II: Bacterial Populations. *Bull. Math. Biol.*, 2008.

[TMVC+08] C. R. Terenna, T. Makushok, G. Velve-Casquillas, D. Baigl, Y. Chen, M. Bornens, A. Paoletti, M. Piel, and P. T. Tran. Physical Mechanisms Redirecting Cell Polarity and Cell Shape in Fission Yeast. *Current Biology*, 2008.

[Tré05] E. Trélat. *Contrôle optimal: théorie & applications*. Vuibert Paris, 2005.

[Tur15] O. Turanova. On a model of a population with variable motility. *Mathematical Models and Methods in Applied Sciences*, 2015.

[UPSS08] M. C. Urban, B. L. Phillips, D. K. Skelly, and R. Shine. A Toad More Traveled: The Heterogeneous Invasion Dynamics of Cane Toads in Australia. *The American Naturalist*, 2008.

[Vil03] C. Villani. *Topics in optimal transportation*, volume 58 of *Graduate Studies in Mathematics*. American Mathematical Society, Providence, RI, 2003.

[Vil09] C. Villani. *Optimal transport*, volume 338 of *Grundlehren der Mathematischen Wissenschaften*. Springer-Verlag, Berlin, 2009. Old and new.

[VLS10] N. Vladimirov, D. Lebiedz, and V. Sourjik. Predicted Auxiliary Navigation Mechanism of Peritrichously Flagellated Chemotactic Bacteria. *PLoS Comput Biol*, 2010.

[VNN13] V. A. Volpert, Y. Nec, and A. A. Nepomnyashchy. Fronts in anomalous diffusion–reaction systems. *Philosophical Transactions of the Royal Society of London A: Mathematical, Physical and Engineering Sciences*, 2013.

[WAB84] R. C. Weast, M. J. Astle, and W. H. Beyer. *1985: CRC handbook of chemistry and physics*. CRC Press, Inc., Boca Raton, FL, 1984.

[WES13] K. W. Wachter, S. N. Evans, and D. Steinsaltz. The age-specific force of natural selection and biodemographic walls of death. *PNAS*, 2013.

[WGP+06] P. Weber, A. Giese, N. Piening, G. Mitteregger, A. Thomzig, M. Beekes, and H. A. Kretzschmar. Cell-free formation of misfolded prion protein with authentic prion infectivity. *Proceedings of the National Academy of Sciences*, 2006.

[WGP+07] P. Weber, A. Giese, N. Piening, G. Mitteregger, A. Thomzig, M. Beekes, and H. A. Kretzschmar. Generation of genuine prion infectivity by serial PMCA. *Veterinary microbiology*, 2007.

[Wir02] F. Wirth. The generalized spectral radius and extremal norms. *Linear Algebra and its Applications*, 2002.

[WRM+08] P. Weber, L. Reznicek, G. Mitteregger, H. Kretzschmar, and A. Giese. Differential effects of prion particle size on infectivity in vivo and in vitro. *Biochemical and biophysical research communications*, 2008.

[WSAWL03] R. Wedlich-Soldner, S. Altschuler, L. Wu, and R. Li. Spontaneous cell polarization through actomyosin-based delivery of the Cdc42 GTPase. *Science*, 2003.

[WSWSL04] R. Wedlich-Soldner, S. C. Wai, T. Schmidt, and R. Li. Robust cell polarity is a dynamic state established by coupling transport and GTPase signaling. *The Journal of cell biology*, 2004.

[WWL00] M. Wachsmuth, W. Waldeck, and J. Langowski. Anomalous diffusion of fluorescent probes inside living cell nuclei investigated by spatially-resolved fluorescence correlation spectroscopy. *J. Mol. Biol.*, 2000.

[XHPE10] C. Xue, H. J. Hwang, K. J. Painter, and R. Erban. Travelling waves in hyperbolic chemotaxis equations. *Bull. Math. Biol.*, 2010.

[Xin00] J. Xin. Front propagation in heterogeneous media. *SIAM Rev.*, 2000.

[Xue13] C. Xue. Macroscopic equations for bacterial chemotaxis: integration of detailed biochemistry of cell signaling. *Journal of Mathematical Biology*, 2013.